# Genetic studies of inner ear development in *Xenopus tropicalis*

Holly Victoria Ironfield B. Sc. (Hons)

Thesis submitted to University College London for the degree of Doctor of Philosophy

2011

Division of Developmental Biology

National Institute for Medical Research
Medical Research Council

## Statement of Declaration

I, Holly Ironfield, declare that the work presented in this thesis has been conducted and completed in the laboratory of Dr. Lyle Zimmerman, in the Division of Developmental Biology, at the National Institute for Medical Research. I confirm that this thesis describes my original work and has not been previously submitted as part of any other degree course or to another university. References are cited where appropriate.

In chapter 3, the seven candidate inner ear phenotypes (fig. 3.3) were originally identified in a forward genetic screen by Dr. Tada Goda. Also, technical assistance was provided by Dr. Joachim Kurth to identify linkage of the *bunny* lesion to chromosome 2 (fig. 3.21).

In chapter 5, technical assistance was again provided by Dr. Joachim Kurth to identify the SSLP markers flanking the telomeric side of the *komimi* lesion. Dr. Joachim Kurth also sequenced *otoconin-90* in both wild type and *komimi* tadpoles, which was used to identify the lesion responsible for the *kom* phenotype.

Signed: _____ Date:_____

## Abstract

*Xenopus tropicalis* provides an excellent model system for studying inner ear development. At ear-forming stages the head is transparent, so this organ can easily be observed, and the small genome, short generation time, and genomic resources makes this species amenable to genetic studies. A group of recessive mutants displaying inner ear defects were obtained from a pilot mutagenesis and gynogenetic screen. The primary inner ear defect was identified for each mutant and each lesion mapped to a chromosome arm. Two mutants, *seasick* (*ssk*) and *komimi* (*kom*) were selected for high resolution positional cloning and phenotypic characterization.

The *ssk* mutant was identified due to enlarged otoconial crystals, decreased pigmentation, and balance defects. Positional cloning showed that the *ssk* phenotype is caused by a premature stop codon in the δ subunit of the adapter protein (AP)-3 complex. AP-3 is required to transport proteins from the endosome and golgi to lysosome-related organelles, a class of organelles that degrade intracellular proteins but also have cell-specific functions such as ionic regulation and pigment synthesis. *ap3δ1* is expressed in the endolymphatic sac, which regulates the ionic composition of the fluid filling the inner ear, suggesting that the otoconial defect may be the result of an ionic imbalance. AP-1 also transports proteins from the endosome to the lysosome-related organelles. Upregulation of AP-1 subunits are observed in response to *ssk*, suggesting that AP-1 may compensate for loss of or decreased levels of AP-3 function.

In *kom* mutants a single large otoconium forms over each macula, and tadpoles exhibit strong balance defects such as circular swimming. Also, the cells comprising the macula are dysmorphic and lack the columnar structure found in wild type. Positional cloning shows that the *kom* phenotype is caused

by a splicing defect causing partial loss of the otoconin-90 signal peptide and likely stops incorporation of the protein into the core of otoconial crystals.

This work successfully demonstrates that *X. tropicalis* forward genetics is a valuable tool for studying the development of the inner ear.

## Acknowledgements

I would like to thank my supervisor, Lyle Zimmerman, for his support and encouragement throughout the length of this project. Also, I am grateful to Tim Geach, Eli Vendrell, Joachim Kurth, Anita Abu-Daya and Tosi Amano for providing useful discussions, practical tips, encouragement and most of all friendship.

I would like to thank my friends and family, especially my parents, Diane and Peter, and my brother, Ross, for their unconditional love and understanding of my absence for the last couple of years.

Finally, I would like to thank Matthew, for his unwavering support and patience.

## Contents

## List of figures

## List of tables

## Abbreviations

| | |
|---|---|
| AP | adapter protein |
| *ap2a1* | *adapter protein 2 alpha 1* |
| *ap3b1* | *adapter protein 3 beta 1* |
| *ap3d1* | *adapter protein 3 delta 1* |
| *ap4e1* | *adapter protein 4 epsilon 1* |
| *ap3u1* | *adapter protein 3 mu 1* |
| *ap1g1* | *adapter protein 1 gamma 1* |
| *ask* | *airsick* |
| BPPV | benign paroxysmal positional vertigo |
| *bun* | *bunny* |
| BrdU | Bromodeoxyuridine |
| CNS | central nervous system |
| *bxe* | *boxer's eye* |
| *dct* | *dopachrome tautomerase* |
| DIG | dioxygenin |
| *dum* | *dumbo* |
| EDTA | ethylenediaminetetraacetic acid |
| ENU | N-ethyl-N-nitrosourea |
| ER | endoplasmic reticulum |
| EST | expressed sequence tag |
| FCS | fetal calf syndrome |
| hCG | human chorionic gonadotropin |
| IC | Ivory Coast |
| *kom* | *komimi* |
| *leg* | *legolas* |
| LROs | lysosome-related organelle |
| MS222 | tricaine |
| N | Nigerian |
| N1-ICD | notch 1 – intracellular domain |

| | |
|---|---|
| NMDA | N-Methyl-D-aspartic acid |
| *ntl* | *no tail* |
| *oc90* | *otoconin 90* |
| *oep* | *one eyed pinhead* |
| OMP | otolith matrix protein |
| PCR | polymerase chain reaction |
| PFA | paraformaldehyde |
| PLA2 | phospholipase A2 |
| PMCA2 | plasma membrane calcium ATPase |
| PNS | peripheral nervous system |
| RT-PCR | reverse transcription – polymerase chain reaction |
| S1K | schedule 1 kill |
| SAG | statoacoustic ganglion |
| SNP | single nucleotide polymorphism |
| SRP | signal recognition particle |
| SSC | saline sodium citrate |
| SSLP | simple sequence length polymorphism |
| *ssk* | *seasick* |
| TBE | tris borate EDTA |
| TBS | tris borate saline |
| TBST | tris borate saline tween |
| TBSBT | tris borate saline bovine serum albumin tween |
| TILLING | targeting induced lesions in genomes |
| TUNEL | terminal deoxynucleotidyl transferase |
| WISH | whole mount in situ hybridisation |
| wt | wild type |

# Chapter 1

# Introduction

# Introduction

Deafness and balance disorders are the most common form of sensory impairment in the human population. It is estimated that 1 in every 2,000 children are born deaf or hard of hearing, and 42% of people over the age of 50 experience hearing loss and balance dysfunction (Price & Fisher, 2001). Hereditary deafness and balance disorders often involve inner ear developmental defects, and hearing loss may result from genetic defects, noise, drugs, aging and disease. The study of hearing and balance impairment in humans is limited by the inability to follow inner ear development, therefore animal models are required for in depth analysis to determine how these disorders develop.

## *1.1 Current models for studying the inner ear*

Current model organisms for studying inner ear development include mouse, chick, zebrafish and *Xenopus laevis*. Gene knockouts and genetic screens carried out in mice have been incredibly valuable, as the mouse inner ear is structurally almost identical to that of human (Morsli et al., 1998). Work carried out in mice has helped to uncover the molecular basis of human diseases such as pendrin syndrome (Yoshino et al., 2004), which results from an ionic imbalance in the inner ear. The disadvantage to working with mice is that their embryos develop internally, therefore observing live embryos is very difficult. Also they produce small litter sizes, large-scale screens are costly, and generating mouse knock out lines is time consuming and laborious.

Studies using zebrafish have made a significant contribution to understanding inner ear development. Zebrafish display a fairly typical vertebrate inner ear (Whitfield, 2002) (fig. 1.1 A), and the development of large numbers of externally developing, optically clear embryos makes it amenable to developmental genetic studies. Many mutants displaying a primary inner ear defect have been recovered from forward genetic screens, several of which have been mapped to

human disease loci, such as *myoVIIa* which is one of the causes of the deaf blindness syndrome, usherin (Ernest et al. 2000). However, teleosts' evolutionary history includes a whole genome duplication event resulting in sub- and neo-functionalization of many genes as well as wide scale re-shuffling of chromosomal organization (Postlethwait et al., 2000). Given this diversification of paralog functions, many gene functions and pathways may not be strictly representative of those of higher vertebrates.

*X. laevis* has proven to be a valuable organism for studying inner ear development. The head is optically clear at tadpole stages, and the inner ear exhibits many key structural similarities to those of higher vertebrates (see section 1.2). Also, amphibians have a remarkable ability to regenerate damaged sensory epithelial cells (Bhattacharyya and Kumar, 2005; Taylor and Forge, 2005). Gain-of- and loss-of-function studies have demonstrated that genes expressed in the inner ear share conserved roles with mammalian and avian development (Quick & Serrano, 2005; Schlosser & Ahrens, 2004). As *Xenopus* eggs are fertilized externally, all embryonic stages are accessible and can be observed in live embryos, offering a great advantage over rodent models. Also, *Xenopus* is ideal for embryological manipulations including ablations, grafts and explants. Embryos are produced in large quantities (>1000 per mating) and can be obtained all year round. However, genetic studies are very difficult in *X. laevis* due to its large ($3.1 \times 10^9$ bp) allotetraploid genome and long generation time (8 months – 2 years).

In recent years *Xenopus tropicalis* has been gaining popularity as a new genetic model organism. It shares the same embryonic advantages for embryology and gain-of-function molecular studies as *X. laevis*, but has one of the smallest tetrapod genomes ($1.5 \times 10^9$bp) distributed over 10 chromosomes, and has a relatively short generation time (5 – 6 months) making it amenable to genetic studies (Amaya et al. 1998; Goda et al. 2006; Hirsch et al. 2002). Crucially, the evolutionary history of *X. tropicalis* does not include a whole genome duplication event such as that ancestral to the teleosts lineage, meaning that gene functions

are less subject to sub- and neo-functionalization and more likely to be representative of higher vertebrates. In this study these desirable traits will be exploited using genetic and molecular tools to carry out a detailed analysis of inner ear development in *X. tropicalis*.

## *1.2 Structure and function of the vertebrate inner ear*

The vertebrate inner ear is required for balance and hearing. The balance organs are highly conserved between species and consist of five sensory epithelia: three cristae, and two maculae known as the utricle and the sacculus. The cristae are each located at the base of one of three semicircular canals, and their function is to detect changes in head orientation. The utricle is positioned along the anterior wall of the inner ear where it detects horizontal motion and the sacculus, which lies along the medial wall, detects vertical motion (Kil and Collazo, 2001) (fig. 1.1). Teleosts and amphibians also contain a lagena, an organ required for the detection of gravity (Kil and Collazo, 2001).

The auditory sensory epithelia vary between species depending on their degree of hearing specialization. In teleosts, the sacculus and lagena also have auditory functions, and in zebrafish this allows the animal to be sensitive to an acoustic range of 100 – 5000Hz (Bass and McKibben, 2003) (fig. 1.1 A). Amphibians also rely on the sacculus and lagena for auditory detection, however, they develop two extra sensory epithelia, the basilar papilla and amphibian papilla (fig. 1.1 B). The four auditory sensory epithelia found in amphibians allow them to detect a greater acoustic resolution over a comparable frequency range to teleosts (Bever et al. 2003; Quick and Serrano 2005). In birds, the auditory sensory epithelia consist of a sacculus and an elongated basilar papilla, which provide a greater acoustic resolution than found in amphibians (fig. 1.1 C). Mammals are the most specialized taxon in detecting auditory stimuli. They develop the organ of Corti, a highly specialized epithelium homologous to the lagena, which in humans can

The balance organs of the inner ear are highly conserved between species and consist of five sensory epithelia: the cristae (red) which sit at the base of the semicircular canals and detect head movement, and the utricle and saccule which detect horizontal and vertical motion, respectively. Teleosts and amphibians also have a lagena, which is required for the detection of gravity.

The auditory organs vary between species depending on their degree of hearing specialization.

**(A)** In teleosts, the utricle and sacculus also act as auditory structures.

**(B)** Amphibians also depend upon the utricle and sacculus but also develop two other sensory epithelia, the basilar papilla and amphibian papilla, which allow them to detect sound at a greater resolution than the teleosts.

**(C)** In birds, the auditory organs consist of the sacculus and an elongated basilar papilla.

**(D)** The mammalian auditory organs consist of the sacculus and a highly specailzed epithelium known as the organ of Corti. It can detect the greatest acoustic range and resolution of all the taxon.

**Figure 1.1: The vertebrate inner ear**

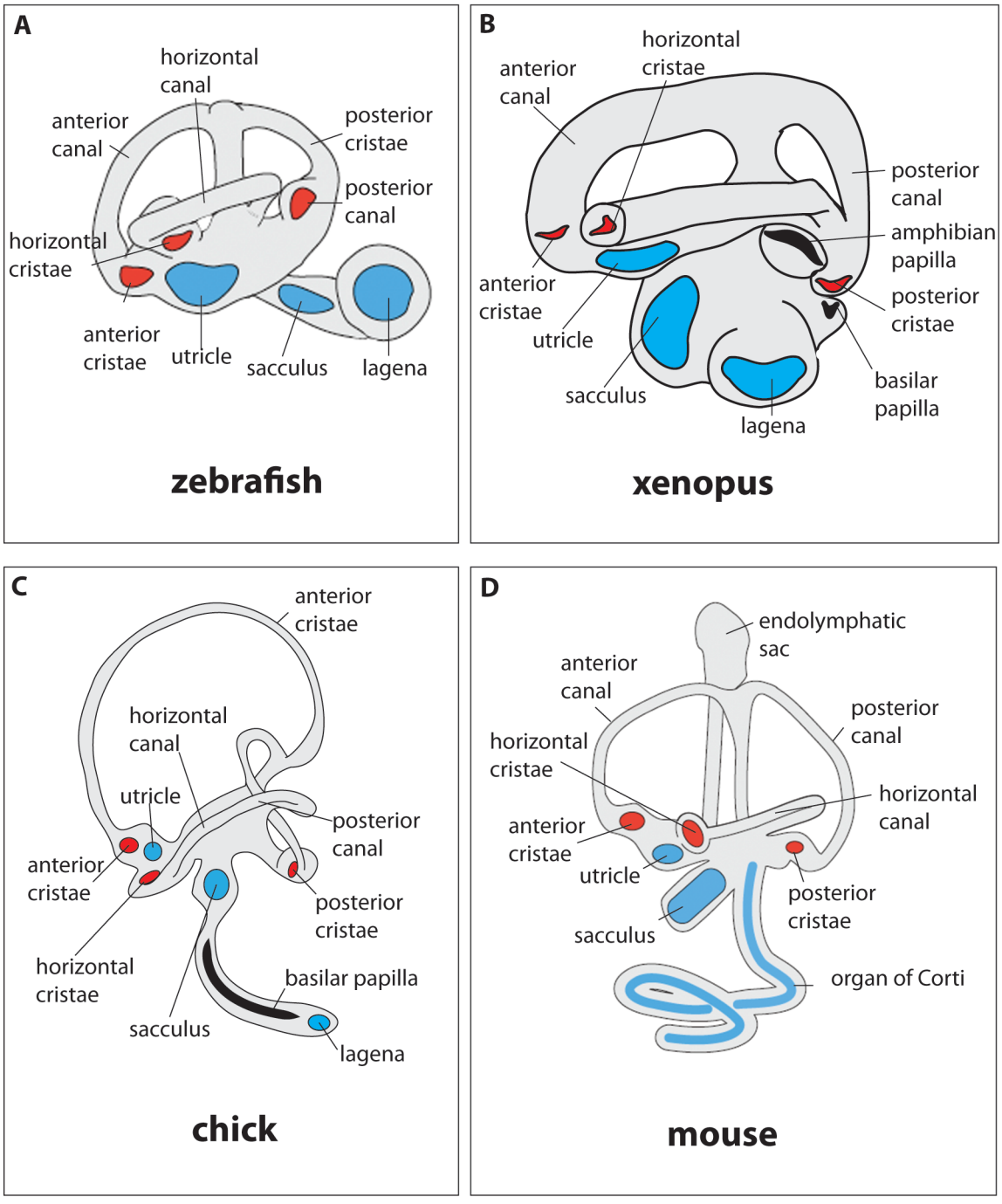


Adapted from Bever et al., 2006; Kelley, 2006; Schneider & Pujades, 2007; Whitfield, 2000

detect acoustic frequencies at a range of 20Hz – 20kHz (Schwander et al., 2010) (fig. 1.1 D).

The maintenance of the ionic environment of the inner ear is critical for the correct function of the sensory epithelia. The endolymphatic sac is an organ that develops in all vertebrates, producing the endolymphatic fluid that fills the lumen of the inner ear. The endolymphatic sac then acts to maintain the concentration of specific ions such as $Ca^{2+}$, $K^{+}$ and $H^{+}$ (Tu et al., 1998; Wangemann et al., 2007). Pigment cells also function to regulate the ionic environment of the endolymph. The melanocytes in mammals and birds and the melanophores in amphibians along with the vestibular dark cells regulate endolymphatic $K^{+}$ concentration (Tu et al., 1998; Wangemann et al., 1995).

### *1.3 Morphological development of the Xenopus inner ear*

Different vertebrate species display striking differences in inner ear morphology (fig. 1.1), particularly in the auditory structures, which relate to the species' degree of hearing specialization. The inner ear arises from a thickened region of head ectoderm, the otic placode, which forms adjacent to the developing hindbrain. In *Xenopus laevis,* development is staged according to detailed anatomical criteria defined by Nieuwkoop and Faber (1975). Comparison of wild type *X. tropicalis* inner ear development (Zimmerman lab, unpublished data) to published *X. laevis* data (Bever et al., 2003; Quick and Serrano, 2005) shows no notable morphological differences in inner ear development, therefore Nieuwkoop and Faber (1975) staging criteria has been used throughout. The otic placode is first morphologically visible at stage 21 and resides next to rhombomeres 4 and 5 (fig. 1.2 A) (Bever et al., 2003; Quick and Serrano, 2005). The otic placode then invaginates to form the otic cup (fig. 1.2 B), which by stage 28 buds away from the overlying ectoderm to form the otic vesicle (fig. 1.2 C) (Bever et al., 2003; Quick and Serrano, 2005). During otic vesicle formation, the otic tissue receives signals from the hindbrain and the surrounding mesendoderm to specify the

**(A)** The inner ear develops from a thickened region of head ectoderm, known as the otic placode. In *Xenopus* this first becomes morphologically visible at stage 21 and forms adjacent to rhombomeres 4 and 5.

**(B)** The otic placode invaginates into the underlying mesoderm and forms the otic cup. As invagination is occuring, cells at the base of the otic cup become specified to form either neuroblasts or sensory cells.

**(C)** By stage 28 the otic cup buds away from the overlying ectoderm to form the otic vesicle. The neuroblasts delaminate from the otic tissue and colonise the statioacoustic ganglion (SAG) and serve to innervate the sensory cells.

**(D)** At stage 37 two discrete sensory epithelia, the utricle and the saccule, are visible developing in the medial region of the otic vesicle. The endolymphatic tissue starts to bud out from the dorsal region of the otic vesicle.

**(E)** The three cristae are morphologically visible by stage 41, and the utricle buds into an interconnecting chamber. The endolymphatic sac has also formed.

**(F)** The three semicircular canals are visible by stage 45.

**(G)** By stage 54 the lagena has formed inside a chamber in ventral part of the inner ear. The amphibian papilla and basilar papilla also develop in the posterior region.

**Figure 1.2: Xenopus inner ear morphogenesis**

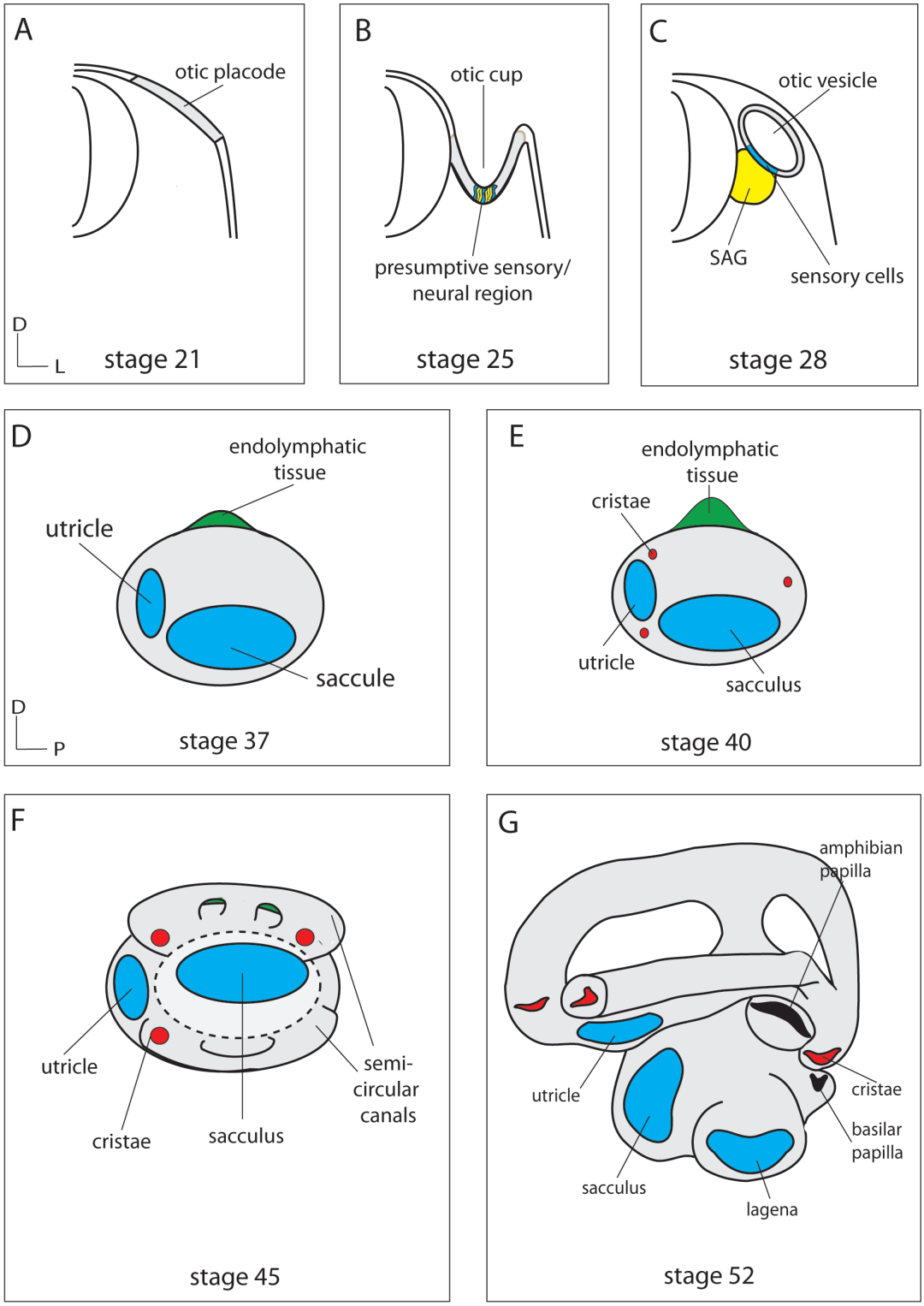

presumptive sensory region (see 1.4) (Mendonsa and Riley, 1999; Woo and Fraser, 1998). A proportion of the cells in the presumptive sensory region develop into neuroblasts, which delaminate from the otic tissue and differentiate to form the neurones that innervate the inner ear. The cells remaining in the presumptive sensory region differentiate to form the cells of the sensory epithelia (fig. 1.2 B - C) (Bever et al., 2003; Quick and Serrano, 2005).

The next phase of development involves the morphogenesis of the otic vesicle to form the complex three-dimensional structure of the adult inner ear. At stage 37, the sensory cells have formed two discrete sensory epithelia, the utricle and the saccule, which form in the ventro-medial region of the otic vesicle (fig. 1.2 D). The endolymphatic tissue is also morphologically visible as a budding of tissue from the dorsal region of the otic vesicle (fig. 1.2 D). By stage 41, the three cristae are visible, and the utricle has budded into a separate chamber that interconnects with the rest of the inner ear (fig. 1.2 E). The endolymphatic tissue has also elongated to form the endolymphatic sac (fig. 1.2 F), and by stage 45, the semicircular canals are also visible. The ventral region of the inner ear has extended by stage 54 and houses the lagena (fig. 1.2 G). The amphibian and basilar papillae also develop in the posterior region of the inner ear (fig. 1.2 G). To support these morphological changes, the developing inner ear also recruits neighboring mesenchymal cells to coalesce and form cartilage to encase the membranous structure (Frenz & Van De Water, 1991).

### *1.4 Induction and patterning*

All of the structures of the inner ear are derived from the otic placode, a thickened region of head ectoderm that forms adjacent to the hindbrain. Induction of the otic placode is controlled by signals from the mesoderm and neural ectoderm. Whereas the mesoderm contains the initial signals for placode induction, the adjacent hindbrain is thought to complement these signals by directing later stages such as setting up asymmetrical gene expression in the otic

tissue, cell fate decisions and morphogenesis of the inner ear (for reviews see Fekete and Wu, 2002; Riley and Philips, 2003; Whitfield and Hammond, 2007).

### *1.4.1 Induction of the otic placode*

The otic tissue is first induced during gastrulation by the mesendoderm as it migrates underneath the presumptive otic tissue. Two types of mesendoderm, the prechordal and cephalic, are known to produce inductive signals. The inductive role of the prechordal mesendoderm is demonstrated by the of the loss-of-function phenotype of *one eyed pinhead* (*oep*) in zebrafish, which encodes the TGF-β signaling receptor cripto and lacks all of this tissue and exhibits a 90-minute delay in the expression of otic markers (Mendonsa and Riley, 1999). If both the prechordal and cephalic mesendoderm are lost, as occurs in double mutants of *oep* and the brachyury mutant *no tail* (*ntl*), this delay in induction is increased to 120 hours (Mendonsa and Riley, 1999). During gastrulation the mesendoderm only has a brief period of contact with the presumptive otic tissue, however, the cephalic mesendoderm contributes to the mesenchyme surrounding the placode where it can continue a sustained period of induction (Mendonsa and Riley, 1999). During post-neurula stages, otic tissue induction is reinforced and in turn patterned by signals originating from the hindbrain and notochord. This has been demonstrated in the zebrafish by transplanting hindbrain tissue into the ventral side of the embryo, where it induces ectopic otic vesicle formation adjacent to the graft (Woo and Fraser, 1998).

Fgf's are strong candidates for the signals that induce otic tissue. *Fgf3* is expressed in the prechordal and paraxial cephalic mesendoderm, and in zebrafish both *fgf3* and *8* are expressed in the rhombomere 4 primordium, which lies adjacent to the presumptive otic tissue. In the zebrafish *fgf8* mutant, *acerebellar* (*ace*), the otic vesicle is small and abnormally patterned however, when *fgf3* morpholino is injected into *ace* mutants the otic tissue is ablated altogether (Philips et al., 2001). The role of fgf3 appears to be conserved across vertebrates (Lombardo et al., 1998), however, involvement of other fgf homologs

varies between species. In mouse, *fgf10* but not *fgf8* is expressed in the hindbrain and mesendoderm surrounding the otic tissue (S. Mansour personal communication cited in Riley & Philips, 2003) and in chick *fgf19* appears to take on this role (Ladher et al., 2000).

### *1.4.2 Axial specification*

#### *1.4.2.1 Anteroposterior axial specification*

The otic tissue develops adjacent to the hindbrain rhombomeres. Each rhombomere expresses a unique set of genes, making them strong candidates for regulating the specification of the anterior-posterior axis. Mutants for the transcription factor mafb support this theory. In mafb mutants rhombomeres 5 and 6 are replaced by a single compartment with characteristics similar to rhombomere 4 (McKay et al., 1994; Sadl et al., 2003), resulting in anterior otic markers such as *hmx3* and *pax5* extending posteriorly (Kwak et al., 2002).

Fgf3 signaling might be the cause of anterior otic specification. In mafb mutants, *fgf3* expression expands posteriorly and the inner ear mutant phenotype can be rescued by morpholino mediated fgf3 knockdown (Kwak et al., 2002). However, *fgf3* is also expressed in the anterior otic tissue, therefore the rescue of the otic phenotype may be the result of the knockdown of otic *fgf3* and not due to effects of fgf3 signaling from the hindbrain (Kwak et al., 2002) (fig. 1.3 A).

Shh signaling, emanating from the floor plate and notochord, has been demonstrated to specify posterior otic identity (fig. 1.3 A) (Hammond et al., 2003). In shh-depleted zebrafish embryos, posterior structures fail to form and anterior structures are duplicated to form a mirror image, whereas overexpression results in the reverse phenotype as posterior structures are duplicated instead (Hammond et al., 2003). Work carried out in *Xenopus* recapitulates this, as overexpression of the shh inhibitor *hip* also results in mirror duplications of anterior structures (Waldman et al., 2007). The caveat with this model is that the level of shh signaling from the midline is equal along the anterioposterior axis

**Figure 1.3: Otic tissue axial patterning**

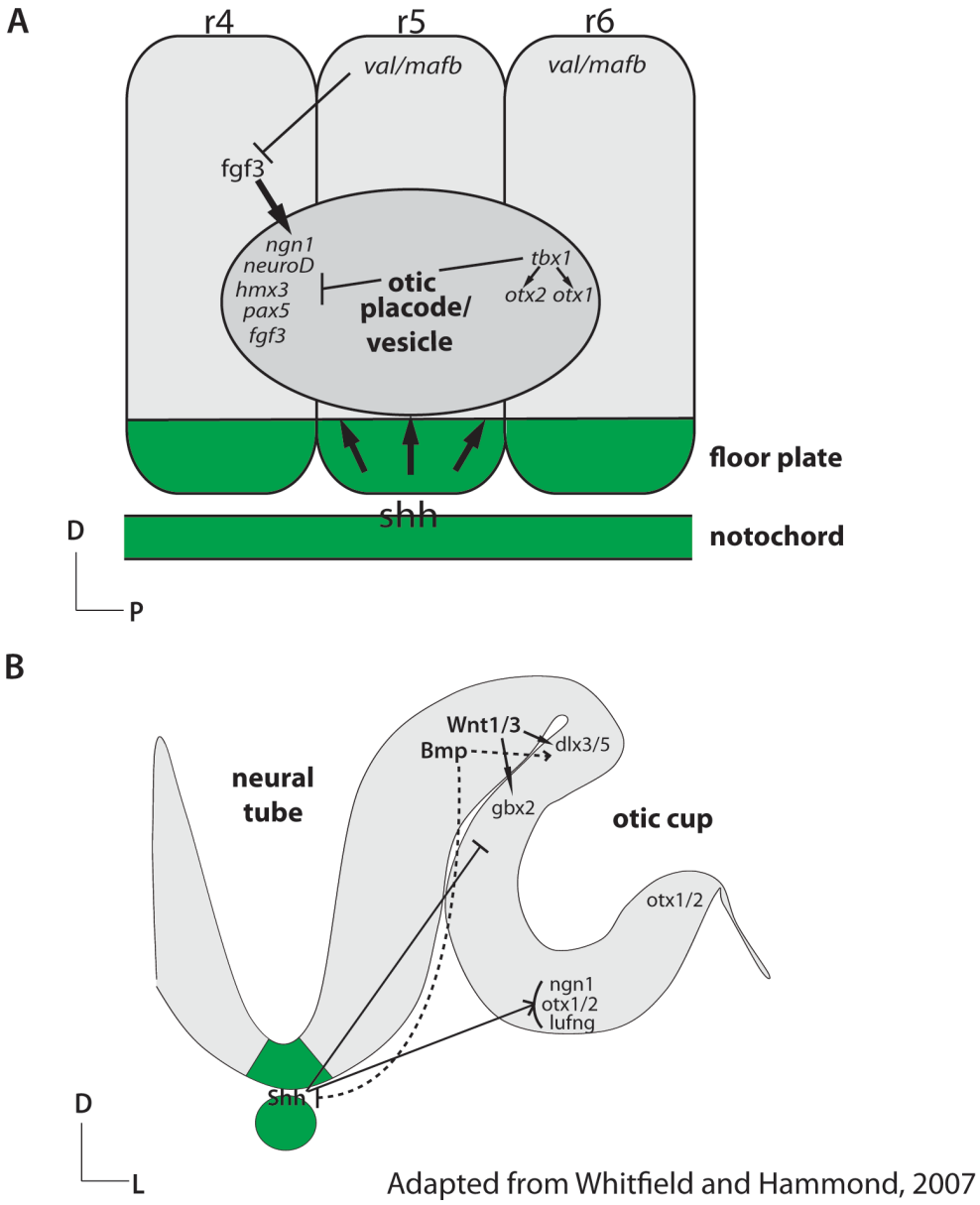


Adapted from Whitfield and Hammond, 2007

**(A)** Schematic of factors influencing anterior-posterior patterning in the otic tissue. Fgf3 from the hindbrain and Shh from the floor plate and notochord have been shown to provide anteriorizing and posteriorizing signals, respectively.

**(B)** Schematic of the factors influencing dorsoventral and mediolateral patterning. Wnts from the hindbrain act as a dorsalizing and lateralizing signals (see text), while Shh specifies ventral fate. It has also been hypothesised that Bmps may act to restrict the dorsal influence of Shh.

(Hammond et al., 2003). A possible explanation is that shh specified cells migrate towards the posterior pole of the otic tissue, however this theory is yet to be tested experimentally. *Tbx1* is likely to be a key downstream target of posterior otic specification signals. It is expressed within the posterior region of the developing otic tissue. In *tbx1* null mice, anteriorly expressed genes such as *lufng*, *ngn1* and *neuroD* expand into the posterior otic domain and posteriorly expressed genes such as *otx1* and *otx2* are abolished (Vitelli et al., 2003). This suggests that *tbx1* acts to restrict the expression of anteriorly expressed genes, therefore maintaining posterior otic identity (fig. 1.3 A).

*1.4.2.2 Dorsoventral axial specification*

The floor plate and the roof plate of the neural tube are likely to be the sources of signals specifying the dorso-ventral axis of the otic tissue. Wnts secreted from the roof plate have been shown to confer dorsal otic patterning (fig. 1.3 B). Mouse double knockouts of *wnt1*/*wnt3a* result in a decrease in the expression of dorsal transcription factors such as *dlx5*, *dlx3* and *gbx2*, and in turn a failure to develop dorsal structures such as the semicircular canals and the endolymphatic duct (Riccomagno et al., 2005). However, blocking Wnt signaling in the hindbrain only affects the expression of a subset of dorsally expressed genes, suggesting that other signaling pathways may also be in operation (Riccomagno et al., 2005). Bmps are expressed in the roof plate. Since it is known that in the neural tube Bmps counteract Shh signaling emanating from the floor plate (Patten & Placzek, 2002), it is possible that these signaling molecules play similar roles in the otic tissue to confer dorso-ventral axial patterning.

Shh is expressed in the floor plate and provides signals for ventral specification of otic tissue (Lui et al., 2002). In *shh* null mouse embryos, the expression of ventral otic transcription factors such as *otx1*, *otx2*, *lufng*, *ngn1* and *neuroD* are all reduced, and ventral structures such as the cochlea fail to form (Riccomango et al., 2002). Dorsally expressed genes such as *dlx5* and *gbx2* also expand ventrally suggesting that Shh blocks downstream Wnt signaling (fig. 1.2 B) (Riccomango et al., 2002; Riccomango et al., 2005). However, manipulation of

Wnt signaling has no observable effect on the expression range of downstream Shh factors, indicating that restriction of Shh activity is not mediated by Wnts (fig. 1.3 B) (Riccomango et al., 2002; Riccomango et al., 2005).

#### *1.4.2.3 Mediolateral axial specification*

The signals patterning the mediolateral axis are probably the least understood. It has been observed in mouse mutants affecting rhombomere patterning (e.g. the mafb mutant *kreisler*, *hoxa1*$^{-/-}$) that the endolymphatic duct, a medial structure, fails to form, while the lateral canal and cristae remain unaffected (Choo et al. 2006; Mark et al., 1993). At the molecular level, medially expressed transcription factors such as *gbx2* and *wnt2b* are downregulated, while those laterally expressed such as *otx2* expand medially (Choo et al., 2006). This phenotype of downregulated medial genes and expansion of laterally expressed genes is recapitulated in the *gbx2* knockout mouse, suggesting that this is a key transcription factor responding to mediolateral hindbrain patterning (Lin et al., 2005).

Despite the fact that Wnts are expressed in the dorsal hindbrain, fate mapping has shown that many Wnt responsive cells lie along the medioventral side of the otic tissue (Riccomango et al., 2005). This is consistent with observations that ventral structures develop abnormally in *wnt1/3*$^{-/-}$ mice (Riccomango et al., 2005). A separate fate mapping study in chick indicated that cells in the lateral otic vesicle originate from the ventral posterior rim of the closing otic cup (Brigande et al., 2000a). These studies suggest that lateral otic cells are first specified is the dorsal otic tissue, migrate ventrally throughout the medial otic tissue, and then move dorsally to achieve their lateral location (Bok et al., 2007).

### *1.4.3 Specification of the prosensory and neural cells*

The inner ear is composed of a large variety of cell types, nearly all of which are derived from the otic placode (Schlosser and Northcutt 2000; Schlosser and

Ahrens 2004). To produce these diverse cell types, placodal cells undergo a series of cell fate decisions. The first is whether or not to form the presumptive sensory cells (see fig 1.2 B). This decision is mediated by notch-1 signaling through its ligand serrate-1, using a process known as lateral induction (fig. 1.4 A) (Daudet and Lewis, 2005; Daudet et al., 2007). Notch-1 is expressed throughout the early otic vesicle, however its ligand serrate-1 (jagged-1 in mammals) is expressed specifically within the presumptive epithelia (Adam et al., 1998). Serrate-1 and notch-1 enter into a positive feedback loop and influence the expression of pro-sensory transcription factors such as *lufng* (fig. 1.4 A) (Daudet and Lewis, 2005). Evidence for lateral induction was first provided in a study where activated notch-1 (notch-1 intracellular domain: N1-ICD) was ectopically expressed in chick by *in ovo* electroporation. N1-ICD induced ectopic *serrate-1* expression and recapitulated the positive feedback loop resulting in the formation of ectopic sensory epithelia (Daudet and Lewis, 2005).

The next cell fate decision is whether the pro-sensory cells form sensory epithelial cells or neuroblasts. The neuroblasts form in the anterior part of the presumptive sensory region, where they then delaminate, migrate and differentiate to form the neurones of the statioacoustic ganglion (SAG) that innervate the sensory epithelia (fig. 1.2) (Fekete and Campero, 2007). These cells are specified to become neuroblasts instead of sensory cells via notch - delta mediated lateral inhibition (fig. 1.4 B) (Adam et al., 1998; Daudet et al., 2007). This has been demonstrated by experimental inhibition of notch, where anterior cells ordinarily fated to remain epithelial, instead differentiate into neuroblasts and delaminate from the otic tissue (Daudet et al., 2007). *Neurogenin* (*ngn-1*) and *neuroD* are critical for the formation of the neuroblasts. In *ngn-1*$^{-/-}$ mice, the SAG is completely absent along with several other cranial ganglia, and the sensory endorgans are reduced in size (Ma et al., 2000). In *neuroD* $^{-/-}$ mice, the delamination of the neuroblasts is delayed and defective resulting in cell death (Liu et al., 2000). This indicates that that while ngn is required for neuroblast specification, neuroD is required for their differentiation

**Figure 1.4: The role of notch signaling in sensory cell fate specification**

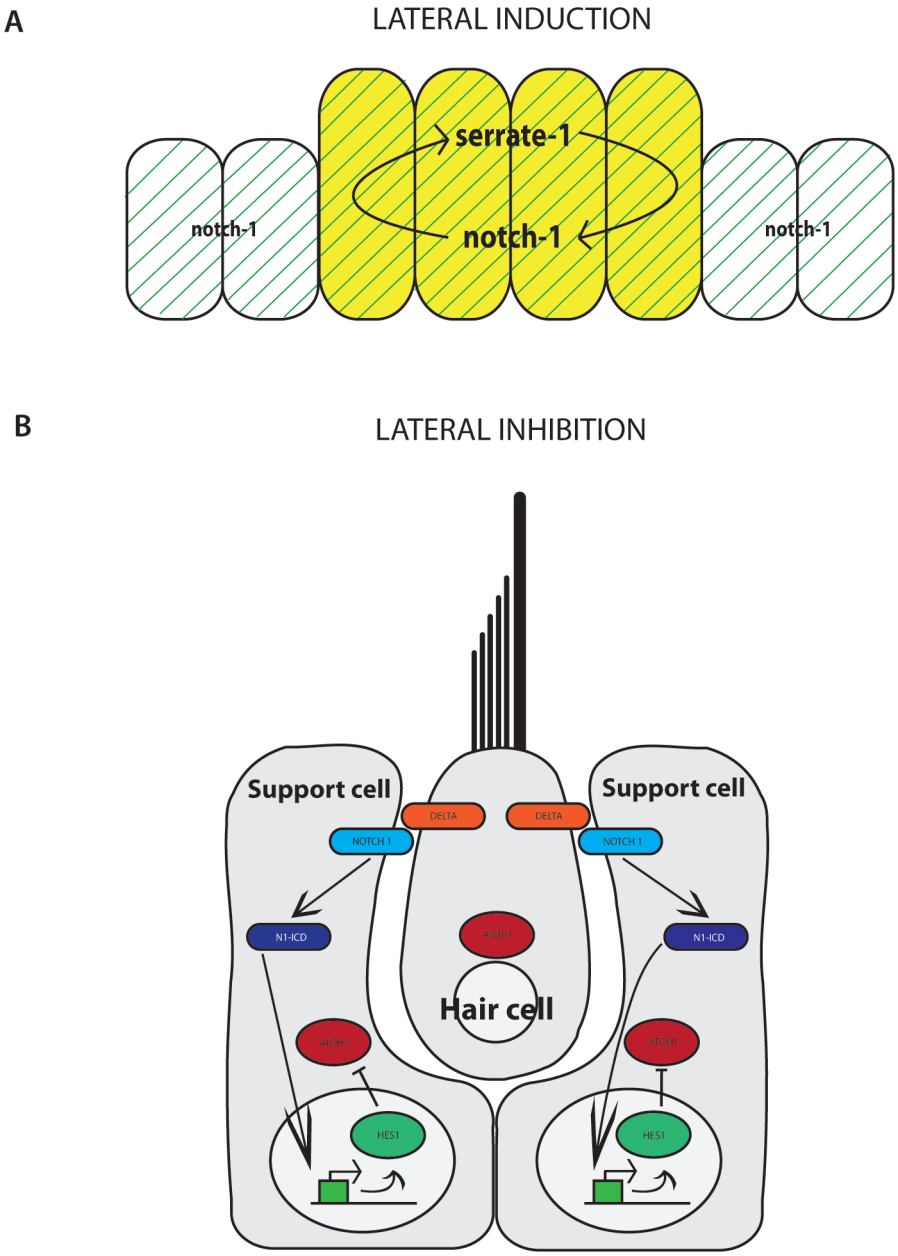


Adapted from Kelley, 2006

**(A)** Serrate-1 expression marks the presumptive sensory epithelium. Where notch-1 and serrate-1 expression domains overlap, they positively upregulate each another and specify the presumptive sensory epithelium region.

**(B)** After the prosensory region has been specified, cells within the region interact by a process of lateral inhibition to determine which cells will differentiate into hair and support cells (see text).

The cells of the sensory epithelia all develop from the cells remaining in the presumptive sensory region. Each sensory epithelium broadly consists of two cell types, hair cells and the support cells. The function of the hair cells is to detect auditory or vestibular stimuli (see introduction section 1.5) while the support cells form a ring around each hair cell and buffer their activity (Morsli et al., 1998; Quick & Serrano, 2005; Wu et al., 1996). The arrangement of hair and support cells is mediated by lateral inhibition using notch-delta signaling (Haddon et al., 1998; Millimaki et al, 2007). The initial sensory region is marked by the expression of *atonal homolog 1* (*atoh1*) which activates notch signaling (Haddon et al., 1998; Millimaki et al., 2007). Delta is stochastically upregulated in some cells and promotes *atoh1* expression resulting in hair cell differentiation. Delta then binds to notch in the neighboring cells, activating it and resulting in upregulation of the inhibitory helix-loop-helix factors, hairy and enhancer of split (HES) 1 and 5. HES 1 and 5 block *atoh1* expression and result in the formation of a support cell (fig.1.4 B) (Fekete and Wu, 2002; Haddon et al., 1998; Millimaki et al., 2007). Observation of the *mind bomb* (*mib*) mutant demonstrates this system, as disruption of delta activity results in overproduction of hair cells at the expense of support cells (Itoh1 et al., 2003).

### *1.4.4 Compartment boundary model*

Positional information is required for the developing sensory epithelia to form in the correct locations in the inner ear. It has been hypothesized that the expression of the transcription factors *lufng*, *pax2* and *fgf3* subdivide the otic vesicle into discrete compartments. *Pax2* and *fgf3* intersect the *lufng* expression domain at the anterior pole of the otic vesicle, along the medial-lateral boundary, creating eight domains (fig. 1.5) (Brigande, et al. 2000; Fekete and Wu, 2002). Each of the sensory epithelia form in only one of these domains, at the boundaries created by the expression of these three transcription factors (fig. 1.5) (Brigande et al., 2000; Fekete and Wu 2002). The model predicts that morphologically elongated sensory epithelia, such as the maculae, will form next to the intersection of two expression domains, while morphologically punctate

**Figure 1.5: The compartment boundary model**

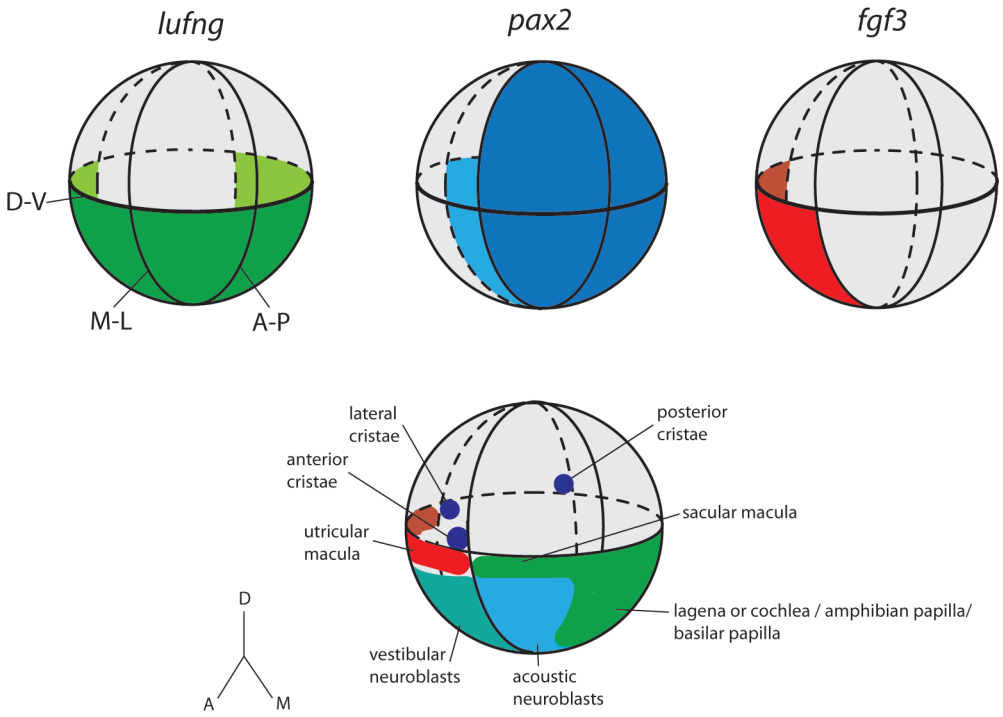


Adapted from Fekete and Wu, 2002

*lufng* is most strongly expressed at the anterior of the otic vesicle and decreases towards the posterior pole. It is one of several factors confering sensory competence to this region, which is subdivided at its anterior pole by the medial expression domain of *pax2* and the antero-ventrolateral expression of *fgf3*. The various sensory epithelia form in close proximity to the boundaries created by these three expression domains, with elongated structures such as the maculae forming at the boundaries of two domains while smaller punctate structures, such as the cristae, form at the intersection of three.

epithelia, such as the cristae, require the intersection of at least three domains to define an exact location (Brigande et al., 2000; Fekete and Wu, 2002).

Evidence for this model is provided by *pax2* null mice, as they fail to form a sacculus, a cochlea, and their innervating neurones, all structures that reside in *pax2* expressing compartments (fig. 1.5) (Burton et al., 2004; Torres et al., 1996). Support is also provided by the observation that in mouse knockouts of *otx1*, a gene expressed in the medioventral compartment (fig. 1.5) (i.e. in the ventral expression in which *lufng* is not expressed), the lateral cristae and semicircular canal fail to form (Acampora et al., 1996). However, Fekete and Wu, 2002 make the point that most of the evidence supporting this model is derived from whole embryo knockouts. As many of these genes, such as *pax2* and *otx1,* are expressed in the hindbrain as well as the otic tissue, it cannot be ruled out that defects in hindbrain signaling may be in part responsible for the observed phenotypes. Therefore, targeted conditional gene knockouts and overexpression studies need to be carried out on the otic tissue to rigorously test this model.

## *1.5 Hair cell structure and function*

### *1.5.1 The structure of the hair cell cilia bundle*

Vertebrate hair cells are polarized epithelial cells characterized by a mechanosensory cilia bundle at their apical pole (Furness et al. 2008; Nayak et al., 2007). The mechanosensory cilia bundle consists of two types of cilia: the stereocilia, which are arranged in two rows in height order; and a single kinocilium located adjacent to the tallest row of stereocilia (fig. 1.6). These cilia are interconnected by different types of filamentous links. Most run parallel to the apical surface of the hair cell, functioning to maintain the integrity of the structure and transmit forces across the cilia bundle (fig. 1.6) (Bashtanov et al., 2004; Goodyear and Richardson 1999). The exception is the tip links that connect the

**Figure 1.6: Hair cell stereocillia bundle**

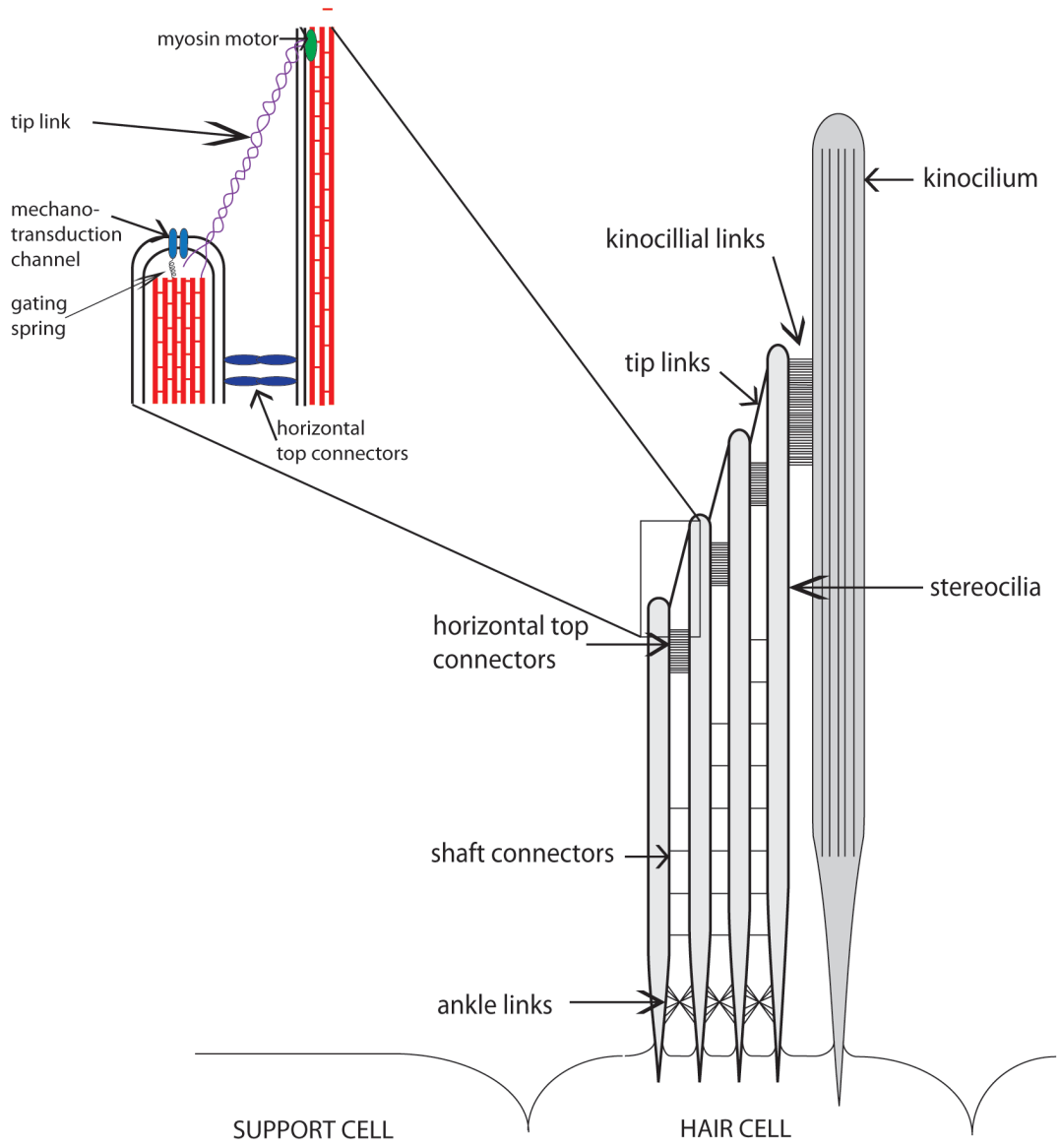


Two rows of stereocilia are arranged in ascending order away from the kinocilium and are held together by filamentous links. Horizontal top connectors, shaft connectors, ankle and kinocilia links all work to maintain integrity and transmit forces across the structure. Tip links connect the tips of the stereocilia and gate mechanotransduction channels when deflected in the excitatory direction.

**Insert**: Stereociliary deflection places stress on the tip links and the gating spring resulting in opening the mechanosensory channel at the tip links lower edge. This results in an influx of $K^{+}$ and $Ca^{2+}$ into the stereocilia, elevating the $Ca^{2+}$ concentration and stimulating neurotransmitter release. The channel is closed by $Ca^{2+}$ binding to the channel and through use of a motor protein at the upper edge of the stereocilia which slips down the actin fibre and releases tension.

tips of different heights of stereocilia to one another and consist of a single strand formed from two helically-intertwined filaments (fig. 1.6) (Bashtanov et al., 2004).

### *1.5.2 Hair cell depolarization*

The tip links function to gate the hair cells' mechanotransduction channels (Pickles et al., 1984; Zhao et al., 1996). When the cilia bundle is deflected, tension is applied to the tip links, which in turn open the attached mechanosensory channel causing an influx of $K^+$ and $Ca^{2+}$ into the hair cell (fig. 1.6) (Corey and Hudseth, 1983). The elevated intracellular concentration of $Ca^{2+}$ stimulates neurotransmitter release at the synapse, generating an action potential in the innervating neuron (Corey and Hudseth, 1983). The channels are subsequently closed by $Ca^{2+}$ binding to the channel, or an element close to the channel, and tension is release by a myosin motor at the top of the tip link slipping down the actin fiber (fig. 1.6).

## *1.6 Development of the otoconia*

Otoconia are dense crystals (0.1-30μm in size) consisting of calcium carbonate with a protein core (fig. 1.7; B). They are anchored to the macula sensory epithelia and function as an inertial mass to increase the sensitivity of the stereocilia to gravity and acceleration (Lim, 1984). In humans ageing, disease and exposure to pharmaceuticals have been shown to degrade the otoconia. In some cases this results in their fragmentation and displacement into the semicircular canals, causing disorders such as Benign Paroxysmal Positional Vertigo (BPPV), the most common form of vertigo (Hughes et al. 2006; Lim 1984; Lundberg et al. 2006).

**(A)** The otoconial complex sits on top of the sensory epithelium, and its function is to transmit mechanical forces to the hair cells that are located below it. The complex is held to the apical surface of the sensory epithelia by a layer of fibrous proteins, such as α and β tectorin, which form rings around the stereocilia of each hair cell. Positioned on top of the fibrous layer is a gelatinous layer, consisting of proteins such as otogelin, in which the otoconial crystals are embedded. Collagen-like proteins such as otolin connect the otoconial crystals to one another and to the gelatinous and fibrous layers.

**(B)** The otoconia consist of a protein core, surrounded by calcium carbonate. The core proteins consist of a dominant otoconin

**Figure 1.7: The Otoconial Complex**

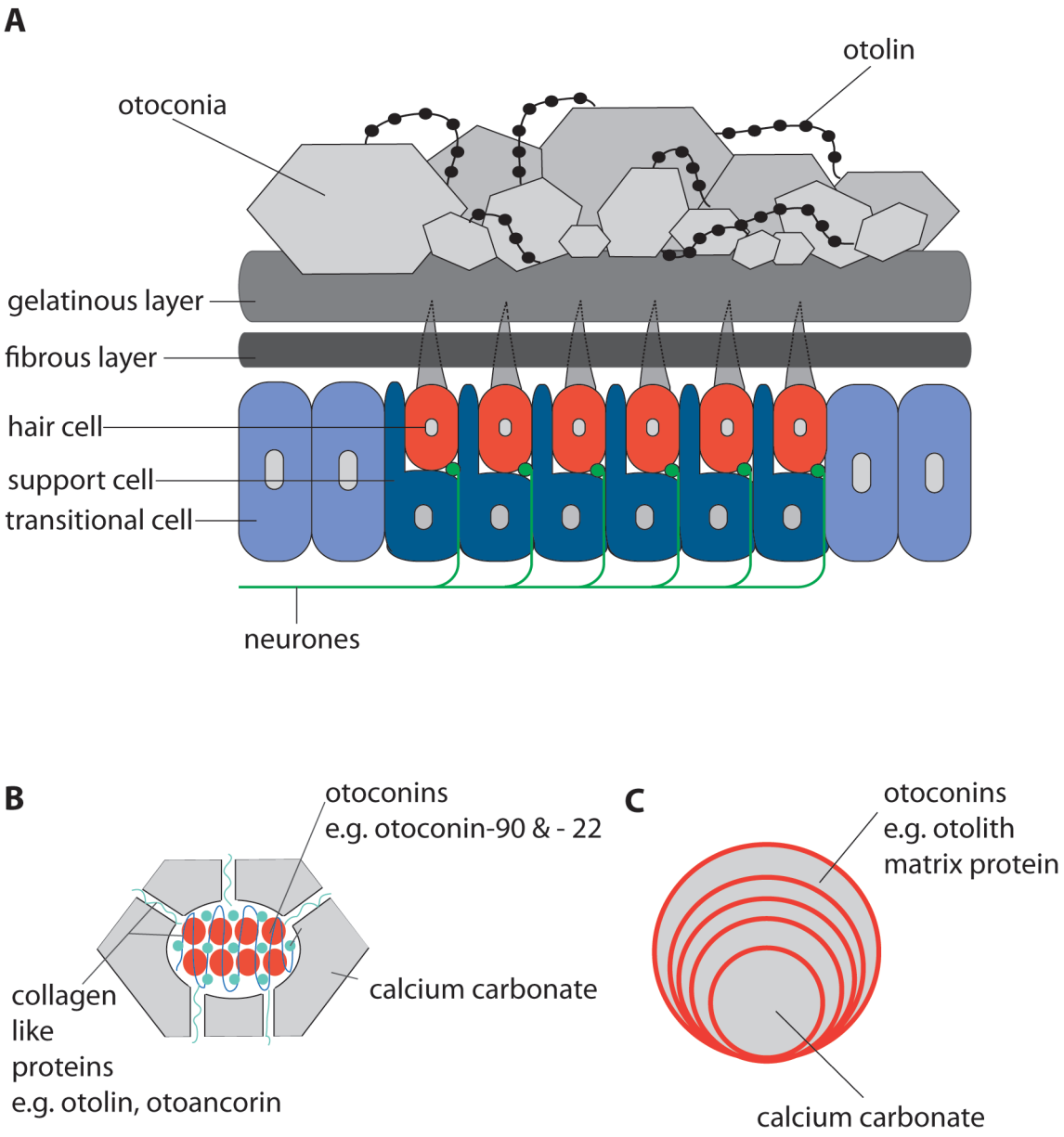

### 1.6.1 The otoconial complex

In mammals, birds and amphibians, otoconial crystals reside in a complex comprising of two layers. The lower layer consists of fibrous proteins, such as α and β tectorin, which surround the hair cell stereocilia, and the upper layer consists of gelatinous proteins, such as otogelin, in which the otoconia are embedded (fig. 1.7 A) (Lim et al., 1984; Lins et al., 2000; Lundberg, et al., 2006). Otoconia only form during embryonic development and so have to be maintained throughout the life of the animal. Teleosts develop a homologous structure to otoconia, known as otoliths. One otolith develops over each macula and they consist of alternating layers of protein and calcium carbonate (fig. 1.7 C) and are also held in place by fibrous and gelatinous layers (Whitfield et al., 2002). Otoliths continue to accrete layers and grow throughout the life of the fish (Whitfield et al., 2002).

### 1.6.2 Otoconial core proteins

Morphology of otoconial crystals differs between species due to the presence of different otoconial core proteins synthesized by the support and transitional cells. The core proteins are collectively known as otoconins, all of which are highly glycosylated and bind $Ca^{2+}$ (Ballarino et al., 1982; Pote et al., 1993; Wang et al., 1998). All otoconins exhibit domains of homology to phospholipase A 2 (PLA2) (Pote and Ross, 1991). The PLA2 domains contain many conserved cysteine residues which are connected by disulphide bonds, allowing otoconins to form rigid protein scaffolds for calcium carbonate to crystallize on (Pote et al., 1993; Wang et al., 1998). Each vertebrate class produces one otoconin in excess of all the others (>90%), and this otoconin affects crystal morphology by influencing which calcium carbonate polymorph is deposited. In amphibians, otoconin-22 (OC22) is the dominant otoconin component in saccular otoconia, directing calcium carbonate to form aragonite and creating orthorhombic crystals (Pote et al., 1993). In amphibian utricular otoconia, otoconin-90 (OC90) predominates resulting in the formation of calcite and creating otoconia with a “rugby football”

shape (Pote and Ross, 1991). In mammals OC90 predominates and so only calcitic otoconia form. In teleosts, otolith matrix protein (OMP) is the dominant protein, causing layers of aragonite to form in the otolith (Murayama et al. 2005; Wang et al. 1998; Yaoi et al. 2003).

Other proteins also play essential roles in the formation and maintenance of the otoconial crystals. Otolin is a collagen-like protein key for both otoconial and otolith formation, distributed throughout the layers of calcium carbonate and maintaining the crystal's structural integrity. In otolin null mice, otoconia are unstable and quickly degrade (Murayama et al., 2005). Also, otogelin and otoancorin are essential to adhere the otoconia to the apical surface of the macula, and when mutated in mice the otoconial complex detaches and moves freely inside the inner ear (Simmler, et al., 2000; Zwaenepoel et al., 2002).

### *1.6.3 The role of ions in otoconial formation*

The endolymphatic fluid fills the lumen of the inner ear, and tight control of its ionic concentration is critical for otoconial crystallization and maintenance. High concentrations of endolymphatic $Ca^{2+}$ are provided by the hair cells, as PMCA2 (plasma-membrane bound calcium-dependent ATPase isoform 2) is enriched in the hair cell bundles and extrudes $Ca^{2+}$. PMCA2 provides $Ca^{2+}$ for otoconial growth, but it also creates a constant stream of $Ca^{2+}$ to maintain crystal structure (Crouch & Schulte, 1996; Kozel et al., 1998). Hair cells also produce carbonic anhydrase, an enzyme required for the production of $H^+$ and $CO_3^-$ (Dou et al., 2004; Shiao et al., 2005). Carbonic anhydride serves a dual function to provide $CO_3^-$ for the formation of calcium carbonate and $H^+$ to keep the pH low so that mineralization does not occur at the base of the hair cells and interfere with their function (Dou et al., 2004; Shiao et al., 2005). The melanophores and dark cells (see 1.2) also express carbonic anhydride and contribute to the endolymphatic $H^+$ and $CO3^-$ (Agrup et al., 1999; Sage et al., 2001; Spicer et al., 1990). Ions are also required as cofactors for enzyme activity. For example $Zn^{2+}$ is an essential cofactor for carbonic anhydrase activity (Erway & Grider, 1984; Erway et al.,

1986) and $Mn^{2+}$ is required for glycoslyating enzymes to modify otoconins (Erway et al., 1986).

### *1.6.4 Model of otoconial biogenesis*

Otoconia biogenesis begins with the formation of protein core particles in the endolymphatic fluid (fig. 1.8 A). This involves the sequestration of $Ca^{2+}$ by the dominant otoconin which in turn recruits other proteins such as otolin (Lundberg et al., 2006; Zhao et al., 2007). The dominant otoconins are expressed throughout the otic vesicle with the major exception of the sensory epithelia (fig. 1.8 A) (Murayama et al., 2004; Wang et al., 1998). $Ca^{2+}$ and $HCO_3^-$ are extruded by the hair cells as well as the dark cells and melanocytes in the roof of the utricular chamber (fig. 1.8 A) (Agrup et al., 1999; Sage et al., 2001; Spicer et al., 1990). These particles then move above the maculae due to endolymphatic flow created by beating cilia (fig. 1.8 B) (Colantonio et al., 2009). It is also likely that the negatively charged protein core particles are attracted to the $H^+$ rich epithelium and that the collagen domain of otolin interacts with integrins on the apical macula surface (fig. 1.8 B) (Lundberg et al., 2006). Calcification of this protein core is rapid and is aided by the extrusion of $Ca^{2+}$ and $HCO_3^-$ from the hair cells and the secretion of minor otoconial proteins from the macula (fig. 1.8 C) (Crouch & Schulte, 1996; Kozel et al., 1998).

## 1.7 *Thesis aims*

The purpose of this thesis was to identify gene functions important for inner ear development through the use of forward genetics in *Xenopus tropicalis*. This was achieved by screening for mutant phenotypes in the progeny of a population of ethylnitrosourea (ENU) mutagenized *X. tropicalis*. This uncovered seven distinct phenotypes that displayed a primary defect in inner ear development, four of which were proven to have a genetic basis. The primary cause of these defects was investigated by examining the phenotype of these mutants through the use

**(A)** $Ca^{2+}$ and $CO_3^-$ are released by the hair cells and the dark cells in the roof of the utricular chamber. They bind to the dominant otoconin which is synthesised and extruded by all cells in the otic tissue with the major exception of the macula cells. The dominant otoconin then recruits other minor otoconins to form proteinaceous core particles.

**(B)** These particles then move towards the macula due to endolymphatic flow created by beating cilia. Also the negatively charged particles are attracted to the $H^+$ rich macula.

**(C)** Calcification of the proteinaceous core particles is rapid and is aided through the extrusion of $Ca^{2+}$ and $HCO_3^-$ from the hair cells and the secretion of other otoco ins from the macula cells. Otogelin and otoancorin work to adhere the otoconial complex to the apical surface of the macula.

**Figure 1.8: Otoconial mineralization model**

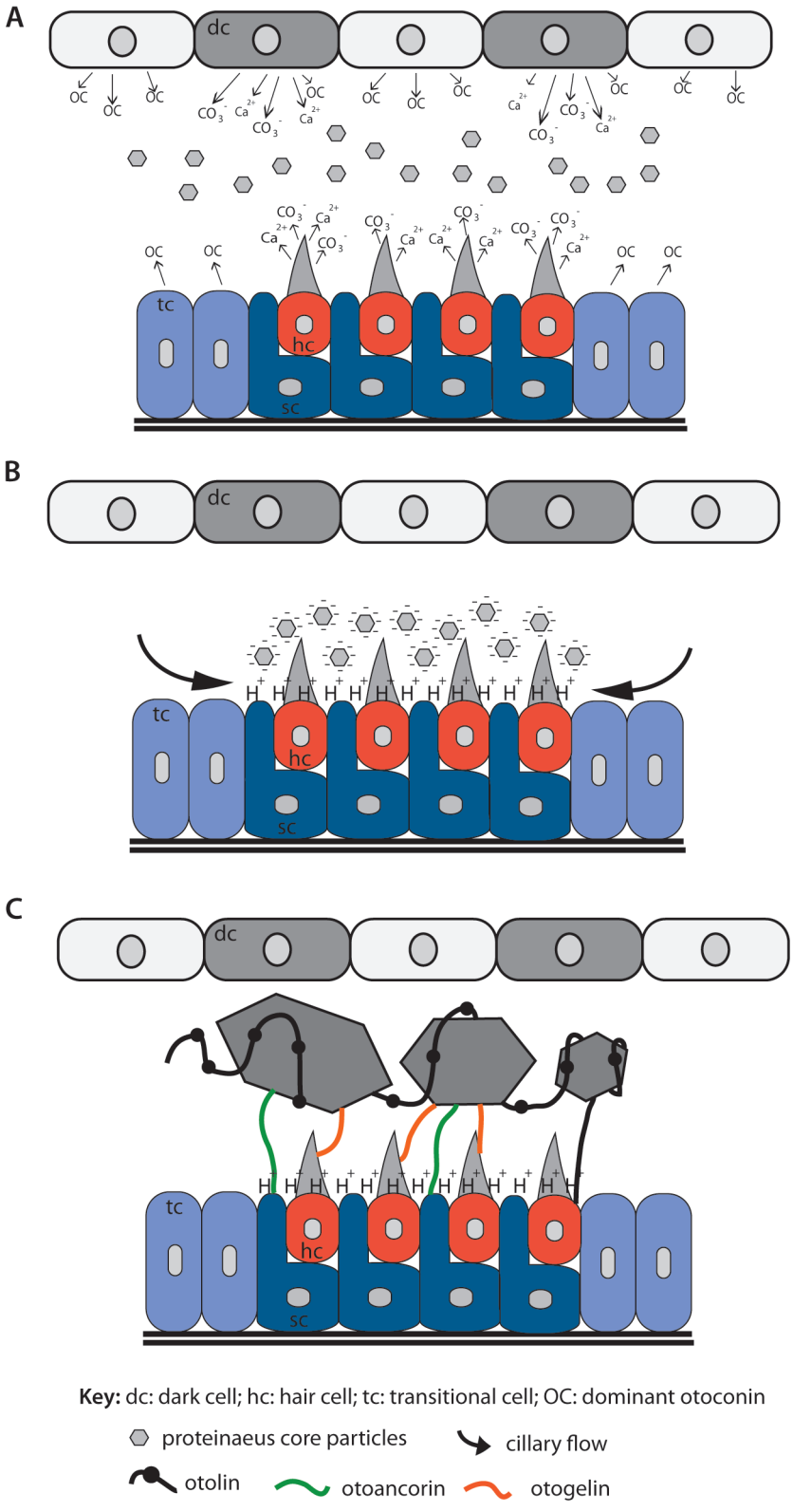

of immunostaining, *in situ* hybridization and histological techniques. This was carried out in tandem with positional cloning to identify the genetic lesion underlying the phenotype. Focus was placed on the *seasick* (*ssk*) and *komimi* (*kom*) mutants that were both originally identified due to otoconial and vestibular behavioral defects.

# Chapter 2

# Materials and Methods

## *2.1 Animal Procedures*

Reagents:

| | | |
|---|---|---|
| MMR (x1) pH 7.7-7.8 | 0.1M | NaCl (Sigma) |
| | 2mM | KCl (Sigma) |
| | 1mM | $MgCl_2$ (Sigma) |
| | 2mM | $CaCl_2$ (Sigma) |
| | 5mM | HEPES (Sigma) |

### *2.1.1 Natural Mating*

Female and male animals received a priming injection of 10 units of gonadotropin hormone (hCG) 1-3 days prior to mating, they were then boosted on the day of the experiment with 100 units hCG and left in a dark place to mate for several hours. Eggs were removed from the tank and treated with 2.2% cysteine (Sigma) in 0.05 x MMR (pH7.7 – 7.8) for 8 minutes at room temperature to remove the jelly coat that surrounds the embryos. The embryos were then rinsed three times with 0.05 x MMR to remove any remaining cysteine and sorted into groups of 300 cleaving embryos per 150mm Petri dish (coated with 0.1% bovine serum albumin (BSA; Sigma) in 0.05 x MMR) in 0.05 x MMR + gentamicin (50μg/ml; Gibco, Invitrogen). Embryos were raised to the desired stage in a 25°C incubator before being harvested.

### *2.1.2 in vitro Fertilization*

Males were schedule 1 killed (S1K) by overanaesthethesia in 0.4% MS222 (Sigma) for 20 minutes followed by decapitation. Testes were removed and placed in a 1.5ml Eppendorf tube containing 0.5 x L15 (Gibco, Invitrogen) + 10% foetal calf serum (FCS) (Gibco, Invitrogen). An Eppendorf pestle was then used to dissociate the tissue and release sperm.

Female frogs received a priming injection of 10 units of hCG 1-3 days prior to laying, and were then boosted 5 hours prior to laying with 100 units hCG. Eggs were manually expressed into a Petri dish containing a drop of 1 x MMR solution

and the sperm solution was placed on top of the eggs and left for 5 minutes at room temperature before flooding with 0.05 x MMR. The embryos were left to develop for 20 minutes before being treated with cysteine as in section 2.1.1 .

### *2.1.3 Gynogenesis*

Females were treated as in 2.1.2 except that prior to addition of sperm, eggs were divided among three Petri dishes for the creation of haploid, gynogenetic and diploid control embryos. Haploid and gynogenetic embryos were obtained by fertilizing eggs with UV-irradiated sperm (50,000 micro joules UV irradiation produced by a Stratalinker (Stratagene); diploid control embryos were fertilized with non-UV treated sperm from the same set of testis. Eggs were incubated with sperm for 5 minutes, then flooded with 0.05 x MMR to activate development. To obtain gynogenetic diploids, a set of haploid embryos was subjected to early cold shock 5 minutes after flooding by placing them in ice cold 0.05 x MMR and incubating them on ice for 7 minutes 30 seconds to block polar body formation. Eggs were then removed from ice and the media replaced with room temperature 0.05 x MMR. The embryos were left to develop for 20 minutes before treating with cysteine as in section 2.1.1 .

### *2.1.4 Raising embryos to adulthood*

Embryos were raised at 25°C in 0.05 x MMR + gentamicin (50μg/ml; Gibco, Invitrogen) for three days post fertilization before being placed at room temperature and transferred into microfiltered water with sea salt added to give a conductivity of ~1000μS. Tadpoles were then fed five times daily with Sera micron (Sera) until approximately four weeks post fertilization, when their diet also includes crushed fish flake (Sera). Once the animals have reached froglet stages they are fed daily on a diet of fish flake and Tetra ReptoMin through to adulthood.

## 2.2 Positional Cloning

### 2.2.1 Genetic Strains

Mutant lesions were induced on an outbred N-strain (Nigerian) background. Polymorphic individuals, for the purpose of positional cloning, were obtained by crossing N-strain carriers crossed to IC-strain (Ivory Coast) wild type individuals.

### 2.2.2 DNA preparation

Reagents:

| | | |
|---|---|---|
| DNA extraction buffer | 50mM<br>1mM<br>0.5% | Tris pH8.8 (Sigma)<br>EDTA (Sigma)<br>Tween (Sigma) |

Genomic DNA was extracted from wild type and mutant tadpoles by placing individual embryos into separate wells of 96 well plates, dry freezing overnight at –80°C, then lysing in 100μl/well DNA extraction buffer plus 100μg/ml proteinase K (Roche) and incubating at 56°C for 90 minutes. Proteinase K was subsequently denatured by heating to 95 °C for 15 minutes.

### 2.2.3 Simple Sequence Length Polymorphisms (SSLP) markers

SSLP markers were obtained from the meiotic map constructed by Amy Sater (University of Houston) and can be accessed on the tropmap database (http://tropmap.biology.uh.edu/credits.html) (Wells, D et al., 2010). Alternatively, bespoke candidate polymorphic markers were identified using Tandem Repeat Finder (http://tandem.bu.edu/trf) (Benson, G., 1999) to find tri- or tetranucleotide repeats in genomic sequence obtained from ensembl (http://www.ensembl.org/index.html). Primers were subsequently designed using Primer3 (http://primer3.sourceforge.net/). The sequences and location of the markers in the version 4 genome assembly are provided in appendix A.

### *2.2.4 PCR Conditions*

Reagents:

| | | |
|---|---|---|
| PCR Reaction Mix | 1ng/μl<br>1μM<br>0.2mM<br>x1<br>0.067 units/μl | Genomic DNA<br>Forward/Reverse primer mix (Sigma)<br>dNTP's (TaKaRa)<br>Taq Buffer (N E Biolabs)<br>Taq (N E Biolabs)<br>DNAse free/RNAse free water (Sigma) |

DNA was denatured at 94°C for 4 minutes, and reagents cycled 35 times to 94°C for 30 seconds, 58°C for 30 seconds and 72°C for 1 minute to allow for denaturing, annealing and elongation steps, respectively, with a final elongation of 72°C for 5 minutes.

### *2.2.5 Polyacrylamide Gel Electrophoresis and Silver Staining*

Reagents:

| | | |
|---|---|---|
| TBE | 89mM<br>2mM | Tris borate (Sigma)<br>EDTA pH 8.0 (Sigma) |
| Denaturing Loading Buffer | 3.7%<br>10mM<br>0.2%<br>0.2% | Formaldhyde (Sigma)<br>EDTA (Sigma)<br>Bromophenol blue (BDH Chemicals)<br>Xylene cyanol (BDH Chemicals) |
| Polyacrylamide Gel | 6%<br>8M<br>2x<br>0.1%<br>0.01% | Acrylamide (Biorad)<br>Urea (Sigma)<br>TBE<br>Temed (Sigma)<br>APS (Sigma)<br>MilliQ water |
| Silver stain solution | 12mM | Silver nitrate |
| Developing Solution | 0.3M<br>0.006% | $Na_2CO_3$ (Sigma)<br>Formaldehyde (Sigma)<br>MilliQ water |

Polyacrylamide gels (39cm x 33cm; 75 wells) were pre-run in 1 x TBE at 60V for 20 minutes. Sample and denaturing loading buffer were mixed in a 1:1 ratio and denatured at 95 °C for 3 minutes prior to loading and running at 55V for 2 hours 30 minutes. Gels were developed by fixing in 10% ethanol for 10 minutes and in 2% nitric acid for 3 minutes prior to staining in silver nitrate for 20 minutes and developing in sodium hydroxide.

## *2.3 Sequencing*

Total RNA was extracted using Trizol (Invitrogen), DNAse I (Promega) treated and subsequently used to synthesize cDNA using the Enhanced Avian HS RT-PCR kit (Sigma HSRT-100) following manufacturer's instructions. *ap3δ1* cDNA was amplified (as in section 2.2.4) in four overlapping segments using the primers in table 2.1, while oc90 was sequenced by amplifying two sets of overlapping segments, both were sent to Beckman Lmt. for sequencing. Once received sequences were aligned using SeqMan and traces examined using 4Peaks.

Table 2.1: PCR primer sequences used to amplify *ap3δ1* for sequencing

| | **Forward Primer** | **Reverse Primer** | **Product Size** | **Region of cDNA Amplified** |
|---|---|---|---|---|
| *ap3δ1* - 1 | TCTCAGTGGGAGGAGAGCAT | AGTTGTTGGTGGACGAGGTC | 806 | 7 - 812 |
| *ap3δ1* - 2 | AGAATCACTGCGTCCTGCTT | TGCAGATGTCAATAATTTTGGTG | 680 | 640 - 1319 |
| *ap3δ1* - 3 | CGGAATGGTATCCAAGAAAAA | GCACAAACTGGGGCAGTC | 590 | 1201 - 1790 |
| *ap3δ1* - 4 | TTAAGGCCAAAGGTCACCAC | CTGCTTGCTCCTACGTTCCT | 687 | 1625 - 2311 |
| *oc90 – A* | AAATAGCTGTGCGCTGGGTGG | TCTCTAAGCCGTGACGACGAAAGTG | 910 | -28 - 943 |
| *oc90 - B* | GTACGGAACTTGGCACT | CGGAGGAACGGACCGCTCGC | 800 | 882 - 1647 |

## *2.4 Microinjection*

Morpholinos targeted against the *X. tropicalis ap3δ1* mRNA transcript were designed by and purchased from Gene Tools LLC. One was targeted against the transcriptional start site, a second was targeted to block a splicing donor of exon 10 and the third was designed to act as a control (table 2.2). A total of 10ng of morpholino was injected into 2-cell wild type embryos (5ng into each cell). Unilateral controls were also produced by injecting only one cell of 2-cell wild type embryos with 5ng of morpholino.

Prior to injecting, morpholinos were mixed with rhodamine dextran (5µg/µl) and denatured at 65°C for 3 minutes. All injections were carried out with needles

(Harvard Apparatus) pulled to a diameter of 0.58mm. Wild type embryos were produced by in *vitro* fertilization (see 2.1.2) and were submerged in 0.05 x MMR + 3% ficoll during and for 2 hours post injection.

The efficiency of the *ap3δ1* exon 10 splice blocking morpholino was tested by designing PCR primers to flank the exon (table 2.3).

Table 2.2: Morpholino sequences

| | |
|---|---|
| *ap3d1* translation blocking morpholino (5'-3') | CGGAGCGCCATACGGACGCACAAAA |
| *ap3d1* 10$^{th}$ exon splice blocking morpholino (5'–3') | ACAAGAAATACAAGAGATACCTGTA |
| control morpholino (5'-3') | CCTCTTACCTCAGTTACAATTTATA |

Table 2.3: Primer sequences flanking exon10

| | **Forward Primer** | **Reverse Primer** | **Wild Type Product Size** | **Morphant Product Size** |
|---|---|---|---|---|
| *ap3d1*exon 10 - 11 junction | GTGCACTTACCCCTTTGGAG | CATTCAAAGTTGGTGATATA TTGG | 514 | 618 |

## *2.5 RT-PCR*

Total RNA was extracted using Trizol (Invitrogen), DNAse I treated (Promega) and subsequently used to synthesize cDNA using Enhanced Avian HS RT-PCR kit (Sigma HSRT-100) following manufactures instructions. Transcripts of interest were amplified from the 3' end of the cDNA (table 2.4) for 26, 27, 28 and 29 cycles using the reaction conditions described in section 2.2.4. DNA products were resolved on 1% agarose.

Table 2.4: PCR primer sequences used for RT-PCR:

| | **Forward Primer** | **Reverse Primer** | **Product Size (bp)** | **Region of cDNA Amplified** | **Total Length of cDNA** |
|---|---|---|---|---|---|
| *ap3δ1* | TTAAGGCCAAAGGTCACCAC | CTGCTTGCTCCTACGTTCCT | 687 | 1625-2311 | |
| *ap3β1* | CCAGAGAAAGGGTTTGTTCG | CCGTAATCTTGTCGAAGAGC | 389 | 1125-1513 | 1515 |
| *ap3μ1* | TGCAGATGAGATGAGAGAGA GTG | TTCAATGTTCACACATTTTACAGA | 389 | 1452-1840 | 1842 |
| *ap1γ1* | TTAGATTTGTTGGGCGGAAA | GCAGCTGGAATGTCTTTGGT | 376 | 2102-2477 | 2577 |
| *ap2α1* | GCACAGGTACAGCAGGTGGT | TCTCAATGTAAGCTTGGACAAGAG | 486 | | |
| *ap4ε1* | CAGTGTCTGGCTGCATCAGT | CAGTCAAGCAACGTGGAAGA | 364 | | |

## *2.6 Gene Expression Patterns*

### *2.6.1 Embryo fixation*

Reagents:

| | | |
|---|---|---|
| MEMFA pH7.4 | 10mM<br>0.2mM<br>0.1mM<br>0.37% | MOPS<br>EDTA<br>$MgSO_4$<br>formaldehyde |

Staged embryos were fixed at room temperature for 1 hour in MEMFA and then washed and stored in 100% methanol.

### *2.6.2 Synthesis of DIG-labeled antisense oligonucleotide probes*

Reagents:

| | | |
|---|---|---|
| Probe synthesis mix | 1x<br>20% (v/v)<br>10% (v/v)<br>10% (v/v)<br>20% (v/v) | DIG labeled NTPs<br>DTT<br>RNasin<br>RNA Polymerase (T7 or SP6)<br>MilliQ water |

Antisense digoxigenin labeled oligonucleotide probes were synthesized from ESTs obtained from Geneservice (table 2.6). Restriction enzymes and polymerases used to linearize and synthesize RNA, respectively, are provided in table 2.6. Probe synthesis mix was placed at 37 °C for 3 hours, treated with

DNAse I at 37 °C for 30 minutes and then purified using Amersham Micro Spin S-400 HR columns, following manufactures instructions.

Table 2.6: ESTs

| Gene | NCBI ID | Vector | Restriction Enzyme | RNA polymerase | Probe size |
|---|---|---|---|---|---|
| *lunfg* | TGas122a06 | pCS107 | EcoR1 | T7 | 400 |
| *bmp4* | TNeu015d14 | pCS107 | Xma1 | T7 | 694 |
| *slug* | TNeu122h01 | pCS107 | EcoR1 | T7 | 817 |
| *dct* | TTpA009b19 | pCS107 | EcoR1 | T7 | 638 |
| *ap3δ1* | TGas106a12 | pCS107 | EcoR1 | T7 | 494 |
| *ap1γ* | TGas046e03 | pCS107 | EcoR1 | T7 | 664 |

### *2.6.3 Whole Mount in situ Hybridization*

Reagents:

| | | |
|---|---|---|
| Maleic Acid Buffer pH7.5 | 500mM<br>750mM | Maleic acid<br>NaCl |
| Triethanol Amine pH7.5 | 100mM<br>2% | Triethanol amine<br>Glacial acetic acid |
| SSC | 150mM<br>15mM | sodium chloride<br>trisodium cirtrate |
| Denhardts | 2%<br>2%<br>2% | Nuclease-free BSA<br>Ficoll<br>PVP-40 |
| BMB Blocking reagent | 2% | BMB blocking reagent (Boehringer-Mannheim) (in MAB) |
| Hybridisation Buffer | 100μg/ml<br>1x<br>5x<br>0.1% (w/v)<br>500mM<br>5mM<br>1mg/ml | Heparin<br>Denharts solution<br>SSC<br>Tween 20<br>EDTA<br>Formamide<br>Yeast RNA |
| Alkaline Phosphatase buffer | 100mM<br>100mM<br>50mM<br>0.1%<br>5mM | Tris-HCl<br>NaCl<br>$MgCl_2$<br>Tween 20<br>levaminsole |
| Bleaching Solution | 0.5%<br>0.5x<br>5mM | Formaldehyde<br>SSC<br>$H_2O_2$ |

Embryos were processed for *in situ* hybridization as described in (Sive 2000). For fluorescent *in situ* hybridization, samples were incubated with HRP-coupled anti-fluorescein antibody (1:1000 dilution) (Roche) and developed using a TSA Plus Cyanine 3 system kit (PerkinElmer, Inc.), following manufacturers'

instructions. Embryos were bleached for 30 minutes, viewed under a Leica Axiophot microscope and imaged using AcQuia software. Contrast and brightness of images were processed using Adobe Photoshop.

### *2.7 Immunofluorescence*

*X. tropicalis* embryos were fixed in 4% PFA, decalcified by overnight incubation in 15mM EDTA and permeabilized by 1 hour incubation in 5% Triton X-100 (in 4% PFA) all at room temperature. Samples were blocked with 1% BSA in TBST (TBSBT), incubated at 4°C overnight with a primary antibody in 10% lamb serum (in TBSBT), washed with TBSBT and incubated at 4°C overnight with the appropriate secondary antibody.

To detect hair cell bodies, donkey polyclonal anti-S-100 was used with an Alexafluor 556 conjugated secondary antibody. Neurones innervating sensory endorgans and the neuromasts of the lateral line were detected using monoclonal mouse anti-acetylated tubulin antibody and an Alexafluor 488 conjugated secondary. All samples were also incubated with dapi to stain the nuclei. Samples were mounted in Flow Fade / Anti Fade solution.

Table 2.7: Antibodies

| **Primary Antibody** | **Dilution** | **Secondary Antibody** | **Dilution** |
|---|---|---|---|
| Polyclonal rabbit anti-S-100 (Ref: Z0311 DAKO) | 1:500 | Anti-rabbit Alexa 556 (Ref: A21428 Molecular Probes) | 1:1000 |
| Polyclonal mouse anti-acetylated tubulin (Ref: T7451 Sigma) | 1:500 | Anti-mouse Alexa 488 (Ref:A21942 Molecular Probes) | 1:1000 |

Staining of actin in hair cell stereocilia and in cell membranes was obtained by overnight incubation with Alexafluor 488 conjugated phalloidin. Phalloidin-stained samples were cleared by successive 30 minute incubations with 25%, 50% and 75% glycerol (*aq*) and the epithelium covering the otic vesicle removed using tungsten needles. Samples were mounted in 75% glycerol.

Table 2.8: Fluorescent-tagged probes

| Probe | Dilution |
|---|---|
| phalloidin | 1:50 |
| dapi | 1:1000 |

Immunofluorescence was detected using scanning laser confocal microscopy (Zeiss). Data were processed using Volocity (Perkin Elmer Company).

### *2.8 fm1-43 staining*

Tadpoles were anaesthethesia in 0.4% MS222 (in 0.05 x MMR) and placed in 20μM fm1-43 (in 0.05 x MMR) for 5 minutes before rinsing in 0.05 x MMR and imaging under fluorescence using a Leica axiophot microscope.

### *2.9 Sectioning*

Embryos were fixed in Bouin's overnight at 4 °C and dehydrated by successive 15 minute washes with 25%, 50% and 70% ethanol (aq). Yellow staining from the Bouin's solution was then removed by washing with 1% NH4 in 70% ethanol for 2 hours. Further dehydration was then carried out by washing with 80%, 90% and 95% ethanol (aq).

For embedding in JB4 (Polysciences, Inc.), embryos were incubated in 95% ethanol and JB4 embedding solution A in a ratio of 1:1 overnight at 4 °C followed by another overnight incubation in solution A plus a catalyst (12.5mg/ml). Finally,

embryos were embedded in solution A plus catalyst and embedding solution B in a ratio of 25:1.

For sectioning otoconia, specimens were embedded in Technovit (Kutzer) to maintain the otoconial crystal structure, however JB4 was favoured for all other experiments due to decreased levels of sample shrinkage. The same protocol for embedding in JB4 was used for embedding in Technovit.

Wild type and mutant sections were cut into 10μm transverse sections using a Leica RM 2165 microtome, mounted onto glass slides (ThermoScientific) and stained with hematoxylin and eosin (Sigma). Sections were imaged using a Zeiss axiophot microscope and Openlab 4.0.2 software.

# Chapter 3

## A forward genetic screen of chemically induced mutations uncovers mutations affecting inner ear development in *Xenopus tropicalis*

## 3.1 Introduction

*Xenopus tropicalis* is gaining popularity as a genetic model organism. Its small genome ($1.5x10^9$bp) (Hellsten et al., 2010), production of large quantities of externally developing embryos, and short generation time make it amenable to genetic studies (Amaya et al., 1998; Goda et al., 2006; Noramly et al., 2005; Khokha et al., 2009; Wells et al., 2011). Techniques such as ablations, grafts and explants, which are well established in *Xenopus laevis*, can easily be adapted for use in *X. tropicalis* (see introduction section 1.1) (Hirsh et al., 2002; Offield et al., 2000). Prior to my arrival in the Zimmerman laboratory, a pilot forward genetic screen for chemically induced mutations in *X. tropicalis* was carried out with the aim of uncovering novel gene functions and exploiting these attractive embryological and genetic traits to study them (Goda et al., 2006). Phenotypes were scored at post-neurulation stages to avoid background noise associated with nonspecific gastrulation defects (Goda et al., 2006). The screen was broad in scope and deficits affecting the development of tissues and organs such as the muscle, heart, eye, and ear along with defects in axial patterning were detected (http://www.nimr.mrc.ac.uk/research/lyle-zimmerman/enu-phenotype-database).
This thesis focuses on characterization of mutations showing a primary defect in the development of the inner ear and identification of the underlying genetic lesions by positional cloning.

### 3.1.1 Mutagenesis strategy

To create the F1 mutagenised population, *in vitro* chemical (N-ethyl-N-nitrosourea; ENU) mutagenesis of mature *X. tropicalis* sperm was carried out, followed by *in vitro* fertilization of wild type eggs (fig 3.1) (Goda et al., 2006). In order to obtain a high mutation rate in the pilot screen, post-meiotic sperm were mutagenized, meaning only one strand of the paternal DNA carried a given mutation, creating an F1 population of mosaic individuals (Goda et al., 2006). The strand containing the lesion was then distributed to one of two cells at first cleavage, resulting in a maximum 50% mosaic heterozygous embryo, such that

**Figure 3.1: Mutagenesis strategy**

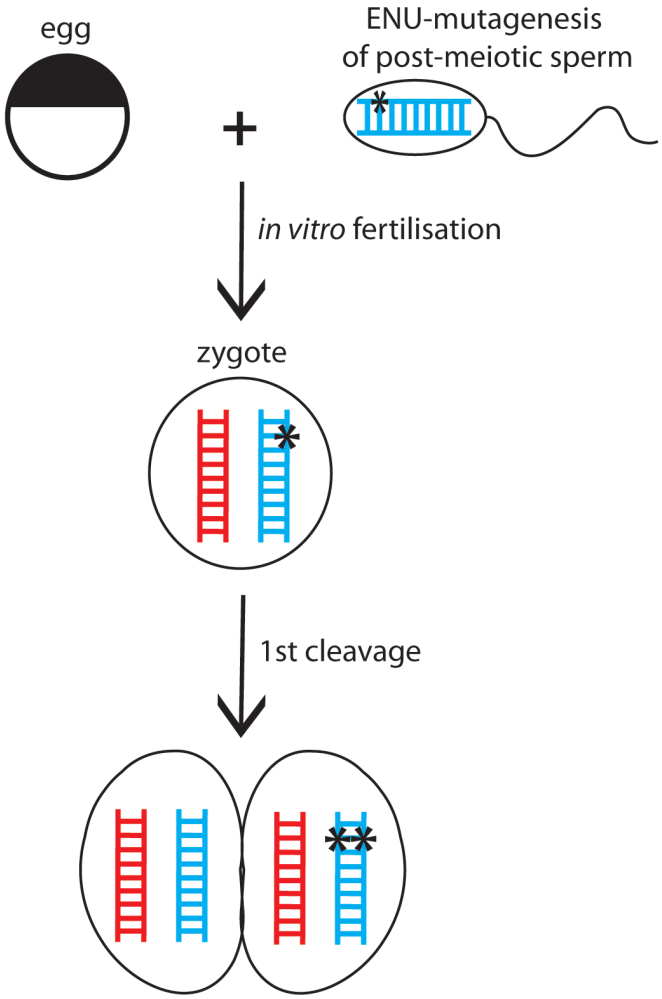


*In vitro* ENU-mutagenesis of post-meiotic sperm results in one strand of paternal DNA carrying the mutated lesion. The mutated sperm is used to *in vitro* fertilize a wild type egg to produce a zygote that is hemi-heterozygous for the mutated lesion. At the first cell division one cell does not inherit the lesion while the other becomes heterozygous.

as much as of 25% of germ cells might carry a specific lesion (fig. 3.1). Since many ENU lesions are not repaired for several cell divisions (Ikegami et al., 1999), some mutants may have been even more mosaic in founder germlines.

### *3.1.2 Screen strategy*

The F1 pioneer generation was raised to sexual maturity and gynogenetic offspring of adult females were screened for recessive mutant phenotypes to identify carriers (see methods section 2.1.3, fig. 3.2 A). Females that produced the same candidate mutant phenotype in successive rounds of gynogenesis were outcrossed (fig. 3.2 B - C), their progeny raised to maturity, and the resulting F2 females screened by gynogenesis to identify heritable defects (fig. 3.2 D). Female F2 carriers were then crossed with male siblings and their progeny scored for Mendelian ratios of specific phenotypes (fig. 3.2 E), to identify male carriers (Goda et al., 2006).

The inner ear phenotypes were identified on a morphological basis, with the major anatomical features screened for being: size and shape of the otic vesicle, size and number of maculae (sensory epithelia associated with otoconia i.e. utricle and saccule, see Introduction 1.6.1), and size and morphology of the otoconial crystals. Balance defects such as circular swimming and difficultly orientating were also screened for (Goda et al., 2006). The otic vesicle and otoconia are large and visible externally from the embryo throughout stages 37 to 45. Structures that can only be visualized using molecular probes, such as the maculae, cristae and endolymphatic tissue, were not directly screened. However, malformations in development of otoconia can sometimes be attributed to broader defects in inner ear development, as many different cell types and gene functions are required to synthesize the components of the crystals and control the ionic environment required for their growth (see Introduction 1.5) (Goda et al., 2006).

**(A)** The progeny were raised to produce a F1 mosaic founder population.

**(B)** F1 females were used to generate gynogenetic embryos which were screened for embryonic defects. If a phenotype was identified, the F1 was rescreened to determine whether the phenotype could be reproduced.

**(C)** F1 females carrying defects were outcrossed using wild type males.

**(D)** Potential F2 female carriers were screened by the production and inspection of gynogenetic tadpoles, while males were screened by mating to a known female carrier and inspecting the offspring. Heritability of a defect confirms an underlying genetic cause.

**(E)** Mutant embryos can then be produced by mating known carriers.

**Figure 3.2:** Screening strategy

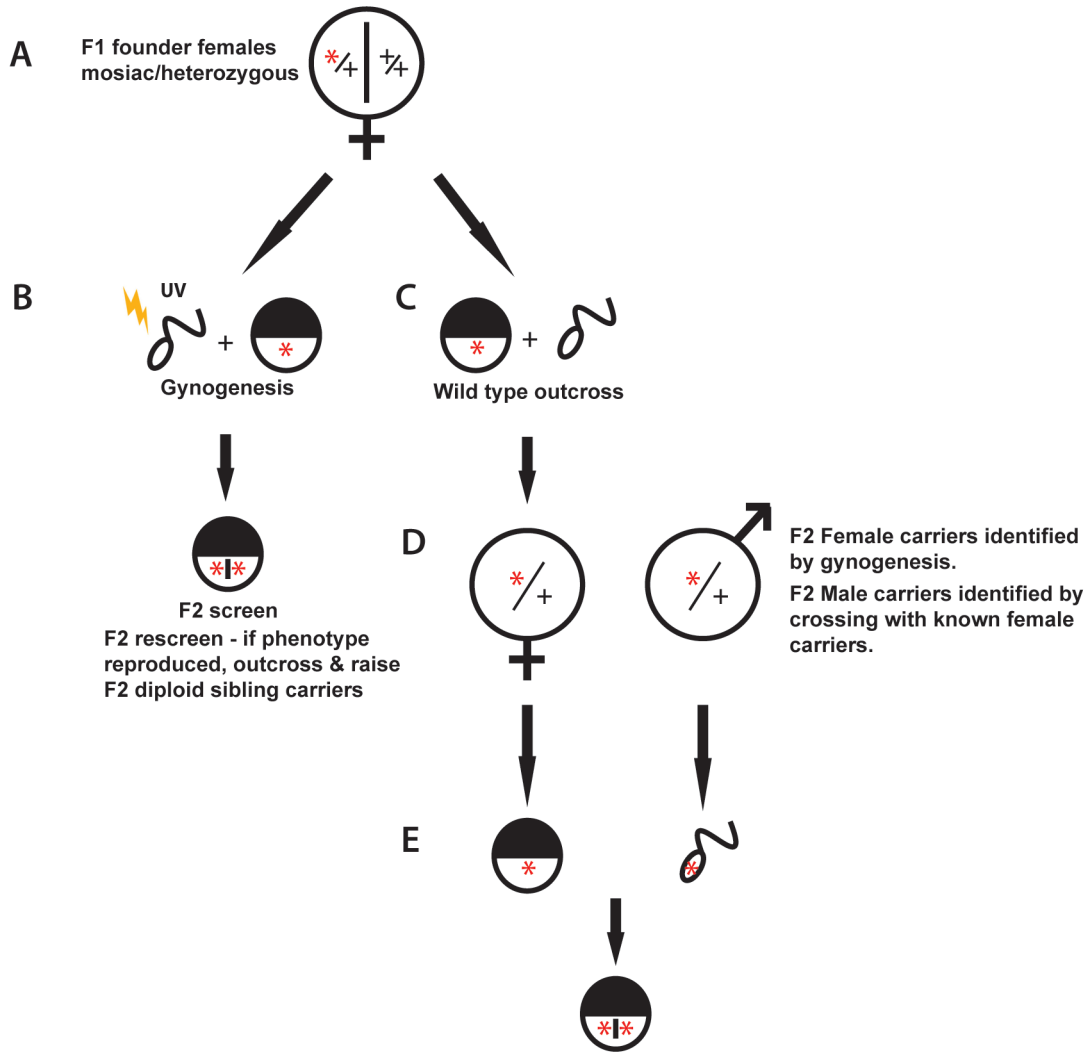


Adapted from Goda et al., 2006

### *3.1.3 Seven candidate inner ear phenotypes were identified in gynogenetic offspring of the F1 generation*

A screen of gynogenetic progeny of the F1 mutagenized population revealed seven candidate mutant phenotype displaying a primary defect in the development of the otic vesicle and/or otoconia. These phenotypes fall broadly into two categories. The first are those that display defects in otic vesicle size such as *dumbo* (*dum*) (fig. 3.3 B) and *bunny* (*bun*) (fig. 3.3 C), which show enlarged and small otic vesicles, respectively. The second group exhibits otoconial defects, such as the large otoconia observed in *seasick* (*ssk*) (fig. 3.3 D) and *legolas* (*leg*) (fig. 3.3 E), the abnormal crystal structure displayed in *komimi* (*kom*) (fig. 3.3 F), the detachment of otoconia from the maculae observed in *carsick* (*csk*) (fig. 3.3 G), and the reduction in size of the utricular otoconial patch seen in *airsick* (*ask*) (fig. 3.3 H). As otic vesicle and otoconial development depend on many biological processes, it is likely that some of these mutants will exhibit broader developmental defects.

### *3.1.4 Strategy for characterizing mutant phenotypes and positional cloning*

The focus of this chapter is to determine the primary inner ear defect and to locate the approximate genomic position of the mutant locus. Based on these data, two mutants will be selected and mapped at high resolution to identify the underlying genetic lesion.

#### *3.1.4.1 Strategy for phenotypic characterization*

To describe the primary inner ear defect in each mutant, I will use histological techniques and molecular probes to visualize the gross structure of the inner ear and specific cell types within it. All characterization is initially carried out on stage 45 tadpoles, as many of the structures of the inner ear such as the utricle, sacculus and endolymphatic tissue can be identified morphologically. The sensory epithelia of the maculae and cristae, the endolymphatic tissue, and the semicircular canals can all be easily identified in histological preparations (Bever

**Figure 3.3: Inner ear phenotypes identified in the mutated F1 *X. tropicalis* population**

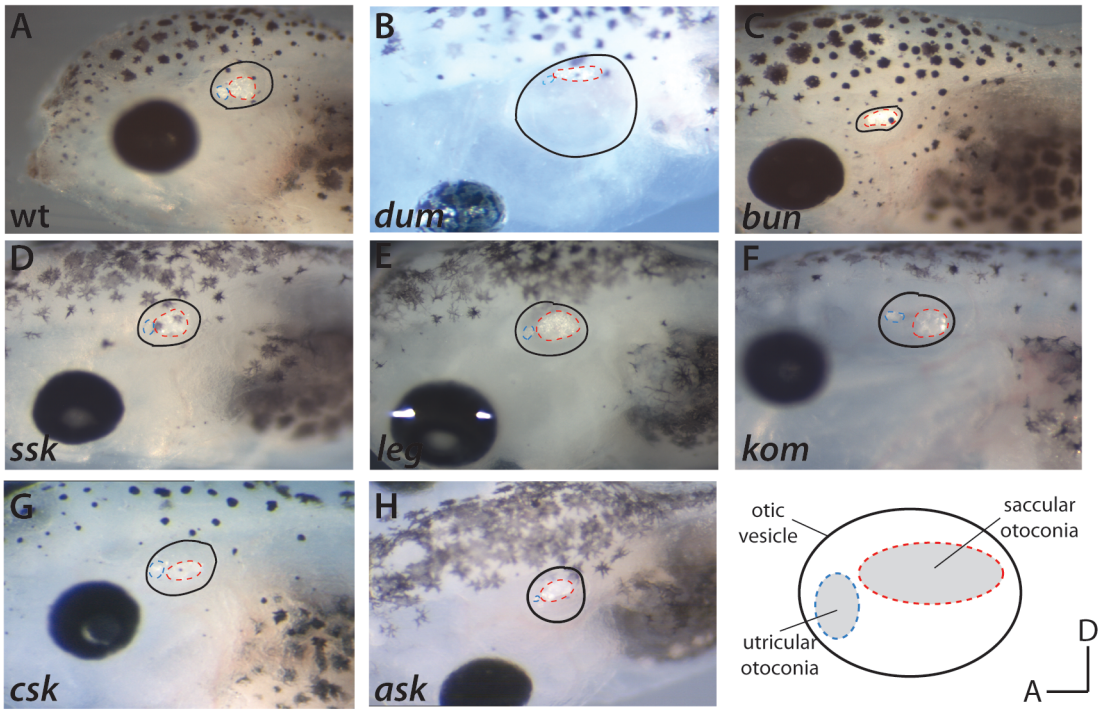


Images provided by Tada Goda

Seven phenotypes displaying a primary defect in inner ear development were identified in the gynogenetic progeny of the F1 population of mutagenised *X. tropicalis*.

**(A)** In wild type tadpoles the utricular (blue dashed line) and saccular (red dashed line) otoconia are clearly visible externally from the embryo.

**(B)** *dumbo* (*dum*) tapoles display an enlarged otic vesicle.

**(C)** *bunny* (*bun*) tadpoles lack utricular otoconia.

**(D)** *seasick* (*ssk*) tadpoles display enlarged otoconia.

**(E)** *legolas* (*leg*) tadpoles display large dysmorphic otoconia.

**(F)** *komimi* (*kom*) tadpoles display single large aggregates sitting over the utricule and-saccule.

**(G)** Otoconia in *carsick* (*csk*) tadpoles are detached from the sensory epithelia and are distributed throughout the lumen of the otic vesicle.

**(H)** The utricular otoconia is reduced in size in *airsick* (*ask*) tadpoles.

et al., 2003; Quick & Serrano, 2005). The structures of the innervating neurones and of the hair and support cells in the maculae, and the innervating neurones, can be visualized using molecular probes (Quick & Serrano, 2005). Also, by stage 45 the sensory structures are asymmetrically arranged to allow them to detect changes in head orientation (Bever et al., 2003; Quick & Serrano, 2005), providing a strong indication of whether the otic tissue has received the correct axial cues.

*3.1.4.2 Strategy for positional cloning*

Generating gynogenetic embryos is simple in *X. tropicalis* (see chapter 2 section 2.1.3 and fig. 3.4 A) and provides a useful tool for rapidly mapping most mutant lesions to a chromosome (Khokha et al., 2010). Gynogenetically created embryos, which retain a complete set of sister chromatids from meiosis II (fig. 3.4 A), are homozygous at centromeric loci. Embryos that are phenotypically mutant at a recessive allele are by definition homozygous at that locus. Gynogenetic mutant embryos derived from a heterozygous carrier mother consist of those with no crossovers between the mutant-linked parental centromere and the mutant locus (fig. 3.4 B), plus those with two or more intervening crossovers, half of which restore linkage to parental centromeres (fig. 3.4 C). The most abundant class of recombination events, single crossovers, result in heterozygous wild type embryos (fig. 3.4 B). Pools of gynogenetic mutant embryos are therefore likely to show linkage between the mutant locus and the cognate centromere, and can be used to rapidly assign mutations to a specific chromosome. Only the most distal mutant loci, where multiple recombination events outnumber single crossovers, will not appear linked to their centromere (Khokha et al., 2010). This technique has been developed by myself and other members of the *X. tropicalis* community, and has been used successfully to rapidly map several mutant lesions to chromosomes (Geach et al., 2010; Khokha et al., 2010; Zimmerman lab unpublished data).

For lesions located relatively close to the centromere (up to ~40cM), the frequency at which recessive mutant phenotypes are observed is an inverse

**(A) (i)** During meiosis, homologous chromosomes recombine and the gamete divides to produce an oocyte containing two sister chromatids.
**(ii)** To produce maternally-derived diploid tadpoles (gynogenotes), eggs are fertilized by UV-irradiated sperm, thus allowing oocyte activation without providing a paternal genetic component. Such eggs will form haploids without further treatment.
**(iii)** Gynogenotes are obtained by subjecting the zygote to early cold shock to inhibit extrusion of one set of maternal chromatids in the second polar body.
**(iv)** The haploid is rescued to a viable diploid background on which recessive phenotypes carried by the mother may be uncovered.

**(B)** Gynogenetic tadpoles are homozygous at centromeric loci as they retain a complete set of sister chromotids from meiosis II. Homozygousity must be maintained at the mutant loci to produce phenotypically mutant tadpoles. Mutant phenotypes produced by lesions located close to the centromere are unlikely to exhibit crossover events between the centromere and the lesion and so centromeric polymorphisms will show clear linkage to the mutant lesion.

**(C)** Centromeric linkage can be diluted by multiple cross-overs forming between the centromere and the lesion, the probability of which increases with distance from the centromere. **(i)** Homozygous mutant embryos exhibiting two-strand double cross-overs remain linked to the parental centromere while **(ii)** four-strand double cross-overs cause the lesion to become linked to the non-parental centromere. As four-strand double cross-overs accumulate for distal loci, centromeric linkage becomes more difficult to detect.

**Figure 3.4: Gynogenetic embryos display linkage to cognate centromeres**

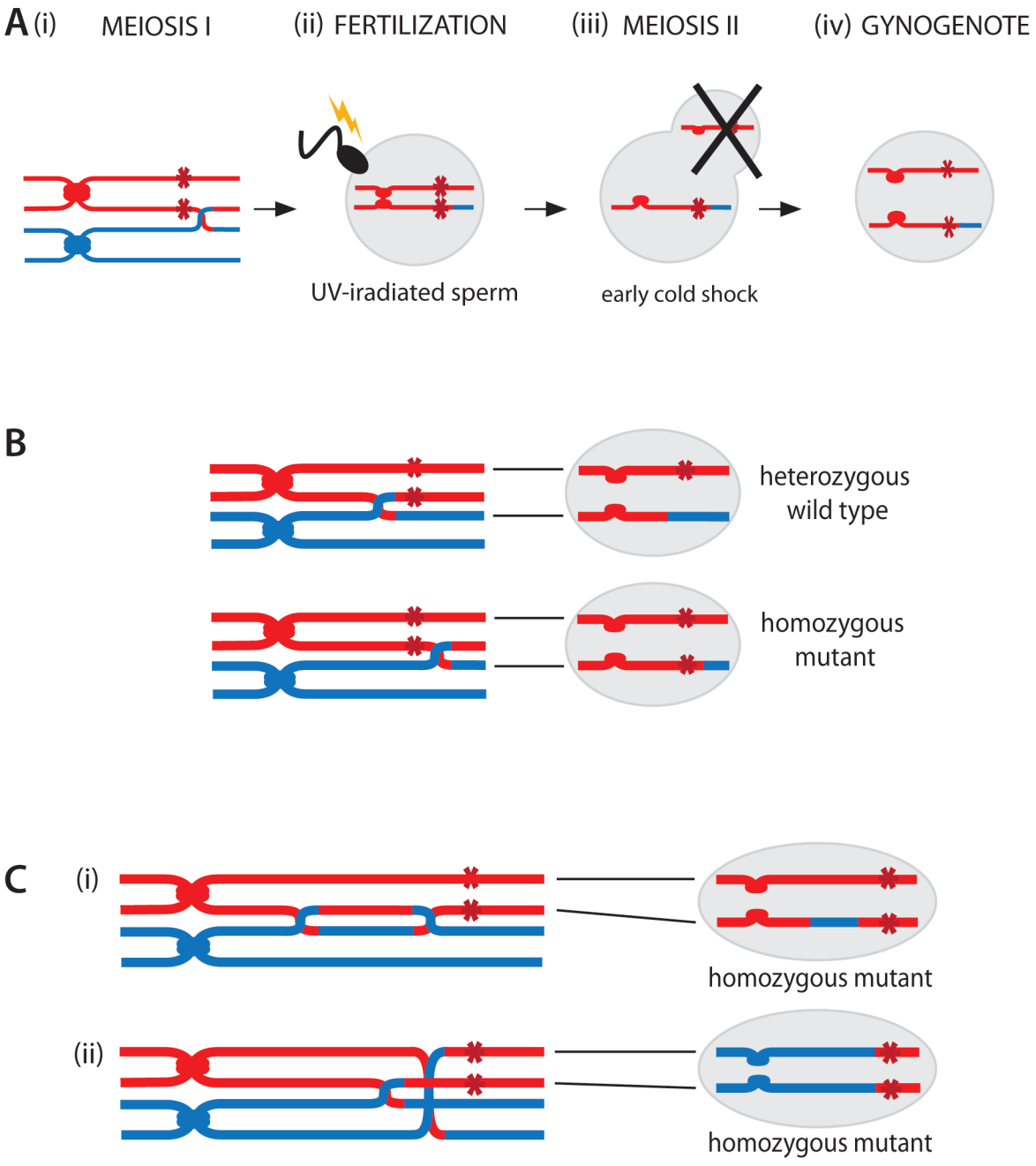

function of the mutation-centromere distance. The closer a lesion is to the centromere, the lower the probability of a recombination event occurring between the lesion and the centromere and the higher the proportion of homozygous mutant embryos that are produced. This means that the ratio of mutant gynogenetic embryos to the total number of gynogenotes can be used to calculate an approximate mutation-centromere distance using the following equation (Khokha et al., 2010):

gene-centromere distance (cM) = 50(1-(2 x mutant n° / total n° of embryos))

Also, I compiled a list of genes with well-characterized roles in inner ear development (appendix B; fig. 3.5) and identified orthologous genes in the *X. tropicalis* genome by BLAST searching. If linked markers are identified on the same chromosome as a candidate gene, SSLP markers near orthologs could be tested to evaluate linkage. This strategy will quickly identify or eliminate candidate genes.

## *3.2 Characterization and low resolution mapping of the X. tropicalis inner ear mutants*

### *3.2.1 Four mutants displaying a primary defect in inner ear formation were recovered in the forward genetic screen*

To confirm heritability of these candidate phenotypes, F1 female carriers were crossed with wild type males and the F2 progeny raised to sexual maturity. The F2 populations for *ssk*, *kom*, *leg* and *bun* were raised by Dr. Goda prior to starting my PhD. Dr. Goda and I identified carriers by screening the gynogenetic progeny produced by the F2 females for the mutant phenotypes. The *dum*, *csk* and *ask* F2 populations were raised and the gynogenetic progeny screened by myself.

**Figure 3.5: Candidate genes**

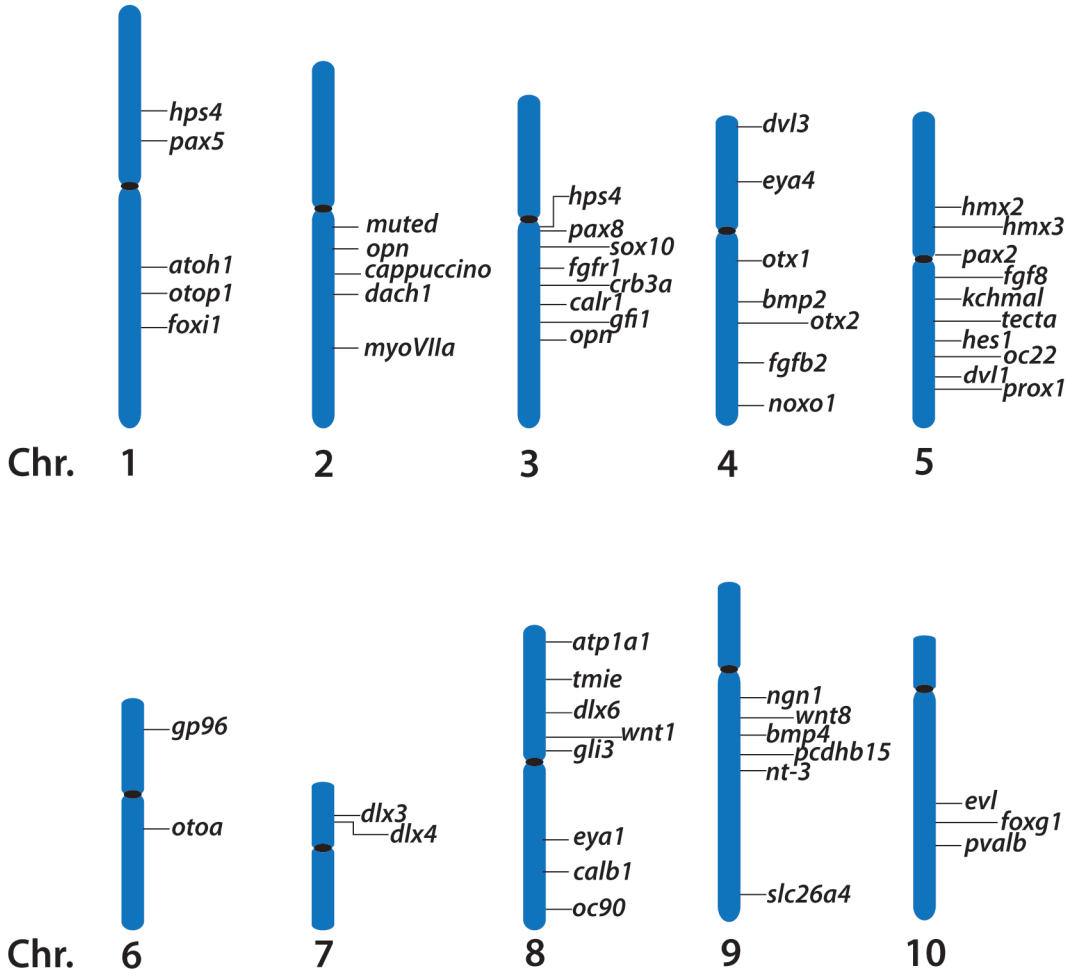


A list of candidate genes known to display mutant phenotypes resembling the *X. tropicalis* inner ear mutants has been compiled from the literature. The locations of these genes in the X. tropicalis genome have been identified using the ensembl genome browser (www.ensembl.org/xenopus tropicalis/Intro/Index) and the meiotic map (Wells et al., 2011).

Of the original seven inner ear phenotypes, *ssk*, *kom*, *leg* and *bun* were re-identified in gynogenetic progeny of cognate F2 females, confirming that they have an underlying genetic cause (table 3.1). I did not recover the *dum*, *csk* and *ask* phenotypes from the F2 individuals I scored (table 3.1). However as the F1 population derived from in vitro mutagenesis is mosaic for induced mutations, a low proportion of the F2 population may have inherited the mutated lesion, and it may be necessary to increase the number of F2 individuals screened to confirm heritability.

To identify male carriers, the F2 female carriers were crossed to sibling males and the offspring screened for their respective mutant phenotypes. Male carriers were obtained for the *ssk*, *kom* and *bun* mutations, each producing Mendelian 3:1 wild type to mutant ratios (table 3.1), consistent with simple recessive genetic lesions. I have yet to identify a male carrier for the *leg* mutation, so Mendelian ratios cannot be assessed.

### *3.2.2 Characterization and low resolution mapping of the seasick (ssk) mutant*

#### *3.2.2.1 ssk have enlarge otoconia, decreased pigmentation and balance defects*

The *ssk* inner ear phenotype is first discernable at stage 37, as otoconia appear slightly enlarged compared to those of wild type siblings (fig. 3.6 A – B; utricle denoted by blue dashed line and sacculus denoted by red dashed line). By stages 41 and 45, otoconia progressively increase in size (fig. 3.6 C – F; utricle denoted by blue dashed line and sacculus denoted by red dashed line) and tadpoles exhibit balance defects such as inability to orientate correctly while swimming. In addition to the inner ear phenotype, *ssk* tadpoles also have decreased melanophore and iridophore pigmentation (see chapter 4 fig. 4.1) and die during metamorphosis (stages 60 - 65).

## Table 3.1: Heritability of the F1 inner ear phenotypes

| Allele | F1 gynogenesis | F2 gynogenesis | F3 gynogenesis | Sibling cross | Mutant-centromere distance |
|---|---|---|---|---|---|
| *seasick* (*ssk*) | 34/192 (17.7%) | 11/46 (23.9%) | 297/849 (35.0%) | 20/105 (19%) | 15cM |
| *komimi* (*kom*) | 22/210 (10%) | 10/49 (20%) | 188/1,777 (11%) | 41/159 (26%) | 39cM |
| *bunny* (*bun*) | | 31/89 (35%) | 33/91 (36%) | 384/1382 (28%) | 14cM |
| *legolas* (*leg*) | 11/70 (16%) | 6/56 (11%) | - | - | 35cM |
| *dumbo* (*dum*) | 5/151 (3%) | - | - | - | - |
| *carsick* (*csk*) | 3/13 (23%) | - | - | - | - |
| *airsick* (*ask*) | 10/67 (15%) | - | - | - | - |

The data represents the number of phenotypically mutant gynogenotes out of the total number of gynogenotes produced by females from each generation. The column entitled “sibling cross” represents the number of mutant tadpoles out of the total number of tadpoles produced from matings between two sibling carriers of the mutation. The mutant-centromere distance is calculated using the equation described in section 3.1.4.2 .

**Figure 3.6: External phenotype of *ssk* inner ear**

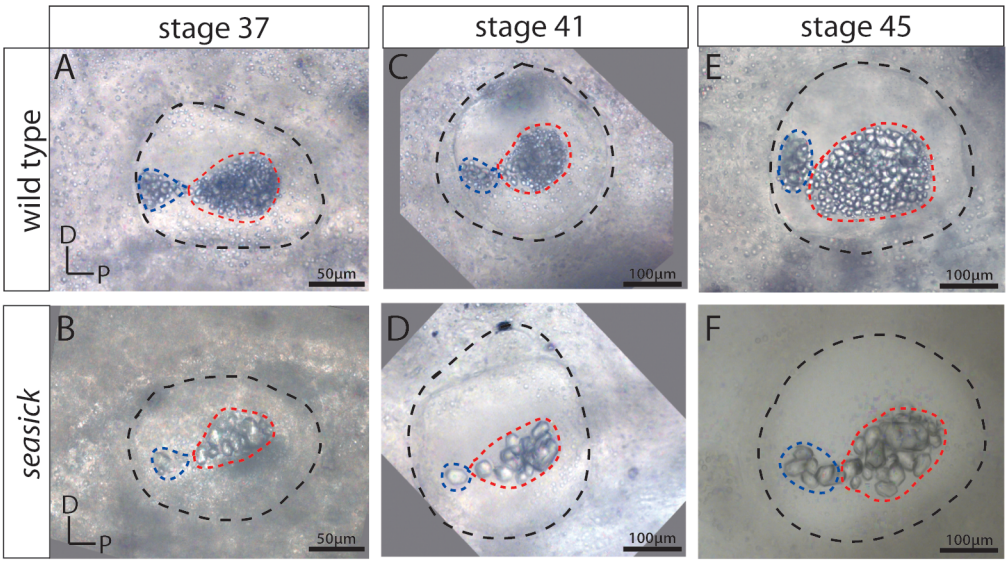


DIC images of *ssk* otic vesicles.

**(A-B)** The *ssk* phenotype is first discernable at stage 37 due to the presence of enlarged otoconia over both the utricular (blue dashed line) and saccular (red dashed line) maculae.

**(C-F)** The otoconia progessively increase in size through stages 41 and 45, and *ssk* tadpoles start to exhibit behavioural vestibular defects, such as an inability to orientate themselves correctly while swimming.

*3.2.2.2 Gross morphology of the inner ear appears unaffected in ssk tadpoles*

Histological sections show that the gross morphology of the *ssk* inner ear has no obvious defects. The interconnecting utricular and saccular chambers (fig. 3.7 B - C), along with their corresponding maculae (fig. 3.7 D - E) form at the correct size and location. Epithelial projections forming the lumen of the semicircular canals are observed (fig. 3.7 D - E), as is the endolymphatic duct (fig. 3.7 F - G). The statoacoustic ganglion (SAG) develops in close proximity to the maculae and the neural tube (fig. 3.7 D – E; black dashed lines), and when viewed at higher magnification (x100) cellular morphology also appears to be unaffected (fig. 3.6 H – I; black dashed line). The columnar structure of the hair and support cells forming the sacculus does not differ from wild type (fig. 3.7 J – K; black dashed lines). Stereocilia bundles form correctly at the apical end of the hair cells (fig. 3.7 J - K; black arrowheads), and the otoconial membrane (fig. 3.7 J - K; red arrowheads) that connects the otoconia to the maculae and facilitates transmission of mechanical force to the hair cells, is also present. These data suggest that at stage 45, the gross morphology of the inner ear, the maculae and the SAG is unaffected by the *ssk* lesion.

*3.2.2.3 Sensory epithelial patterning, differentiation and innervation appears unaffected in ssk tadpoles*

I used fluorescein-tagged phalloidin to visualize the actin in the hair cell stereocilia and cell boundaries in the inner ear of stage 45 wild type and *ssk* tadpoles. The stereocilia of the saccular (fig. 3.8 B - C; dotted line) and utricular (fig. 3.8 B - C; dashed line) macula hair cells are clearly visible, as are the cristae located at the base of the semicircular canals (fig. 3.8 B - C; red arrows). At higher magnification, the saccular hair cells, separated from one another by a ring of supporting cells, can be seen in both *ssk* and wild type tadpoles (fig. 3.8 D – E), in a pattern resulting from classical notch-delta signaling (see introduction section 1.3.3) (Morsli et al., 1998; Quick & Serrano, 2005; Wu et al., 1996).

Antibody staining of S-100, a calcium binding protein expressed in the cell bodies of differentiated hair cells (Abbate, F et al., 2002), shows that hair cell size and

**(A)** Schematic of lateral view of a stage 45 inner ear. Red dashed lines indicate location of sections.

**(B-G)** At stage 45, the *ssk* inner ear displays no obvious gross morphological defects. The interconnecting utricular and saccular chambers along with their corresponding maculae are clearly visible, as are the epithelial projections of the semicircular canals, the statioacoustic ganglion (SAG) and the endolymphatic duct. The size of the otic tissue is also comparable to wild type. Each image is orientated so that dorsal is to the top and lateral is to the right.

**(H-I)** Viewed at high magnification, the cellular morphology of the SAG appears to be unaffected. The neuronal cell bodies appear comparable in size and both are tightly associated with the neural tube (NT) and the maculae. Each image is orientated so that lateral is to the top and ventral is to the right.

**(J-K)** The hair and support cells of the macular display the same columnar structure as the wild type. The hair cell stereocilia form at the apical pole of the cell (black arrowhead) and the otoconial membrane (red arrowhead) forms also. Each image is orientated so that lateral is to the top and ventral is to the right.

**Figure 3.7: Gross morphology of the inner ear appears unaffected in *ssk* embryos**

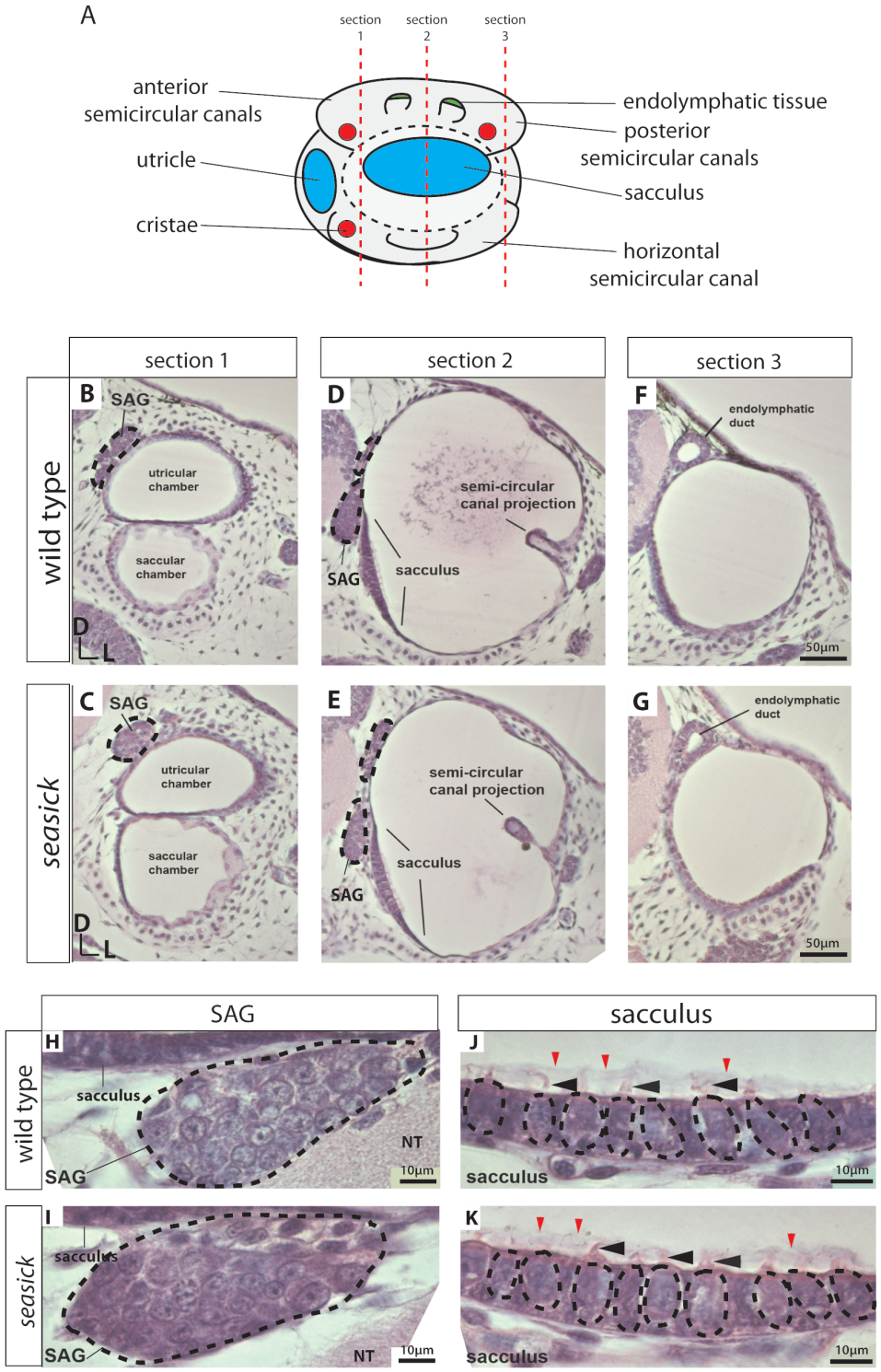

**(A)** Schematic of the utricular, saccular and cristae sensory epithelia plus the innervating neurones. The "I" nerve bundle innervates the utricle and then branches to innervate the anterior and horizontal cristae. The "II" nerve bundle innervates the sacculus and the "III" nerve bundle innervates the posterior cristae.

**(B-C)** The hair cell stereocilia of the utricular (dashed lined) and saccular (dotted line) maculae are clearly visible in both wild type and *ssk*, as are the cristae (red arrows) at the base of the semicircular canals. Both forms of sensory epithelia are comparable in size in *ssk* and wild type.

**(D - E)** A classic notch-delta mediated patterning of hair cells surrounded by a ring of support cells is visible in both wild type and ssk maculae.

**(F - G)** S-100 staining of hair cell bodies reveals that hair cell size and density does not notably differ between wild type and *ssk*.

**(H - I)** Anti-acetylated tubulin staining of the hair cell kinocilia and neurones shows that the hair cells of the maculae and cristae are innervated correctly (neurone bundle I - red arrowhead; neurone bundle II – white arrowhead; neurone bundle III blue arrowhead).

**(J)** In stage 45 tadpoles, the number of utricular and saccular hair cells doesn't differ between wild type and *ssk* (hair cells counts carried out on S-100 antibody staining; n=4).

**Figure 3.8: Sensory epithelial patterning, differentiation and innervation appear unaffected in *ssk* mutants**

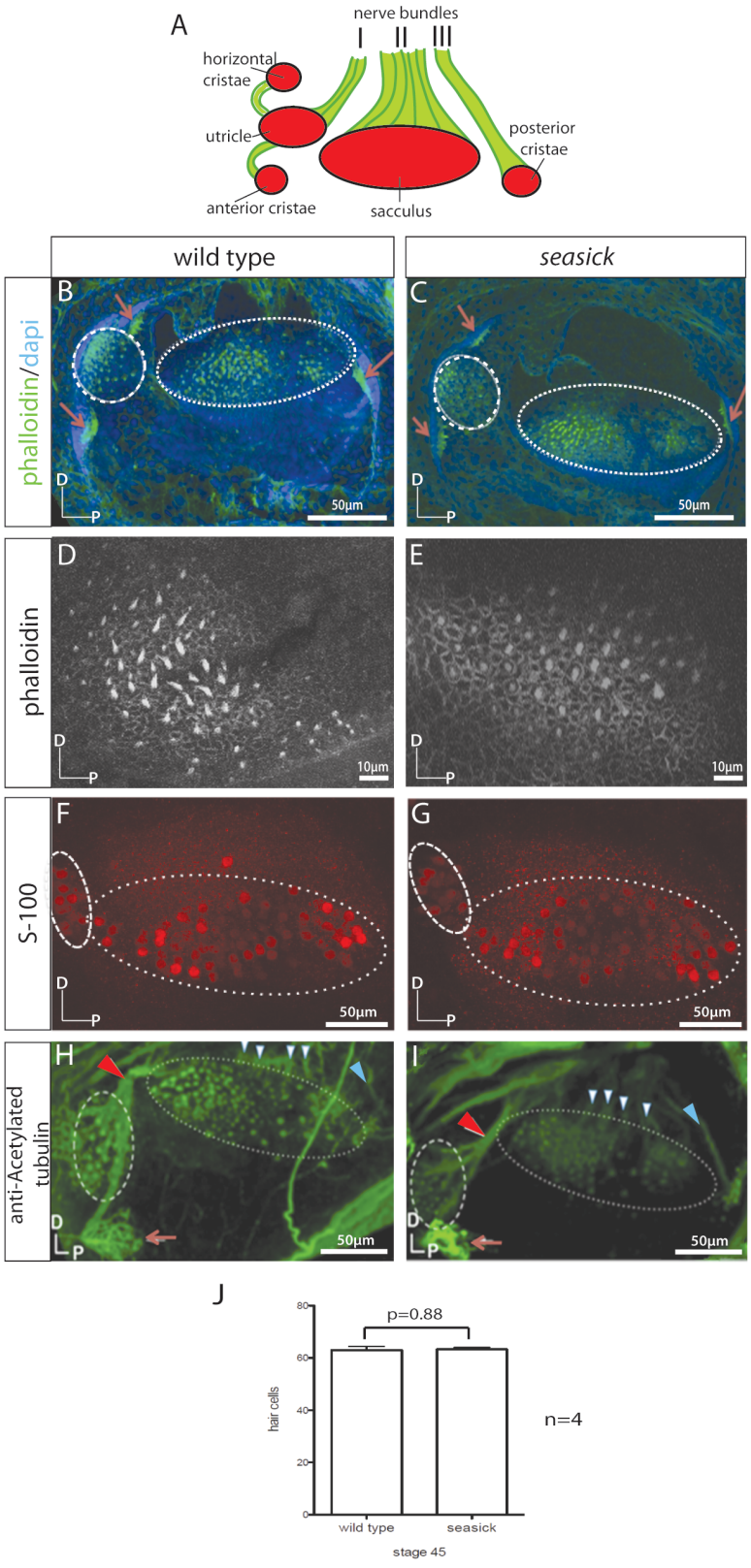

density does not notably differ between *ssk* and wild type tadpoles (fig. 3.8 F, G & J; sacculus denoted by dotted line; utricle denoted by dashed line; p=0.88). Anti-acetylated tubulin staining allows visualization of the kinocilium and the neurones innervating the hair cells, and shows that the hair cells of the maculae and the cristae (fig. 3.8 H - I; neurone bundle I - red arrowhead; neurone bundle II – white arrowhead; neurone bundle III blue arrowhead) are innervated correctly.

*3.2.2.4 ssk is linked to the p-arm of chromosome 1*

Out of a total of 895 gynogenetic tadpoles, 308 displayed the *ssk* phenotype. Using these data the mutation-centromere distance can be calculated as ~15cM (table 3.1). To map the *ssk* lesion to a chromosome, pools of DNA obtained from wild type and *ssk* gynogenetic tadpoles were assayed for linkage to polymorphic SSLP markers located close to each centromere. *ssk* is linked to the chromosome 1 centromeric SSLP marker 013H11 in pools of DNA obtained from 20 wild type and 20 *ssk* gynogenetic embryos (fig. 3.9 A).

To determine an approximate location of the *ssk* lesion on chromosome 1, pools of DNA from gynogenetically derived wild type and *ssk* tadpoles were assayed for linkage to polymorphic SSLP markers on the p and q-arms of chromosome 1. Where possible, SSLP markers located on the same scaffolds as candidate genes were selected (for candidate genes see fig. 3.5 and appendix B table B.1). *ssk* shows the strongest linkage to SSLP marker 019E09 which is located ~ 10cM from the centromere on the p-arm (fig. 3.9 B).

*3.2.2.5 Conclusions*

The inner ear defect in *ssk* mutants appears to be limited to the development of the otoconial crystals. The gross morphology of the inner ear along with the patterning of the hair and support cells does not notably differ from wild type, nor does innervation of the sensory cells in the sensory epithelia of the maculae and cristae. The melanophores and iridophores are also defective in *ssk* mutants, as both cell types display hypopigmentation (see fig. 4.1). Melanophores residing in

## Figure 3.9: *ssk* shows linkage to the centromere of chromosome 1 in pools of gynogenetically derived embryos

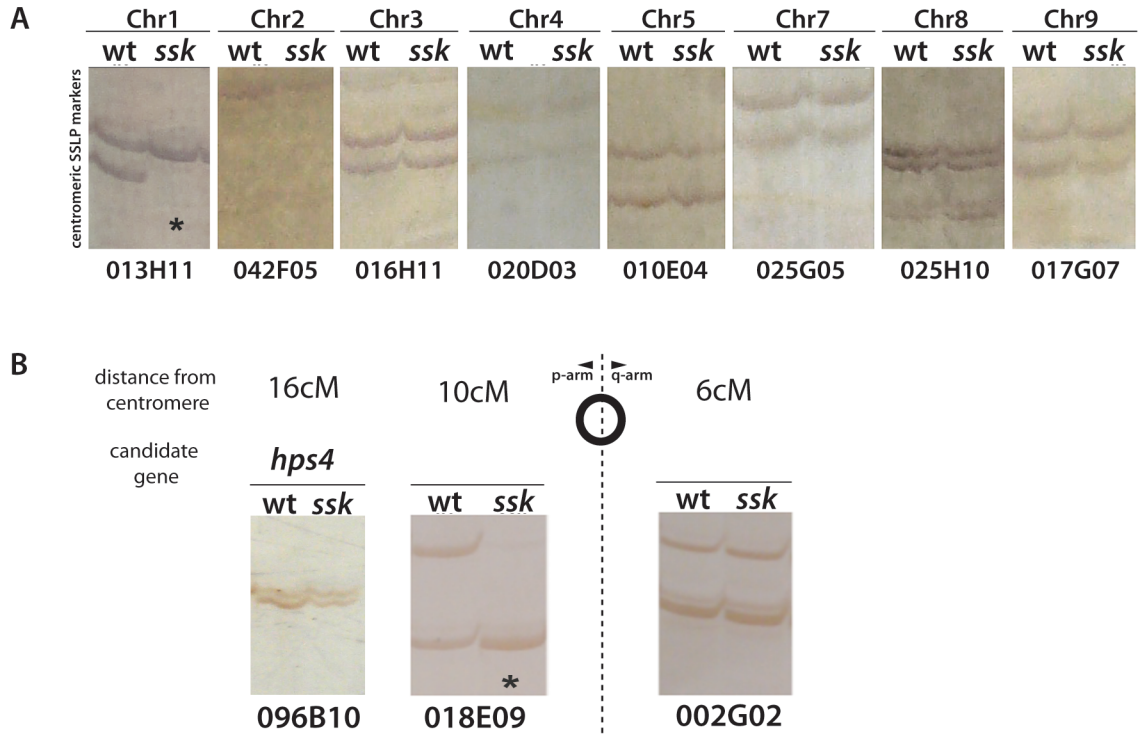


**(A)** Pools of gynogenetically-derived wild type and *ssk* DNAs were assayed for linkage to centromeric polymorphisms for the 10 *X. tropicalis* chromosomes. *ssk* exhibits linkage to a chromosome 1 centromeric SSLP marker 013H11 ("*"). Centromeric markers for chromosomes 6 and 10 were not assayed due to difficulty in obtaining polymorphisms.

**(B)** Pools of gynogenetically-derived wild type and *ssk* tadpoles were assayed for linkage to polymorphic SSLP markers spread across chromosome 1. Where possible, SSLP markers located close to candidate genes were selected. *ssk* exhibited the strongest linkage to marker 018E09.

the inner ear are known to aid the regulation of ions such as $Ca^{2+}$ and $K^{+}$ (Tu et al., 1998), therefore one hypothesis is that the otoconial defect may be attributed to defects in this cell type. It is also possible that a problem in ionic regulation could be caused by defects in other cell types such as the endolymphatic tissue or that malformations in the synthesis and/or processing of otoconial proteins may be responsible.

The linkage analysis using gynogenetic tadpoles indicates that the lesion lies ~15cM from the centromere on the p-arm of chromosome 1, and does not show linkage to any of the candidate genes tested in this region. The *ssk* lesion shows the strongest linkage to the SSLP marker 018E09, located ~10cM from the centromere on the p-arm of chromosome 1.

### *3.2.3 Characterization and low mapping cloning of the komimi (kom) mutant*

#### *3.2.3.1 External phenotype of the kom inner ear*

*kom* tadpoles display large dysmorphic otoconial aggregates instead of multiple small otoconia found in wild type siblings. At stages 37 and 41, *kom* tadpoles often only display one otoconium located over the sacculus (fig. 3.10 A – D; utricle denoted by blue dashed line and sacculus denoted by red dashed line), but by stage 45 most mutants display both utricular and saccular otoconia (fig. 3.10 E – F; utricle denoted by blue dashed line and sacculus denoted by red dashed line). *kom* embryos also exhibit strong balance defects such as circular swimming, difficulty reorientating themselves when placed upside down and a poor startle reflex. Homozygous mutants are viable and can develop to sexual maturity.

#### *3.2.3.2 Gross morphology of the inner ear is unaffected in kom tadpoles, however, the columnar structure of the macular sensory epithelia is lost*

No detectable differences in the gross morphology between stage 45 wild type and *kom* inner ears are observed in histological sections. The major structures of

**Figure 3.10: External phenotype of *kom* inner ear**

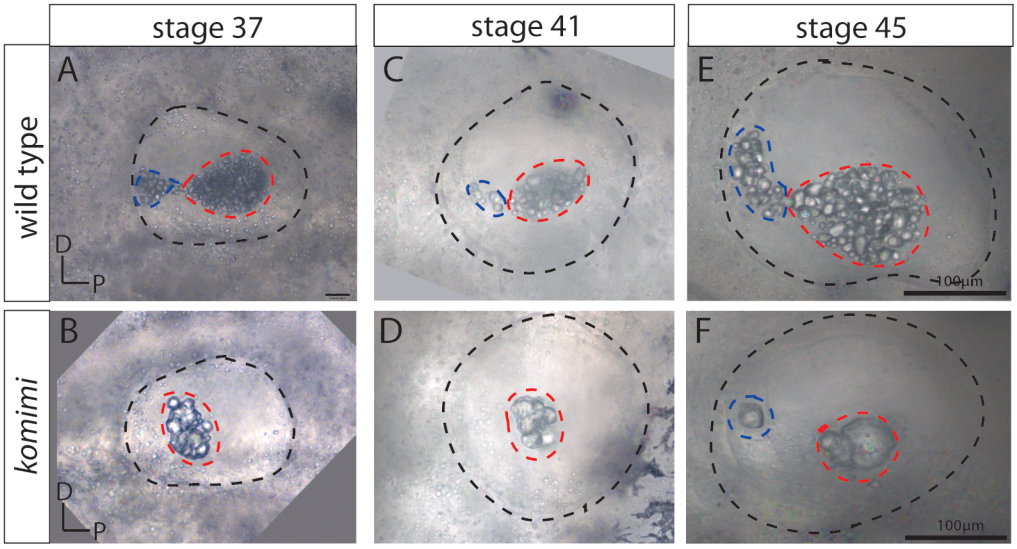


DIC images of otic vesicles in *kom*.

**(A-D)** Stage 37 and 41 *kom* tadpoles display a large dysmorphic otoconial crystal located over the saccule (blue dashed line) instead of the multiple small crystals observed in wildtype siblings.

**(E-F)** By stage 45 most *kom* tadpoles display a crystal over both the utricle (red dashed line) and saccule. *kom* tadpoles also display strong vestibular defects such as circular swimming and an inability to reorientate themselves while swimming.

**(A)** Schematic of lateral view of a stage 45 inner ear. Red dashed lines indicate location of sections.

**(B - G)** At stage 45, the gross morphology of the *kom* inner ear does not appear to differ from wild type. The interconnecting utricular and saccular chambers and the saccular maculae are clearly visible, as are the epithelial projections of the semicircular canals, the SAG and the endolymphatic duct. Images are orientated so that dorsal is to the top and lateral is to the left.

**(H - I)** Viewed at high magnification, the cellular morphology of the *kom* SAG is comparible to the wild type. The kom neuronal cell bodies do not appear to differ in size from the wild type and both are tightly associated with the NT and the maculae. Images are orientated so that lateral is to the top and ventral is to the right.

**(J - K)** In *kom*, the hair and support cells of the macula lack the columnar structure of the wild type. The cells are dysmorphic and vary greatly in size. The hair cells form hair cell stereocilia bundles at the apical pole (black arrowheads), and the otoconial membrane forms (red arrowhead), however many cells do not appear to span the whole apical-basal axis of the epithelia (green arrowhead).

Images are orientated so that lateral is to the top and ventral is to the right.

**Figure 3.11: The columnar structure of the macular sensory epithelia is lost in *kom* mutants**

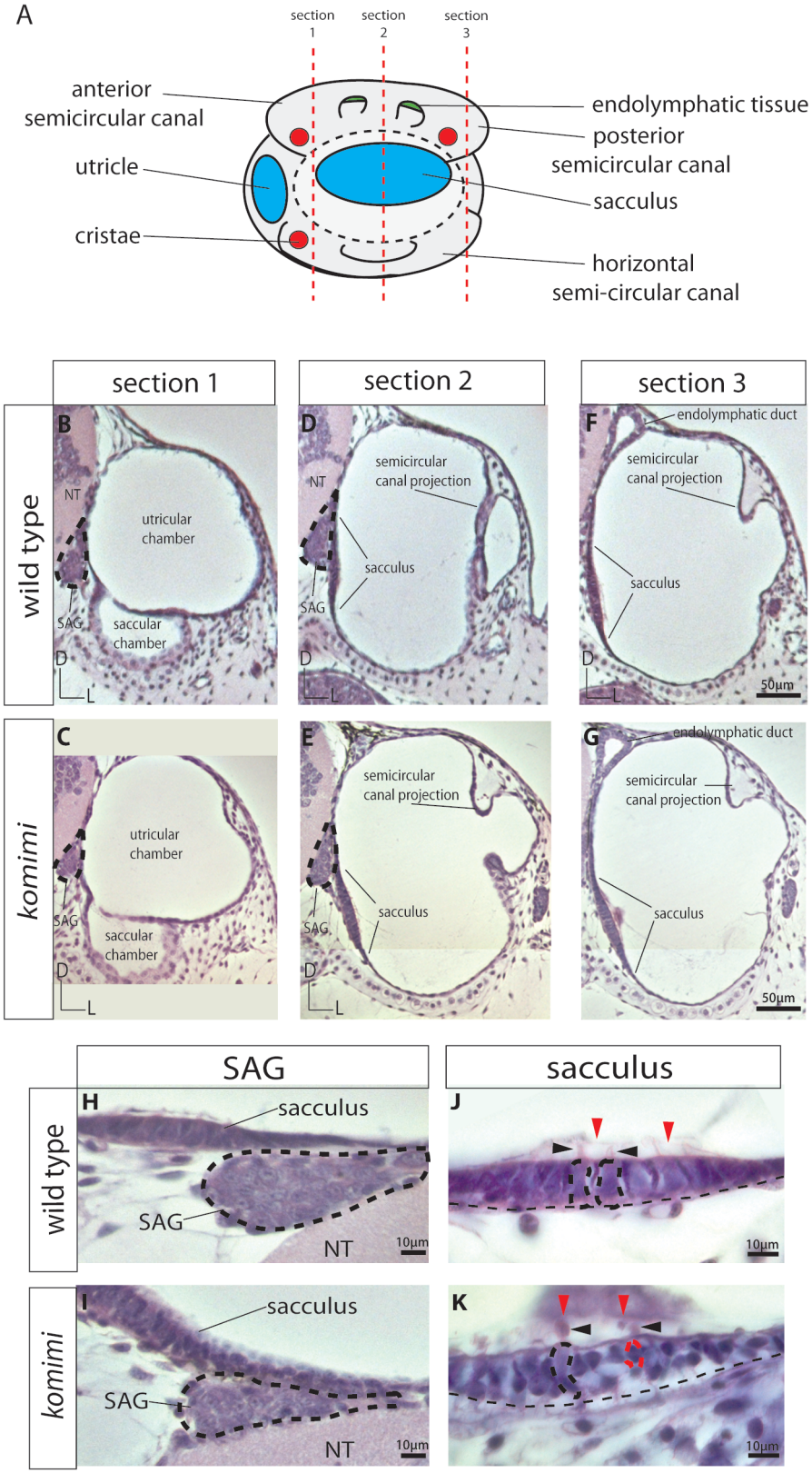

the inner ear such as the utricular and saccular chambers (fig. 3.11 B - C), their corresponding maculae (fig. 3.11 D - E), the developing semicircular canals (fig. 3.11 D - E) and the endolymphatic duct (fig. 3.11 F - G) all form at a comparable size and location. The SAG develops in close proximity to the neural tube and the maculae and the cellular morphology does not visibly differ from the wild type (fig. 3.11 H – I; black dashed line). However, when viewed at high magnification, defects in the maculae are visible. In the wild type inner ear, the hair and support cells of the maculae are tightly associated with one another forming a columnar structure. In *kom* embryos, these cells are dysmorphic and appear to differ in size within the epithelia. The hair cells retain apical-basal polarity, as stereocilia bundles do form at the apical pole (fig. 3.11 I - J; black arrowheads) of the cell however many cells do not appear to span the whole apical-basal axis (fig. 3.11 J; red dashed line) as is observed in the wild type (fig. 3.11 I; black dashed line).

*3.2.3.3 Sensory epithelial cell size differs greatly in kom*

Fluorescein-tagged phalloidin shows that each sensory epithelium resides at a comparable location and size (fig. 3.12 B – C). Viewed at higher magnification, the saccular hair cells are surrounded by a ring of support cells, however the size of the apical surface of the hair cells, and the associated stereocilia bundle, differ greatly within the epithelia (fig. 3.12 D – E). The phenotype is again reflected by the S-100 immunostaining of the hair cell bodies, with hairs cell ranging from approximately half the size to three times the size of the wild type (fig. 3.12 F – G). The number of hair cells does not notably differ from wild type (fig. 3.12 J) and innervation of the sensory epithelia does not appear to be affected (fig. 3.12 H – I).

*3.2.3.4 kom is linked to the q-arm of chromosome 6*

Out of a total of 2059 gynogenetic tadpoles, 224 displayed the *kom* phenotype, giving an estimate of the mutation-centromere distance of ~40cM. To map the *kom* lesion, I tested SSLP markers located close to the centromere of each chromosome for linkage to the *kom* lesion. This shows that *kom* is weakly linked to the SSLP marker 015G09, which is located close to the centromere of

**(A)** Schematic of lateral view of a stage 45 inner ear. Red dashed lines indicate location of sections.

**(B - G)** At stage 45, the gross morphology of the *kom* inner ear does not appear to differ from wild type. The interconnecting utricular and saccular chambers and the saccular maculae are clearly visible, as are the epithelial projections of the semicircular canals, the SAG and the endolymphatic duct. Images are orientated so that dorsal is to the top and lateral is to the left.

**(H - I)** Viewed at high magnification, the cellular morphology of the *kom* SAG is comparible to the wild type. The kom neuronal cell bodies do not appear to differ in size from the wild type and both are tightly associated with the NT and the maculae. Images are orientated so that lateral is to the top and ventral is to the right.

**(J - K)** In *kom*, the hair and support cells of the macula lack the columnar structure of the wild type. The cells are dysmorphic and vary greatly in size. The hair cells form hair cell stereocilia bundles at the apical pole (black arrowheads), and the otoconial membrane forms (red arrowhead), however many cells do not appear to span the whole apical-basal axis of the epithelia (green arrowhead).

Images are orientated so that lateral is to the top and ventral is to the right.

**Figure 3.12: Sensory epithelial cell size differs greatly in *kom***

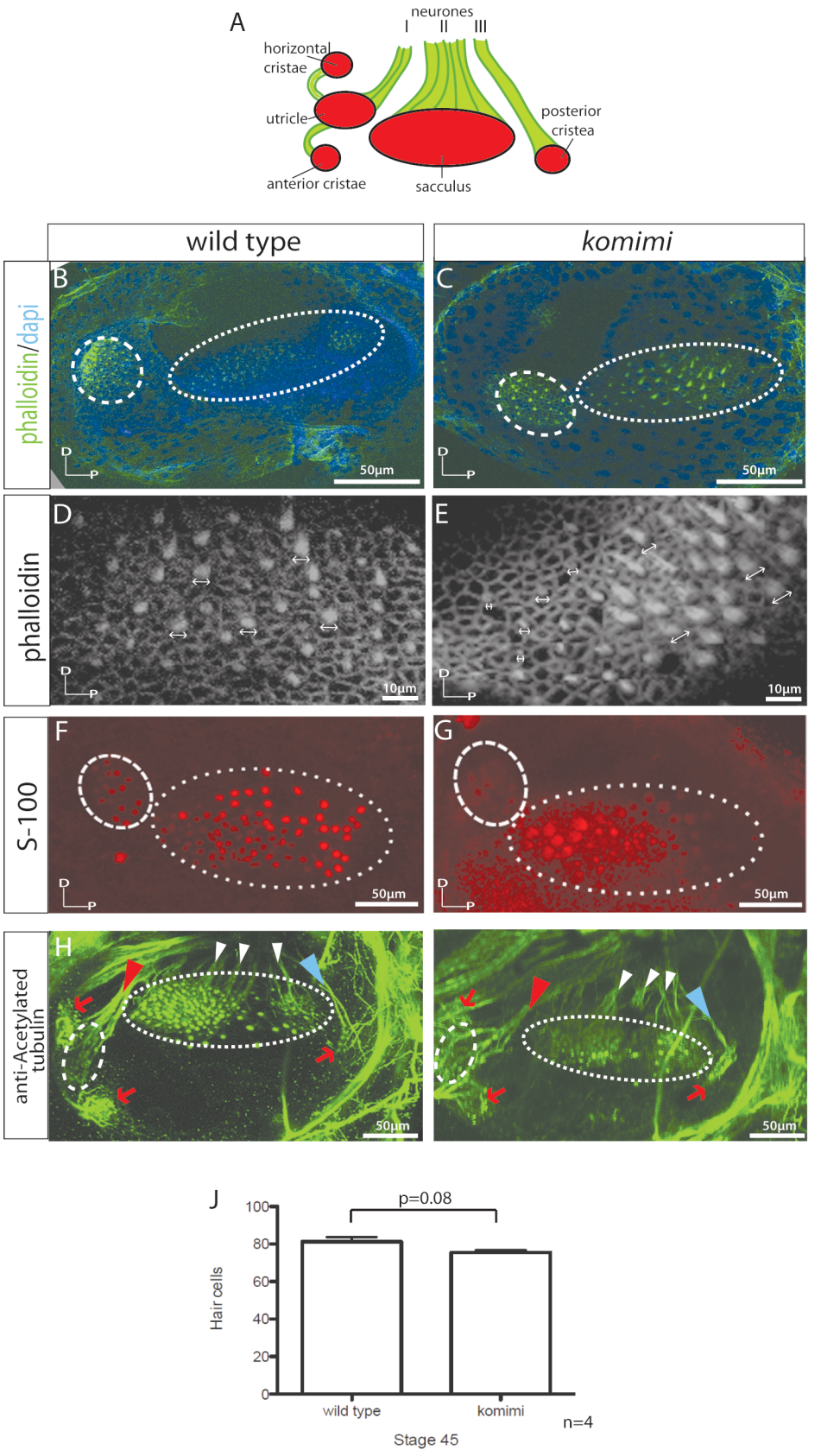

chromosome 6 (fig. 3.13 A; denoted by "*"). This weak centromere linkage is consistent with the distal chromosomal location suggested by the gynogenetic phenotype ratio (see section 3.1.4.2). I tested an additional 20 individual *kom* tadpoles for the chromosome 6 centromeric SSLP marker 015G09 to determine whether *kom* is linked to chromosome 6. The *kom* tadpoles show a clear bias for one allele (17 *kom* tadpoles have the N-strain allele, 3 *kom* tadpoles have the IC-strain allele), suggesting that *kom* is linked to the centromere of chromosome 6.

An approximate location of the *kom* lesion on chromosome 6 was determined by assaying pools of wild type and *kom* gynogenetic tadpoles for linkage to SSLP on the p- and q-arms of chromosome 6. Where possible, SSLP markers located on the same scaffold as candidate genes were selected (appendix B table B.1, fig. 3.5). *kom* displays linkage to SSLP markers 008B06 and 121G10 on the q-arm.

*3.2.3.5 Conclusions*

In *kom*, a single large dysmorphic otoconial crystal develops over each macula, the macular cells vary greatly in size, and many appear not to span the whole apical-basal axis, causing the epithelia to lose the columnar structure observed in wild type. Many mechanisms could be responsible for this phenotype. Abnormal timing of epithelial differentiation may result in the observed cellular morphology, or a defect in cell adhesion could cause the cells to lose their elongated structure. Macular cells play a key role in the development of the otoconia, as they synthesize otoconial proteins such as otolin, the hair cell stereocilia acts as a nucleation point for crystal growth, and the macular cells control the local ionic environment that is essential for crystallization (see introduction 1.6). Therefore it is plausible that *kom* causes a defect in the maculae that is in turn responsible for the abnormal otoconial morphology. There is also the possibility that the macular phenotype is caused by mechanical stress exerted by the excessive otoconial mass. The loss of columnar structure observed in the *kom* epithelia could be the result of apoptosis caused by mechanical cell damage.

## Figure 3.13: *kom* shows linkage to the centromere of chromosome 6 in pools of gynogenetically derived embryos

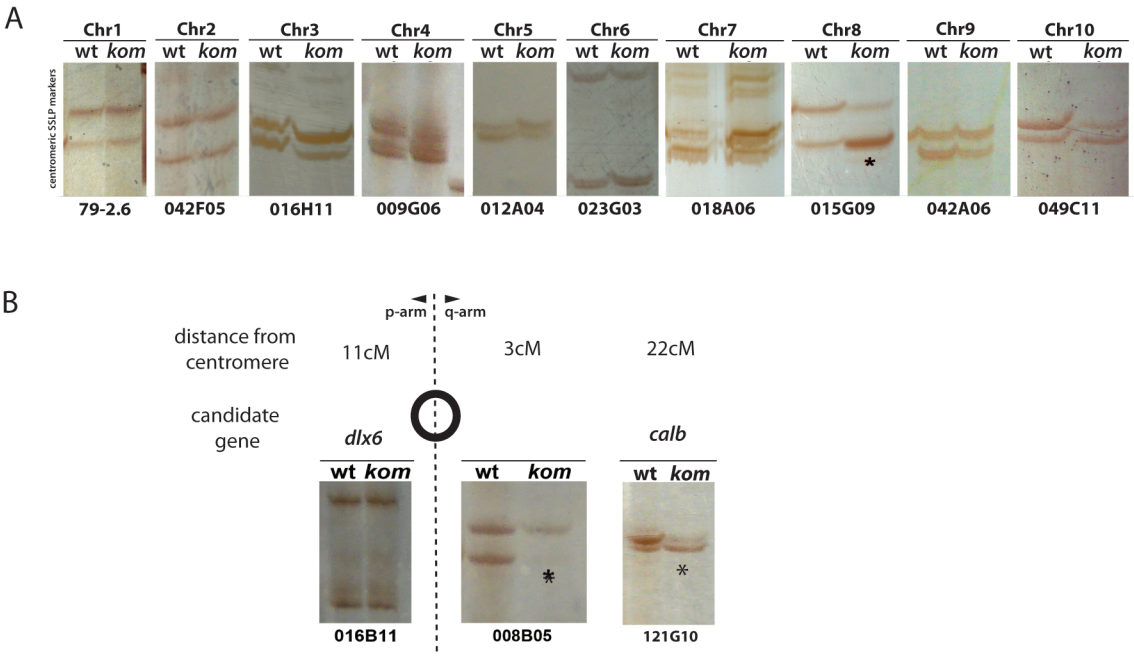


**(A)** Pools of gynogentically-derived wild type and *kom* embryos were assayed for linkage to polymorphoric SSLP markers close to the centromeres of the 10 *X. tropicalis* chromosomes. *kom* shows weak linkage to the centromeric SSLP marker for chromosome 6 015G09 ( "*" ).

**(B)** Pools of gynogenetically derived wild type and *kom* tadpoles were assayed for linkage to polymorphic SSLP markers on the p- and q-arms of chromosome 6. Where possible, SSLP markers located close to candidate genes were selected. *kom* exhibited the strongest linkage to marker 008B06.

The *kom* lesion shows weak linkage to the centromere of chromosome 6. The lesion also has a large estimated mutation-centromere distance of ~40cM, indicating that it is very distal to the centromere. Strong linkage is observed to SSLP markers 008B06 and 121G10, both of which are located in the q-arm of chromosome 6.

### *3.2.4 Characterization and low resolution mapping of the legolas (leg) mutant*

#### *3.2.4.1 External phenotype of the leg inner ear*

The *leg* phenotype is first detectable at stage 37 by the presence of enlarged otoconia which continue to increase in size from stages 41 and 45 (fig. 3.14 A – F; utricle denoted by blue dashed line and sacculus denoted by red dashed line). No obvious vestibular defects are observed, however few *leg* tadpoles have been examined since the mutant can only be obtained by gynogenesis, as a male carrier is yet to be identified.

#### *3.2.4.2 Gross morphology of the inner ear appears unaffected in leg tadpoles*

Histological sections indicate that the gross morphology of the inner ear has no observable defects. The interconnecting saccular and utricular chambers are present (differences in size are due to orientation of section) and the sacculus is visible in the medial wall of the saccular chamber (fig. 3.15 B - C). The epithelial projections of the developing semicircular canals are also visible as is the endolymphatic duct (fig. 3.15 F - G). When viewed at high magnification (x100), the cellular morphology of the SAG does not appear to differ from the wild type. The neuronal cell bodies appear comparable in size between *leg* and wild type, and both are in close association with the neural tube and macular epithelia (fig. 3.15 H – I; black dashed line). The hair and support cells of the maculae have the same columnar structure as in the wild type (fig. 3.15 J – K; black dashed line). The hair cell stereocilia are also clearly visible at the apical pole of the hair cells (fig. 3.15 J - K; black arrowhead) along with the otoconial membrane (fig. 3.15 J - K; red arrowhead).

**Figure 3.14: External phenotype of *leg* inner ear**

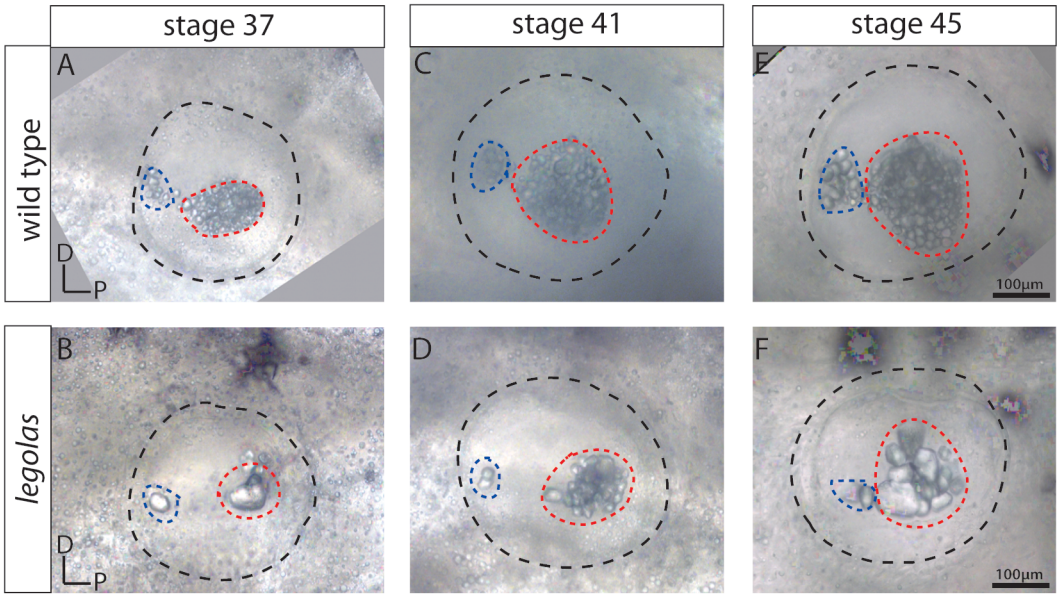


DIC images of *leg* otic vesicles.

**(A-B)** *leg* phenotype is first discernable at stage 37 due to the presence of enlarged otoconial crystals.

**(C-F)** The otoconial crystals in *leg* continue to increase in size through stages 41 and 45 in *leg* relative to wild type.

**(A)** Schematic of lateral view of a stage 45 inner ear. Red dashed lines indicate location of sections.

**(B - G)** At stage 45, the gross morphology of the *leg* inner ear displays no obvious defects. The interconnecting utricular and saccular chambers are present (dashed line marks the approximate location of the opening between the two chambers) and the sacculus is clearly present in the medial wall of the saccular chamber. The epithelial projections of the semicircular projections are clearly visible, as are the statioacoustic-ganglion (SAG) and endolymphatic duct. Images are orientated so that dorsal is to the top and lateral is to the right.

**(H - I)** At high magnification, the cellular morphology of the SAG does not appear to differ from wild type. The neuronal cell bodies appear comparable in size, and both are tightly associated with the neural tube (NT) and the macular. Images are orientated so that lateral is to the top and ventral is to the left.

**(J - K)** The hair and support cells of the maculae display the same columnar structure as wild type. The hair cell stereocilia form at the apical pole of the cell (black arrowhead) and the otoconial membrane (red arrowhead) forms also. Images are orientated so that lateral is to the top and ventral is to the left.

**Figure 3.15: Gross morphology of the inner ear appears unaffected in *leg* tadpoles**

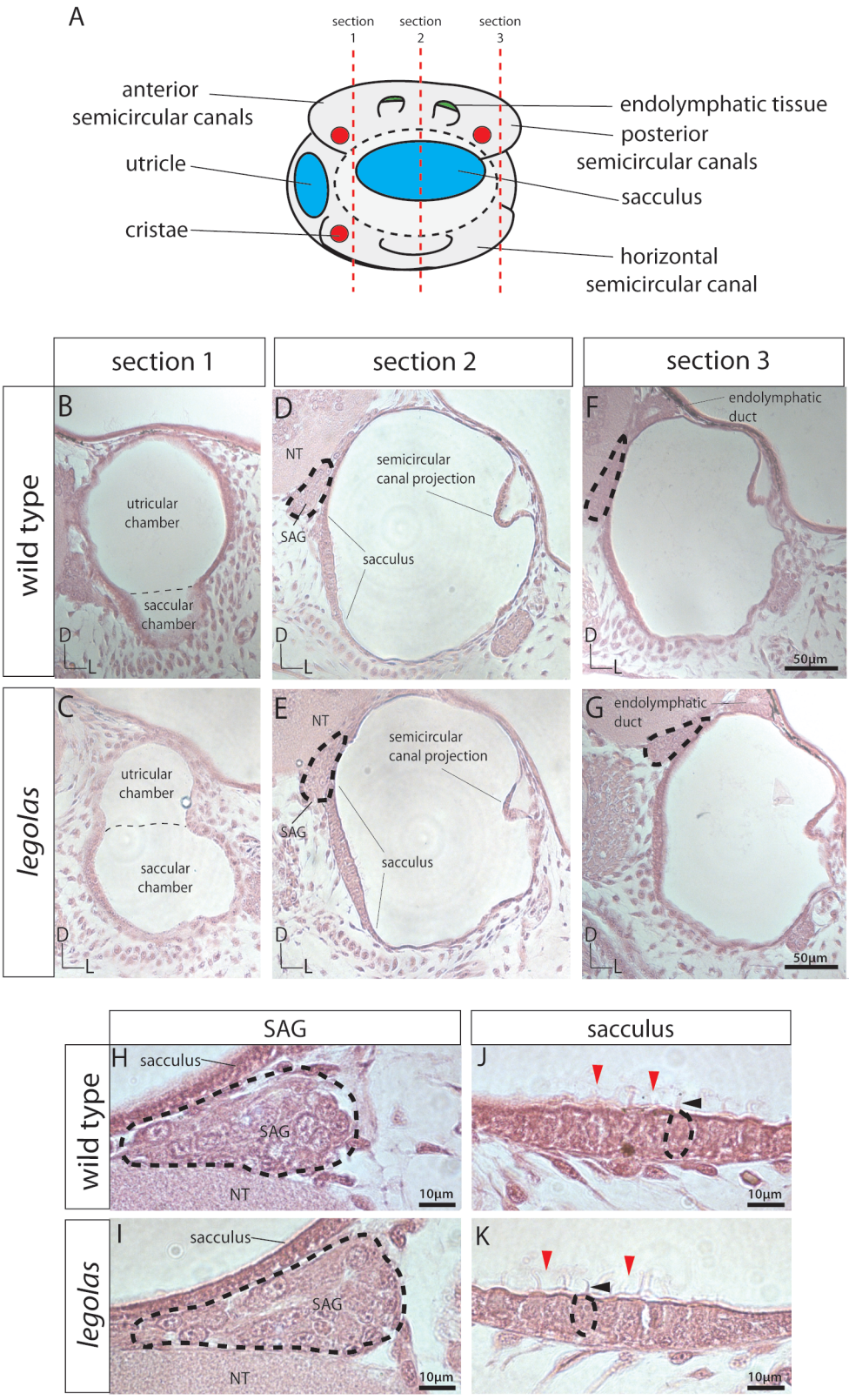

*3.2.4.3 Differentiation, patterning and innervation of the sensory epithelia are unaffected in leg tadpoles*

Fluorescein-tagged phalloidin staining of actin reveals that the size and location of the sensory epithelia in the inner ear do not appear to differ from wild type (fig. 3.16; B - C). When viewed at high magnification, the saccular hair cells are clearly surrounded by a ring of support cells in both *leg* and wild type (fig. 3.16 D - E). S-100 staining of the hair cell bodies also reveals that the hair cell size and density is comparable (fig. 3.16 F - G, J; p=0.58) and anti-acetylated tubulin staining of the innervating neurones also does not reveal any noticeable defects (fig. 3.16 H - I; neurone bundle I - red arrowhead; neurone bundle II – white arrowhead; neurone bundle III blue arrowhead).

*3.2.4.4 leg is linked to the q-arm of chromosome 5*

Out of a total of 219 gynogenetic tadpoles, 32 displayed the leg phenotype, allowing the mutation-centromere distance to be calculated at ~35cM (table 3.1). To determine which chromosome the *leg* lesion resides on, I assayed pools of DNA obtained from wild type and *leg* gynogenetic tadpoles for linkage to centromeric SSLP markers. Strong linkage is observed to marker 026H07, located near the centromere of chromosome 5 (fig. 3.16 A).

I assayed SSLP markers located on the p and q-arms of chromosome 5 for linkage to the *leg* lesion using pools of DNA obtained from wild type and *leg* gynogenetic tadpoles. Where possible I selected SSLP markers located on the same scaffolds as candidate genes. Gynogenetic *leg* tadpoles show linkage to several SSLP markers along the q-arm, with the strongest linkage observed to marker 017D07 (fig. 3.16 B).

*3.2.4.4 Conclusions*

At stage 45, *leg* tadpoles do not display any obvious external morphological defects other than the presence of enlarged otoconial crystals. Further investigation of the inner ear phenotype reveals that gross morphology, cellular patterning and innervation are unaffected. Although *leg* tadpoles may have broader defects not observed in the external phenotype, available data suggests

**(A)** Schematic of the utricular, saccular and cristae sensory epithelia plus the innervating neurones in stage 45 tadpoles. The "I" nerve bundle innervates the utricle and then branches to innervate the anterior and horizontal cristae. The "II" nerve bundle innervates the sacculus and the "III" nerve bundle innervates the posterior cristae.

**(B - C)** The hair cell stereocilia of the utricular (dashed lined) and saccular (dotted line) maculae, stained with fluoroscein-tagged phalloidin, are clearly visible in both wild type and *leg*.

**(D - E)** The saccular epithelial cells are clearly spaced so that each hair cell is surrounded by a ring of suport cells, as expected by classic notch-delta signaling.

**(F - G)** Hair cell size and density does not notably differ between wild type and *leg* tadpoles, as shown by S-100 staining of hair cell bodies.

**(H - I)** Anti-acetylated tubulin staining of the neurones innervating the macula and cristae sensory epithelia are present in both wild type and *leg* tadpoles (neurone bundle I - red arrowhead; neurone bundle II – white arrowhead; neurone bundle III blue arrowhead).

**(J)** In stage 45 tadpoles, the number of utricular and saccular hair cells does not differ between wild type and *leg* (hair cells counts carried out on S-100 antibody staining; n=4).

**Figure 3.16: Sensory epithelial patterning, differentiation and innervation appear unaffected in *leg* mutants**

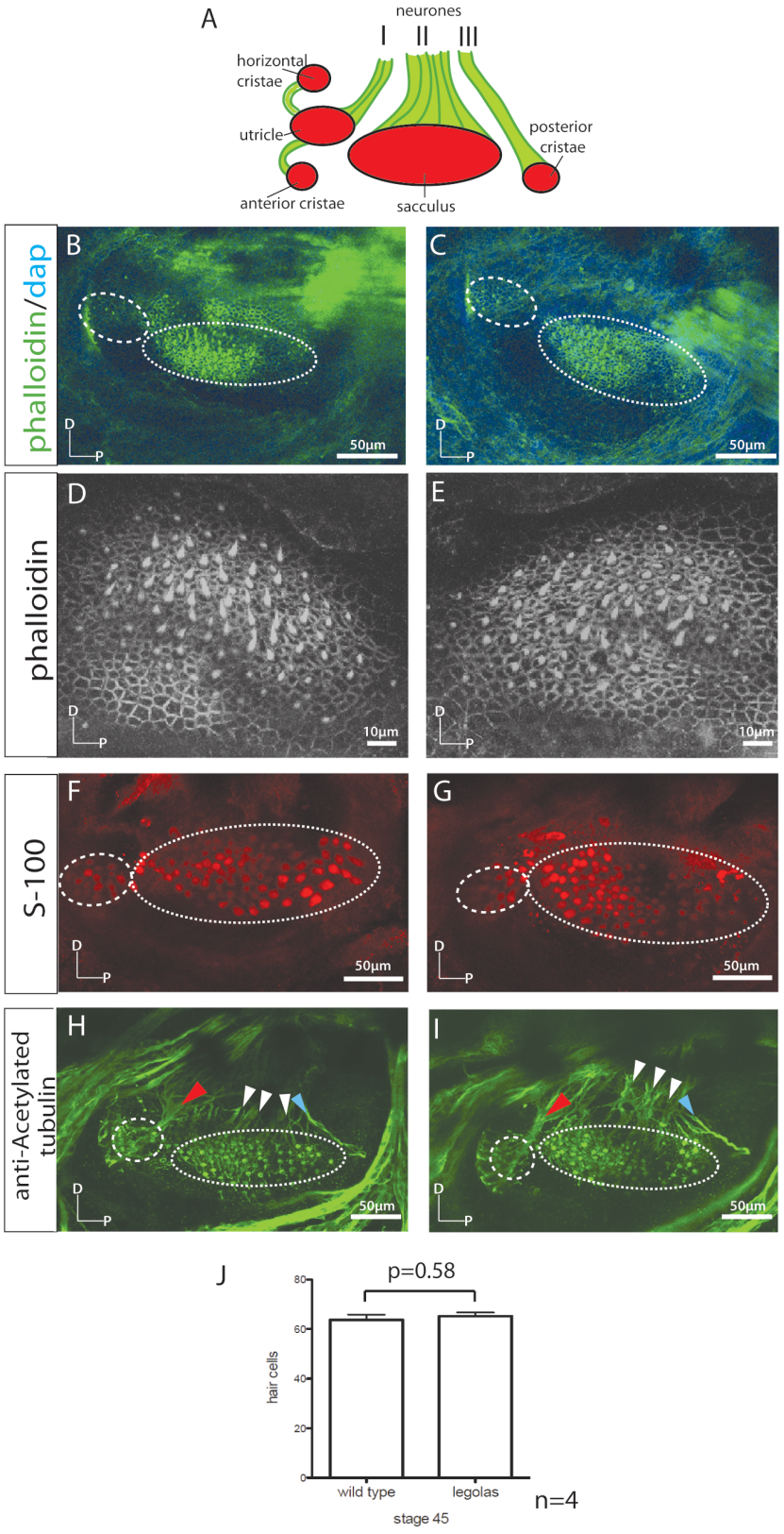

**Figure 3.17:** ***leg*** **shows linkage to the centromere of chromosome 4 in pools of gynogenetically derived embryos**

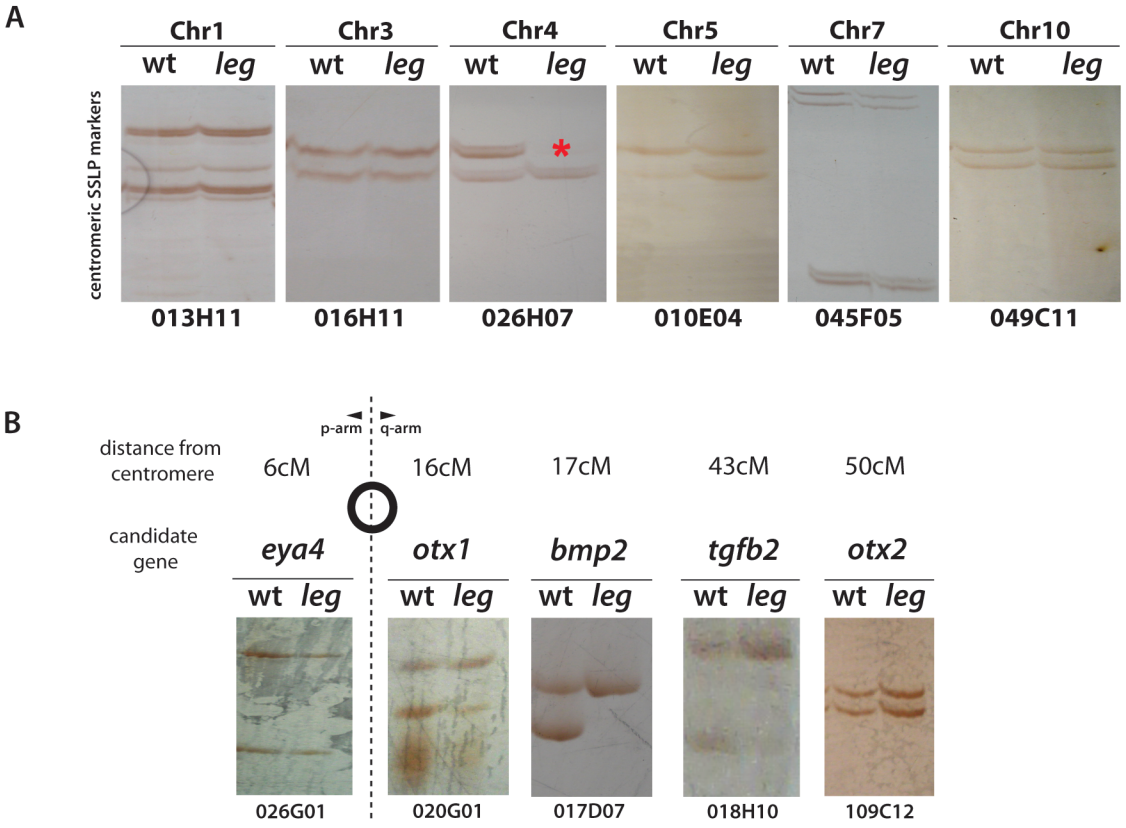


**(A)** Pools of gynogentically derived wild type and *leg* embryos were assayed for linkage to polymorphoric SSLP centromeric markers. *leg* exhibits linkage to the centromeric SSLP marker 045F05 on chromosome 4 ( "*" ). Chromosome 2, 6, 8 and 9 not assayed due to difficulty finding polymorphic SSLP markers.

**(B)** Pools of wild type and *leg* gynogenetic DNAs were assayed for linkage to polymorphic SSLP markers on the p- and q-arm of chromosome 4. Where possible, SSLP markers located close to candidate genes were selected. *leg* exhibited the strongest linkage to marker 017D07.

that the primary defect is in otoconial formation. Failure to synthesize and export otoconial proteins could cause the *leg* phenotype, as these proteins are required to regulate the growth of the otoconial crystals (see introduction section 1.6) (Ballarino et al., 1982; Pote et al., 1993; Wang et al., 1998).

The *leg* lesion is located ~35cM from the centromere on the q-arm of chromosome 5 and shows linkage to SSLP markers 017D07 and 018H10.

### *3.2.5 Characterization and low resolution mapping of the bunny (bun) mutant*

#### *3.2.5.1 External development of the bun inner ear*

The *bun* mutant has a small otic vesicle and only one sensory epithelium associated with otoconia, however the otoconia appear not to differ from wild type (fig. 3.18 A – F). The otic vesicle increases in size through stages 37 to 45, but always remains smaller than wild type (fig. 3.18 A - F). *bun* tadpoles also have strong balance defects such as circular swimming and difficulty reorientating themselves when turned upside down. Mutants are not viable and die at approximately stage 47.

#### *3.2.5.2 bun tadpoles have small dysmorphic otic vesicles containing a macular epithelium enlarged along the apical-basal axis*

Histological sections of stage 45 tadpoles show that the *bun* otic vesicle is smaller than that of wild type siblings. It contains only one chamber, housing a macular epithelium that is enlarged along the apical-basal axis (fig. 3.19 C - H). There are no epithelial projections developing out of the lateral wall of the otic vesicle (fig. 3.19 E - F), suggesting that the semicircular canals are not developing at this stage, however the endolymphatic duct is present (fig. 3.19 G - H). In wild type inner ears, the periphery of the otic vesicle is tightly associated with neural crest-derived cartilage, called the otic capsule, which provides structural support for the developing inner ear (fig. 3.19 C, E & G) (Quick and Serrano, 2005). In *bun* tadpoles, the otic capsule forms at a comparable location

**Figure 3.18: External phenotype of *bun* inner ear**

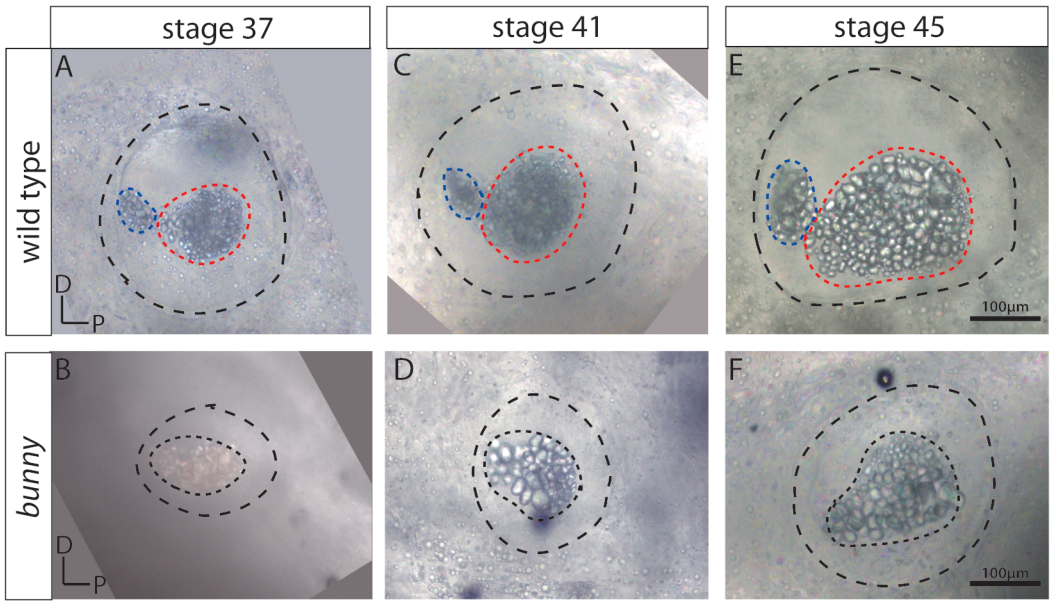


DIC images of *bun* otic vesicles.

**(A-F)** *bun* tadpoles have a small otic vesicle compared to wild type siblings and only one macula associated with otoconia. The *bun* otic vesicle increases in size throughout stages 37-45 but always remains smaller than wild type at corresponding stages. *bun* tadpoles also display vestibular behavioural defects such as circular swimming and an inability to correctly orientate themselves.

**(A-B)** Schematics of stage 45 wild type and *bun* inner ears.

**(C-H)** At stage 45, the otic vesicles in *bun* are greatly reduced in size. In wild type tadpoles, the periphery of the otic vesicle is in close contact with the cartilage of the otic capsule. In *bun* the otic capsule remains in the wild type location but the small otic vesicle is detached from it. Only one chamber is present, and it contains a greatly thickened saccular macula. The membranous projections of the developing semicircular canals are also absent; however, the endolymphatic duct does form. Images are orientated so that dorsal is to the top and lateral is to the right.

**(I-J)** The neuronal cell bodies of the SAG (black dashed lines) appear comparable in size to wild type, however they lack proximity to the NT and maculae due to the smaller size of the otic vesicle. The axons branching out from the SAG appear elongated in *bun* tadpoles (black arrowheads) compensating for the greater length between the NT and the maculae. Images are orientated so that lateral is to the top and ventral is to the right.

**(K-L)** The hair and support cells of the saccular macula display a columnar structure in both wild type and *bun* , however in *bun* the apical-basal length of these cells isgreatly increased (black dashed lines). The hair cell stereocilia are visible at the apical pole of the hair cells (black arrowheads) and the otoconial membrane (red arrowheads) is visible also. Images are orientated so that lateral is to the top and ventral is to the right.

**Figure 3.19:** ***bun*** **tadpoles exhibit small dismorphic otic vesicles and contain a single enlarged macula**

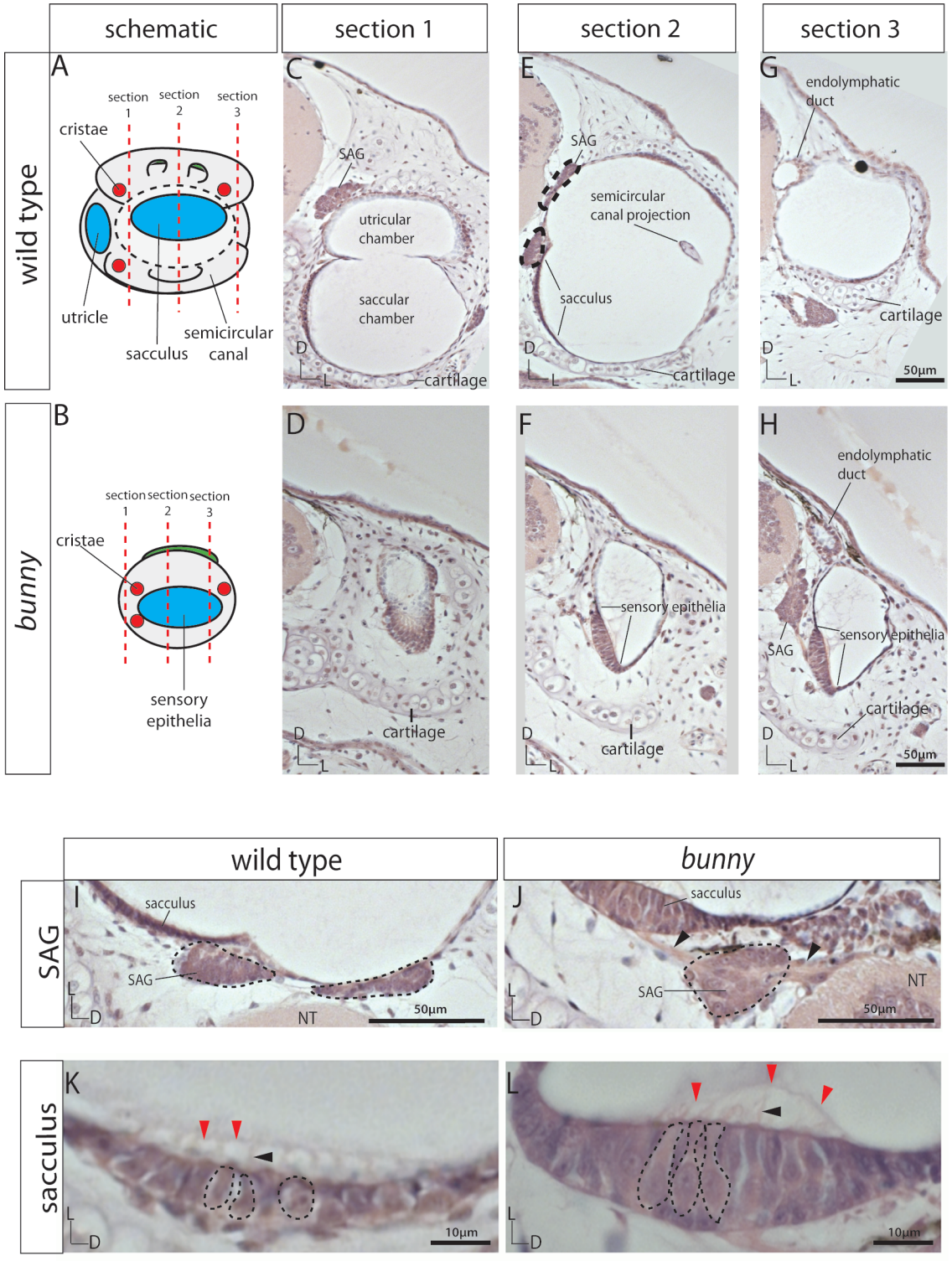

to the wild type but the small otic vesicle forms detached from the cartilage and is surrounded by mesenchyme tissue (fig. 3.19 D, F & H).

In stage 45 wild type tadpoles the neuronal cell bodies of the SAG form two lobes, one located dorsally and one ventrally, which develop in close association with the neural tube and the sensory epithelia that it innervates (fig. 3.19 E; black dashed line). In *bun* only one lobe is visible (fig. 3.19 H; black dashed line). Due to the decreased size of the otic vesicle, the SAG sits detached from the otic tissue and the neural tube, in the intervening mesenchyme cells. The axons connecting the SAG to the neural tube and the sensory epithelia are elongated to compensate for the greater distance (fig. 3.19 J; black arrowheads). The size of the neuronal cell bodies do not notably differ from the wild type. However, it difficult to discern from histological data whether the size of the whole SAG is abnormal in *bun* and wild type (fig. 3.19 G - H).

The hair cells of the *bun* macula exhibit apical-basal polarity, as stereocilia bundles are clearly visible at the apical pole (fig. 3.19 K – L; black arrowhead). Also, the hair and support cells form a columnar structure as observed in the wild type (fig. 3.19 K – L; black dashed lines). However the apical-basal axis is greatly elongated, creating a thickened epithelium (fig. 3.19 K - L).

*3.2.5.3 bun tadpoles develop fewer macular hair cells*

S-100 (fig. 3.20 G – H) and fluorescein-tagged phalloidin (fig. 3.20 C – D) staining of hair cell bodies and stereocilia respectively, show that there is no clear distinction between the utricular (fig. 3.20 C & G; dashed line) and saccular (fig. 3.20 C & G; dotted line) maculae in *bun* mutants (fig. 3.20 D & H; dashed line). It is not clear whether only one macular sensory epithelium has formed or whether the utricular and saccular macular are fused (fig. 3.20 D & H; dashed line). However acetylated tubulin staining shows that the neural bundle that innervates the utricule and the horizontal and anterior cristae is still present in *bun* mutants (fig. 3.20 J; red arrowhead). S-100 staining also shows that all three cristae form

**(A - B)** Schematics of the wild type and *bun* sensory epithelia and the nerve bundles innervating them. The "I" nerve bundle innervates the utricle and then branches to innervate the anterior and horizontal cristae. The "II" nerve bundle innervates the sacculus and the "III" nerve bundle innervates the posterior cristae.

**(C - D)** Hair cell stereociliary bundles of only one macula are visible by fluorescein-tagged actin staining in *bun* (note difference in scale between wild type and *bun*).

**(E -F)** The arrangement of hair and support cells complies with a classical notch-delta pattern in both *bun* and wild type.

**(G - H)** S-100 staining of hair cell bodies confirms the presence of only one macula, the location of which is comparable to the sacculus.

**(I - J)** The neurones innervating nerve bundles "I" (red arrowhead), "II" ( white arrowheads) & "III" (blue arrowheads) are present in both *bun* and wild type.

**(K - L)** S-100 staining, along with anti-Acetylated tubulin staining of the hair cell kinocilia, reveals that all three cristae are present in the *bun* inner ear.

**(M)** At stage 45, only ~65% of the wild type hair cells form in *bun* mutants (p=000.1).

**Figure 3.20: *bun* tadpoles produce fewer macular hair cells**

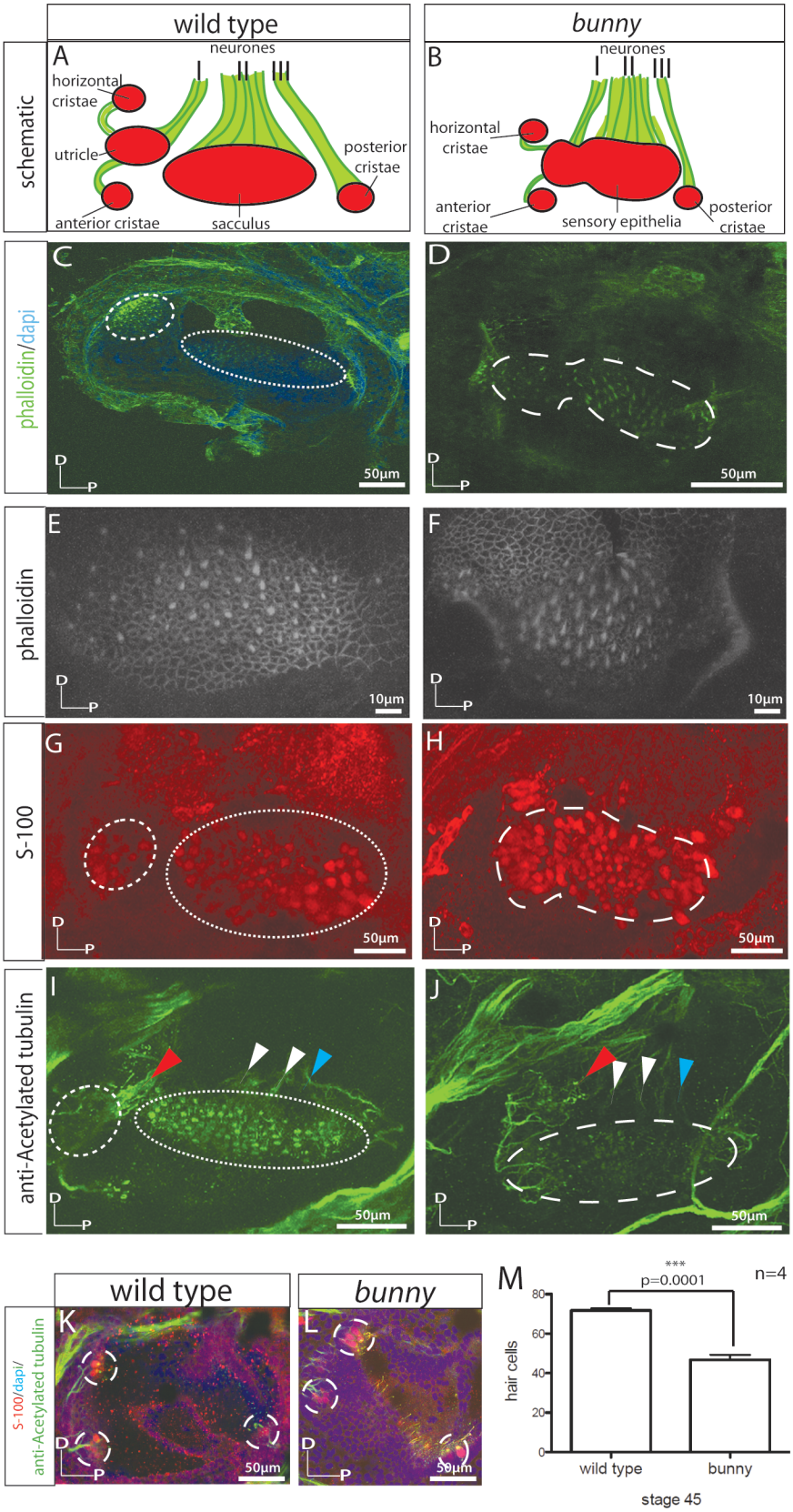

in *bun* mutants and acetylated tubulin staining shows they are innervated (fig. 3.20 K – L; dashed line).

Viewed at high magnification, fluorescein-tagged phalloidin staining shows that the classical notch-delta derived pattern of hair cells surrounded by support cells (see introduction section 1.4.3) is maintained in the *bun* macular epithelium (fig. 3.20 E – F). Fewer macular hair cells are present in stage 45 *bun* mutants compared to wild type siblings (S-100 positive cells counted; p=0.0001).

*3.2.5.4 bun is linked to the p-arm of chromosome 2*

Out of a total of 180 gynogenotes, 64 displayed the *bun* phenotype, allowing the distance to be calculated at ~14cM (table 3.1). Attempts to map the *bun* lesion to a chromosome by gynogenetic linkage to centromeric SSLP markers was unsuccessful due to difficulty identifying polymorphic markers in the female carriers. Instead linkage to SSLP markers was assayed in 40 individual *bun* tadpoles obtained from a conventional mating between *bun* carriers. Linkage of the *bun* allele to marker 043H07, which is located ~4cM from the centromere on the q-arm of chromosome 2 was identified, as only 3 recombination events were observed out of the 40 genomes assayed (fig. 3.21 A). Polymorphic SSLP markers located on other chromosomes are unlinked (data not shown).

SSLP markers located across the q-arm of chromosome 2 were assayed for recombination events in the same 40 *bun* tadpoles. Fewer recombination events were identified in markers located progressively closer to the centromere, however as the centromeric marker 133H07 displays 3 recombination events, this suggests that the *bun* lesion lies on the p-arm. SSLP markers on the p-arm could not be assayed as this entire region is missing from the current meiotic map (fig. 3.21 B).

*3.2.5.5 Conclusions*

In *bun* tadpoles the otic vesicles are smaller (fig. 3.18), at stage 45 there are ~35% fewer macular hair cells (fig. 3.20 M), and the macular cells are enlarged

## Figure 3.21: *bun* shows linkage to the p-arm of chromosome 2

A Chromosome 2 SSLP marker 043H07

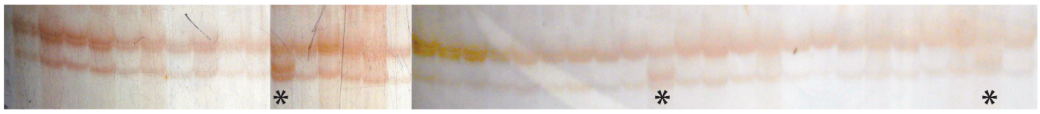

B

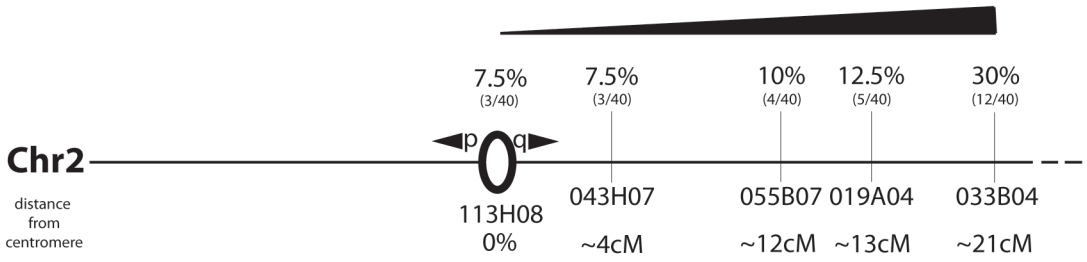


**(A)** Linkage of *bun* to chromosome 2 was identified as the SSLP marker 043H07 located onchromosome 2, displays only 3 recombination events out of the 40 *bun* genomes assayed. No linkage was observed to SSLP markers located on any other chromosome tested (data not shown).

**(B)** SSLP markers along the q-arm of chromosome 2 were assayed for recombination-events in the same 40 *bun* genomes. Fewer recombination events were observed in markers progressively closer to the centromere. The centeromeric SSLP marker 133H07 exhibits 3 recombination events out of the 40 genomes assayed, indicating that the *bun* lesion lies on the p-arm. SSLP markers on the p-arm have not been assayed as no scaffolds have been mapped to this arm.

along the apical-basal axis (fig. 3.19). At stage 45, the semicircular canals are failing to form (fig. 3.19), and there is no clear distinction between utricular and saccular maculae (fig. 3.20). However, patterning of the rest of the otic vesicle, such as the formation of the cristae (fig. 3.20 K - L), the neurones innervating the sensory epithelia (fig. 3.20 I - L), and the patterning of hair and support cells in the macular (fig. 3.20 E - F) does not appear to differ from wild type.

A possible cause of this phenotype is a defect in cell proliferation. Work carried out by Quick and Serrano (2007) shows that in *Xenopus laevis* there is a high level of proliferation at the edge of the macular epithelium and at the base of the developing semicircular canals, during stages 32 – 47. Reduced levels of cell proliferation could cause the utricular and saccular maculae to appear merged as the cells that spatially separate these two epithelia might not form, also causing failure of semicircular canals to develop. The increased size of the macular cells along the apical-basal axis could be the result of cells growing in preparation for division but then failing to divide. Analysis of BrdU incorporation into cells dividing in the otic tissue would help test this hypothesis.

The *bun* lesion is located on the p-arm of chromosome 2, ~14cM from the centromere. This is a poorly assembled region of the *X. tropicalis* genome as no scaffolds have been mapped to the entire p-arm. An improved meiotic map needs to be constructed before conventional positional cloning can be carried out on this mutation. Alternatively, it may be possible to identify the lesion by direct genomic sequencing of mutant embryos.

## *3.3 Discussion*

### *3.3.1 Phenotypes uncovered in the screen*

The pilot forward genetic screen of ENU-induced mutations revealed seven inner ear phenotypes in the gynogenetic progeny of the F1 generation, four of which

were successfully recovered in the progeny of the F2 generation. A range of phenotypes were uncovered, such as defects in the patterning of the otic tissue, the development of the maculae and the development of the otoconia. The underlying lesions of the four confirmed mutants were found to reside on different chromosomes, and therefore the phenotypes must be the product of mutations affecting different genes.

Screening for otoconial defects was a successful strategy as six of the seven phenotypes were identified due to crystal malformations. Otoconial formation relies on the correct development of many cell types, such as the hair and support cells of the maculae, to produce the correct ionic environment for crystal growth and to synthesize the crystal components (reviewed in Hughes et al., 2006; Lundberg et al., 2006). This means that otoconia provide a useful indicator of broader inner ear phenotypes, such as defects in the maculae, which were identified without being directly screened for. Surprisingly, in *bun* mutants, the otoconial crystals did not differ in size or morphology from the wild type, despite the malformation of the gross structure if the inner ear and the macular defect.

Although these phenotypes were primarily identified due to defects in the inner ear, it is likely that some of the phenotypes will be the result of broader developmental defects. The hindbrain plays an essential role in inducing and patterning the otic tissue (see introduction section 1.3), therefore it is conceivable that an inner ear defect may be secondary to a defect in this tissue. The zebrafish *valentino* (*val*) mutant, which encodes a bZip transcription factor, provides a good example. In *val* mutants anterior-posterior patterning of the hindbrain is disrupted which in turn affects patterning of the inner ear (Kwak et al., 2002). The *val* transcript is only expressed in the hindbrain, yet when the mutant is viewed externally the inner ear defect is the most striking phenotype (Kwak et al., 2002).

The neuromasts of the lateral line and the inner ear hair cells are structurally very similar and share many of the same developmental pathways (reviewed in Baker

et al., 2008; Streit, 2001). Therefore it is not surprising that in the large-scale screens for inner ear mutant phenotypes in the zebrafish defects in the neuromasts were detected too (Whitfield et al., 1996; Malicki et al., 1996). The function of the lateral line is to detect vibrations in the water, allowing the animal to detect movements nearby (Bleckmann et al., 1989; Dijkgraaf, 1963). In the *kom* mutant, tadpoles often fail to respond to vibration or physical stimuli, therefore it can be hypothesized that the lateral line may exhibit defects as well.

In several vertebrate screens, it has been noted that pigmentation defects are often associated with problems with hearing and balance (Hardisty-Hughes et al., 2010; Malicki et al., 1996; Whitfield et al., 1996). Pigmentation and hearing are associated due to the presence of neural crest-derived melanophores (melanocytes in mammals) that reside in a region of the inner ear called the strial vascularis where they help regulate the ionic environment (Wangemann et al., 1995). The *ssk* mutant has a melanophore defect as well as abnormal otoconial development, therefore it is possible that the inner ear phenotype may be caused by a melanophore defect.

### *3.3.2 Advantages and limitations of the forward genetic screen*

#### *3.3.2.1 ENU-mutagenesis*

ENU induces point mutations through the alkylation of nucleic acids, causing nucleotide mis-pairing and base substitution during DNA replication, or substitution of the alkylated base with another base (Balling, 2001; Goda et al., 2006). A single lesion is likely to only affect one gene by altering the coding sequence, however it is possible that an animal may carry many lesions affecting different genes. As with any type of mutagenesis, the concentration of the mutagen needs to be titrated so that mutant phenotypes can be recovered without polluting the genetic background with lesions.

The F1 founder female carrying the *ssk* lesion was found to also carry a second mutation causing paralysis of the heart, designated *muzak* (*muz*) (Abu-daya et

al., 2009). Low resolution positional cloning determined that both lesions reside on the p-arm of chromosome 1. Due to the close proximity of the two lesions, many individuals had to be screened to segregate the *ssk* mutation. The *leg* F1 founder also carried a mutation affecting cranial facial development, designated *boxers eye* (*bxe*). Positional cloning determined that these lesions reside on different chromosomes and so only ~1/2 of the F2 carriers of either lesion carried both (Zimmerman laboratory unpublished data). Although the remaining mutants didn't show any obvious additional phenotypes, it is still possible that these animals carry other mutations that cause subtle defects. However, *ssk*, *kom* and *bun* are all recovered in sibling crosses in a Mendelian ratio, supporting the hypothesis that a single gene mutation is responsible for the phenotype.

*3.3.2.2 Production of a mosaic F1 generation*

Out of the seven phenotypes identified in the F1 population, only four were recovered in the progeny of the F2 generation. One explanation is that the phenotype may not have an underlying genetic cause and therefore cannot be inherited. Another possibility is that the F1 founder female could display a high level of mosaicism (see section 3.1.1). This means that if the remaining three phenotypes do have an underlying genetic cause, it is possible that only a small fraction of the F2 population has inherited the lesion. Large numbers of individuals need to be screened in order to determine whether the phenotype is heritable and therefore has an underlying genetic cause. Mosaicism could have been eliminated by mutating spermatogonia *in vivo*, however this method causes a high mortality rate in the treated male frogs and is also difficult to tritrate as unlike *in vitro* mutagenesis dominant F1 mutant phenotypes are not visible (Zimmerman laboratory unpublished data).

*3.3.2.3 Gynogenesis creates a bias to uncovering centromeric linked loci*

Screening the gynogenetic progeny of the F1 founding population is advantageous over a standard three-generation screen, as only one generation intervenes between mutagenesis and screening (section 3.1.2; fig. 3.2), saving on time and husbandry. However, this strategy creates a bias to uncovering

lesions located proximal to the centromere. Lesions located close to the centromere have a low probability of recombination events occurring between them, causing homozygosity to be maintained and a larger proportion (up to 50%) of gynogenetic embryos will be phenotypically mutant (see section 3.1.4.2; fig. 3.4 B) (Goda et al., 2006; Khokha et al., 2009). Embryos homozygous for lesions located distally from the centromere will be produced at a lower frequency, as intervening crossover events are more likely (Goda et al., 2006; Khokha et al., 2009). A standard three-generation screen would remove this bias, as mutations caused by lesions located across the genome would be uncovered in equal frequencies. However the mosaicism caused by mutating post-meiotic sperm means that very large numbers of F2 couples would have to be mated and screened, meaning that this strategy is not compatible with *in vitro* mutagenesis. Despite this bias, the gynogenetic screen has recovered a number of mutations (e.g. *kom*), which map to the most distal parts of the genome, suggesting that this strategy is not limited to centromeric regions.

### *3.3.3 Advantages and limitations of the X. tropicalis genome assemblies and meiotic map*

The *X. tropicalis* genome assembly used throughout this project consists of over 19,000 scaffolds, 272 of which cover 50% of the genome and are each over 1.56Mb in size (Hellsten et al., 2010). A subset of the larger scaffolds are arranged into linkage groups, and the approximate genetic distance from one another predicted using SSLP linkage analysis to create a meiotic map (Wells et al., 2011; http://tropmap.biology.uh.edu/). Scaffolds incorporated into the meiotic map are predicted to cover ~66% of the physical genome (Wells et al., 2011), so some regions of the map have gaps where no scaffolds had been positioned. In this assembly *ssk* resides in a region with a high density of mapped scaffolds, the *kom* and *leg* lesions are in regions where mapped scaffolds are sparser, and the *bun* lesion is located on a chromosome arm where no scaffolds have been mapped. The density of mapped scaffolds in the region of the meiotic map that the lesions are located will greatly influence the ease in which mutations can be

mapped by positional cloning. Throughout the project the *X. tropicalis* genome assembly has undergone several revisions and recently the newest version of the assembly consists of chromosome-sized scaffolds, which will greatly aid positional cloning.

### *3.3.4 Future studies*

The focus of this screen was to identify phenotypes affecting organogenesis and axial patterning. However, inner ear development begins during gastrulation when the presumptive otic tissue receives inductive signals from the mesoderm migrating beneath it (see introduction section 1.4.1). In order to study the entire development of the inner ear, screening embryos at earlier time points is necessary. Studying early phenotypes is difficult in a gynogenetic screen, as distinguishing by morphological inspection between non-specific gastrulation defects and those caused by an underlying genetic lesion can be very difficult. Early phenotypes would be more easily detected in a standard three-generation screen, as phenotypes would be expected in Medialian ratios, suggesting an underlying genetic cause. Also, screening for expression of a specific panel of genes, such as *pax2*, *fgf3* and *otx2*, by *in situ* hybridization could provide a more sensitive strategy for identifying earlier defects.

The ability to visualize hair cells in live embryos would allow detailed analysis of sensory hair cell development. A parvalbumin-3 GFP *X. tropicalis* transgenic has recently been developed in the Grainger lab (personal communication) and is expressed specifically in the hair cells of the inner ear and in the neuromasts of the lateral line. Crossing the parvalbumin-3 GFP transgenic line with mutant lines that have known sensory epithelial defects, such as *kom* and *bun*, would allow real-time analysis of the mutant's epithelial development. Also, mutagenesis carried out on the parvalbumin-3 GFP transgenic line would enable focused screens to be carried out to identify defects on the developing sensory epithelia.

### *3.4 Summary*

A group of seven candidate inner ear mutant phenotypes were identified in the gynogenetic progeny of a mutagenized population of *X. tropicalis*, four of which were recovered in the progeny of the F2 population. These mutant phenotypes include defects in the size and morphology of the otoconial crystals, size of the otic vesicle, development of the semicircular canals, and development of the sensory epithelia. Low-resolution mapping confirms that these mutations reside on different chromosomes and therefore affect different gene functions.

The next two chapters of this thesis focus on identifying the lesions and the biological processes responsible for the *ssk* and *kom* phenotypes. A conventional positional cloning approach will be adopted to map the effected lesions, and further characterization of the phenotypes will be undertaken to understand the biological function of the mutated gene.

# Chapter 4

## The *Xenopus tropicalis* mutant *seasick* (*ssk*) disrupts adapter protein-3 function

## 4.1 Introduction

The *seasick* (*ssk*) phenotype is characterized by enlarged otoconia, lack of iridophore pigmentation and small melanophores that are punctate in appearance. Tadpoles also have difficulty balancing and are unable to orientate themselves correctly while swimming. In the previous chapter I determined that the lesion causing the *ssk* phenotype is located on the p-arm of chromosome 1 (see section 3.2.2.4). I also showed that structural defects in the inner ear are limited to the development of the otoconia in stage 45 *ssk* tadpoles (see section 3.2.2).

In this chapter I aim to uncover the lesion responsible for the *ssk* phenotype by carrying out high resolution positional cloning and sequencing of candidate genes. I also further characterize the otoconial and pigmentation defects to help identify the mechanisms that may be defective in *ssk* mutants.

## 4.2 Gross phenotypic characterization of the seasick (ssk) mutant

### 4.2.1 *ssk* tadpoles have enlarged otoconia and reduced melanophore and iridophore pigmentation

The *ssk* phenotype is first visible at stage 37, when melanophores on the flank and head appear small and punctate compared to wild type (fig. 4.1 A - B; dashed lines, C - D), and the otoconia are slightly enlarged (fig. 4.1 E - F; dashed line). At stage 45, *ssk* melanophore pigmentation remains punctate (fig. 4.1 G - J), however a small proportion of pigment can be seen at the periphery of the cell (fig. 4.1 I - J). Otoconia are visibly much larger than wild type (fig. 4.1 K & L), and tadpoles begin to exhibit balance defects. By stage 54, *ssk* tadpoles have fewer melanophores, and the melanophores contain less pigment than in wild type (fig. 4.1 M & N). The melanophores located in the inner ear also contain less pigment

**(A - F)** Stage 37 *ssk* tadpoles have small punctate melanophores located on their flank, tail and head (D dashed line & E), compared to the large stellate melanophores that develop in wild type (A dashed line & B). The otoconial crystals (C & F dashed lines) are also slightly enlarged in *ssk*.

**(G - L)** Stage 45 wild type melanophores are highly pigmented and stellate, while *ssk* melanophores are smaller, punctate and have less pigment (H & K). Otoconial crystals are clearly much larger than the wild type (I & L dashed lines).

**(M - V)** Stage 54 *ssk* tadpoles have fewer melanophores than wild type tadpoles (M & P).The iridophores located over the gut and heart severly lack pigmentation (N & Q) and the melanophores located in the otic vesicle also have decreased levels of pigmentation compared to wild type (O & R dashed line).

**Figure 4.1: *ssk* external phenotype**

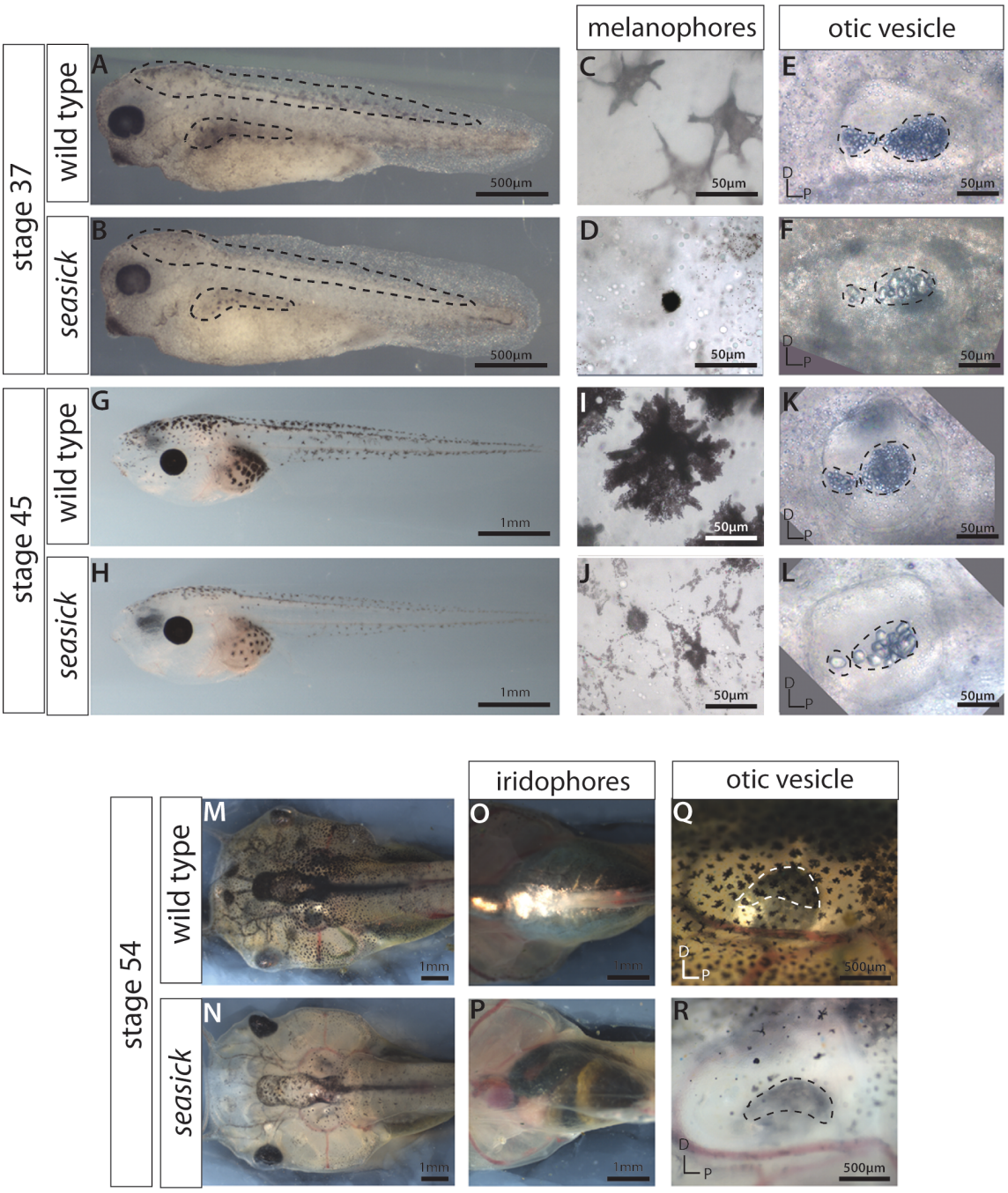

(fig. 4.1 Q & R) and the iridophores, located over the heart and gut, also lack pigmentation (fig. 4.1 O & P).

### *4.2.2 Excessive otoconial growth in ssk*

To observe otoconial morphology, I dissected otoconia out of wild type and *ssk* tadpoles and observed them under a brightfield microscope at stages 37, 41, 45 and 54 (n=5). At stage 37, otoconial crystals appear slightly enlarged compared to wild type (fig. 4.2 A – B; table 4.1), by stage 41 the difference in crystal size is more pronounced (fig. 4.2 C – D; table 4.1) and by stage 45 *ssk* otoconial crystals begin to fuse (fig. 4.2 E – F; table 4.1). By stage 54, the *ssk* otoconia have formed large aggregates that fill most of the inner ear (fig. 4.2 G – H; table 4.1).

To investigate the association of the otoconial crystals with the apical surface of the macular sensory epithelia, I took transverse sections through the sacculus of stage 45 wild type and *ssk* tadpoles, and stained them with haematoxylin and eosin. In wild type tadpoles, a large number of small otoconia form in close contact with the apical surface of the sacculus (fig. 4.2 I), while in *ssk*, the enlarged otoconia are in contact with a much smaller region (fig. 4.2 J).

### *4.2.3 Macular sensory epithelial development is not affected in ssk*

Otoconial development relies on the cells of the macula to synthesize otoconial proteins, such as otolin (Murayama et al., 2005), and to create an ionic environment in which calcium carbonate can crystallize (Crouch & Schulte, 1996; Dou et al., 2004; Kozel et al., 1998; Shiao et al., 2005) (see introduction, section 1.5). In the previous chapter no macular defects were detected in stage 45 *ssk* tadpoles (see chapter 3 section 3.2.2). However the maculae are well developed

**Table 4.1: Comparison of wt and *ssk* otoconial crystal length**

| Stage | | Mean (μm) | Standard deviation | N | Range (μm) |
|---|---|---|---|---|---|
| 37 | wt | <1 | - | 5 | <1 |
| | *ssk* | 2.4 | 1.1 | 5 | <1 – 4 |
| 41 | wt | 1.8 | 1.1 | 5 | <1 – 3 |
| | *ssk* | 3.2 | 1.7 | 5 | ~1 – 5 |
| 45 | wt | 2.1 | 2.1 | 5 | <1 – 6 |
| | *ssk* | 24.4 | 10.6 | 5 | 10 – 50 |
| 54 | wt | 7.4 | 7.6 | 5 | 1 – 20 |
| | *ssk* | 90 | - | 1[§] | 90 |

[§] Only 1 stage 54 *ssk* tadpole was sampled as few *ssk* tadpoles survive to this stage.

**Figure 4.2**: *ssk* tadpoles exhibit excessive otoconial growth

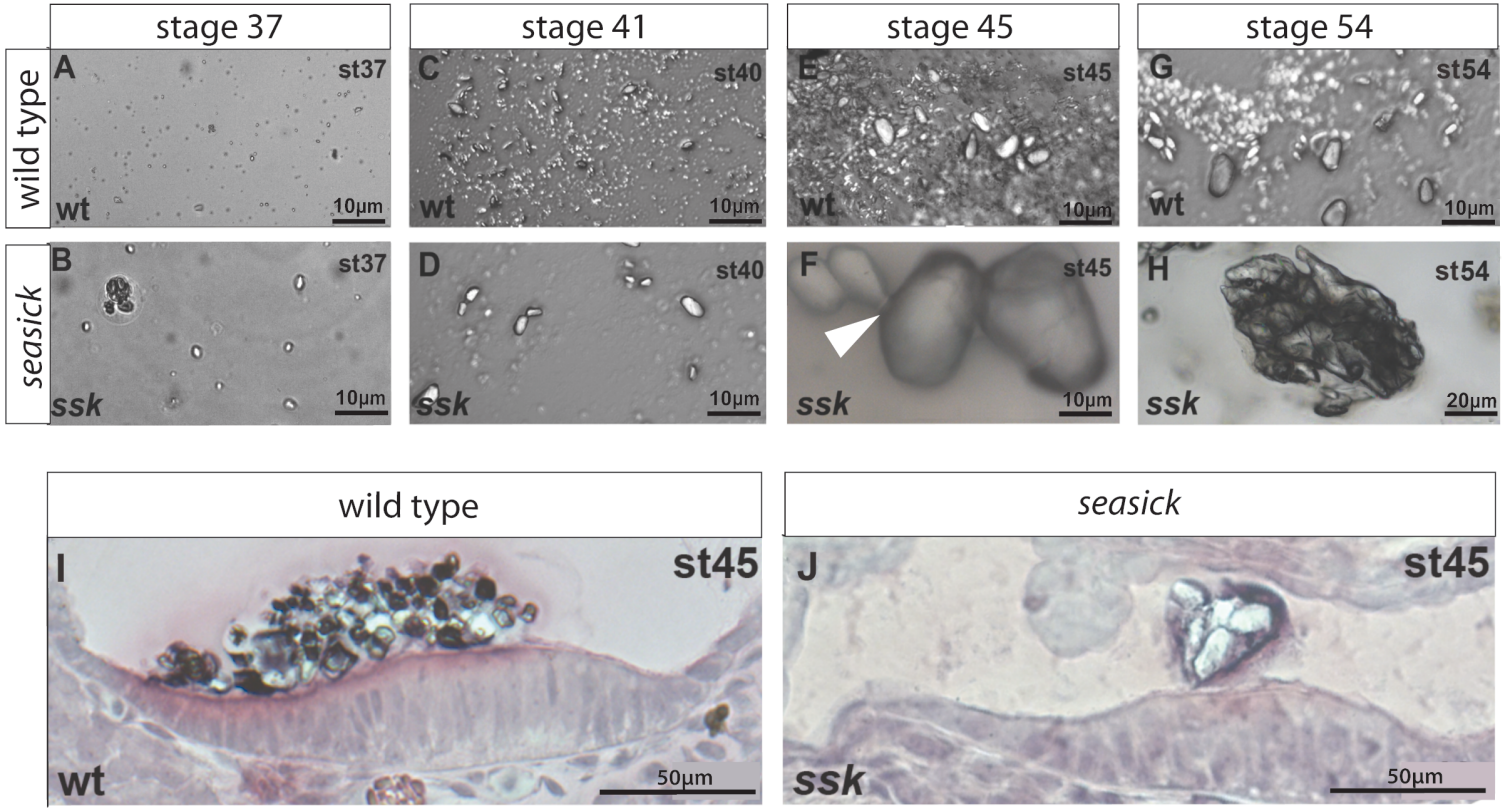


**(A - H)** Otoconia dissected out of wild type and *ssk* tadpoles at stages 37,41, 45 and 54 and imaged under brightfield microscopy. *ssk* otoconia grow excessively and fuse to form large agglomerates.

**(I- J)** Transverse sections through the sacculus of stage 45 tadpoles stained with haemotoxylin and eosin. Sections show that wild type otoconia are in close contact along the whole apical surface of the sacculus while the large otoconia found in *ssk* have limited contact with the sensory epithelium**.**

**(A - I)** At stage 37, the hair cells in both the utricle and the sacculus are visible in both wild type and *ssk* tadpoles ( A - C).Throughout stages 41 and 45 the utricle and sacculus increases in size in both wild type and *ssk* (D - I) and by stage 45 the cristae are visible (G - I). The locations of each sensory epithelium are comparable between wild type and *ssk*.

**Figure 4.3: Hair cell differentiation and patterning is unaffected in *ssk* embryos**

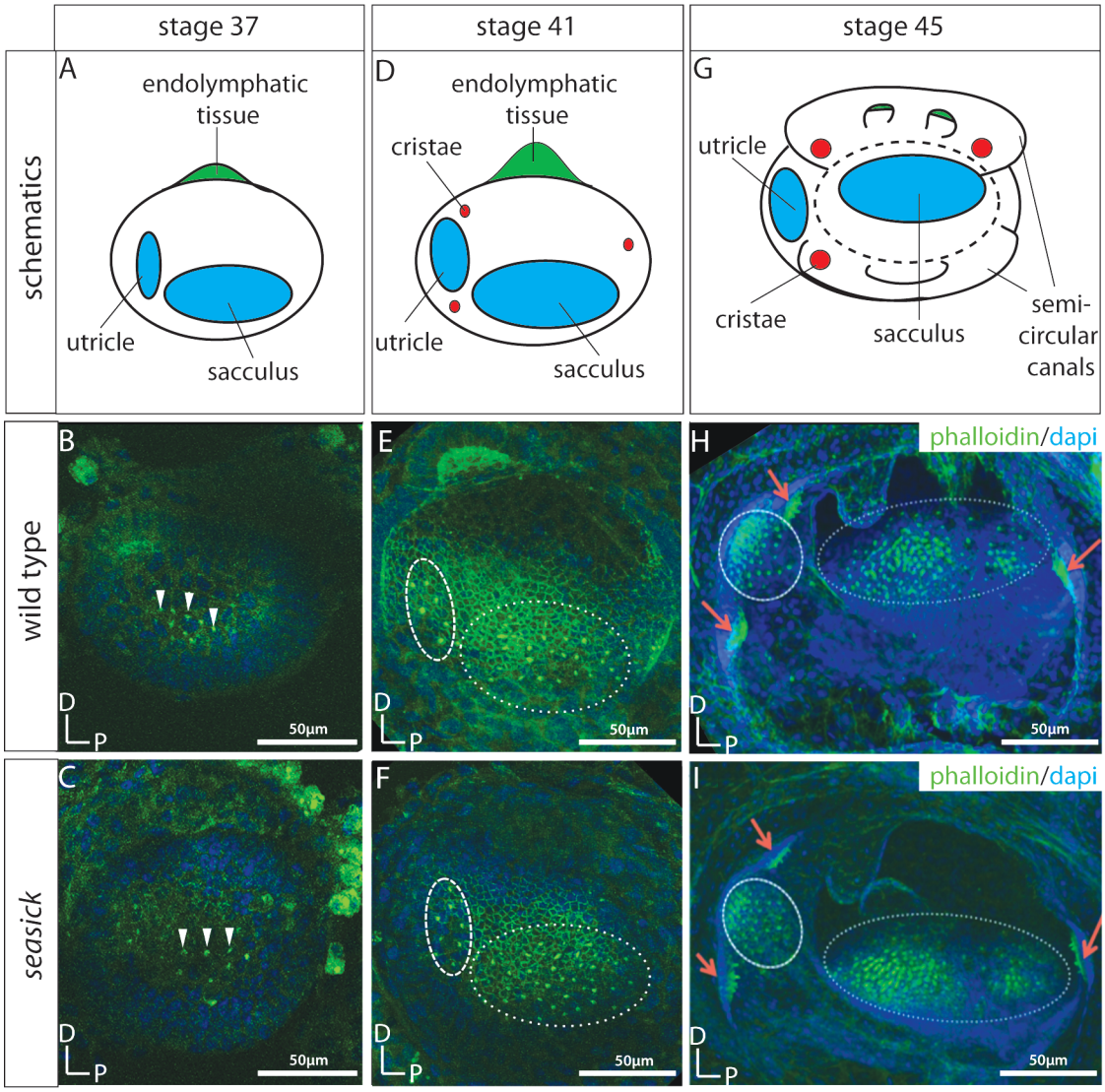

at this stage, and it is possible that earlier defects, such as a delay in macula formation, may be responsible for the otoconial defect. To determine whether *ssk* otoconial phenotype is caused by a defect in the spatial or temporal development of the maculae, I used fluorescein-tagged phalloidin to stain cell boundaries and hair cell stereocilia bundles.

At stage 37, the hair cells of the utricle and sacculus are clearly visible in both wild type and *ssk* tadpoles (fig. 4.3 A - C). Throughout stages 41 and 45 the maculae increase in size in both wild type and *ssk* (fig. 4.3 D - I), and by stage 45, the three cristae are visible as well (fig. 4.3 G - I). The locations of each of the sensory epithelia are comparable between wild type and *ssk* (fig. 4.3 A - I).

### *4.2.4 Neural crest specification and migration is unaffected in ssk*

*Ssk* tadpoles have defective melanophores and iridophores, which are both derivatives of the neural crest. To determine whether *ssk* mutants have any defects in other neural crest derivatives, I evaluated the expression of markers of neural crest specification, migration and differentation.

To observe neural crest induction and migration, I looked at the expression of the neural crest marker *slug* (Mayor et al., 1995) by WISH at stages 13 (n=50) and 22 (n=50). The *ssk* phenotype cannot be identified morphologically before stage 37, so if defects in neural crest induction and migration occur in *ssk*, these would be seen in a Mendelian ratio (1:3) in embryos from crosses of carriers. I did not detect any differences in the level of *slug* expression or the pattern of migrating neural crest cells (fig. 4.4; D & G; black arrowheads), suggesting that neural crest induction and migration is unhindered in *ssk* embryos (fig. 4.4 A - F).

The head cartilage and the peripheral nervous system (PNS), like melanophores and iridophores, are derived from neural crest precursor cells. I examined cartilage

**Figure 4.4: Neural crest specification and migration is unaffected in *ssk* embryos**

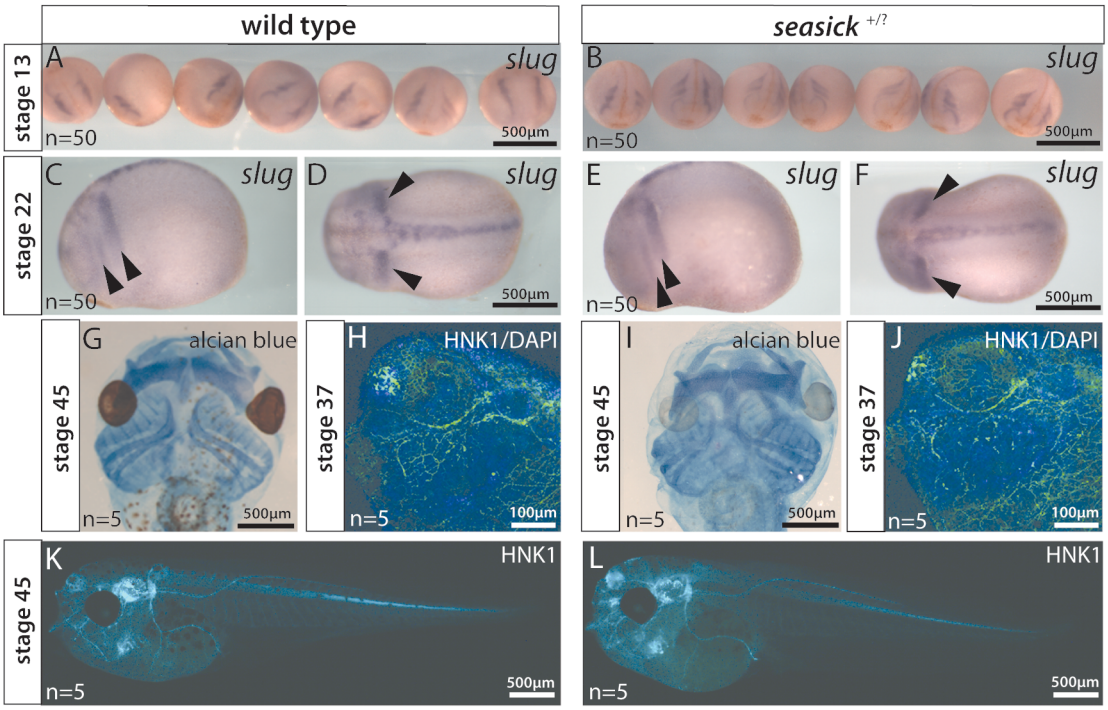


**(A-F)** *slug* WISH carried out on pools of 50 wild type and 50 *ssk* embryos, at stages 13 (A & B) and 22 (C - F) shows no detectable difference in pattern of neural crest migration (C - F black arrowheads) or the level of expression (representative images of embryos displayed).

**(G & I)** Cartilage stained using alcian blue in stage 45 tadpoles shows no detectable differences in *ssk* compared to wild type.

**(H, J, K - L)** Peripheral nervous system stained with anti-HNK1shows no difference.

formation by staining stage 45 tadpoles with alcian blue, thus revealing that the patterning of this structure does not differ in *ssk* from wild type (fig. 4.4 G & I) (n=5). HNK-1 antibody staining of the PNS at stage 37 (fig. 4.4 H - J; n=5) and 45 (fig. 4.4 K - L) (n=5) likewise showed no defects in neural formation or patterning. The *ssk* tadpoles also respond to touch, indicating that the PNS is functioning correctly.

### *4.2.5 Normal melanophore morphology in ssk suggests defective melanosome formation and trafficking*

I investigated melanophore morphology to determine whether the phenotype is the result of a defect in the gross cellular morphology or if it is specific to pigment biogenesis. *Dopachrome tautomerase* (*dct*) encodes an enzyme required for melanin synthesis and is expressed at high levels throughout melanophores (Guyonneau et al., 2004). Fluorescent WISH for *dct* was carried out to act as a marker for the cell morphology. Melanin is synthesized and held in small intracellular vesicles called melanosomes that can be visualized under brightfield microscopy. The cells were imaged using fluorescent and brightfield confocal microscopy to ascertain the morphology of the melanophores and the sub-cellular location of the melanosomes.

In stage 37 wild type melanophores, the melanosomes vary in location from being aggregated centrally in the cell (fig. 4.5; A white arrowhead) to being dispersed throughout the cell (fig. 4.5; A red arrowhead) (n=5). Stage 37 *ssk* melanophores are comparable in size and morphology to wild type. However no melanosomes are visible in many *ssk* melanophores (fig. 4.5 B; white arrowhead), and in cells where they are visible, the melanosomes are aggregated centrally in the cell (fig. 4.5 B; green arrowhead) (n=5). In stage 41 and 45 tadpoles this phenotype is more pronounced. Wild type melanophores are highly dendritic with densely packed melanosomes located throughout the

**Figure 4.5: Normal melanophore morphology suggests defective vesicular trafficking in *ssk***

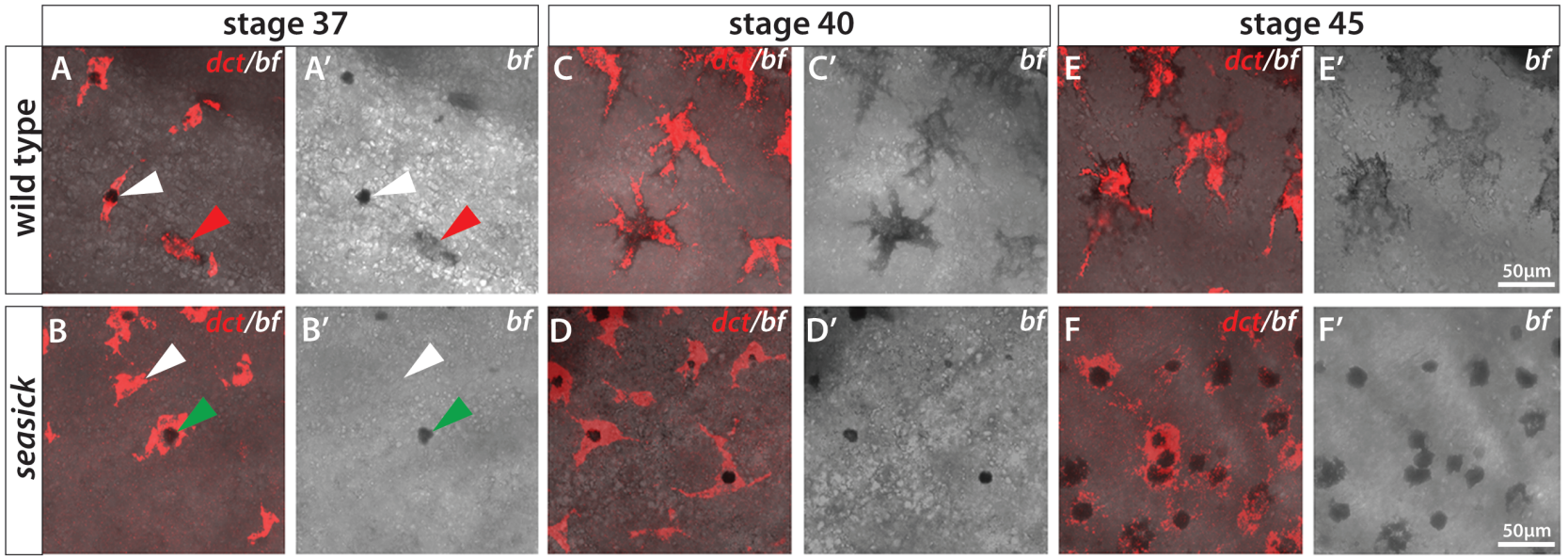


**(A-F)** Confocal mircroscopy images of dorsal cranial melanophores, stained by fluorescent WISH for *dopochrome tautomerase* (*dct*) (red) and merged with brightfield images. This demonstrate that *ssk* melanophores display a normal dendritic morphology, but abnormal melanophore distribution, creating a punctate appearance.

cell, while *ssk* melanophores are also dendritic but the melanosomes are fewer and clearly aggregated centrally in the cell (fig. 4.5 C - F) (n=5).

## *4.3 Identification and confirmation of the ssk lesion*

### *4.3.1 ssk maps to a 3.5Mb interval containing ap3δ1*

To identify the gene responsible for the *ssk* phenotype, positional cloning was carried out to locate the affected genetic locus. In the previous chapter I discovered that the *ssk* lesion shows linkage to SSLP marker 018E09 on the p-arm of chromosome 1 (see chapter 3 section 3.2.2.4). To locate the genomic region encompassing the lesion, I analyzed single *ssk* tadpoles, obtained from a sibling cross, with polymorphic SSLP markers located on the telomeric and centromeric sides of 018E09. Analysis shows that markers 021H07 on scaffold_158 and 021H03 on scaffold_555 flank the *ssk* lesion (fig. 4.6). To refine this interval, more markers were analyzed in the region between these two flanking markers until analysis of 1021 mutants revealed 6 and 6 recombination events for markers 028D11 and 123G04, respectively (fig. 4.6). This defines a genetic interval of 3.5Mb in which the *ssk* lesion is located (fig. 4.6) spanning 4 scaffolds (112, 327, 386 and 289) in the version 4.1 genome assembly. These scaffolds are known to reside in this interval as the sequences of these scaffolds align with the recently released version 7 genome assembly, which consists of chromosome-sized scaffolds. A total of 57 gene models are predicted to reside in this region (table 4.1).

SSLP markers 327_1 and 327_4, located on scaffold_327, are linked strongly to the *ssk* lesion as no recombination events occur in the 1021 tadpoles analyzed (fig. 4.6). I evaluated the gene models of scaffold_327 and identified adapter protein-3 delta subunit (*ap3δ1*), a gene 309kb from marker 327_4, as a strong candidate gene (fig. 4.6). *ap3δ1* encodes the delta subunit of the adapter protein-3 (AP – 3) complex, which is involved in intracellular protein transport (Simpson

**Figure 4.6: *ssk* maps to a 3.5 Mb interval on the p-arm of chromosome 1**

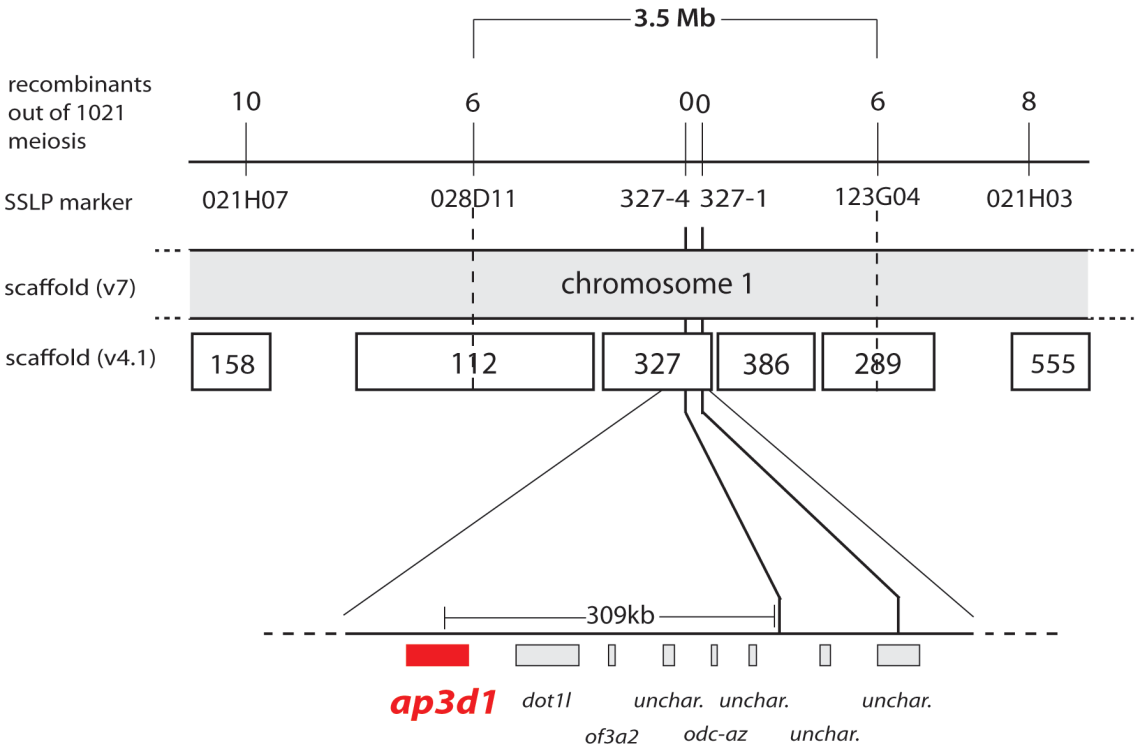


Analysis of polymorphic SSLP markers on the p-arm of chromosome 1 identified markers 021H07 on scaffold_158, and 021H03 on scaffold_555, as flanking the mutation. Further analysis of of markers in this interval narrowed down the region to 3.5Mb, flanked by markers 028D11 on scaffold_112 and 123G04 on scaffold_289.

The 3.5Mb interval spans scaffolds 112, 327, 386 and 289. Polymorphic SSLPmarkers on scaffold_327 yield no recombinants, suggesting strong linkage to the *ssk* lesion. *ap3δ1* is a strong candidate gene as the mouse mutant mocha is phenotypically similar to *ssk*. *ap3δ1* is located 309kb from marker 327_4 .

## Table 4.2: Genes located in the *ssk* genetic interval

| Gene | Scaffold | Location | Name/Function |
|---|---|---|---|
| *unchar.* | 112 | 1,324,640 – 1,355,086 | - |
| *sall1* | 112 | 1,977,950 – 1,996,411 | *Spalt*-like, zinc finger protein |
| *cyld* | 112 | | cylindromatosis (turban tumor syndrome) |
| *arl2bp* | 112 | 2,336,404 – 2,350,977 | GTPase associated factor |
| *rspry1* | 112 | 2,355,970 – 2,385,891 | E2 ubiquitin conjugating enzyme |
| *unchar.* | 327 | 1 – 38,650 | - |
| *unchar.* | 327 | 87,391 – 94,754 | tyrosine kinase |
| *unchar.* | 327 | 159,588 – 160,745 | - |
| *lingo3* | 327 | 195,358 – 197,172 | Ig-domain transmembrane protein |
| *oaz1* | 327 | 228,097 – 235,189 | ornithine decarboxylase antizyme |
| *sf3a2* | 327 | 283,522 – 291,179 | mRNA splicing factor |
| *plekhjl* | 327 | 291,325 – 302,480 | Pleckstrin homology |
| *dot1* | 327 | 312,093 – 365,543 | histone methyltransferase |
| *unchar.* | 327 | 349,197 – 375,561 | - |
| *unchar.* | 327 | 383,549 – 384,804 | - |
| ***ap3d1*** | **327** | **415,707 – 456,586** | **protein trafficking** |
| *mobk12a* | 327 | 505,063 – 516,745 | Cell cycle associated protein |
| *csnklg2* | 327 | 651,966 – 676,797 | casein kinase |
| *unchar.* | 327 | 713,675 – 905,275 | - |
| *unchar.* | 327 | 697,676 – 705,296 | - |
| *ankle1* | 327 | 742,573 – 811,015 | oncogene |
| *arhgef18* | 327 | 841,981 – 874,583 | Rho/Rac guanine nucleotide exchange factor |
| *unchar.* | 327 | 967,161 – 984,100 | galactosyltransferase |
| *lsm4* | 327 | 1,002,241 – 1,012,043 | mRNA splicing factor |
| *unchar.* | 327 | 1,189,012 – 1,206,043 | - |
| *tox3* | 327 | 1,262,210 – 1,285,683 | neuronal survival factor |
| *unchar.* | 386 | 36,960 – 52,467 | - |
| *unchar.* | 386 | 67,532 – 70,677 | K+ channel |
| *rps28p9* | 386 | 156,869 – 160,031 | ribosomal protein |

| Gene | Scaffold | Location | Name/Function |
|---|---|---|---|
| *kank3* | 386 | 173,547 – 190,629 | tumor suppressor factor |
| *angpyl4* | 386 | 279,031 – 286,816 | - |
| *rab11b.1* | 386 | 306,309 – 317,005 | oncogene |
| *rab11b.2* | 386 | 310,923 – 346,624 | oncogene |
| *march2* | 386 | 322,776 – 330,622 | ubiquitin ligase |
| *lonp1* | 386 | 348,675 – 364,096 | degrades oxidatively damaged proteins in mitrochondria |
| *unchar.* | 386 | 409,365 – 412,094 | - |
| *med11* | 386 | 559.670 – 565,244 | RNA polymerase II factor |
| *ndufa11* | 386 | 575,414 – 579,450 | NADH dehydrogmease complex |
| *vmac* | 386 | 583,754 – 585,572 | intermediate filament associated factor |
| *caps* | 386 | 596,034 – 600,035 | calcium activated protein |
| *ranbp3* | 386 | 608,631 – 637,070 | TGFb signaling factor |
| *slcla6* | 386 | 665,703 – 676,430 | - |
| *unchar.* | 386 | 692,250 – 693,346 | - |
| *rfx2* | 386 | 698,760 – 712,622 | spermatogonogensis |
| *acsbg2* | 386 | 762,920 – 777,832 | acyl-CoA synthetase |
| *mllt1* | 386 | 7783,911 – 794,046 | - |
| *acer1* | 386 | 796,817 – 819,226 | alkaline ceramidase |
| *anp32c* | 386 | 839,371 – 846,384 | histone acetylation |
| *myolf* | 386 | 881,978 – 911,161 | - |
| *adamtsl0* | 386 | 941,122 – 994,543 | - |
| *zap70* | 386 | 1,010,945 – 1,035,199 | protein kinase |
| *unchar.* | 289 | 279 – 19,361 | - |
| *unchar.* | 289 | 29,596 – 45,474 | - |
| *efna2* | 289 | 227,992 – 326,625 | boundary formation |
| *unchar.* | 289 | 362,937 – 364,031 | - |
| *cirbp* | 289 | 385,657 – 388,465 | cold inducible RNA binding protein |
| *midn* | 289 | 452,441 – 461,637 | neurogenesis factor |

et al., 1996; Le Borgne et al., 1998). *ap3δ1* is one of many genes implicated in the human pathology Hermansky-Pudlak Syndrome. The mouse *ap3δ1* null, *mocha*, shares several features with the *ssk* phenotype. Both *ssk* and *mocha* have decreased levels of melanophore pigmentation (melanocytes in mammals), have balance problems and develop defective otoconia, although in *mocha* small abnormal otoconia form (Simpson et al., 1996; Le Borgne et al., 1998; Kantheti et al., 1998) instead of the fused enlarged crystals observed in *ssk*.

### *4.3.2 ssk encodes a mutant allele of adapter protein-3 delta subunit (ap3δ1)*

I sequenced *ap3δ1* cDNA from pools of five wild type and five *ssk* tadpoles to determine whether *ssk* encodes a mutation in this gene. This revealed a thymine to guanine transversion at base pair position 283 (fig. 4.7 A), 4 bases 3' from the beginning of exon 10 (fig. 4.7 B). The *ssk* lesion abolishes a leucine codon and replaces it with a premature stop codon (fig. 4.7 A), causing any AP3δ1 protein synthesized to be truncated from 1160 residues down to 287 (fig. 4.7 C). The premature stop codon is located in the head domain of AP3δ1, deleting the hinge and ear domains in *ssk* (fig. 4.7 C).

### *4.3.3 Morpholino-mediated knockdown of AP3δ1 phenocopies the ssk phenotype*

To confirm that a deficit in AP3δ1 function is responsible for the *ssk* phenotype, I injected antisense morpholino oligonucleotides, designed to target *ap3δ1* mRNA, into wild type embryos. One morpholino targets the translation start site ATG and the second blocks splicing at the exon 10/intron 10 junction (fig. 4.8 A). I injected the morpholinos into embryos at the 2-cell stage. In one set of experiments I injected morpholinos bilaterally, and in a second experiment I injected morpholinos unilaterally, to provide an internal control.

**(A)** Sequence analysis of *ap3δ1* cDNA obtained from a pool of **(i)** 5 wild type sibling and **(ii)** a pool of 5 *ssk* embryos reveals a thymine to guanine transversion at position 283 (3′ from the transcriptional start site). This abolishes a leucine codon and replaces it with a premature stop codon.

**(B)** The lesion is located on the fourth base of exon 10.

**(C)** Schematic of the AP3δ1 protein domains and the truncated peptide synthesized in *ssk* mutants.

**Figure 4.7:** ***ssk*** **interval contains a truncated allele of adapter protein-3 delta subunit (*ap3δ1*)**

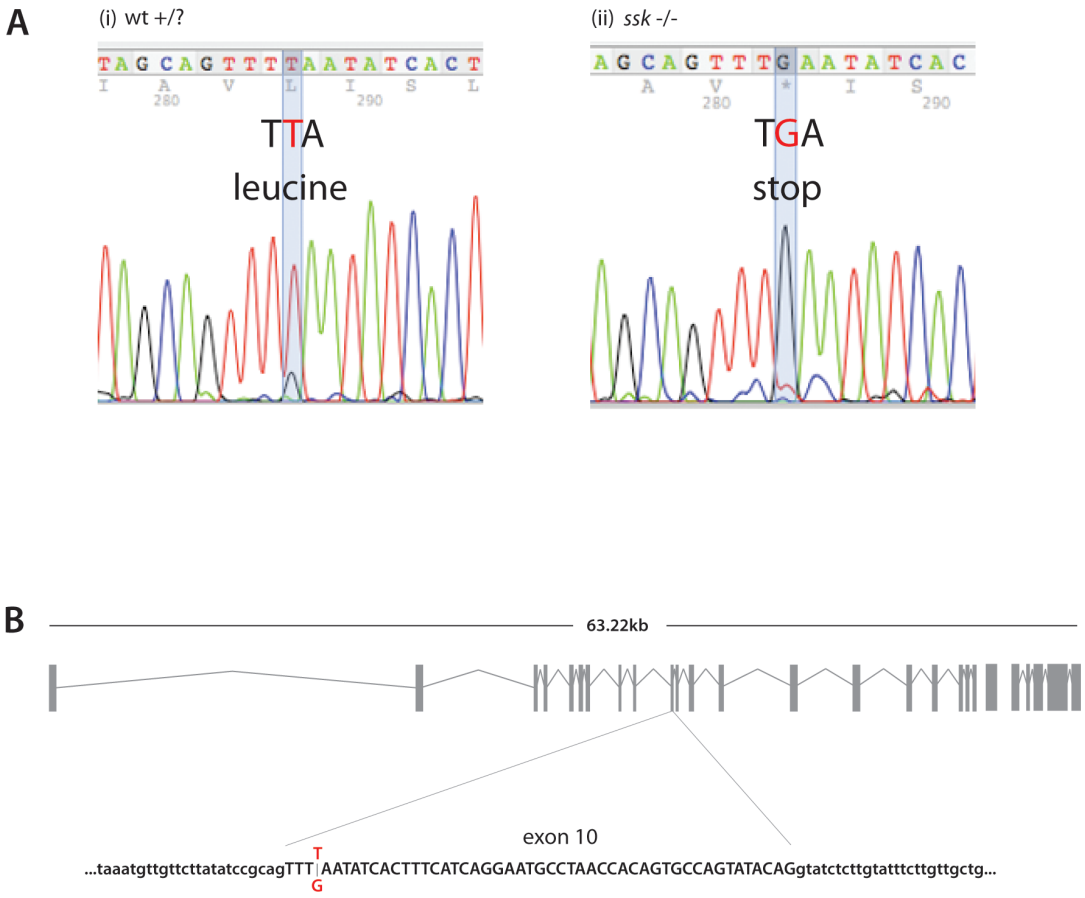

**(A)** MO-targeted locations in the *ap3δ1* transcript.

**(B-C)** Embryos injected with a control morpholino all display a wild type phenotype.

**(D-E)** *ssk* embryos display decreased levels of melanophore pigmentation and enlarged otoconia.

**(F-G)** ATG-morpholino injected embryos displayed hypopigmented melanophores and enlarged otoconia (bilateral injection shown – 39/42 p = 0.0001).

**(H-I)** Exon10/Intron10 splice blocking morpholino (bilateral injection shown – 19/30 p = 0.0001).

**(J)** **(i)** Schematic of primer locations flanking intron 10 **(ii)** PCR amplification of region spanning intron 10.

**Figure 4.8: *ap3δ1* morpholinos phenocopy *ssk***

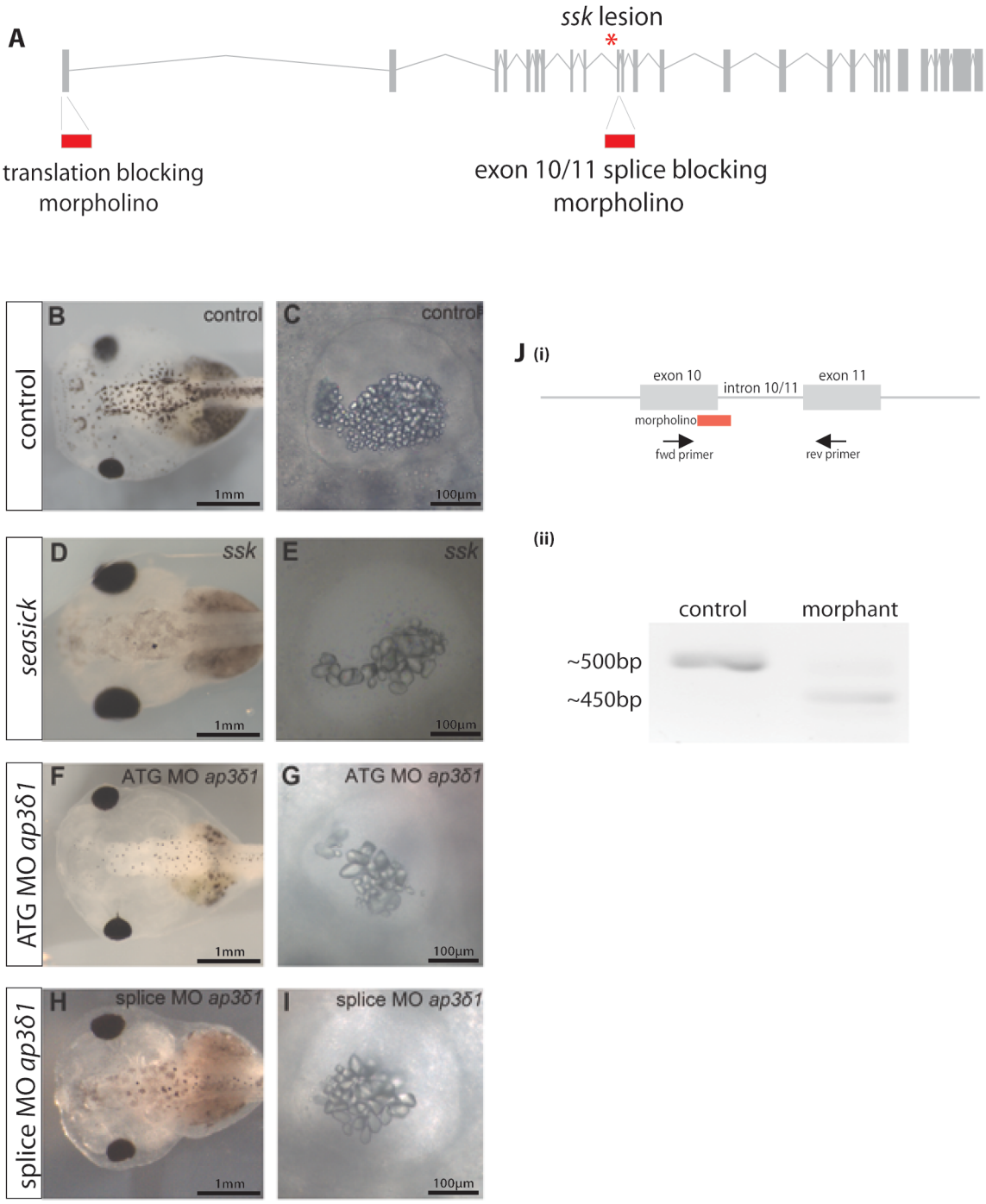

**Table 4.3: Injection of *ap3δ1* morpholino**

| Morpholino | Concentration (ng/embryo) | Unilateral or bilateral injection | Number of phenocopies | P value |
|---|---|---|---|---|
| **ATG-MO *ap3δ1*** | 10ng | Bilateral | 9/16 (56%) | 0.0001 |
| **ATG-MO *ap3δ1*** | 5ng | Unilateral | 7/25 (28%) | 0.0002 |
| **Splice blocking – MO ATG-MO *ap3δ1* (exon10/intron 10)** | 10ng | Bilateral | 39/42 (92.8%) | 0.0001 |
| **Splice blocking – MO ATG-MO *ap3δ1* (exon10/intron 10)** | 5ng | Unilateral | 19/30 (63%) | 0.0001 |
| **Control-MO** | 10ng | Bilateral | 0/142 (0%) | - |
| **Control-MO** | 5ng | Unilateral | 0/52 (0%) | - |

Injection of both the translation blocking and the splice blocking morpholinos caused a significant number of morphants to phenocopy *ssk* (fig. 4.8 B – I; table 4.2). Also, unilaterally injected embryos only phenocopy the mutation in one half of the tadpole (table 4.2). To confirm the efficiency of the splice blocking morpholino, PCR primers designed to flank intron 10 were used to amplify cDNA synthesized from bilaterally injected morphants. All morphants tested show ~50bp increase in amplicon size, consistent with a failure to splice out intron 10 from the mRNA (fig. 4.8 J).

### *4.3.4 Developmental expression profile of ap3δ1*

To determine the spatial and temporal expression pattern of *ap3δ1,* I carried out WISH on wild type embryos at a range of developmental stages. RT-PCR carried out on wild type eggs shows that *ap3δ1* is expressed maternally (fig 4.9 A) and WISH shows that transcripts are localized to the animal pole of stage 8 blastula embryos (fig 4.9 B - C). Expression then becomes localized to the neural plate during neurulation (stage 13) (fig. 4.9 D - F).

At stage 26, *ap3δ1* is strongly expressed in the dorsal region of the otic placode (fig. 4.9 G - H; red arrowhead). Weaker expression is also visible in the neural tube (fig. 4.9 G - H; black arrowheads), hindbrain (fig. 4.9 G - H; black arrowheads), eye, and the migrating neural crest cells (fig. 4.9 G - H; purple arrowheads). By stage 30, *ap3δ1* expression remains strongest in the dorsal otic tissue (fig. 4.9 I - J red arrowhead, K red dashed line), however a weaker expression domain has expanded to encompass the entire otic tissue (fig. 4.9; black dashed line). Expression in the dorsal and ventral neural tube, hindbrain, eye, and neural crest becomes more pronounced, and expression in the developing pronephros (fig. 4.9 I; blue arrowhead, L; blue dashed line) becomes visible (fig. 4.9 I - L). By stage 34, *ap3δ1* is expressed at lower levels throughout the otic tissue, while expression remains high in the neural tube, hindbrain, eye, neural crest and pronephros (fig. 4.9 M - P). In stage 41 tadpoles, otic *ap3δ1*

**(A)** RT-PCR (27 cycles) carried out on wild type eggs shows that *ap3δ1* is maternally expressed.

**(B - T)** *ap3δ1* WISH carried out on wild type embryos on a range of stages (n=25, representative images shown).

At blastula stages *ap3δ1* is expressed in the animal pole (B & C) and by neurula stages is expressed in the neural ectoderm (D-F) and remains expressed in the neural tissue at all stages investigated (G - H, I - J, M - N, S - T black arrowheads).

From the otic placode at stages through to the formation of the otic vesicle at stage 30, *ap3δ1*is strongly expressed in the dorsal region of the otic tissue (G - K red arrowheads; M red dashed line). By stages 34 and 41, *ap3δ1* is expressed broadly thoughout the otic tissue at lower levels.

*ap3δ1* is also strongly expressed in the pronephros (I, M & Q blue arrowhead; L, P & T blue dashed line) and neuromasts (S green arrowheads) and at lower levels in the migrating neural crest cells (I & M purple arrowheads).

**Figure 4.9: *ap3δ1* wild type expression profile**

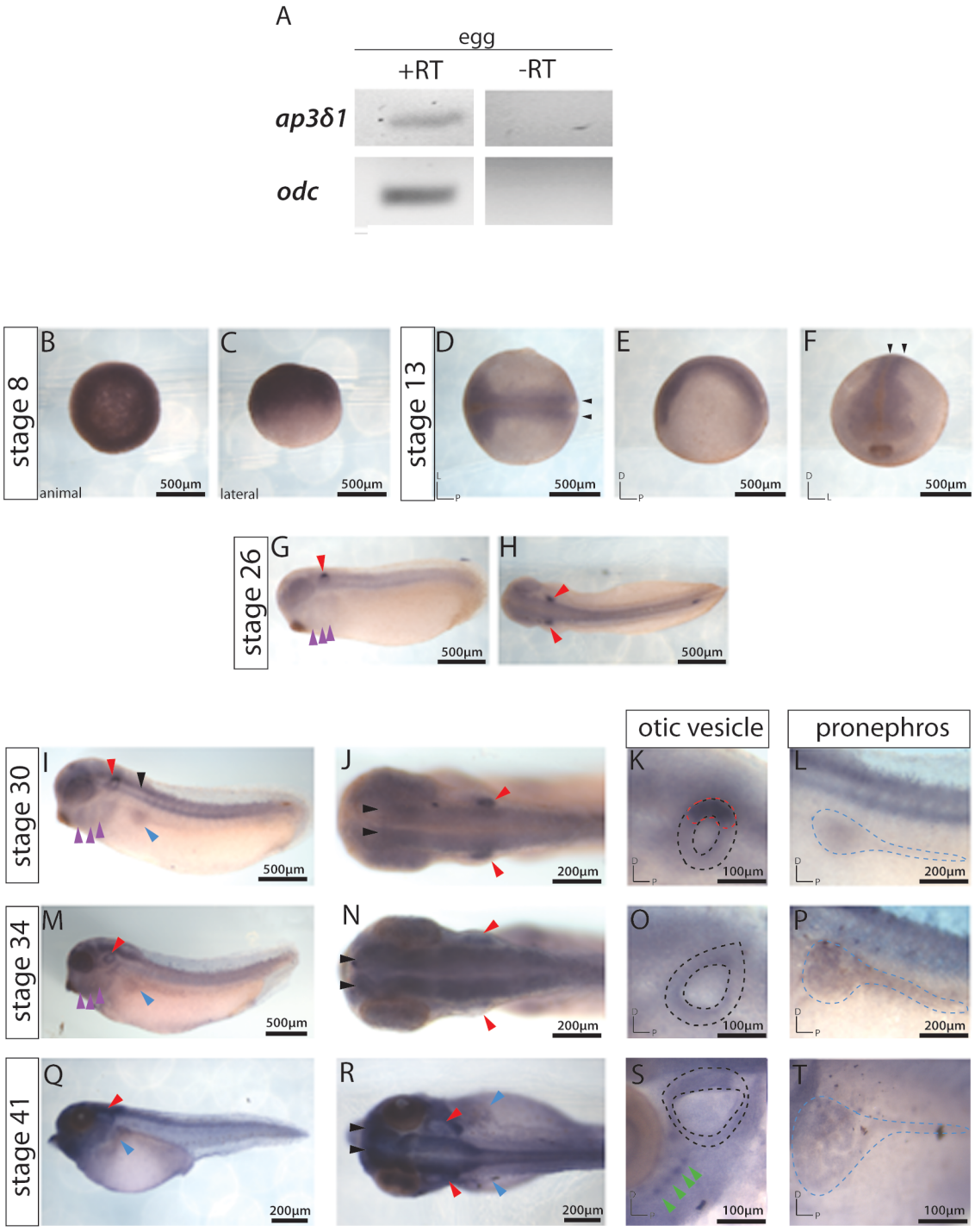

expression is at its highest in the endolymphatic tissue (fig. 4.9 Q - T red arrowhead), and high expression is also observed in clusters of cells in the same region as the neuromasts (fig. 4.9 S green arrowheads). High levels of expression are maintained in the eye, hindbrain, dorsal neural tube and the pronephros (fig. 4.9 Q - T).

## *4.4 Molecular characterization of the ssk phenotype*

### *4.4.1 AP3δ1 is part of a heterotetrameric complex required for vesicle formation, protein cargo recognition and intracellular translocation*

AP3δ1 exists as one subunit in the AP-3 heterotetrameric complex (fig. 4.10 A). AP-3 consists of two large subunits, δ and β, along with an intermediate subunit μ and a small subunit, σ. The subunits are assembled so that the $NH_2^-$terminal domains of the δ and β subunits along with the μ and σ subunits form the "head" out of which protrude the adaptin COOH-terminal "ear" domains, connected by a flexible "hinge" (fig. 4.10; A).

AP-3 is one of four identified adapter protein complexes, all of which are involved in recognizing and transporting proteins throughout the intracellular environment (Robinson & Bonifacino, 2001). Each consists of homologous β, μ and σ subunits and a unique large subunit, such as the AP-3 δ subunit (fig. 4.10 A). In each AP complex, the "head" domain is involved in cargo recognition and the "ear" and "hinge" domains of the β subunit recognize vesicular coat proteins such as clathrin (fig. 4.10 B - C) (Robinson & Bonifacino, 2001). The AP-3 complex is primarily involved in transporting protein cargo from the endosome and golgi complex to lysosome-related organelles (LROs) (fig. 4.10 D) (Dell' Angelica et al., 1999; Kantheti et al., 1998; Theos et al., 2005). LROs contain lysosomal proteins but also have cell type specific components that are required for specialized functions (Dell' Angelica et al., 1999; Kantheti et al., 1998; Theos et al., 2005).

**(A)** Schematic of the basic structure of heterotetrameric adapter protein (AP) complexes. All four AP complexes consist of a β, σ and μ subunit but differ in the fourth containing either a γ, α, δ or ε subunit.

**(B)** The head of the AP complex recognises and interacts with specific protein cargo

**(C)** The "ear" domain of the β-subunit binds to vesicular coat proteins, such as clathrin. The AP complex and the vesicular coat proteins assemble to form a coated pit and in turn a vesicle which can undergo intracellular transport.

**(D)** Sorting pathways mediated by AP complexes.

**Figure 4.10:** Adapter protein (AP) complexes are required for vesicle formation, cargo recognition and transport

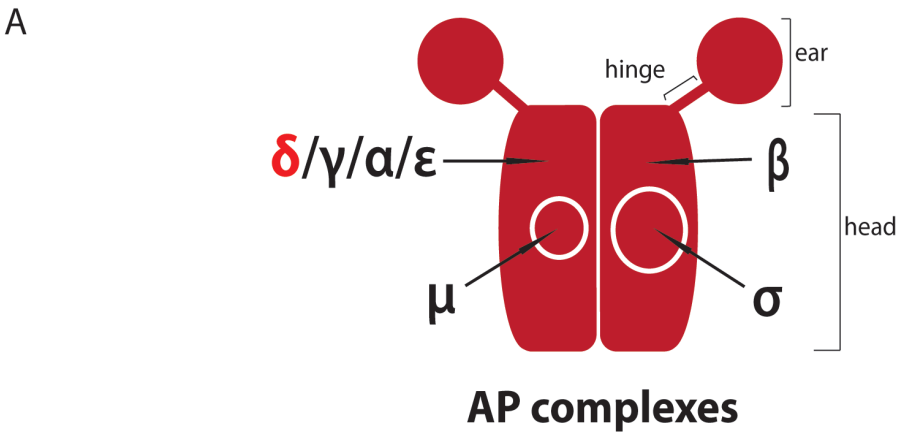


(Adapted from Boehm & Bonifacino, 2001)

Examples of LROs include melanosomes, platelet dense granules and synaptic vesicles (Dell' Angelica et al., 1999; Kantheti et al., 1998; Theos et al., 2005).

### *4.4.2 ap3δ1 transcripts are downregulated in ssk embryos*

I carried out whole mount *in situ* (hybridization) WISH of *ap3δ1* to determine whether the level and pattern of expression differs between wild type and *ssk*. At stage 25, before *ssk* can be phenotyped ~23% (5/22) of embryos obtained from a cross of *ssk* carriers clearly show decreased expression (fig. 4.11 B - C) cobsistant with a Mendelian ratio. Expression is completely lost in the neural tube and hindbrain, however, low levels of expression are still visible in the dorsal invaginating otic cup (fig. 4.11 B – C; red arrowheads). No such decrease is observed in wild type controls (0/25) (fig. 4.11 A) and negligible staining is present in the sense control (0/25) (fig. 4.11 D).

At stages 41 and 45, *ap3δ1* is downregulated in *ssk* embryos (fig. 4.11 E - F, I - J, M - N, Q - R). This downregulation was confirmed by RT-PCR data in stage 45 tadpoles (fig. 4.11 U). Some staining is still visible at reduced levels in the hindbrain (fig. 4.11 I - J black dashed line), the branchial arches (fig. 4.11; purple arrowhead) and the otic vesicle (fig. 4.11 J; red arrowhead). The decrease in *ap3δ1* expression is mostly likely the result of nonsense-mediated decay (Whitfield et al., 2004) degrading the mutated transcript.

### *4.4.3 Expression of the remaining AP-3 subunits is unaffected by the ssk lesion*

I have shown that *ap3δ1* is downregulated in response to the *ssk* lesion. As the product of *ap3δ1* forms part of a complex, regulatory mechanisms may exist to control the synthesis of the other subunits. To determine whether expression of the AP-3 β and μ subunits are altered at the mRNA level, I carried out RT-PCR in wild type and *ssk* tadpoles at stages 41 and 45. RT-PCR at both stages 41 and 45 show no change in the level of expression of *ap3β1* or *ap3μ1* (fig. 4.12).

**(A-D)** *ap3δ1* WISH at stage 25 on pools 25 wid type (A) and 25 *ssk* embryos (A) (B-D). *ap3δ1* is downregulated in ~25% of the embryos obtained from *ssk* carriers. Sense control embryos show negligable staining.

**(E-S)** *ap3δ1* WISH on wild type (E, G, I & K) and *ssk* (F, H, J, L) tadpoles at stages 41 and 45 show decreased expression in *ssk* embryos. Sense control embryos show negligble staining.

**(U)** RT-PCR (27 cycles) on stage 45 wild type and *ssk* tadpoles show decreased levels of *ap3δ1*expression. Ornithine decarboxylase (odc) has been used as a control.

**Key:** arrow heads; red - otic tissue, black - neural tissue, blue - pronephros, green - neuromasts

**Figure 4.11: *ap3δ1* is downregulated in *ssk***

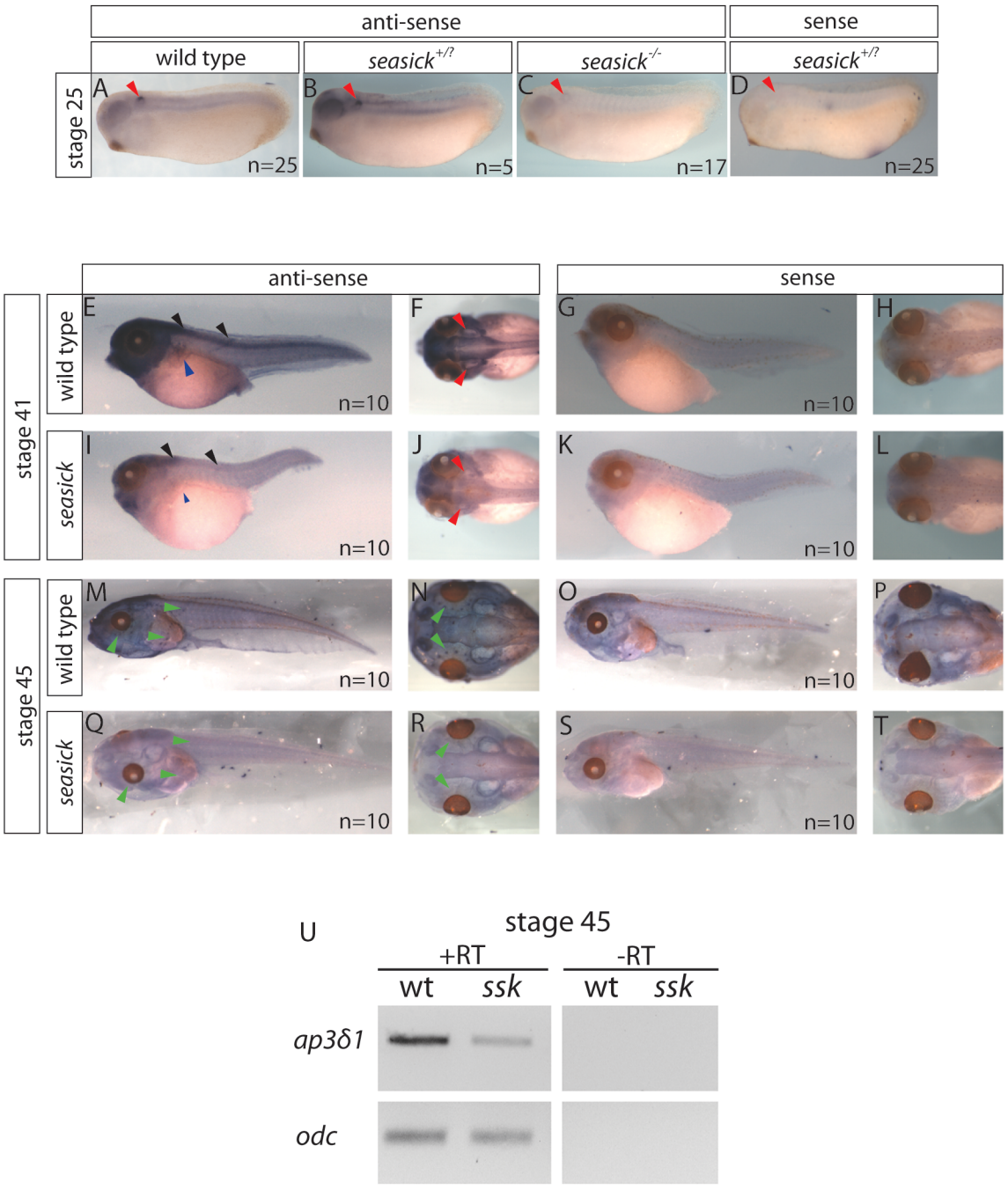

**Figure 4.12: Expression of *β & μ* AP-3 subunits is unaffected in *ssk* mutants**

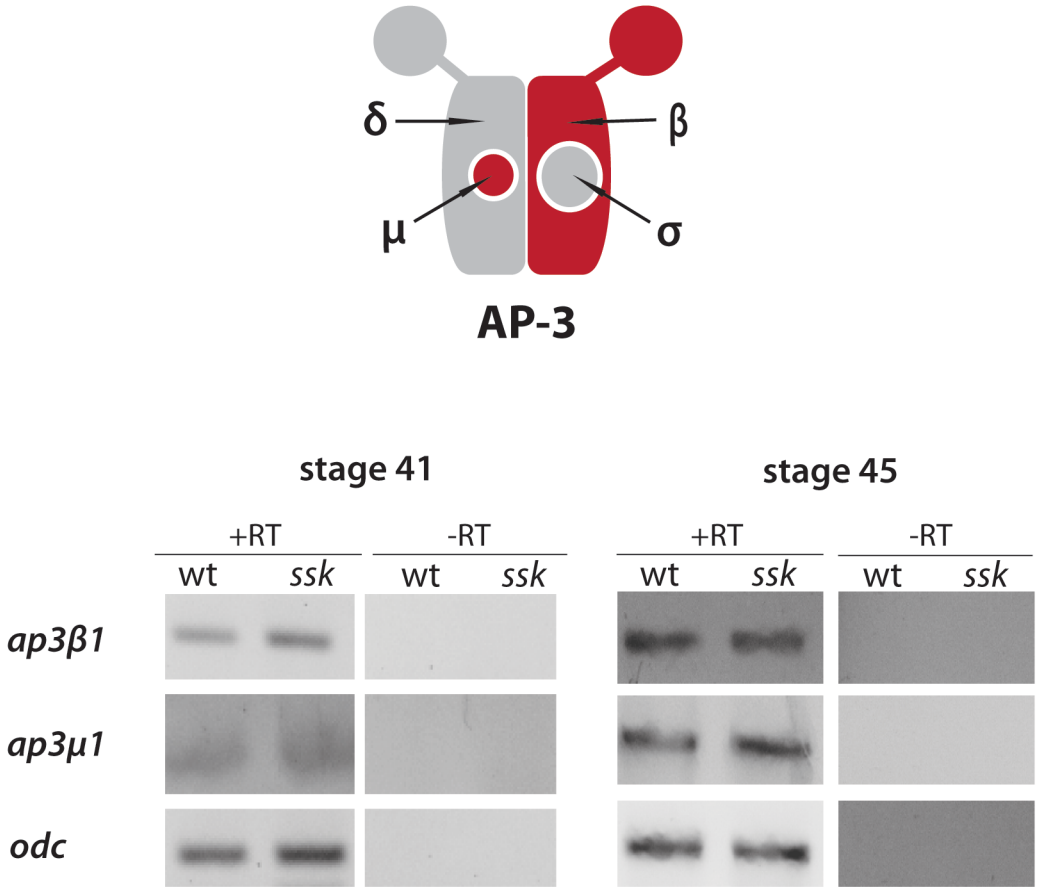


The β and μ subunits in the AP-3 complex show no change in expression level as a result of the *ssk* lesion, when anaylyzed by RT-PCR at stages 41 and 45 (RT-PCR carried out on pools of 5 embryos, bands at 27 PCR cycles displayed).

### *4.4.4 ap1γ1 is upregulated in response to ssk*

In yeast it has been shown there is partial functional redundancy between the AP complexes, as the different AP complexes are able to bind and transport some of the same protein cargos (Janvier et al., 2003; Kyttala et al., 2005; Theos et al., 2005). The *ssk* lesion disrupts AP-3 function, so it is possible that the remaining AP complexes could exhibit regulatory changes in order to compensate. To investigate this, I analyzed the level of transcription, by RT-PCR, of the subunits homologous to *ap3δ1* residing in each of the remaining AP-complexes. At both stages 41 and 45, the level of expression of the α subunit of AP-2 (*ap2α1*) and the ε subunit of AP-4 (*ap4ε1*) do not noticeably differ in *ssk* from wild type (fig. 4.13 B & C). However, the γ subunit of AP-1 (*ap1γ1*) is clearly upregulated in *ssk* mutants at both stages analyzed (fig. 4.13 A).

To confirm that *ap1γ1* is upregulated in response to *ssk*, I carried out WISH in wild type and *ssk* embryos at stages 25, 41 and 45. At stage 25, *ap1γ1* expression does not appear to differ between wild type and *ssk* (fig. 4.14 A - B), however at stages 41 and 45, *ap1γ1* is clearly upregulated (fig. 4.14 D - E, H - I, L - M, P - Q). *ap1γ1* is ubiquitously expressed at all stages analyzed, and negligible staining is observed in sense controls (fig. 4.14 F - G, J - K, N - O, R - S).

## *4.5 Discussion*

### *4.5.1 The ssk lesion disrupts ap3δ1 function and provides the first confirmed lower vertebrate model for Hermansky-Pudlack syndrome*

The *ssk* phenotype is likely to be caused by a lesion located in *ap3δ1*, creating a premature stop codon and truncating any synthesized protein to approximately one quarter of its original size. The *ap3δ1* transcript encodes the δ subunit of the

**(A) (i)** Schematic of the AP-1 complex, AP1γ1 subunit depicted in grey.
**(ii)** RT-PCR at stage 41 and **(iii)** stage 45 demonstrates that the level of ap1γ1 transcript increases between wild type and *ssk*.

**(B)(i)** Schematic of the AP-2 complex, AP2α1 subunit is depicted in grey.
**(ii)** RT-PCR at stage 41 and **(iii)** stage 45 demonstrates that the level of *ap2α1* transcript does not differ between wild type and *ssk*.

**(C)(i)** Schemcatic of the AP-4 complex, AP4 1 is depicted in grey.
**(ii)** RT-PCR at stage 41 and stage 45 **(iii)** demonstrates that the level of *ap4ε1* does not differ between wild type and *ssk*.

**Figure 4.13:** ***ap1γ1*** **is upregulated in ssk tadpoles while** ***ap2α1*** **and** ***ap4ε1*** **expression remains unaffected**

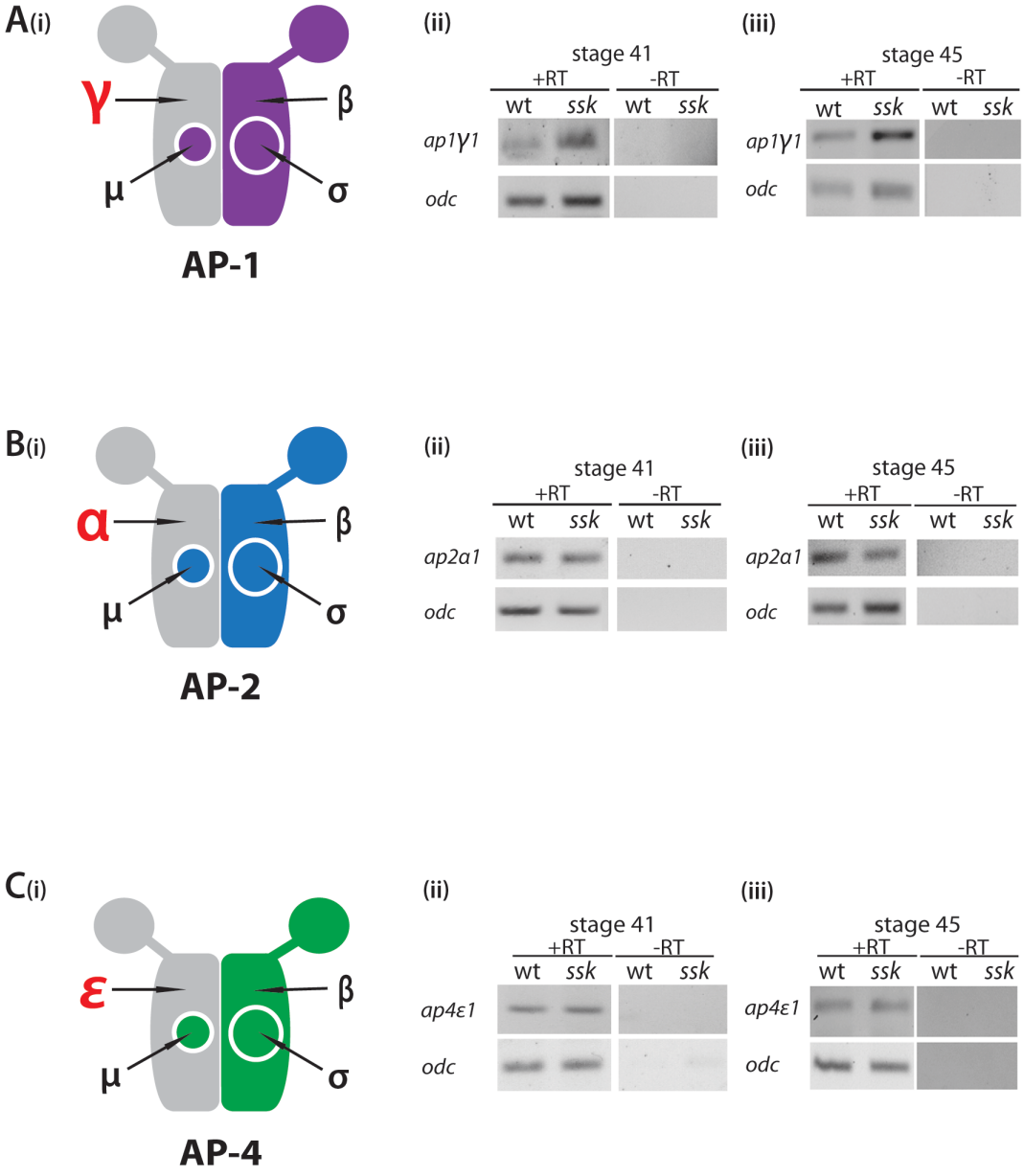

## Figure 4.14: *ap1γ1* is upregulated in *ssk* at tadpole stages

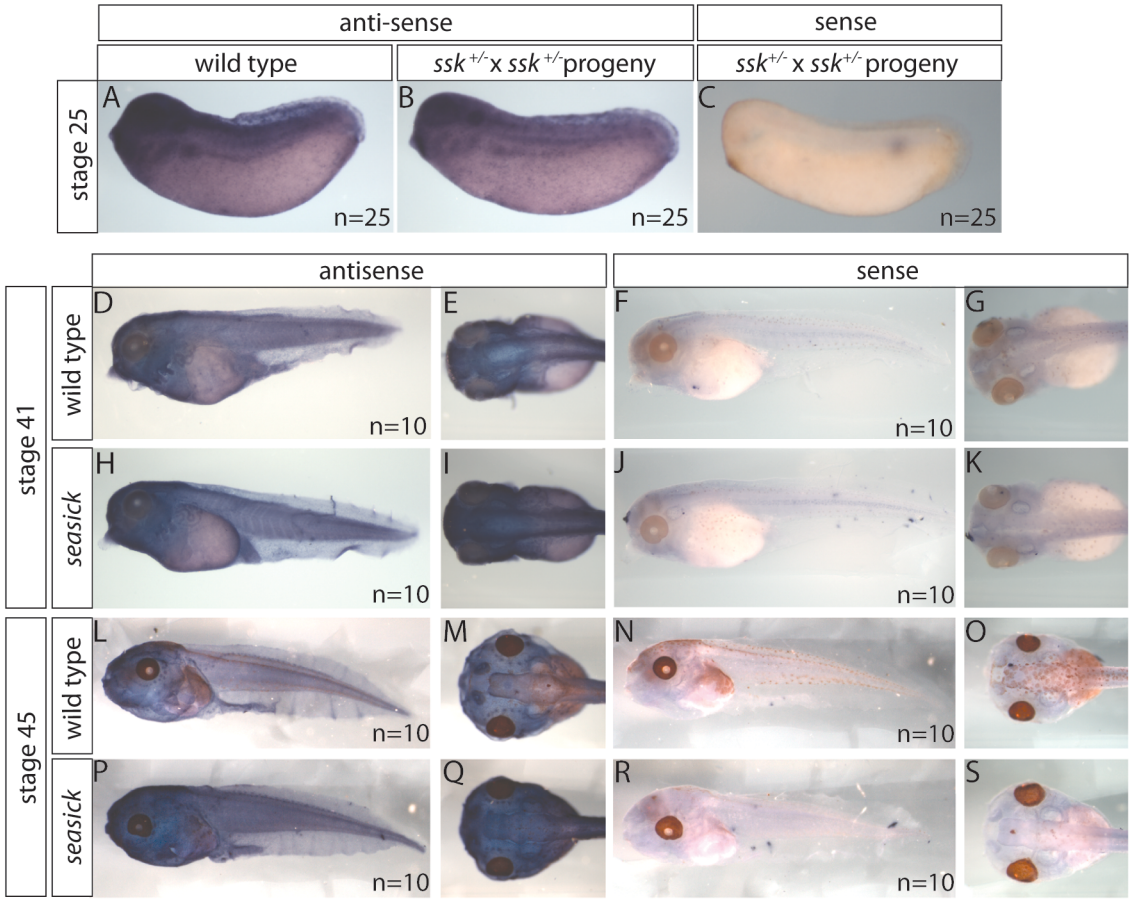


**(A-C)** *ap1γ1* WISH at stage 25 on pools of wild type embryos (A) and embryos obtained from *ssk* carriers (B-C). *ap1γ1* is ubiquitously expressed and has no detectable difference in expression between embryos obtained from *ssk* carriers and wild type embryos. Sense control embryos show negligable staining.

**(D-S)** *ap1γ1* WISH on wild type (E, G, I & K) and *ssk* (F, H, J, L) embryos at stages 41 and 45 show increased expression in *ssk* embryos. Sense control embryos show negligable staining.

AP-3 complex and is mutated in the human disease type 2 Hermansky-Pudlack syndrome (Dell' Angelica et al., 1999; Hermansky & Pudlak, 1959; Kantheti et al., 1998). This disease is characterized by albinism, seizures, poor blood clotting and otoconial defects (Gahl et al., 1998; Huizing et al., 2000). These symptoms are caused by defective trafficking of proteins to lysosome-related organelles (LROs) such as melanosomes, synaptic vesicles and platelet dense granules (Dell' Angelica et al., 1999; Kantheti et al., 1998; Theos et al., 2005). The *ssk* mutant is the first confirmed mutant in a lower vertebrate that can serve as a model for this disease.

The lesion in *ap3δ1* probably creates a null or a strong hypomorph as very little of the protein is synthesized, and diminishing the amount of endogenous protein by morpholino injection accurately phenocopies the mutant, suggesting that the truncated protein in *ssk* mutants has little or no function. Also, in mouse cell lines, mutations in the δ and β subunits affecting the AP-3 "head domain" (see fig. 4.10 A) cause degradation of the whole complex (Kantheti et al., 1998; Le Borgne et al., 1998; Peden et al., 2002; Simpson et al., 1996). Degradation occurs because the head domains of the δ and β subunits are required for inter-subunit binding, therefore if this domain is lost the subunits cannot assemble as a complex (Kantheti et al., 1998; Le Borgne et al., 1998; Peden et al., 2002; Simpson et al., 1996). In *ssk*, AP3δ1 is truncated so that only half of the head domain is synthesized, so it is possible that that this may result in the degradation of the whole complex. In *ssk*, the mutation in *ap3δ1* does not cause downregulation of the remaining AP subunits at the mRNA level (fig. 4.12), however regulation of any of the AP-3 subunits at the protein level has not been tested due to lack of suitable antibodies.

Rescuing the phenotype with a wild type *ap3δ1* construct would remove any ambiguity that the premature stop codon found in *ap3δ1* is responsible for the *ssk* phenotype. Also, injecting mutant embryos with different alleles could be carried out to determine the function of different protein domains. As the *ssk*

phenotype can only be morphologically identified by stage 37, injection of wild type mRNA would need to remain in the embryo for several days. To achieve this, the *ap3δ1* gene could be cloned into a plasmid containing a constitutively active promoter such as β-actin. Also, as no suitable antibodies are currently available, myc-tagged constructs of wild type and *ssk ap3δ1* could be injected into wild type embryos to compare the subcellular localization of these transcripts. Also myc-tagged constructs of AP-3 subunits could be injected into *ssk* embryos. If the product of these constructs were able to associate with cell membranes this would indicate that the subunits were assembling into a complex, however this would not determine whether the complex retained any function (Peden et al., 2002).

### *4.5.2 The ssk otoconial phenotype may be the result of an ionic imbalance in the endolymphatic fluid*

The gross morphological development of the inner ear is unaffected in *ssk* mutants (fig. 4.3), however the otoconial crystals grow excessively and fuse (fig. 4.2), and tadpoles exhibit balance defects. The balance defects may be attributed, at least in part, to the presence of enlarged otoconia. In transverse sections of the *ssk* sacculus, there is a limited area of the sensory epithelium in contact with the otoconia. As the otoconia are enlarged, their increased mass may overstimulate the hair cells they are in contact with while hair cells that are not attached to any otoconia will be understimulated (see introduction section 1.6).

During early inner ear development *ap3δ1* is strongly expressed in the presumptive endolymphatic tissue (fig. 4.9 & fig. 4.11), suggesting that mis-trafficking of proteins to LROs in this tissue may be responsible for the otoconial defect. At present it is unknown what function LROs may have in the endolymphatic tissue, however work carried out on the *mocha* and *pearl* mice (*ap3δ1* null and *ap3β1* hypomorph, respectively) shows that supplementing

pregnant dams with either $Zn^{2+}$ and/or $Mn^{2+}$ partially rescues the otoconial phenotype (Balkema et al., 1983; Feng et al., 1999; Rolfsen & Erway, 1984). $Zn^{2+}$ and $Mn^{2+}$ are known to act as co-factors for enzymes involved in otoconial formation. $Zn^{2+}$ is essential for carbonic anhydrase activity, an enzyme required to produce $CO_3^-$ to form $CaCO_3$ (Erway & Grider, 1984; Erwya et al., 1986), while glycosylating enzymes, which modify the core otoconin proteins (see introduction section 1.5), depend on $Mn^{2+}$ for their activity (Erway et al., 1986). This suggests that in mice AP-3 may carry transporters or binding proteins to LROs where they act to store $Zn^{2+}$ and $Mn^{2+}$ and regulate their release into the endolymphatic fluid. To determine whether a deficiency of $Zn^{2+}$ and $Mn^{2+}$ is responsible for the otoconial phenotype in *ssk*, $Zn^{2+}$ and/or $Mn^{2+}$ could be added to the media that the mutants are raised in to see if this rescues the phenotype.

The melanophores located in the inner ear (see introduction section 1.2) also function to modulate the ionic environment of the endolymphatic fluid, such as the concentration of $K^+$ and $Ca^{2+}$ (Tu et al., 1998). $Ca^{2+}$ is required to produce $CaCO_3$ for otoconial development (see introduction section 1.6), while both $K^+$ and $Ca^{2+}$ are essential for hair cell depolarization (see introduction section 1.5.2). In *ssk* tadpoles, the melanophores have decreased levels of pigmentation (fig. 4.1; Q & R), indicating that transportation of proteins via AP-3 to the melanosomes is hindered.

To determine whether the melanophore defect plays a role, the otic placode could be transplanted from a *ssk* embryo into a wild type. As melanophores are derived from the neural crest, wild type melanophores would migrate from the host embryo into the mutant otic tissue. If the phenotype were less severe this would indicate that the melanophores are contributing to the inner ear defect.

### 4.5.3 The ssk phenotype suggests a requirement of AP-3 for melanosome intracellular transport

In *ssk* melanophores, the melanosomes aggregate centrally and fail to disperse throughout the cell, suggesting a role for AP-3 in moving melanosomes throughout the intracellular environment. Defective microtubule-dependent transport of LRO has also been observed in mouse T-lymphocytes, where a null mutation in *ap3β1* results in a failure to transport lytic granules to the immunological synapse, reducing the cells' cytotoxicity and in turn the animals immune response (Clark et al., 2003). At present, the mechanism of action remains unclear. One hypothesis is that defects in AP-3 result in mislocalisation of membrane proteins that are required to link the LROs to the cell cytoskeleton or cytoskeletal motors, although this is yet to be tested.

### 4.5.4 AP-3 has tissue specific roles during embryonic development

The *ap3δ1* transcript exhibits a tissue specific expression pattern during early embryonic development. As well as the endolyphatic tissue and melanophores, *ap3δ1* displays strong expression in the neural tissue, eye, migrating neural crest, neuromasts and pronephros (fig. 4.12). Defects in these tissues have been observed in patients with Hermanky-Pudlak syndrome (Huizing et al., 2001; Shotelersuk et al., 2000). At present, potential phenotypes in these tissues have not been examined in *ssk*, however some of these defects have been characterized in homologous tissues in the *mocha* mouse.

In *mocha*, it has been shown that AP-3 traffics protein cargo from the golgi and endosomes to synaptic vesicles in the central nervous system (CNS). Two of these cargos are the zinc transporters ZnT3 and ZnT4 (Kantheti et al., 1991). Zinc has a vital function in the synaptic vesicles as it aids modulation of currents mediated by NMDA and GABA receptor-gated ion channels (Xie & Smart, 1991), and loss of AP-3 function results in seizures in *mocha* mice (Kantheti et al.,

1998). Defects in the kidneys were also examined in mocha, as loss of AP-3 function reduced the secretion of lysosomal enzymes from the kidney proximal tubule cells, decreasing the animal's ability to degrade waste products (Swank et al., 1991). As *ap3δ1* is strongly expressed in developing CNS and in the pronephros (fig. 4.12), it is possible that similar deficits are present in the *ssk* mutant.

### *4.5.5 AP-3 and AP-1 exhibit cross-regulation*

Expression of *ap1γ1* is upregulated in response to *the ssk* lesion, indicating cross-regulation between the AP complexes. This could be an indication that more AP-1 is produced to compensate for a lack of AP-3 function. Although AP-1 predominantly transports cargo from the endosome to the golgi, a fraction of AP-1 is known to move in a parallel route to AP-3 and transports cargo from the endosome to the LROs (see 4.10 D) (Janvier et al., 2003; Kyttala et al., 2005; Theos et al., 2005). It has also been shown in other model systems that AP-1 can carry out some of the functional roles of AP-3. For example, in mouse melanocytes tyrosinase is one of the protein cargos selected by AP-3 (Höning et al., 1998). It was also shown that AP-1 can also bind tyrosinase and that in *ap3β1*$^{-/-}$ mouse melanocyte cell lines that the number of AP-1 vesicles containing tyrosinase increases, a proportion of which reached the melanosomes, suggesting that AP-1 can compensate for this role (Theos et al., 2005).

It must be noted that although *ap1γ1* is upregulated at the transcriptional level, this may not be true at the protein level. Appropriate antibodies need to be obtained to carry out western blots to determine whether the level of AP1Y1 protein differs between wild type and *ssk*. Also, to assess whether AP-1 is functionally compensating for AP-3, sub-threshold levels of *ap1γ1* morpholino could be injected into *ssk* embryos to determine whether this results in a more severe phenotype.

### 4.5.6 Future studies

#### 4.5.6.1 Generating 100% mutant embryos through germline transplantation

Creating *ssk* carriers that produce 100% mutant offspring would be incredibly useful, as experiments could be carried out on large numbers of mutant embryos before they are morphologically identifiable. Germ-line transfer, a technique where the host embryos germ-line is suppressed and replaced by a tissue graft containing homozygous mutant germ-line cells, could achieve this. Development of the host germ-line can easily be suppressed in *X. tropicalis* by morpholino knockdown of germ-line determinants such as *dead end* and *deadsouth*, plus the robust nature of *X. tropicalis* embryos allows grafts to be carried out with ease. The production of homozygous *ssk* carriers would greatly aid future studies of *ssk* as experiments could be carried out on large numbers of mutants at early stages without the need for genotyping. An alternative approach would be to create a stable BAC transgenic line carrying a wild type copy of *ap3δ1* plus *gfp* controlled by a ubiquitous promoter on a *ssk* background. Heterozygotes for the BAC transgene could then be crossed and all the progeny testing negative for GFP will be homozygous mutant *ssk*.

#### 4.5.6.2 Determination of AP3δ1 protein domain function

The severe truncation of *ap3δ1* caused by the *ssk* lesion is likely to result in forming a null or a strong hypomorph. The AP3δ1 protein consists of three main domains: the head (which contains two protein-protein interaction sub-domains), the hinge and the ear (fig. 4.7 C and fig. 4.10). Work carried out on mouse cell lines has identified a regulatory role of the ear domain in recruiting the AP-3 complex to cell membranes (Peden et al., 2002), but little is known about the remaining domains. Injection of RNA constructs into *ssk* embryos could be used to rescue the mutant phenotype, and by deleting regions of the wild type transcript the effects of losing specific protein domains could be examined. Injection of RNA constructs into the offspring of homozygous *ssk* carriers (see

section 4.5.6.1) would be useful as all of the embryos injected would be mutant and any phenotype would be specific to the loss of the AP3δ1 domain of interest.

#### *4.5.6.3 Dissecting the roles of ap3δ1 by tissue specific knockouts*

At present it is unclear which tissue in the inner ear is responsible for the *ssk* otoconial phenotype. During embryonic development *ap3δ1* is expressed strongly in the endolymphatic tissue and the melanophores, but during tadpole stages it is also expressed throughout the otic vesicle (fig. 4.9). I have hypothesized that the otoconial phenotype may be the result of an ionic imbalance caused by defective protein trafficking in the endolymphatic tissue and/or the melanophores. However, it is also possible that protein trafficking defects resulting from later expression of *ap3δ1* throughout the otic vesicle may have an influence on crystal maintenance. Tissue specific knockouts of a transgenic *ap3δ1* on a *ssk* genetic background would allow the role of different tissues in the inner ear to be studied individually. This could be achieved by creating a floxed *ap3δ1* BAC transgenic tagged by gfp on a $ssk^{-/-}$ background and crossing it to a cre transgenic under the control of tissue specific promoters (fig. 4.15). This would allow the tissue specific phenotype of *ap3δ1* in the inner ear to be examined in a wild type background.

The *ap3δ1* transcript has a tissue specific expression pattern during early embryonic development, as it is expressed in tissues such as the CNS, eye, pronephros and lateral line. Tissue specific knockout of *ap3δ1* could also be used to examine the function of the AP-3 complex in these tissues in the context of a wild type background. This technique would allow phenotypes to be studied past the point where *ssk* remains viable, enabling the role of AP-3 in tissues such as the kidney to be studied.

#### *4.5.6.4 Identification of AP-3 interacting proteins*

AP-3 function requires interaction with many proteins targets either to regulate the complex, transport it throughout the intracellular environment or act as cargo.

**Figure 4.15: Tissue specific knock-out of *ap3δ1***

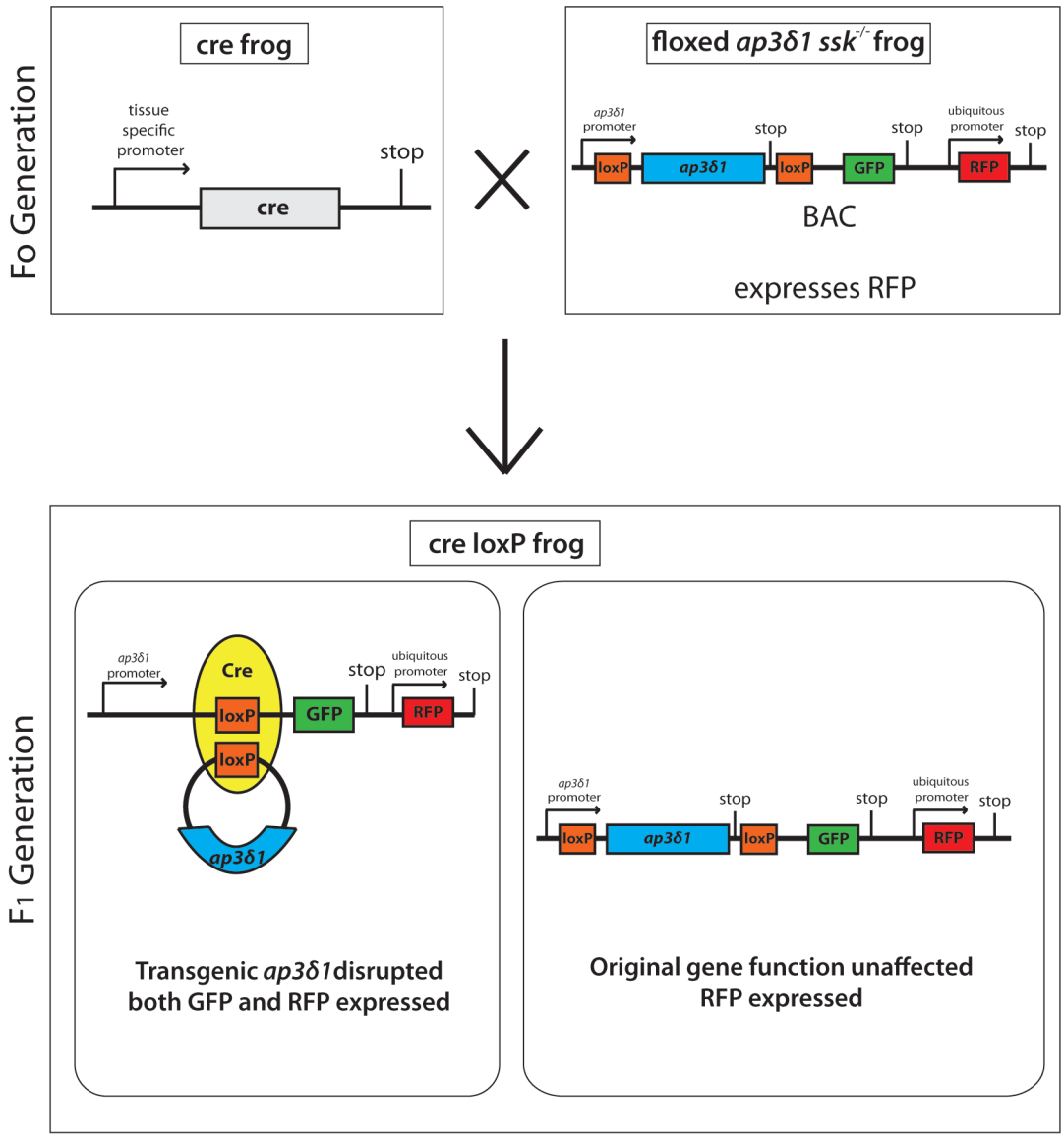


Expression of a BAC transgenic floxed *ap3δ1* line under the control of a *ap3δ1* promoter in *ssk* tadpoles will rescue the mutant phenotype.

Crossing the transgenic *ap3δ1* line with a cre line under the control of a tissue specific promoter produces offspring where the transgenic *ap3δ1* is removed in a given cell type. Removal of the *ap3δ1* transcript allows GFP to be expressed and act as a reporter .

At present few of these interacting proteins have been indentified. The *ssk* mutant could be utilized to obtain and identify these interacting proteins by co-immunoprecipitation (co-IP) and mass spectrometry, respectively. Comparison between AP-3 co-IP carried out on wild type and on *ssk* embryos would be very useful as proteins identified in both experiments could be reliably eliminated as non-specific targets.

#### *4.5.6.5 Identification of proteins regulating the AP-3 pathway*

Gain-of-function screens, such as injecting cDNAs into *ssk* embryos and comparing their phenotype to wild type injected embryos, could identify proteins that regulate the AP-3 pathway. The *X. tropicalis* full-length cDNA collection currently consists of ~9,000 transcripts. To streamline the experiment, transcripts could be injected into embryos in batches of 100 RNAs and if a phenotype were observed for a given batch, injections of single RNAs could be carried out. Gain-of-function screens are well established in *Xenopus* species and provide an efficient means of identifying AP-3 interacting factors that cannot easily be carried out in other AP-3 models such as mouse due to the low numbers and inaccessibility of embryos.

## *4.6 Summary*

The *ssk* phenotype is characterized by enlarged otoconial crystals, punctate melanophore pigmentation and decreased levels of iridophore pigmentation. Positional cloning, sequencing and phenocopying of candidate genes demonstrated that a premature stop codon in *ap3δ1* is responsible for the phenotype. *ap3δ1* encodes the δ-subunit of the AP-3 complex. AP-3 functions to recognize and transport specific protein cargos from the endosome and golgi to LRO's, a type of organelle exhibiting similarities to lysosomes but also displaying cell specific functions such as pigment synthesis or acting as an ion reservoir (Dell' Angelica et al., 1999; Kantheti et al., 1998; Theos et al., 2005). During

embryonic development, *ap3δ1* is strongly expressed in the developing endolymphatic sac and melanophores, and becomes expressed throughout the inner ear by tadpoles stages. The endolymphatic tissue and melanophores function to maintain the ionic environment of the inner ear, suggesting that the otoconial defect could be a result of an ionic imbalance. However, lack of AP-3 function in the rest of otic vesicle may also have an influence on crystal maintenance. AP-1 is known to transport protein from the endosome to LROs as well as AP-3, and upregulation of the AP-1 subunit *ap1γ1* is observed in response to the *ssk* lesion. The upregulation of *ap1γ1* indicates the presence of a cross-regulatory mechanism between the AP complexes, and may indicate that AP-1 is compensating for loss-of or decreased levels of AP-3 function, although this has yet to be tested at the functional level.

The severe truncation of AP3δ1 most likely results in a null phenotype, making *ssk* amenable to a number of functional studies. The role of different AP3δ1 protein domains could be determined by injecting RNA constructs of specific domains into *ssk* embryos and assessing the ability of each domain to rescue the mutant phenotype. Also, developing a transgenic line to rescue the *ssk* phenotype and deleting it in specific tissues could be used to investigate the tissue specific functions of AP-3. Co-IP and gain-of-function screens could identify proteins interacting with AP-3 as well. At present, the only other vertebrate model of AP-3 are the mouse *mocha* and *pearl* mutant lines (*ap3δ1* null and *ap3β1*, respectively) (Feng et al., 1999; Kantheti et al., 1998). *X. tropicalis* provides a big advantage over these mouse models as each of these experiments can rapidly be carried out on large numbers of intact embryos, providing a convenient system for furthering our understanding of AP-3 function.

# Chapter 5

# The *Xenopus tropicalis* mutant *komimi* (*kom*) results from a splicing defect in *otoconin-90*

## *5.1 Introduction*

In *komimi* (*kom*) mutants, a single large otoconium forms over each macula and tadpoles exhibit strong balance defects such as circular swimming. In chapter 3 I showed that the *kom* lesion is located on the q-arm of chromosome 6 (see section 3.2.3.4). I also showed that the cells comprising the saccular macula are dysmorphic and lack the columnar morphology found in wild type (see section 3.2.3.2).

The aim of the experiments described in this chapter is to identify the lesion responsible for the *kom* phenotype by high resolution mapping and sequencing of candidate genes. I also further characterize the inner ear defects to help identify the mechanisms that may be affected in *kom* mutants.

## *5.2 Gross phenotypic characterization of the komimi (kom) inner ear*

### *5.2.1 The kom phenotype is characterized by large dysmorphic otoconia and vestibular behavioral defects*

The *kom* phenotype is identifiable by the presence of a single enlarged dysmorphic otoconium over each macula; no other defects are externally visible (fig. 5.1 A - D). Mutant tadpoles also exhibit balance defects such as circular swimming, difficulty reorientating themselves when placed upside down and decreased response to physical stimulation (fig. 5.1).

**Figure 5.1: *kom* external phenotype**

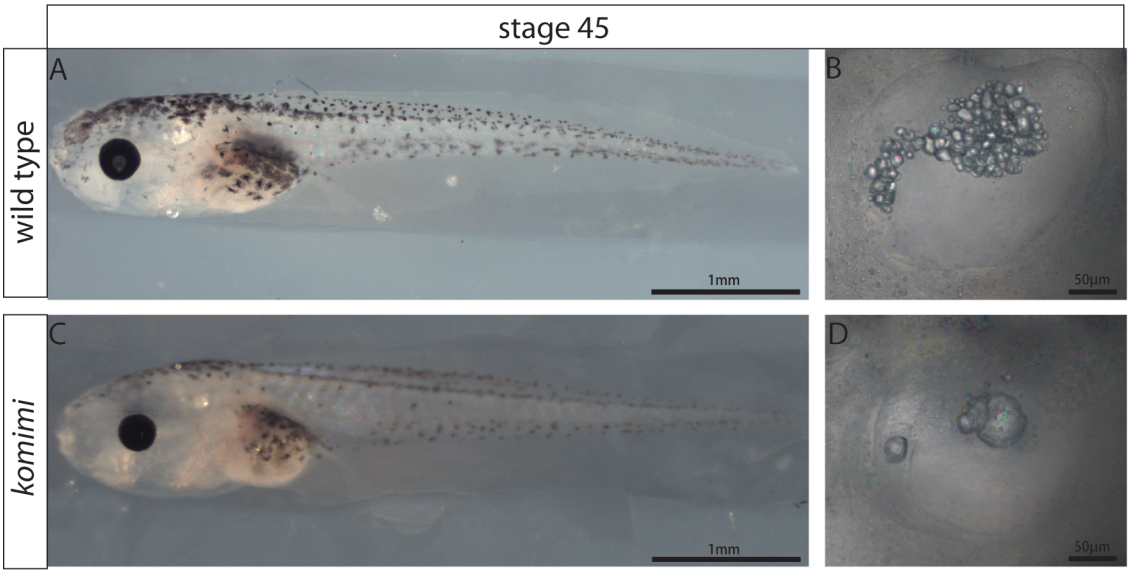


The *kom* phenotype is characterized by the presence of a single enlarged otoconium located over each macula sensory epithelia.

### 5.2.2 *kom* mutants develop single enlarged dysmorphic otoconial crystals over each macula

To further characterize the otoconial phenotype, I dissected otoconia out of wild type and *kom* sibling tadpoles at stages 41, 45, 47 and 54 and observed them under a brightfield microscope (n=5). At stage 41, one or two otoconial crystals are present in the *kom* inner ear that are visibly much larger than those found in wild type (fig. 5.2 A – B; wt otoconia <1µm in length, *kom* otoconia ~30µm in length). By stage 45, the *kom* otoconial crystals have increased in size and appear to be composed of several large crystals that have fused together to form agglomerates (fig. 5.2 C – D; wt otoconia <1µm - ~3µm, *kom* otoconia ~ 110µm). The *kom* otoconial agglomerates appear to reach their maximum size by stage 47 (fig. 5.2 E – F; wt otoconia <1µm - 6µm, *kom* otoconia ~145µm), as otoconia dissected out of stage 54 tadpoles do not notably differ in size (fig. 5.2 G – H; wt otoconia 1 - 20µm, *kom* otoconia ~155µm).

To investigate the association of the otoconial crystals with the apical surface of the macular sensory epithelia, I took transverse sections through the sacculus of stage 45 wild type and *kom* tadpoles, and stained them with haematoxylin and eosin. In wild type tadpoles, multiple small otoconia reside in close contact with the apical surface of the sacculus (fig. 5.2 I), while in *kom*, the large otoconial agglomerates are in contact with very little of the epithelia (fig. 5.2 J). Also, as discussed in section 3.2.3.2, the cells that comprise the saccular macula are dysmorphic and differ greatly in size within the epithelium (fig. 5.2 J).

### 5.2.3 Macular sensory cells differ in size throughout the epithelium

Analysis of stage 45 *kom* otic vesicles in chapter 3 shows that the cells comprising the macular sensory epithelia are dysmorphic, lack the columnar organization found in wild type and differ in size within the epithelium (see chapter 3 section 3.2.3). To determine the developmental stage that this phenotype becomes visible, I used fluorescein-tagged phalloidin to stain cell

**Figure 5.2: *komimi* embryos develop enlarged dysmorphic otoconia over each macula**

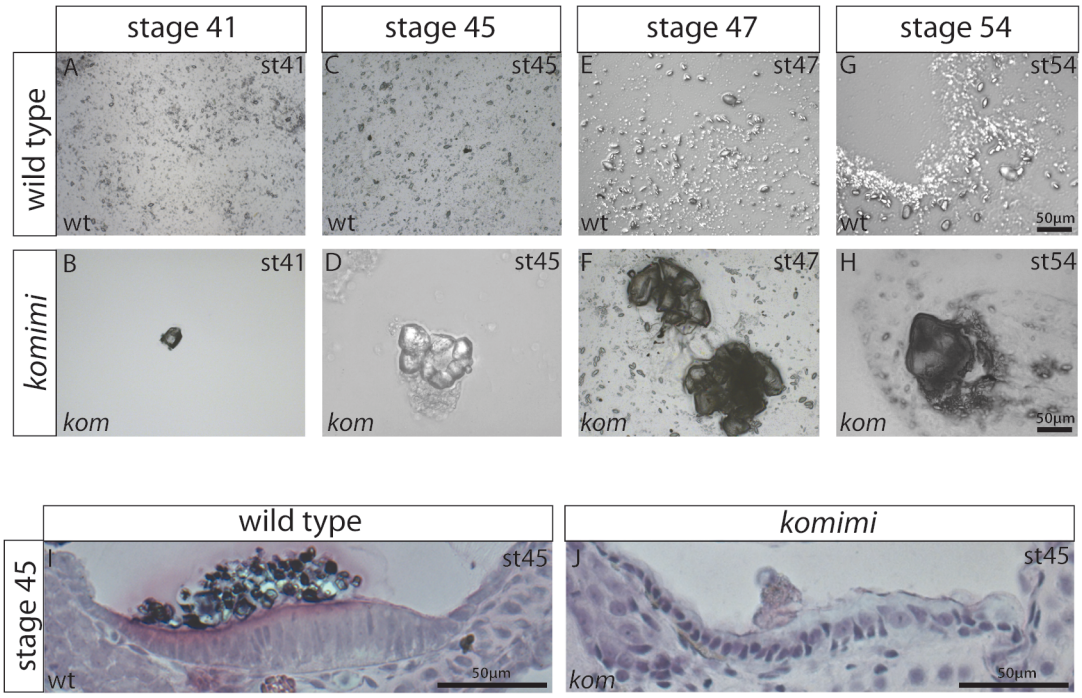


**(A-H)** Otoconial crystals are grossly enlarged and dysmorphic in *kom* embryos and fuse to form large agglomerates.

**(I-J)** Enlarged otoconia have reduced contact with the sensory epithelium, and the sensory epithelium itself lacks the columnar morphology of a differentiated wild type epithelium.

**(A – E)** (A) Schematic of stage 37 inner ear. (B & D) Fluoroscein-tagged phalloidin staining of stage 37 wild type and *kom* otic vesicles Hair cell stereocilia bundles are clearly visible in both wild type and *kom*. (C & E) Hair cells are comparable in size both within the epithelia and between wild type and *kom*.

**(F – J)** (F) Schematic of stage 41 inner ear. (G & I) Hair cells of both the utricular (dashed line) and saccular (dotted line) maculae are visible in both wild type and *kom* tadpoles at comparable locations. (H & J) In wild type, hair cells are uniform in size throughout the epithelium (white arrowheads & double headed arrows) while in *kom* hair cells differ greatly in size (white arrowheads and double headed arrows) and some stereocilia bundles appear frayed (yellow arrowhead).

**(K – O)** (K) Schematic of stage 45 inner ear. (L & N) The utricle (dashed line) and sacculus (dotted line) are present at comparable locations between wild type and *kom*. (M & O) High magnification of the saccular hair cells shows that they differ greatly in size in *kom*.

**Figure 5.3:** Macular sensory cells differ in size throughout the epithelium in *kom*

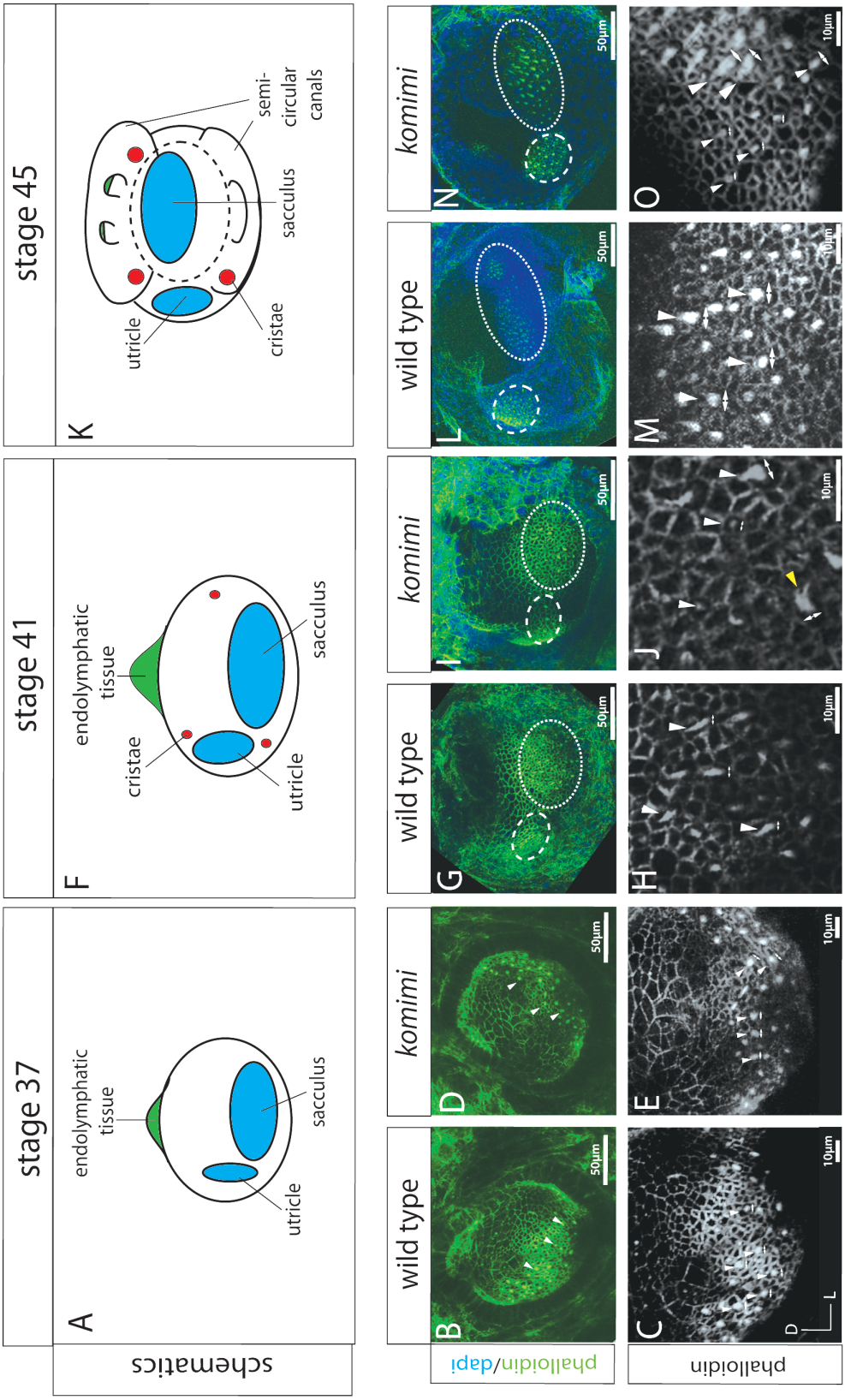

boundaries and hair cell stereocilia bundles in *kom* and wild type tadpoles at a range of developmental stages (n=5).

At stage 37, the hair cell stereocilia bundles are clearly visible at a comparable size in both wild type and *kom* tadpoles (fig. 5.3 A – E). By stage 41, the utricle (dashed line) and sacculus (dotted line) are clearly distinguishable in both *kom* and wild type (fig. 5.3 F, G & I). Viewed at high magnification (x63) the size of the saccular cells differs greatly throughout the epithelium in *kom* tadpoles, unlike the wild type epithelium where the cells appear uniform in size (fig, 5.3 H & J; white arrowheads & double arrows). Some of the stereocilia bundles in *kom* tadpoles also appear splayed (fig. 5.3 J; yellow arrowhead). This phenotype continues to be observed in stage 45 *kom* tadpoles (fig. 5.3 K – O).

### *5.2.4 Specification and early differentiation of the sensory region of the inner ear appears unaffected in kom*

The macular phenotype described in fig. 5.3 and section 3.2.3 could be caused by a specification defect in the pro-sensory region of the otic vesicle and/or the differentiation of the sensory epithelial cells. To explore this hypothesis, the temporal and spatial expression pattern of several genes involved in specification and differentiation of the sensory regions of the inner ear have been investigated by WISH. *kom* can only be morphologically identified from stage 37, so if defects in the expression of these markers occur at earlier stages they will be observed in Mendelian ratios (1:3) in embryos derived from a mating of two carriers.

#### *5.2.4.1 Pro-sensory cell specification is unaffected in kom mutants*

*lunatic fringe* (*lufng*) is one of the earliest markers to be expressed in the pro-sensory region of the otic vesicle and is found in cells that will give rise to the utricle and sacculus (Cole et al., 2000; Fekete and Wu, 2002). Stages 25, 30, 37 and 41 were assayed by WISH to determine whether there are any visible differences in the expression of *lufng* (n=50). No difference in the temporal or

**Figure 5.4: *lufng* expression pattern does not differ between *kom* and wild type embryos**

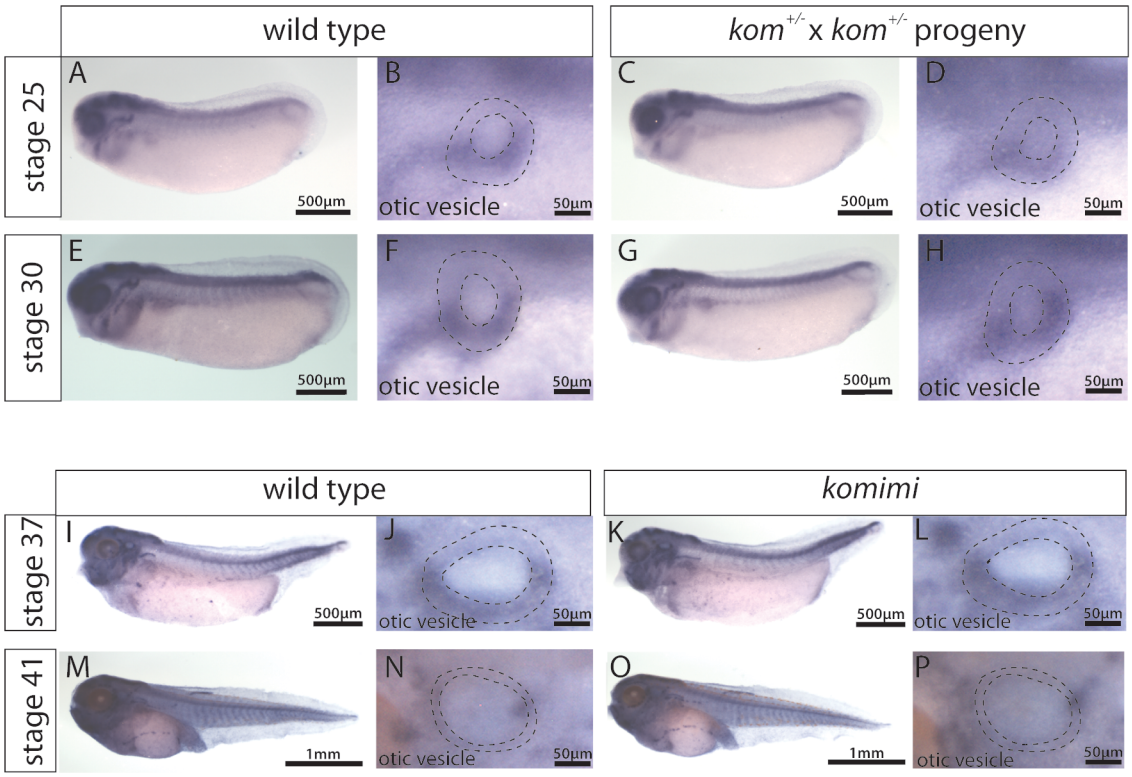


**(A - G)** To determine whether pro-sensory cell specification is affected in *kom, lufng* WISH was carried out on stage 25 and stage 30 wild type embryos (A - B, E - F) and embryos obtained from a mating of *kom* carriers (C - D, G - H). *lufng* is expressed in the ventral region of the otic vesicle, as well as in each of the neurogenic placodes, the brain, neural tube and pronephros. No differences in the level or pattern of expression were observed.

**(I - P)** *lufng* WISH was carried out on stage 37 and 41 wild type (I - J, M - N) and *kom* (K - L, O - P) tadpoles. At stage 37, *lufng* continues to be expressed in the ventral region of the otic vesicle but by stage 41 this expression ceases. Throughout both stages 37 and 41, *lufng* continues to be expressed in the tissues derived from the neurogenic placodes, along with the brain, neural tube and pronephros. By stage 41, *lufng* is also expressed in the neuromasts of the lateral line. No difference in the level or pattern of expression was observed between wild type and *kom* in any of these tissues at both stages examined.

spatial expression pattern is observed in any of the stages assayed (fig. 5.4 A - P).

*bone morphogenetic protein 4* (*bmp4*) is essential for cristae specification as it is expressed in the presumptive cristae cells (Wu and Oh, 1996) and inhibition of its function using noggin coated beads stops cristae formation (Geriach et al., 2000). No differences in the temporal or spatial expression pattern were observed or the level of expression for any of the stages investigated (n=50) (fig. 5.5 A - L).

#### *5.2.4.2 Early hair cell differentiation is unaffected in kom mutants*

In the inner ear *myosin VIIa* is specifically expressed in differentiated hair cells and encodes an unconventional myosin required for hair cell bundle integrity (Ernest et al., 2000). No differences in the level, timing or spatial pattern of expression is observed between mutant and wild type embryos (n=50) (fig. 5.6 A - L), suggesting that the sensory epithelia are able to differentiate.

### *5.2.5 Structure and activity of lateral line neuromasts do not notably differ in kom from wild type*

The hair cells of the inner ear and the neuromasts of the lateral line share a common evolutionary history and as a result they are structurally similar and share many developmental pathways (Adamska M et al., 2000; Baker et al., 2008). *kom* tadpoles display strong balance behavioral defects as well as a delayed response to physical stimulation. As the role of the lateral line is to sense physical stimuli, it is possible that this organ has developed incorrectly or is malfunctioning. I studied the structure of the lateral line neuromasts in wild type and *kom* stage 41 tadpoles by immunostaining the neuromasts kinocilia using anti-acetylated tubulin antibody (fig. 5.7 A – D; n=10). I also investigated the function of the neuromasts mechanotransduction channels using the amphipathic dye fm1-43 (fig. 5.7 E – H; n=10). Fm1-43 enters hair cells through

**Figure 5.5: *bmp4* expression is not affected in *kom***

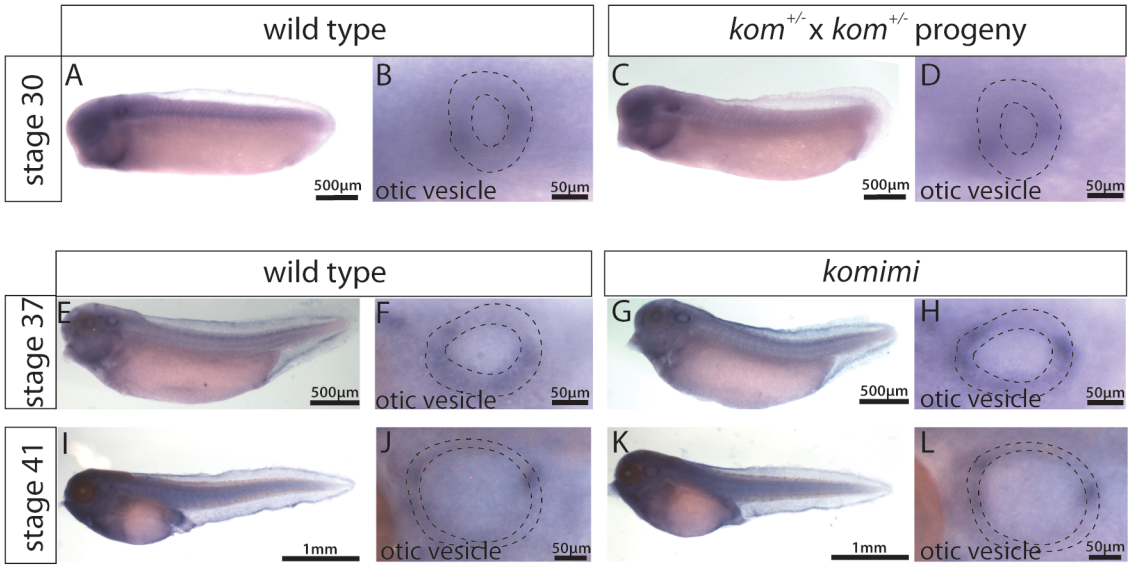


**(A - D)** To determine whether cristae specification is affected in *kom*, *bmp4* WISH carried out in stage 30 wild type embryos (A - B) and embryos obtained from a mating of *kom* carriers (C - D). In the otic vesicle, *bmp4* has an anterior and posterior pole of expression. It is also expressed in the neurogenic placodes and the neural tube. No difference in this pattern or level of expression was observed.

**(E - K)** *bmp4* WISH carred out on stages 37 and 41 wild type (E - F, I - J) and *kom* (G - H, K - L) tadpoles. *bmp4* exhibits two anterior poles of expression and one posterior pole of expression in the otic vesicle, corresponding to the developing cristae. Expression is also exhibited in tissues derived from the neurogenic placodes, brain, neural tube and pronephros. No difference in the level or pattern of expression was observed between wild type and *kom* tadpoles.

**Figure 5.6: *myoVIIa* expression is not affected in *kom***

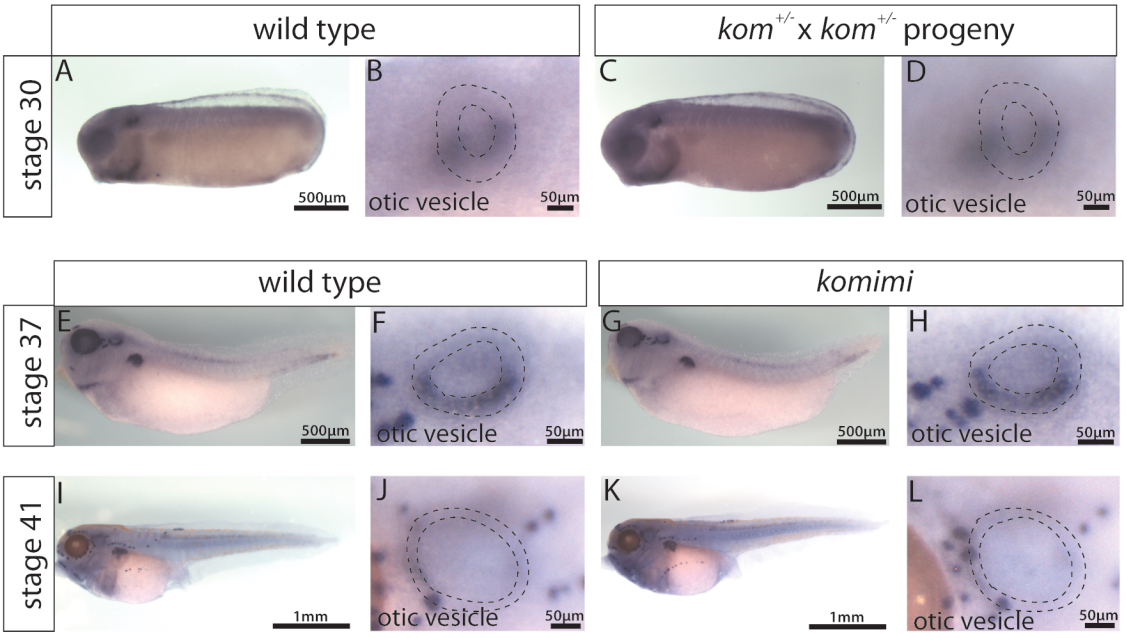


**(A - D)** To determine whether hair cell differentiation is affected in *kom*, *myoVIIa* WISH was carried out on stage 30 wild type embryos (A - B) and embryos obtained from a mating of *kom* carriers (C - D). *myoVIIa* is expressed in the ventral region of the otic vesicle, along with the neurogenic placodes, brain, neural tissue and pronephros. No difference in the level or pattern of expression is apparent.

**(E - L)** *myoVIIa* WISH carried out on stage 37 and 41 wild type and *kom* tadpoles. At stage 37, *myoVIIa* continues to be expressed in the ventral region of the otic vesicle but by stage 41 this expression ceases. Throughout both stages 37 and 41 *myoVIIa* is strongly expressed in the eye and pronephros with weaker expression in the neur genic placodes and the neural tube. By stage 41, *myoVIIa* is also expressed in the neuromasts of the lateral line.

**Figure 5.7: Neuromast structure and activity of the mechanotransduction channel appears unaffected in *kom***

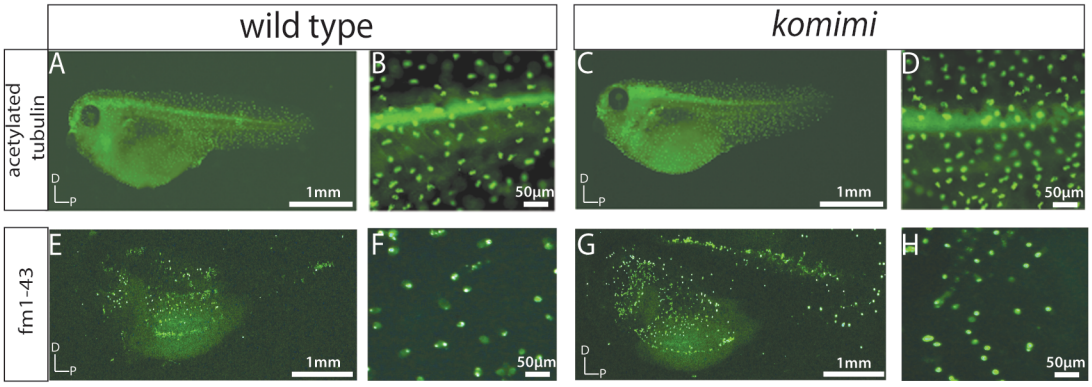


**(A - D)** Neuromast kinocilia were stained using anti-acetylated tubulin. No notable difference in neuromast structure was observed between stage 41 wild type and *kom*.

**(E - H)** Fm1-43 is internalized in stage 41 neuromasts, indicating that the mechanosensory channels are active.

the mechanotransduction channels and fluoresces brightly when intercalated into membranes, such as those of the endoplasmic reticulum and mitochondria, allowing the dye to selectively label active hair cells (Gale et al., 2001; Nishikawa and Saski, 1996). Observations of both the structure and activity of *kom* neuromasts showed no notable difference between wild type and *kom* (fig. 5.7 A – H).

## *5.3 Identification of the kom lesion*

### *5.3.1 The kom lesion resides in a 1.7Mb interval containing oc90*

To understand the genetic cause of the *kom* phenotype, high resolution mapping cloning was carried out to identify a small genetic interval in which the lesion resides. In chapter 3 I showed that the *kom* lesion is linked to SSLP markers 008B06 and 121G10 on the q-arm of chromosome 6 (section 3.2.3.4; fig. 3.13). To define the genetic interval containing the *kom* lesion, SSLP markers flanking the lesion were identified by testing single *kom* tadpoles, obtained from a sibling cross, with polymorphic SSLP markers located on the telomeric and centromeric sides of 008B06 and 121G10. Analyzing a set of 96 mutant embryos revealed that SSLP markers 015A12 (1 recombinant) and 033G06 (2 recombinants) flanked the telomeric and centromeric sides of the lesion, respectively, defining *kom* in an interval of 2.4Mb (fig. 5.8).

Analyzing recombinants in a larger set of tadpoles further narrowed this interval until 188 mutant embryos revealed that SSLP markers 015B05 (2 recombinants), on scaffold_496, and 033G06 (5 recombinants), on scaffold_459, flanked the lesion (fig. 5.9). This defined an interval of 1.7Mb spanning over scaffolds 496, 776 and 459 (fig. 5.8). These scaffolds are known to reside in this interval as the sequence of these scaffolds align with the recently released version 7 genome assembly, which consists of chromosome sized scaffolds.

**Figure 5. 8**: *kom* maps to a 1.7Mb interval on the q-arm of chromosome 6

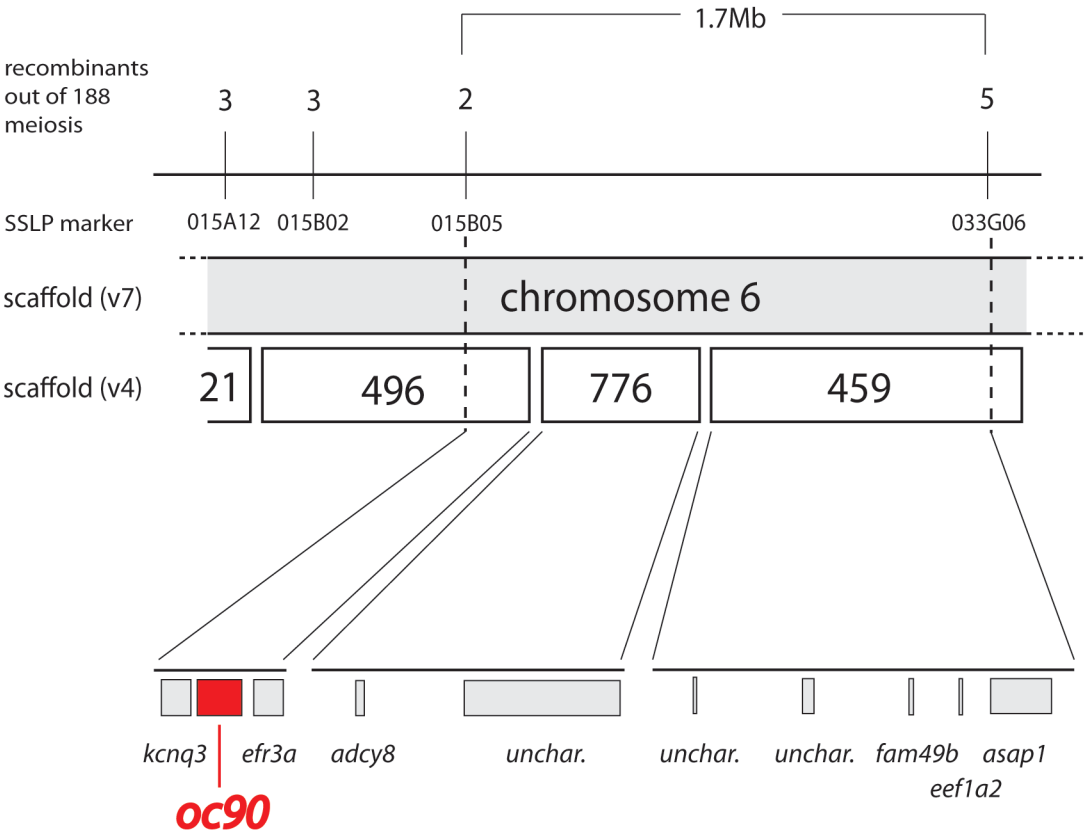


Analysis of polymorphic SSLP markers on the q-arm of chromosome 6 identified markers 015B05 on scaffold_496 and 033G06 on scaffold_459 as flanking the mutation. This defines a genetic interval of 1.7Mb.

The 1.7Mb interval spans scaffolds 496, 776 and 459. *oc90* is a strong candidate gene as it encodes a core otoconin protein and mouse mutations in this gene exhibit large dysmorphic otoconia, comparable to those found in *kom*.

## Table 5.1: Genes located in the *kom* genetic interval

| Gene | Scaffold | Location | Function | Expressed in inner ear? | Reference |
|---|---|---|---|---|---|
| *efr3a* | 496 | 18,049 - 74,683 | EFR3 homolog A | yes | _ |
| *oc90* | 496 | 53,614 - 235,898 | otoconin-90; otoconial matrix protein required for otoconial crystallisation and maintenance | yes | Zhao et al., 2007 |
| *kcnq3* | 496 | 212,778 - 269,915 | K+ channel, expressed in the sensory epithelia of the inner ear | yes | Jin et al., 2009 |
| *adcy8* | 776 | 61,215 - 62,126 | adenylate cyclase 8; involved in intracellular signalling | unknown | _ |
| uncharacterized | 776 | 219,062 - 414,115 | unknown | unknown | _ |
| *asap1* | 459 | 134,078 - 257,426 | ArfGAP with SH3 domain; involved in G-protein signalling | unknown | _ |
| *eef1a2* | 459 | 262,213 - 267,726 | eukaryotic translation elongation factor 1 alpha 1; involved in protein synthesis | yes (ubiquitous) | Ryazanov & Spirin, 1990 |
| *fam49b* | 459 | 334,043 - 344,923 | unknown | unknown | _ |
| uncharacterized | 459 | 481,049 - 503,624 | unknown | unknown | _ |
| uncharacterized | 459 | 807,462 - 807,564 | unknown | unknown | _ |

There are 10 genes models predicted to reside in this 1.7Mb region, four of which are expressed in the inner ear (table 5.1). *otoconin-90* (*oc90*) is a strong candidate as it encodes a core otoconial protein which is essential for crystal formation and maintenance (Wang et al., 1998; Zhao et al., 2007).

### *5.3.2 kom is tightly linked to a mutant allele of otoconin-90 (oc90)*

PCR amplification of *X. tropicalis oc90* exons 2 -13 from cDNA shows a clear decrease in size in *kom* compared to wild type, while no difference is observed when amplifying exons 12 – 19 (fig. 5.9 A). Sequencing of *kom* and wild type *oc90* cDNA shows that exon 3 is missing in the *kom* transcript (fig. 5.9 B), however the reading frame remains in frame. Sequencing of the genomic DNA showed that there is an adenine to guanine transition (fig 5.9 C) in the intron 2/3 splice acceptor site (fig. 5.9 C). Exon 3 encodes the last 6 amino acids of the OC90 signal peptide (Appendix C) and the first 20 amino acids of the OC90 protein (fig. 5.10).

## *5.4 Discussion*

### *5.4.1 kom lesion disrupts exon 2 splice accepter site of oc90 causing deletion of part of the signal peptide*

The *kom* phenotype is likely to be caused by a lesion disrupting a splice acceptor site in *oc90*, causing deletion of exon 3 from the mRNA transcript (fig. 5.9). OC-90 is a key component of the otoconial protein core. It contains two phospholipase A2 domains (PLA2) rich in acidic amino acids and is highly glycosylated causing the protein to have a high affinity for $Ca^{2+}$ (Erway et al., 1986; Wang et al., 1998; Zhao et al., 2007). The PLA2 domains also contain several conserved cysteine residues between which multiple disulphide bonds form, creating a rigid structure on which $CaCO_3$ can crystallize (Wang et al.,

**(A)** PCR amplification of exons 2-13 from wild type and *kom* cDNA shows that the *kom* amplicon is smaller than the wild type. Amplification of exons 12-19 from wild type and *kom* cDNA show no difference.

**(B)** Sequencing of wild type and *kom* cDNA shows exon 3 is missing in the *kom* transcript.

**(C)** Sequencing of wild type and *kom* genomic DNA shows that the intron 2/3 splice acceptor site is mutated, resulting in an adenosine to guanine transition.

**Figure 5.9: A lesion in the intron 2/3 acceptor site results in loss of exon 3 from *kom* transcripts**

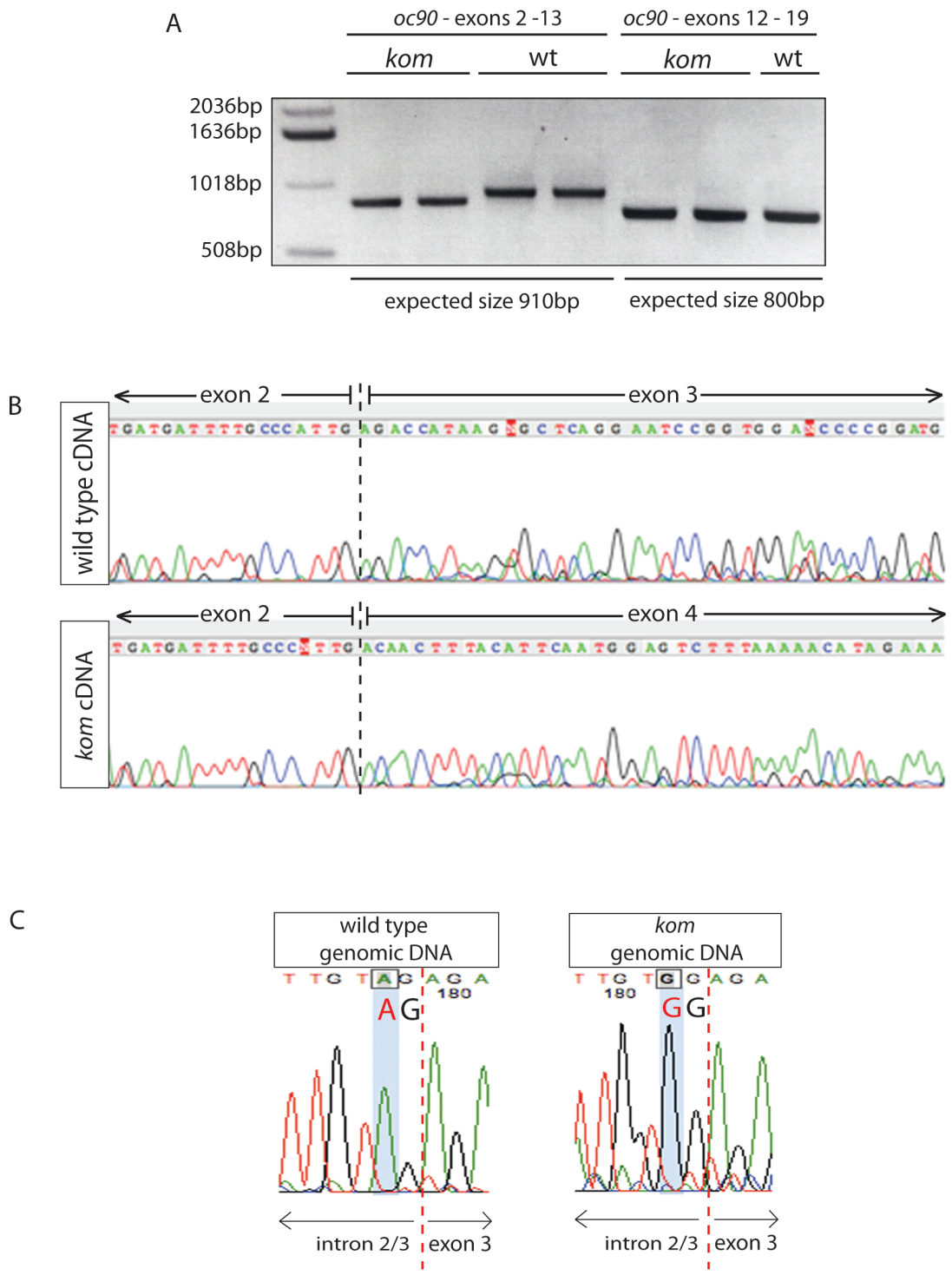

**Figure 5.10:The *kom* lesion causes deletion of part of the OC-90 signal peptide**

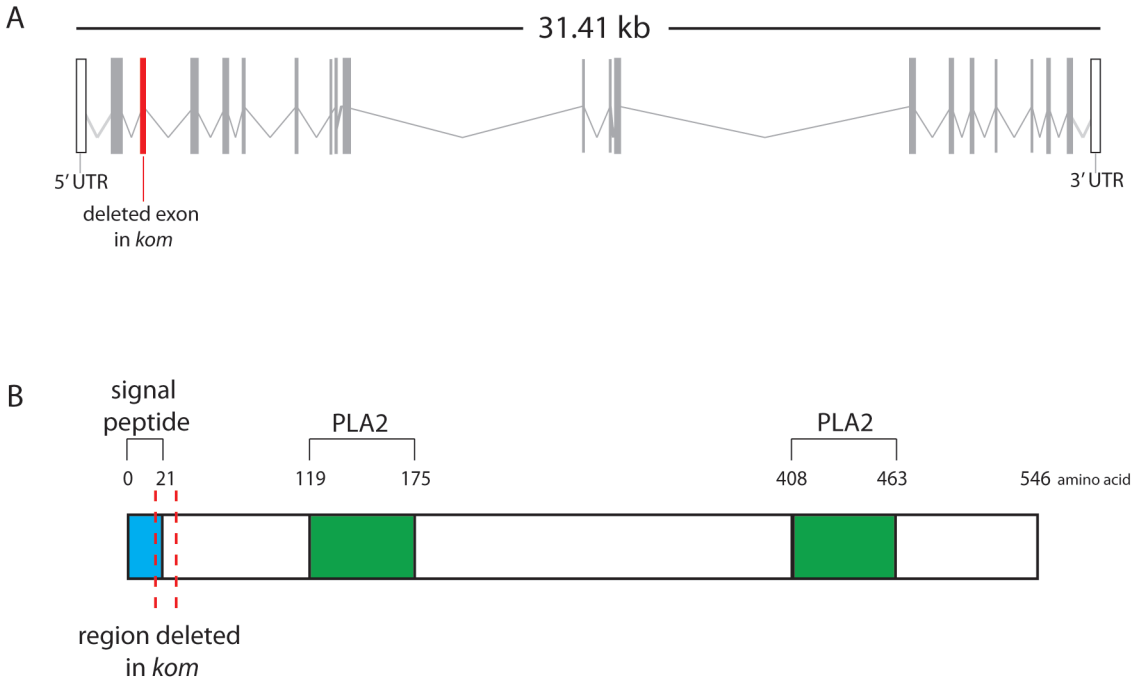


**(A)** Mutation of the *oc90* intron 2/3 splice acceptor site causes deletion of exon 3 from the transcript.

**(B)** The deleted exon in *kom* transcripts removes 26 amino acids from the OC90 protein. The deleted region includes the last 6 amino acids of the signal peptide.

1998; Zhao et al., 2007). In mouse, zebrafish and *X. laevis*, *oc90* is expressed throughout the otic vesicle, with the exception of the sensory epithelial cells, and is secreted into the endolymphatic fluid where it is incorporated into the developing otoconia (Gibert et al., 2011; Petko et al., 2007; Wang et al., 1998; Zhao et al., 2007; see introduction 1.6).

Exon 3 encodes the last 6 amino acids of the predicted OC90 signal peptide (appendix C) and the first 20 amino acids of the mature OC90 protein (fig. 5.9). Disrupting the intron 2/3 splice acceptor site is likely to delete residues encoded by exon 3 causing a slight truncation of the predicted OC90 signal peptide and removal of the signal peptide cleavage site (fig. 5.9 and appendix C). The function of the signal peptide is to target OC90 to the endoplasmic reticulum, where it is expected to undergo post-translational modifications such as glycosylation, before being secreted out of the cell into the endolymphatic fluid (Doudna et al., 2004; Halic et al., 2005; Koch et al., 2003). During translation of the OC90 protein, the newly translated signal peptide is recognized and bound by the signal recognition particle (SRP) (fig. 5.11 A), which halts translation while the ribosome is transported to the endoplasmic reticulum (ER) (fig. 5.11 B). SRP binds to its receptor on the ER and the signal peptide binds to an ER membrane channel, known as a translocon (fig. 5.11 C). Translation is reinitiated and the rest of the protein is moved through the translocon into the ER as it is synthesized (fig. 5.11 D). The SRP then detaches (fig. 5.11 E). At the end of translation the signal peptide is cleaved and the protein is released into the lumen of the ER and continues through the secretary pathway (Doudna et al., 2004; Halic et al., 2005; Koch et al., 2003). In *kom* the loss of the last 6 amino acids of the signal peptide might affect binding of SRP and therefore OC90 may not get transported to the ER. Also the truncated signal peptide may no longer be able to bind efficiently to the translocon and so the OC90 may not be able to enter the ER. Critically, the signal peptide cleavage site is lost (fig. 5.9 and appendix C), so even if OC90 is able to reach and enter the ER it may not be released into the lumen and so does not continue through the

**Figure 5.11: Targeting of secretory proteins to the ER**

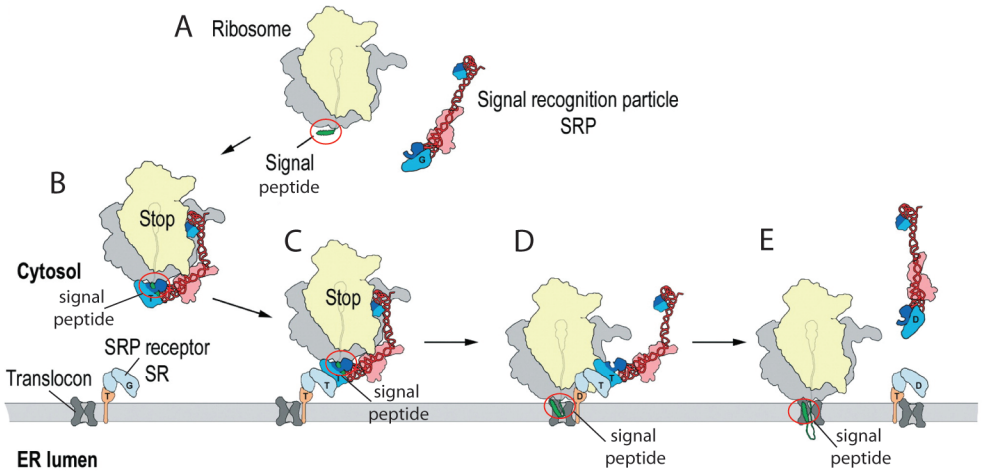


Schematic overview of the co-translational targeting of proteins destined for secretion.

**(A)** SRP interacts with the signal peptide as soon as it emerges from the ribosomal polypeptide exit tunnel.

**(B)** Peptide elongation is halted upon SRP binding.

**(C)** The complex is targeted to the ER membrane by the interaction of SRP with its receptor (SR).

**(D)** The newly synthesized protein is then transferred to the protein channel in the ER membrane (the translocon). The signal peptide binds to the translocon and the newly synthesized protein moves through the channel into the ER.

**(E)** The SRP dissociates. When translation is completed the signal peptide is cleaved and the protein is released into the lumen of the ER.

Adapted from Halic and Beckmann, 2005

secretory pathway. It is therefore possible that in *kom* tadpoles OC90 may fail to move through the secretary pathway to be released into the endolymphatic fluid.

Morpholino knockdown could be used to determine whether OC90 retains any function in *kom*. If injection of a translation blocking ATG morpholino into wild type embryos produced an accurate phenocopy this would suggest that *kom* is a functional null. However, if the ATG morpholino fails to fully phenocopy *kom* but an exon 3 splice blocking morpholino does produce a *kom* phenotype, this would suggest that *kom* OC90 retains some function in the embryo or has a dominant affect. Indication of whether OC90 enters the ER could be obtained through western blot, as if OC90 extracted from *kom* embryos has a significantly lower molecular weight than the wild type this would suggest that post-translational modifications of OC90 are not taking place. Comparing whole mount immunostaining of OC90 between wild type and *kom* would also determine whether the signal peptide is cleaved thus allowing the protein to enter the secretary pathway and be exported into the endolymphatic fluid filling the otic vesicle.

### *5.4.2 Loss of OC90 affects crystallization of both calcitic and aragonitic otoconia*

In *kom* tadpoles, throughout stages 41 – 54 a single large otoconium forms over both the utricle and the sacculus. Closer examination reveals that each otoconium is composed of multiple large crystals that have fused to form agglomerates. OC90 accounts for >90% of the protein core of mammalian and avian otoconia and influences $CaCO_3$ to crystallize in the calcitic polymorph (Pote and Ross, 1991). In amphibians, utricular otoconia are composed of calcite therefore it has been suggested that OC90 may be the dominant otoconin in these crystals (Kurc et al., 1999; Pote and Ross, 1993). Conversely, the core of amphibian saccular otoconia consists of >90% otoconin-22 (OC22) and causes deposition of $CaCO_3$ as aragonite (see introduction 1.6.2) (Kurc et al., 1999; Pote and Ross, 1993). Despite the low amount of OC90 in utricular aragonitic

otoconia, the crystals are still affected in *kom*. OC90 plays a key role during nucleation of otoconia as it recruits other otoconins such as otolin to the protein core as well as proteins associated with the otoconial membrane (Lundberg et al., 2006; Zhao et al., 2007). Expression of otoconins has not been extensively studied in *X. tropicalis*, but relative transcript frequency in cDNA libraries shows that *oc90* is first expressed around stage 35, while *oc22* is expressed much later at approximately stage 50 (Gurdon Institute Xenopus tropicalis EST database http://genomics.nimr.mrc.ac.uk/). As both utricular and saccular otoconia are visible in the otic vesicle around stage 35, it is possible that OC90 plays an early role in recruiting otoconial proteins to the core of aragonitic crystals without forming the bulk of the protein core.

Immunostaining of OC90 during early otoconial development could determine whether OC90 is present in aragonitic otoconia and therefore able to contribute to their development. Also the $CaCO_3$ polymorph deposited in *kom* otoconia could be identified by X-ray diffraction (Zhao et al., 2007) to determine whether both aragonitic and calcitic crystals form *kom*.

### *5.4.3 kom macular phenotype may be caused by mechanical stress or an ionic imbalance in the endolymphatic fluid*

The cells of the maculae appear unaffected in stage 37 *kom* tadpoles, but by stages 41 and 45 the cells differ greatly in size throughout the epithelium and some of the hair cell stereocilia appear splayed (fig. 5.3, fig. 3.11 & fig. 3.12). Analysis of *lufng* WISH suggests that specification of the sensory region is unaffected (fig. 5.4). The expression of cristae marker *bmp4* (fig. 5.5) and the hair cell marker *myoVIIa* (fig. 5.6) indicates that sensory epithelia differentiation is unaffected also. The late onset of the macular phenotype along with the expression data of specification and differentiation markers indicates that early macular development is unaffected in *kom*.

Mechanical stress is a potential cause of the macular phenotype in *kom*. The otoconial agglomerates produced in *kom* tadpoles are many orders of magnitude larger than those found in wild type (fig. 5.2) and it is possible that the excessive mass may damage the sensory cells located beneath them. Enlarged otoconia are also found in the *ssk* and *leg* mutants and these mutants do not display macular defects, however the crystals produced in these mutants only reach half the size of those found in *kom*. Macular damage could be assessed in *kom* tadpoles by TUNEL staining to determine whether the cells are undergoing cell death.

### *5.4.3 kom behavioral phenotype is likely caused by the defective maculae and excessive otoconial mass*

The function of the macular sensory epithelia is to provide balance information, therefore given the macular defect observed in *kom* it is unsurprising that the tadpoles experience problems balancing. Also, as the primary function of the otoconia is to act as an inertial mass to deflect the underlying hair cells, it is likely that the excessive mass of the *kom* otoconia are contributing to the animals distorted sense of balance.

### *5.4.4 Future studies*

OC90 is known to bind otoconial proteins such as otolin and recruit them to the otoconial core, however the full complement of proteins recognized by OC90 is not known. Co-IP of OC90 from a range of developmental stages could be used to obtain the proteins interacting with OC90 followed by mass spectrometry to aid protein identification.

## *5.5 Summary*

The *kom* phenotype is characterized by the presence of a single enlarged otoconium located over each macula and behavioral balance defects such as circular swimming. The *kom* phenotype is likely to be caused by an adenosine to guanine transversion that disrupts the intron 2/3 splice acceptor site in *oc90,* causing deletion of exon 3 from the mRNA (fig. 5.9). Loss of exon 3 results in deletion of the last 6 amino acids of the signal peptide and the first 20 amino acids of the mature protein, potentially hindering movement of OC90 through the secretary pathway. OC90 is a core otoconial protein comprising >90% of the core of calcitic otoconia, while OC22 comprises >90% of the core of aragonitic otoconia. Despite the low proportion of OC90 in aragonitic otoconia, the development of both types of otoconia is affected in *kom.* This is potentially due to OC90 playing a role in the recruitment of otoconial proteins to the early development of both aragonitic and calcitic otoconia.

The early development of the macula does not appear to be affected in *kom* development, however by stage 41 the macular epithelial cells vary greatly in size throughout the epithelia and by stage 45 the uniform columnar structure of the epithelia is lost. At present the cause of this defect is not understood. One possible explanation is that the excessive mass of the *kom* otoconia damages the cells residing beneath it.

# Chapter 6

# Concluding remarks

## 6.1 Summary of findings

### 6.1.1 A pilot forward genetic screen identified four X. tropicalis mutants with a primary inner ear defect

The aim of this thesis is to use *X. tropicalis* forward genetics as a tool to identify novel gene functions important for inner ear development. Seven candidate inner ear phenotypes displaying a primary defect in inner ear formation were identified as part of a forward genetic screen for *X. tropicalis* developmental defects (Goda et al., 2006). Dr. Tada Goda and I determined that the *ssk*, *kom*, *leg* and *bun* phenotypes were heritable and therefore caused by an underlying genetic lesion (see table 3.1). The purpose of this study was to ascertain the primary inner ear defect of each of the four mutants and determine on which chromosome arm the lesion resides. Two mutants were then selected for high resolution positional cloning and further phenotypic characterization to identify the underlying lesion and its role in inner ear development.

The *ssk* mutant has enlarged otoconial crystals, decreased pigmentation and balance defects. Histological sections and immunostaining of hair cell and neural markers show that the gross morphology of the inner ear and the patterning of the sensory epithelia are unaffected in stage 45 mutants. Gynogenetic linkage to centromeric SSLP markers revealed that the *ssk* lesion resides on the p-arm of chromosome 1. In *kom* mutants, a single large otoconium forms over each macula, and tadpoles exhibit strong balance defects such as circular swimming. In stage 45 mutants, the cells comprising the macula are dysmorphic and lack the columnar structure found in wild type, but other morphological features of the inner ear appear normal. The *kom* lesion is linked to SSLP markers on the q-arm of chromosome 6. The *bun* phenotype is characterized by the formation of a small otic vesicle and only one discernable otoconial patch. Further investigation showed that ~35% fewer macular hair cells form in stage 45 *bun* tadpoles and that the epithelium is enlarged along the apical-basal axis. No clear distinction

between the utricular and saccular maculae is visible, and the semicircular canals fail to form. The *bun* lesion shows linkage to the p-arm of chromosome 2. Finally the *leg* mutant was found to also display enlarged otoconia and closer examination reveals no other morphological inner ear defects. The *leg* phenotype is linked to SSLP markers on the q-arm of chromosome 5.

Out of the four identified inner ear mutant phenotypes, *ssk* and *kom* were selected for further study.

### *6.1.2 The X. tropicalis mutation ssk disrupts adapter protein-3 function*

Positional cloning and sequencing of candidate genes identified that *ssk* is caused by a premature stop codon in *ap3δ1* (see fig. 4.6 and 4.7), a gene that encodes a subunit in the AP-3 complex (see fig. 4.10). AP-3 transports protein cargo from the endosome and golgi to lysosome-related organelles (LROs), a class of organelles that degrade intracellular proteins but also have cell specific functions such as ionic regulation and pigment synthesis. Defects in this pathway are known to cause the human pathology Hermansky-Pudlak syndrome.

During embryonic development, the *ap3δ1* transcript is expressed in the endolymphatic sac and in melanocytes (see fig. 4.9), both of which function to maintain the ionic environment of the endolymphatic fluid (Tu et al., 1998; Wangemann et al., 1995; Wangemann et al., 2007). This suggests that the otoconial defect may be the result of an ionic imbalance. Work carried out in the *mocha* mouse supports this theory as providing pregnant dams with $Zn^{2+}$ and $Mn^{2+}$ supplements partially rescues the otoconial phenotype (Balkema et al., 1983; Feng et al., 1999; Rolfsen & Erway, 1984). The *ap3δ1* transcript is also expressed in the brain, neural tube, pronephros, neuromasts and neural crest (see fig. 4.9). Defects in these tissues have been observed in Hermanky-Pudlak syndrome (Huizing et al., 2001; Shotelersuk et al., 2000), however potential phenotypes in these tissues are yet to be investigated in *ssk*.

The AP3δ1 protein is severely truncated in *ssk* mutants. Despite this truncation, some pigment is clearly visible in the melanosomes, and a fraction of these melanosomes are still able to translocate throughout the cell (see fig. 4.5). These observations suggest that at least in the melanophores, some of the AP-3 cargos such as those involved in pigment synthesis, are able to reach the LRO. This phenotype could be caused by the *ssk ap3δ1* retaining some function and acting as a hypomorph. Another possibility is that a different AP complex is compensating for AP-3 function. AP-1 is also known to transport proteins from the endosome to LROs and can bind some of the same protein cargo as AP-3 (Janvier et al., 2003; Kyttala et al., 2005; Theos et al., 2005). The *ap1γ1* transcript is upregulated in response to the *ssk* lesion (see fig. 4.13 and 4.14), indicating cross-regulation between the AP complexes. Whether AP1γ1 is upregulated at the protein level and whether it can functionally compensate for loss of AP-3 function is unknown. Injection of sub-threshold levels of *ap1γ1* morpholino into *ssk* embryos could identify functional redundancy between AP-1 and AP-3. Production of a more severe phenotype would indicate that AP-1 is compensating for lack of AP-3 function.

### *6.1.3 The X. tropicalis mutant kom deletes most of the otoconin-90 signaling peptide*

The *kom* phenotype is characterized by the presence of a single large otoconium over each macular and behavioral balance defects such as circular swimming. Early sensory epithelial development appears unaffected in *kom* however by stage 41 the macular epithelial cells differ greatly in size. Histology and immunostaining of stage 45 tadpoles show that the epithelia is disorganized and lacks the uniform columnar morphology found in wild type. High resolution mapping and sequencing of candidate genes indentified an adenosine to guanine transition in the exon 3 splice acceptor site of *oc90* causing the deletion of exon 3 from the mRNA. OC90 is one of the dominant otoconial proteins comprising the

core of calcitic otoconia (Pote and Ross, 1991). The protein contains two acidic PLA2 domains and is highly glycosylated causing it to have a strong affinity for $Ca^{2+}$ (Erway et al., 1986; Wang et al., 1998; Zhao et al., 2007). OC90 is also known to play a role in recruiting other otoconial proteins to the developing crystal (Lundberg et al., 2006; Zhao et al., 2007). The deletion of exon 3 results in the loss of the last 6 amino acids of the predicted signal peptide and the first 20 amino acids of the mature protein. Disruption of the signal peptide may result in failure of OC90 to move through the secretary pathway, which in wild type would result in post-translational modifications such as glycosylation and secretion into the endolymphatic fluid.

Amphibians develop both calcitic and aragonitic otoconia. In birds and mammals OC90 comprise >90% of the protein core of calcitic otoconia and it has been suggested that OC90 may be the dominant otoconin in amphibian calcitic otoconia, while OC22 is the dominant otoconin to aragonitic otoconia (Kurc et al., 1999; Pote and Ross, 1991; Pote and Ross, 1993). Despite this the development of both aragonitic and calcitic otoconia is affected in *kom*. *oc90* is expressed much earlier in development than *oc22* and as OC90 is known to recruit otoconial proteins to the developing otoconial core, it is possible that OC90 plays a key role in the early development of both otoconia without comprising the bulk of the protein core of aragonitic crystals.

At present the cause of the macular phenotype in unknown, but it is possible that the excessive otoconial mass in *kom* causes damage to the epithelial cells located beneath them.

### *6.2 Advantages and disadvantages of forward genetics*

Studies of mutations identified in forward genetic screens have been invaluable in identifying novel gene functions. The pilot *X. tropicalis* forward genetic screen,

carried out in the Zimmerman laboratory, has identified mutant phenotypes affecting a diverse range of developmental functions (Goda et al., 2006). A positional cloning strategy has been adopted to identify mutant lesions and at present six have been successfully identified (Abu-Daya et al., 2009; Geach et al., 2010; Zimmerman lab unpublished data). Successful positional cloning relies on a high density of polymorphic markers, an adequate recombination rate and an accurately assembled genome in the vicinity of the lesion. If any of these factors are lacking, positional cloning can be very time consuming and laborious. Recent revisions of the *X. tropicalis* genome assembly and meiotic map have greatly improved the accuracy and coverage of the physical genome, which will increase the rate at which lesions can be identified by positional cloning.

Adapting technologies such as exon capture and resequencing of mutant genomes, well established in human and mouse, are also likely to greatly simplify identification of mutations. Exon capture involves sequencing the protein coding regions of all the identified genes in the *X. tropicalis* genome, either form a carrier individual (for direct identification of sequence lesion) or from pools (>50) of mutant and wild type individuals to simultaneously obtain linkage information. The sequences are aligned and compared so that single nucleotide polymorphisms (SNPs) can be identified and their relative abundance can be used as information for mapping. SNPs that are not linked to the mutation will be found in a ~1:1 ratio while those located close to the lesion would show increasing levels of homozygosity in the mutant pool. This nucleotide bias that would increase in frequency with proximity to the lesion and could also identify the lesion responsible for the mutant phenotype. The exon capture protocol can be carried out within a couple of weeks, and pilot studies carried out in the Khokha laboratory have shown that this can be a successful method for rapidly identifying *X. tropicalis* mutant lesions (personal communication). Insertional mutagenesis screens would also provide a valuable approach for obtaining mutants, as once a mutant phenotype is identified the mutated gene can quickly

be identified by PCR amplification and sequencing of the DNA surrounding the inserted transposable element.

### *6.3 Future directions*

The *X. tropicalis* forward genetic screen was broad in scope, and developmental defects in organs such as the muscle, heart, eye, and neural crest were detected as well as mutations affecting the inner ear (Goda et al., 2006). Focused screens for inner ear developmental defects in *X. tropicalis* would be invaluable as the otic placode is morphologically visible and the head becomes progressively transparent, allowing the inner ear to be observed throughout its development (Bever et al., 2003; Quick & Serrano et al., 2005). In the current screen, inner ear defects were identified during otic vesicle stages, however WISH of early induction and patterning markers (e.g. *pax2*, *pax8*, *fgf3*, *hmx3*, *otx2*, *dlx3*; see introduction section 1.4) could allow mutant phenotypes to be detected at much earlier stages. Also, carrying out mutagenesis screens on transgenic hair cell lines would allow live embryos to be screened for developmental sensory epithelial defects. A parvalbumin-3 GFP transgenic, which is expressed specifically in the hair cells on the inner ear and lateral line, has recently been developed (Grainger lab personal communication) and would be amenable to this type of screen.

Amphibians have a remarkable ability to regenerate damaged hair cells in the inner ear, a trait that is not shared by mammals. Hair cells are easily damaged by exposure to noisy environments, ototoxic compounds (such as aminoglycoside antibiotics and platinum-containing chemotherapy drugs), and old age, therefore it is unsurprising that hearing and balance defects are the most common form of human sensory impairment (Bindu and Reddy, 2008; Dror and Avraham, 2009; Van Eyken et al, 2007). Understanding the mechanisms of how amphibians regenerate damaged hair cells could provide information on how to manipulate human hair cells to do the same. Genes involved in *X. tropicalis* hair cell

regeneration could be identified in a forward genetic mutagenesis screen through the use of a transgenic reporter line. Kaede is a fluorescent molecule that slowly undergoes a conformational change causing the fluorescent wavelength emitted to change from the green spectrum to the red spectrum (Ando et al., 2002). A parvalbumin-3 kaede transgenic line exposed to ototoxic drugs could be screened for regeneration defects as newly formed hair cells would emit green light while the original hair cells would emit red.

Identifying mutations in genes known to have a role in inner ear development would also be useful as *X. tropicalis* in amenable to techniques such as tissue transplantation, allowing the signaling properties of mutant genes on wild type tissue to be examined. Work is currently being carried out in the *X. tropicalis* community to establish reverse genetic techniques such as TILLING (targeted induced lesions in genomes) and in the future this will be a valuable source for obtaining mutants (Goda et al., 2006; Stemple personal communication). Zinc-finger nuclease technology has also been adapted to *X. tropicalis* and animals carrying mutations in *noggin* have recently been produced in Prof. Richard Harland's laboratory (Young et al., 2011).

The work presented in this thesis shows that *X. tropicalis* forward genetics is a valuable system for studying inner ear development. The accessibility of large numbers of externally developing embryos as well as the transparency of the otic vesicle allows the inner ear to be observed throughout its development. The chemical mutagenesis and screen identified seven inner ear phenotypes, four were confirmed to have a genetic cause. The underlying lesion causing two of the mutant phenotypes were successfully identified by positional cloning, and analysis of the resulting phenotypes have provided new insights into inner ear development. In the future, carrying out focused screens by analysis of *in situ* hybridization markers and/or through the use of transgenic lines will greatly contribute to our understanding of inner ear development.

# Chapter 7

# Bibliography

Abbate, F., Catania, S., Germana, A., Gonzalez, T., Diaz-Esnal, B., Germana, G. and Vega, J. (2002). S-100 protein is a selective marker for sensory hair cells of the lateral line teleosts. Neuroscience Letters 329, 133-136.

Abu-Daya, A., Sater, A., Wells, D., Mohun, T. and Zimmerman, L. (2009). Absence of heartbeat in the Xenopus tropicalis mutation muzak is caused by a nonsense mutaiton in cardiac mysoin myh6. Developmental Biology 336, 20-29.

Acampora, D., Mazan, S., Avantaggiato, V., Barone, P., Tuorto, F., Lallemand, Y., Brulet, P. and Simeone, A. (1996). Epilepsy and brain abnormalities in mice lacking the Otx1 gene. Nature Genetics 14, 218-222.

Adam, J., Myat, A., Le Roux, I., Eddinson, M., Henrique, D., Ish-Horowicz, D. and Lewis, J. (1998). Cell fate choices and the expression of Notch, Delta and Serrate homologues in the chick inner ear: parallels with Drosophila sense-organ development. Development 125, 4645-4654.

Adamska, M., Leger, S., Brand, M., Hadryst, T., Braun, T. and Bober, E. (2000). Inner ear and lateral line expression of a zebrafish Nkx5-1 gene and irs downregulation in the ears of FGF8 mutant, ace. Mechansims of Development 97, 161-165.

Agrup, C., Bagger-Sjoback, D. and Fryckstedt, J. (1999). Presence of plasma membrane-bound Ca(2+)-ATPase in the secretory epithelia of the inner ear. Acta oto-laryngologica 119, 437-445.

Amaya, E., Offield, M. and Grainger, R. (1998). Frog genetics: Xenopus tropicalis jumps into the future. Trends in Genetics 14, 253-255.

Ando, R., Hama, H., Hino, M., Mizuno, H. and Miyawaki. (2002). An optical marker based on the UV-induced green-to-red photoconversion of a fluorescent

protein. Proceedings of hte National Academy of science of the United States of America 99, 12651-12656.

Baker, C., O'Neill, P. and McCole, R. (2008). Lateral line, otic and epibranchial placodes: developmental and evolutionary links? Journal of Experimental Zoology 310, 370-383.

Balkema, G., Mangini, N. and Pinto, L. (1983). Discrete visual defects in pearly mutant mice. Science 219, 1085-1087.

Ballarino, J. and Howland, H. (1982). Otoconial morphology of the developing chick. American Association of Anatomists 204, 83-87.

Balling (2001). ENU mutagenesis: analyzing gene function in mice. Annual Review of Genomics Human Genetics 2, 463-492.

Bashtanov, M., Goodyear, R., RIchardson, G. and Russell, I. (2004). The mechanical properties of chick (Gallus domesticus) sensory hair bundles: relative contributions of structures sensitive to calcium chelation and subtilisin treatment. Journal of Physiology 559, 287-299.

Bass, A. and McKibben, J. (2002). Neural mechanisms and behaviors for acoustic communication in teleost fish. Progress in Neurobiology 69, 1-26.

Beisel, K., Rocha-Sanchez, S., Ziegenbein, S., Morris, K., Kai, C., Kawai, J., Carninci, O., Hayashizaki, Y. and Davis, R. (2007). Diversity of $Ca^{2+}$ activated $K^{+}$ channel transcripts in inner ear hair cells. Gene 386, 11-23.

Bever, M. and Fekete, D. (2002). Atlas of the developing inner ear in zebrafish. Developmental Dynamics 223, 536-543.

Bever, M., Jean, Y. and Fekete, D. (2003). Three-dimensional morphology of inner ear development in Xenopus laevis. Developmental Dynamics 227, 422-430.

Bhattacharyya, T. K. and Kumar, A. (2005) Vestibular cytotoxicity in gentamicin-treated frogs: a preliminary report. American Journal of Otolaryngology 26(2), 91-95.

Blasiole, B., Canfield, V., Vollrath, M., Huss, D., Mohideen, M., Dickman, J., Cheng, K., Fekete, D. and Levenson, R. (2006) Separate Na, K-ATPase genes are required for otolith formation and semi-circular canal development in zebrafish. Developmental Biology 294, 148-160.

Bleckmann, H., Weiss, O. and Bullock, T. (1989). Physiology of lateral line mechanoreceptive regions in the elasmobranch brain. Journal of comparative physiology 164, 459-474.

Boehm, M and Bonifacino, J.S. (2001). Adaptins: the final recount. Molecular Cell Biology 12(10), 2907-2920.

Bok, J., Chang, W. and Wu, D. (2007). Patterning and morphogenesis of the vertebrate inner ear. International Journal of Developmental Biology 51, 521-533.

Breuskin, I., Bodson, M., Thelen, N., Thiry, M., Borgs, L., Nguyen, L., Stolt, C., Wegner, M., Lefebvre, P. and Malgrange, B. (2010). Glial but not neuronal development in the cochleo-vestibular ganglion requires Sox10. Journal of Neurochemistry 114, 1827-1839.

Brigande, J., Iten, L. and Fekete, D. (2000). A fate map of chick otic cup closure reveals lineage boundaries in the dorsal otocyst. Developmental Biology 227, 256-270.

Brown, S., Wang, J and Groves, A. (2005) Dlx gene expression during chick inner ear development. Journal of Neurobiology 483, 48-65.

Brownstein, Z., Dror, A., Gilony, D., Migirov, L., Hirschberg, K. and Avraham, K. (2008) A novel SLC26A4 (PDS) deafness mutation retained in the endoplasmic reticulum. Archives of Otolaryngology 134, 403.

Burton, Q., Cole, L., Mulheisen, M., Chang, W. and Wu, D. (2004). The role of Pax2 in mouse inner ear development. Developmental Biology 272, 161-175.

Chiang, P., Oiso, N., Gautam, R., Suzuki, T, Swank, R. and Spritz, R. (2003) The Hermansky-Pudlak syndrome 1 (HPS1) and HPS4 proteins are components of two complexes, BLOC-3 and BLOC-4, involved in the biogenesis of lysosome-related organelles. Journal of Biochemistry 278, 20332-20337.

Choo, D., Ward, J., Reece, A., Dou, H., Lin, Z. and Greinwald, J. (2006). Molecular mechanisms underlying inner ear patterning defects in kreisler mutants. Developmental Biology 289, 308-317.

Ciciotte, S., Gwynn, B., Moriyama, K., Huizing, M., Gahl, W., Bonifacino, J. and Peters, L. (2003) Platelet storage pool deficiency associated with inherited abnormalities of the inner ear in the mouse pigment mutants muted an dmocha. Blood 101, 4402-4407.

Clark, R., Stinchcombe, J. D., A, Blott, E., Booth, S., Bossi, G., Hamblin, T., Davies, E. and Griffths, G. (2003). Adapter protein 3-dependent microtubule-mediated movement of lytic granules to the immunological synapse. Nature Immunology 4, 1111-1120.

Colantonio, J., Vermot, J., Wu, D., Langenbacher, A., Fraser, S., Chen, J. and Hill, K. (2009). The dynein regulatory complex is required for ciliary motility and otolith biogenesis in the inner ear. Nature 457, 205-209.

Cole, L., Le Roux, I., Nunes, F., Laufer, E., Lewis, J. and Wu, D. (2000). Sensory organ generation in the chicken inner ear: contribution of bone morphogenetic protein 4, serrate 1, and lunatic fringe. Journal of Comparative Neurology 424, 509-520.

Corey, D. and Hudspeth, A. (1983). Analysis of the microphonic potential of the bullfrog's sacculus. Journal of Neuroscience 3, 942-961.

Corey, D. and Hudspeth, A. (1983). Kinetics of the receptor current in bullfrog saccular hair cells. Journal of Neuroscience 3, 962-976.

Crouch, J. and Schulte, B. (1996). Identification and cloning of site C splice variants of plasma membrane Ca-ATPase in the gerbil cochlea. Hearing Research 101, 55-61.

Daudet, N., Ariza-McNaughton, L. and Lewis, J. (2007). Notch signalling is needed to maintain, but not to initiate, the formation of prosensory patches in the chick inner ear. Development 134, 2369-2378.

Daudet, N. and Lewis, J. (2005). Two contrasting roles for Notch activity in chick inner ear development: specification of prosensory patches and lateral inhibition of hair-cell differentiation. Development 132, 541-551.

Dell'Angelica, E., Shotelersuk, V., Aguilar, R., Gahl, W. and Bonifacino, J. (1999). Altered trafficking of lysosomal proteins in Hermansky-Pudlak syndrome due to mutations in the beta 3A subunit of the AP-3 adaptor. Molecular Cell 3, 11-21.

Dijkgraaf, S. (1963). The functioning an dsignificance of the lateral-line organs. Biological reviews of the Cambridge Philosophical Society 38, 51-105.

Di Palma, F., Belyantseva, I., Kim, H., Vogt, T., Kachar, B. and Noben-Trauth, K. (2002) Mutatiosn in Mcoln3 associated with deafness and pigmentation defects in varitint-waddler (Va) mice. Proceedings of the National Academy of Sciences of the United States of America 99, 14994-14999.

Dou, H., Xu, J., Wang, Z., Smith, A., Soleimani, M., Karet, F., Greinwald, J. and Choo, D. (2004). Co-expression of pendrin, vacuolar H+-ATPase alpha4-subunit and carbonic anhydrase II in epithelial cells of the murine endolymphatic sac. The Journal of Histochemistry and Cytochemistry 52, 1377-1384.

Doudna, J. and Batey, R. (2004). Structural insights into the signal recognition particle. Annual Review of Biochemistry 73, 539-557.

Ernest, S., Rauch, G., Haffter, P., Geisler, R., Petit, C. and Nicolson, T. (2000). Mariner is defective in myosin VIIA: a zebrafish model for human hereditary deafness. Human Molecular Genetics 9, 2189-2196.

Erway, L. and Grider, A. J. (1984). Zinc metabolism in lethal-milk mice. Otolith, lactation, and aging effects. Journal of Heredity 75, 480-484.

Erway, L., Purichia, N., Netzler, E., D'Amore, M., Esses, D. and Levine, M. (1986). Genes, manganese, and zinc in formation of otoconia: labeling, recovery, and maternal effects. Scanning Electron Microscopy 4, 1681-1694.

Etheridge, S., Ray, S., Li, S., Hamblet, N., Lijam, N., Tsang, M., Greer, J., Karods, N., Wang, J., Sussman, D., Chen, P. and Wynshaw-Boris, A. (2008). Murine disheveled 3 functions in redundant pathways with dushevelled 1 and 2 in

normal cardiac outflow tract, chochlea, and neural tube development. PLoS Genetics 4(11), e1000259

Falcon-Perez, J., Starcevic, M., Gautam, R. and Dell'Angelica, E. (2002) BLOC-1, a novel complex containing the pallidin an dmutated proteins involved in the biogenesis of melanosomes and platelet0dense granules. Journal of Biochemistry 277, 28191-28199.

Fekete, D. and Campero, A. (2007). Axon guidance in the inner ear. International Journal of Developmental Biology 51, 549-556.

Fekete, D. and Wu, D. (2002). Molecular anatomy of placode development in Xenopus laevis. Current Opinion in Neurobiology 12, 35-42.

Feng, L., Seymour, A., Jiang, S., TO, A., Pden, A., Novak, E., Zhen, L., Rusiniak, M., Eicher, E., Robinson, M. et al. (1999). The beta3A subunit gene (Ap3b1) of the AP-3 adaptor complex is altered in the mouse hypopigmentation mutant pearl, a model for Hermansky-Pudlak syndrome and night blindness. Human Molecular Genetics 8, 323-330.

Frenz, D. and Van De Water, T. (1991). Epithelial control of periotic mesenchyme chondrogenesis. Developmental Biology 144, 38-46.

Furness, D., Katori, Y., Nirmal Kumar, B. and Hackney, C. (2008). The dimensions and structural attachments of tip links in mammalian cochlear hair cells and the effects of exposure to different levels of extracellular calcium. Neuroscience 154, 10-21.

Gahl, W., Brantly, M., Kaiser-Kupfer, M., Iwata, F., Hazelwood, S., Shotelersuk, V., Duffy, L., Kuehl, E., Troendle, J. and Bernardini, I. (1998). Genetic defects and clinical characeteristics of patients with a form of oculocutaneous albinism

(Hermansky-Pudlak syndrome). New England Journal of Medicine 338, 1258-1264.

Gale, J., Marcotti, W., Kennedy, H., Kros, C. and Richardson, G. (2001). FM1-42 behaves as a permeant blocker of the hair-cell mechanotransducer channel. Journal of Neuroscience 21, 7013-7025

Geach, T. and Zimmerman, L. (2010). Paralysis and delayed Z-disc formation in the Xenopus tropicalis unc45b mutant dicky ticker. BMC Developmental Biology.10, 75-83.

Gerlach, L., Hutson, M., Germiller, J., Nguyen-Luu, Victor, J. and Barald, K. (2000). Addition of the BMP4 antagonist, noggin, disrupts avain inner ear development. Development. 127, 45-54.

Gibert, Y., Sassi-Messai, S., Fini, J., Bernard, L., Zalko, D., Cravedi, J., Balaguerm P., Andersson-Lendahl, M., Demeneix, B. and Laudet, V. (2011). Bisphenol A induces otolith malformations during vertebrate embryogenesis. BMC Developmental Biology. 147, (11) 4.

Goda, T., Abu-Daya, A., Carruthers, S., Clark, M., Stemple, D. and Zimmerman, L. (2006). Genetic screens for mutations affecting development of Xenopus tropicalis. PLoS Genetics 2, e91.

Goodyear, R., Forge, A., Legan , P. and Richardson, G. (2010) A symmetric distribution of cadherin 23 and protocadherin 15 in the kinocilial links of avian sensory hair cells. Journal of Comparative Biology 518. 4288-4297.

Goodyear, R. and RIchardson, G. (1999). The ankle-link antigen: an epitope sensitive to calcium chelation associated with the hair-cell surface and the calycal processes of photoreceptors. Journal of Neuroscience 19, 3761-3772.

Grider, A. J. (Erway, LC). Intestinal metallothioneion in lethal-milk mice with systemic zinc deficiency. Biochemical Genetics 24, 635-642.

Guyonneau, L., Murisier, F., Rossier, A., Moulin, A. and Beermann, F. (2004). Melanocytes and pigmentation are affected in dopachrome tautomerase knockout mice. Molecular cell biology 24, 3396-3403.

Haddon, C., Jiang, Y., SMithers, L. and Lewis, J. (1998). Delta-Notch signalling and the patterning of sensory cell differentiation in the zebrafish ear: evidence from the mind bomb mutant. Development 125, 4637-4644.

Haddon, C. and Lewis, J. (1996). Inner ear formation during the early larval development of Xenopus laevis. Journal of Comparative Neurology 365, 113-128.

Halic, M. and Beckmann, R. (2005). The signal recognition particle and its interactions during protein targeting. Current Opinion in Structural Biology. 15, 116-125.

Hammond, K., Loynes, H., Folarin, A., Smith, J. and Whitfield, T. (2002). Hedgehog signalling is required for correct anteroposterior patterning of the zebrafish otic vesicle. Development 130, 1403-1417.

Hammond, K., Loynes, H., Folarin, A., Smith, J. and Whitfield, T. (2003). Hedgehog signalling is required for correct anteroposterior patterning of the zebrafish otic vesicle. Development 130, 1403-1417.

Hardisty-Hughes, R., Parkers, A. and Brown, S. (2010). A hearing and vestibular phenotyping pipeline to identify mouse mutants with hearing impairment. Nature Protocols 5, 177-190.

Heller, S., Bell, A., Denis, C., Choe, Y and Hudspeth, A. (2002) Parvalbumin 3 is an abundant Ca2+ buffer in hair cells. Journal of the Association for Research in Otolatyngology 3, 488-498.

Hellsten, U., Harland, R., Gilchrist, M., Hendrix, D., Jurka, J., Kapitonov, V., Ovcharenko, I., Putnam, N., Shu, S., Taher, L. et al. (2010). The genome of the Western clawed frog Xenopus tropicalis. Science 328, 633-636.

Hermansky, F. and Pudlak, P. (1959). Albinism associated with hemorrhagic diathesis and unusual pigmented reticular cells in the bone marrow: report of two cases with hsitochemical studies. 1959 14, 162-169.

Hirsch, N., Zimmerman, L., Gray, J., Chae, J., Curran, K., Fisher, M., Ogino, H. and Grainger, R. (2002). Xenopus tropicalis transgenic lines and their use in the study of embryonic induction. Developmental Dynamics 225, 522-535.

Honing, S., sandoval, I. and von Figura, K. (1998). A di-leucine-motif in the cytoplasmic tail of LIMP-II an dtyrosinase mediates selective binding of AP-3. EMBO 17, 1304-1314.

Hughes, I., Thalmann, I., Thalmann, R. and Ornitz, D. (2006). Mixing model systems: using zebrafish and mouse inner ear mutants and other organ systems to unravel the mystery of otoconial development. Brain Research 1091, 58-74.

Huizing, M., Anikster, Y and Gahl, W. (2000). Hermansky-Pudlak syndrome and related disorders of organelle formation. Traffic. 1, 823-835.

Huizing, M., Anikster, Y., Fitzpatrick, D., Jeong, A., D'Souza, M., Rausche, M., JR, T., Kaiser-Kupfer, L., WHite, J. and Gahl, W. (2001). Hermansky-Pudlak syndrome type 3 in Ashenazi Jews and other non-Puerto Rican patients with

hypopigmentation and platelet storage-pool deficiency. American Journal of Human Genetics 69, 1022-1032.

Huizing, M., Boissy, R. and Gahl, W. (2002). Hermansky-Puslak Syndrome: Vesicle formation from yeast to man. Pigment cell research 15, 405-419.

Ibsch, M., Anken, R. and Rahmann, H. (2004). Calcium gradients in the fish inner ear sensory epithelium and otolithic membrane visualized by energy filtering transmission electron microscopy (EFTEM). Advances in space research : the official journal of the Committee on Space Research 33, 1395-1400.

Ikegami, R., Hunter, P. and Yager, T. (1999). Developmental activation of the capability to undergo checkpoint induced apoptosis in the early zebrafish embryo. Developmental Biology 209, 409-433.

Itoh, M., Kim, C., Palardy, G., Oda, T., Jiang, Y., Maust, D., Yeo, S., Lorick, Y., Wright, G., Ariza McNaughton, L. et al. (2003). Mind bomb is a ubiquitin ligase that is essential for efficient activation of Notch signaling by Delta. Developmental Cell 4, 67-82.

Janvier, K., Kato, Y., Boehm, M., Rose, J., Martina, J., Kim, B., Venkatesan, S. and Bonifacino, J. (2003). Recognition of dileucine-based sorting signals from HIV-1 Nef and LIMP-II by the AP-1 gamma-sigma1 and AP-3 delta-sigma3 demicomplexes. Journal of Cell Biology 163, 1281-1290.

Kantheti, P., Qiae, X., Diaz, M., Pden, A., Meyer, G., Carskadon, S., Kapfhamer, D., Sufalko, D., RObinson, M., Noaebels, J. et al. (1998). Mutation in AP-3 delta in the mocha mouse links endosomal tranpsort to storage deficiency in pletelets, melanosomes, and synaptic vesicles. Neuron 1998, 111-122.

Khokha, M., Krylov, V., Reilly, M., Gall, J., Bhattacharya, D., Cheung, C., Kaufman, S., Lam, D., Macha, J., Ngo, C. et al. (2009). Rapid gynogenetic mapping of Xenopus tropicalis mutaitons to chromosomes. Developmental Dynamics 238, 1398-1346.

Kido, T. and Takahashi, M. (1997). Scanning electron microscopic study of amphibians otoconia. Auris, nasus, larynx 24, 125-130.

Kil, S. and Collazo, A. (2001). Origins of inner ear sensory organs revealed by fate map and time-lapse analyses. Developmental Biology 233, 365-379.

Kimitsuki, T., Nakashima, T., Kawano, H. and Komune, S. (2003) Neurotrophin-3 modifies potassium currents in isolated inner hair cells from guinea-pig cochlea. Auris Nasus Larynx 30, 141-145.

Kirjavanien, A., Sulg, M., Heyd., Alitalo, K., Yla-Herttuala, S., Moroy, T., Petrova, T. and Rirvola, U. (2008). Prox1 interacts with Atoh1 and Gfi1, and regulates cellular differentiation in the inner ear sensory epithelia. Developmental Biology 322, 33-45.

Kiss, P., Knisz, J., Zhang, Y., Baltrusaitis, J., Sigmund, C., Thalmann, R>, Smith, R., Verpy, E. and Banfu, B. (2006) Inactivation of NADPH oxidase organizer 1 results in sever imbalance. Current Biology 16, 208-213.

Koch, M., Moser, M. and Muller, M. (2003). Signal recognition particle-dependant protein targeting, universal to all kingdoms of life. Reviews of physiology biochemistry and pharmacology. 146, 55-94.

Kozel, P., Friedman, R., Erway, L., Yamoah, E., Liu, L., Riddle, T., Duffy, J., Doetschman, T., Miller, M., Cardell, E. et al. (1998). Balance and hearing deficits

in mice with a null mutation in the gene encoding plasma membrane Ca2+-ATPase isoform 2. Journal of Biochemistry 273, 18693-18696.

Kozlowski, D., Whitfield, T., Hukriede, N., Lam, W. and Weinberg, E. (2005) The zebrafish dog-eared mutation disrupts eya1, a gene required for cell survival and differentiation in the inner ear and lateral line. Developmental Biology 277, 27-41.

Kurc, M., Farina, M., Lins, U. and Kachar, B. (1999). Structural basis for mechanical transduction in the frog vestibular sensory apparatus: III. The organization of the otoconial mass. Hearing Research 131, 11-21.

Kwak, S., Phillips, B., Heck, R. and Riley, B. (2002). An expanded domain of fgf3 expression in the hindbrain of zebrafish valentino mutants results in mis-patterning of the otic vesicle. Development 129, 5279-5287.

Kyttala, A., Yliannala, K., Schu, P., Jalanko, A. and Luzio, J. (2005). AP-1 and AP-3 facilitate lysosomal targeting of Batten disease protein CLN3 via its dileucine motif. Journal of Biological Chemistry 280, 10277-10283.

Ladher, R., Anakwe, K., Gurney, A., Schoenwolf, G. and Francis-West, P. (2000). Identification of synergistic signals initiating inner ear development. Science 290, 1965-1967.

Le Borgne, R., Alconada, A., Bauer, U. and Hoflack, B. (1998). The mammalian AP-3 adapter-like complex mediates the intracellular transport of lysosomal membrane glycoproteins. The Journal of biological chemistry 273, 29451-29461.

Lim, D. (1984). Otoconia in health and disease. A review. The Annals of otology, rhinology & laryngology. Supplement 112, 17-24.

Lin, Z., Cantos, R., Pantente, M. and Wu, D. (2005). Gbx2 is required for the morphogenesis of the mouse inner ear: a downstream candidate of hindbrain signaling. Development 132, 2309-2318.

Liu, M., Pereira, F., Price, S., Chu, M., Shope, C., Himes, D., Eatock, R., Brownell, W., Lysakowski, A. and Tsai, M. (2000). Essential role of BETA2/NeuroD1 in development of the vestibular and auditory systems. Genes & development 14, 2839-2854.

Lombardo, A., Isaacs, H. and Slack, J. (1998). Expression and functions of FGF-3 in Xenopus development. International Journal of Developmental Biology 42, 1101-1107.

Lu, W., Zhou, D., Freeman, J., Thalmann, I., Ornitz, D. and Thalmann, R. (2010). In vitro effects of recombinant otoconin 90 upon calcite crystal growth. SIgnificance of tertiary structure. Hearing Research 268, 172-183.

Lundberg, Y., Zhao, X. and Yamoah, E. (2006). Assembly of the otoconia complex to the macular sensory epithelium of the vestibule. Brain Research 1091, 47-57.

Ma, Q., Anderson, D. and Fritzsch, B. (2000). Neurogenin 1 null mutant ears develop fewer, morphologically normal hair cells in smaller sensory epithelia devoid of innervation. Journal of the Association for Research in Otolaryngology 1, 129-143.

Mackereth, M., Kwak, S., Fritz, A. and Riley, B. (2005) Zebrafish pax8 is required for otic plaocde induction and plays a redundant role with Pax2 genes in the maintenance of the otic placode. Development 132, 371-382.

Malicki, J., Schier, A., Solnica-Krezel, L., Stemple, D., Neuhauss, S., Stainier, D., Abdelilah, S., Rangini, Z., Zwartkruis, F. and Driever, W. (1996). Mutations affecting development of the zebrafish ear. Development 123, 275-283.

Mark, M., Lufkin, T., Vonesch, J., Ruberte, E., Olivo, J., Dolle, P., Gorry, P., Lumsden, A. and Chambon, P. (1993). Two rhombomeres are altered in Hoxa-1 mutant mice. Development 119, 319-338.

Maroon, H., Walshe, J., Mahmood, R., Kiefer, P., Dickson, C. and Mason, I. (2002). Fgf3 and Fgf8 are required together for formation of the otic placode and vesicle. Development. 129, 2099-2108.

Mayor, R., Morgan, R. and Sargent, M. (1995). Induction of the prospective neural crest of Xenopus. Development 121, 767-777.

McKay, I., Muchamore, I., Krumlauf, R., Maden, M., Lumsden, A. and Lewis, J. (1994). The kreisler mouse: a hindbrain segmentation mutant that lacks two rhombomeres. Development 120, 2199-2211.

Mendonsa, E. and Riley, B. (1999). Genetic analysis of tissue interactions required for otic placode induction in the zebrafish. Developmental Biology 206, 100-112.

Millimaki, B., Sweet, E., Dhason, M. and Riley, B. (2007). Zebrafish atoh1 genes: classic proneural activity in the inner ear and regulation by Fgf and Notch. Development 134, 295-305.

Mitchem, K., Hibbard, E., Beyer, L., Bosom, K., Dootz, G., Dolan, D., Johnson, K., Raphael, Y. and Kohrman, D. (2002). Mutation of the novel gene Tmie results in sensory cell defects in the inner ear of spinner, a mouse model of human hearing loss DFNB5. Human Molecular Genetics 11, 1887-1898.

Morsli, H., Choo, D., Ryan, A., Johnson, R. and Wu, D. (1998). Development of the mouse inner ear and origin of its sensory organs. Journal of Neuroscience 18, 3327-3335.

Murayama, E., Herbomel, P., Kawkami, A., Takeda, H. and Noagasawa, H. (2005). Otolith matrix proteins OMP-1 and Otolin-1 are necessary for normal otolith growth and their correct anchoring onto the sensory maculae. Mechansims of Development 122, 791-803.

Murayama, E., Takagi, Y. and Nagasawa, H. (2004). Immunohistochemical localization of two otolith matrix proteins in the otolith and inner ear of the rainbow trout, Oncorhynchus mykiss: comparative aspects between the adult inner ear and embryonic otocysts. Histochemistry and cell biology 121, 155-166.

Murayama, E., Takagi, Y., Ohira, T., Davis, J. G., Greene, M. I. and Nagasawa, H. (2002). Fish otolith contains a unique structural protein, otolin-1. European Journal of Biochemistry 269, 688-696.

Nayak, G., Ratnayaka, H., Goodyear, R. and RIchardson, G. (2007). Development of the hair bundle and mechanotransduction. International Journal of Developmental Biology 51, 597-608.

Nieuwkoop, P. and Faber, J. (1975). Normal table of Xenopus laevis (Daudin): a systematical and chronogical survey of the developmetn from the fertilized egg till the end of metamorphosis: Garland Publishing Inc.

Nishikawa, S. and Sasaki, F. (1996) Internalization of styryl dye FM1-43 in the hair cells of lateral line organs in Xenopus larvae. Journal of histochemistry and cytochemistry 44(7), 733-741.

Noramly, S., Zimmerman, L., Cox, A., Aloise, R., Fisher, M. and Grainger, R. (2005). A gynogenetic screen to isolate naturally occuring recessive mutations in Xenopus tropicalis. Mechansims of Development 122, 273-287.

Offield, M., Hirsch, N. and Grainger, R. (2000). The development of Xenopus tropicalis transgenic lines and their use in studying lens developmental timing in living embryos. Development 127, 1789-1797.

Okano, J., Takigawa, T., Seki, K., Suzuki, S., Shiota, K. and Ishibashi, M. (2005). Transforming growth factoe beta 2 promotes the formation of the mouse cochleaovestibular ganglion in organ culture. International Journal of Developmental Biology 49, 23-31.

Omori, Y. and Malicki, J. (2006). Oko meduzy and related crumbs genes are determinants of apical cell features in the vertebrate embryo. Current Biology. 16, 945-957.

Patten, I. and Placzek, M. (2002). Opponent activities of Shh and BMP signaling during floor plate induction in vivo. Current Biology 12, 47-52.

Pauley, S., Lai, E. and Fritzsch, B. (2006) FOxg1 is required for morphogenesis and histogenesis of the mammalian inner ear. Developmental Dynamics 325, 2470-2482.

Peden, A., Rudge, R., Lui, W. and Robinson, M. (2002). Assembly and function of AP-3 complexes in cells expressing mutant subunits. Journal of Cell Biology 156, 327-336.

Petko, J., Milimaki, B. Canfield, V., Riley, B and Levenson, R. (2008). Otoc1: a novel otoconin-90 ortholog required for otolith mineralization in zebrafish. Developmental Neurobiology. 68, 209-222.

Phillips, B., Bolding, K. and Riley, B. (2001). Zebrafish fgf3 and fgf8 encode redundant functions required for otic placode induction. Developmental Biology 235, 351-365.

Pickles, J., Comis, S. and Osborne, M. (1984). Cross-links between stereocilia in the guinea pig organ of Corti, and their possible relation to sensory transduction. Hearing Research 15, 103-112.

Postlethwait, J., Woods, I., Ngo-Hazelett, P., Yan, Y. and Kelly, P. (2000). Zebrafish comparative genomics and the origins of vertebrate chromosomes. Genome research 10, 1890-1902.

Pote, K. and Ross, M. (1991). Each otoconia polymorph has a protein unique to that polymorph. Comparative biochemistry and physiology. 98, 287-295.

Pote, K. and Ross, M. (1993). Utricular otoconia of some amphibians have calcitic morphology. Hearing Research 67, 189-197.

Price, E. and Fisher, D. (2001). Sensorineural deafness and pigmentation genes: melanopcytes and the mitf transcriptional network. Neuron 30, 15-18.

Quick, Q. and Serrano, E. (2005). Inner ear formation during the early larval development of Xenopus laevis. Developmental Dynamics 234, 791-801.

Riccomagno, M., Martinu, L., Mulheisen, M., Wu, D. and Epstein, D. (2002). Specification of the mammalian cochlea is dependent on Sonic hedgehog. Genes & development 16, 2365-2378.

Riccomagno, M., Takada, S. and Epstein, D. (2005). Wnt-dependent regulation of inner ear morphogenesis is balanced by the opposing and supporting roles of Shh. Genes & development 19, 1612-1623.

Riley, B. and Phillips, B. (2003). Ringing in the new ear: resolution of cell interactions in otic development. Developmental Biology 261, 289-312.

Robinson, M. and Bonifacino, J. (2001). Adaptor-related proteins. Current Opinion in Cell Biology 13, 444-453.

Rolfsen, R. and Erway, L. (1984). Trace metals and otolith defects in mocha mice. Journal of Hereditary. 75,159 – 162.

Rubel, E. and Fritzsch, B. (2002). Auditory system development: primary auditory neurons and their targets. Annual Review of Neuroscience 25, 51-101.

Sage, C. and Marcus, D. (2001). Immunolocalization of ClC-K chloride channel in strial marginal cells and vestibular dark cells. Hearing Research 160, 1-9.

Sadl, V., SIng, A., Mar, L., Jin, F. and Cordes, S. (2003). Analysis of hindbrain patterning defects caused by the kreisler (enu) mutation reveals multiple roles of Kreisler in hindbrain segmentation. Developmental Dynamics 227, 134-142.

Schlosser, G. and Ahrens, K. (2004). Molecular anatomy of placode development in Xenopus laevis. Developmental Biology 271, 439-466.

Schlosser, G. and Northcutt, R. (2000). Development of neurogenic placodes in Xenopus laevis. Journal of Comparative Neurology 418, 121-146.

Schwander, M., Kachar, B. and Muller, U. (2010). Review series: The cell biology of hearing. Journal of Cell Biology 190, 9-20.

Shiao, J., Lin, L., Horng, J., Hwang, P. and Kaneko, T. (2005). How can teleostean inner ear hair cells maintain the proper association with the accreting otolith? The Journal of comparative neurology 488, 331-341.

Shotelersuk, V., Dell'Angelica, E., Hartnell, L., Bonifacino, J. and Gahl, W. (2000). A new variant of Hermansky-Pudlak syndrome due to mutaitons in a gene responsible for vesicle formation. American Journal of Medicine 108, 423-437.

Simmler, M., Zwaenepoel, I., Verpy, E., Guillaud, L., Elbaz, C., Petit, C. and Panthier, J. (2000). Twister mutant mice are defective for otogelin, a component specific to inner ear acellular membranes. Mammalian Genome 11, 961-966.

Simpson, F., Bright, N., West, M., Newman, L., Darnell, R. and Robinson, M. (1996). A novel adapter-related protein complex. Journal of Cell Biology 133, 749-760.

Sive, H. (2000). Early development of Xenopus laevis: A Laboratory Manual. CSHL Press.

Sollner, C., Schwarz, H., Geisler, R. and Nicolson, T. (2004). Mutated otopetrin 1 affects the genesis of otoliths and the localization of Starmaker in zebrafish. Development genes and evolution 214, 582-590.

Spicer, S., Schulte, B. and Adams, J. (1990). Immunolocalization of Na+,K(+)-ATPase and carbonic anhydrase in the gerbil's vestibular system. Hearing Research 43, 205-217.

Streit, A. (2001). Origin of the vertebrate inner ear: evolution an dinduction of the otic placode. Journal of Anatomy 199, 99-103.

Sumanas, S., Larson, J. and Miller Bever, M. (2003) Zebrafish chaperone protein GP96 is required for otolith formation during ear develepment. Developmental Biology. 261, 443-455.

Swank, R., Reddingtion, M., Howlett, O. and Novak, E. (1991). Platelet storage pool deficiency assocaited with inherited abnormalities of the inner ear in the mouse pigment mutants muted and mocha. Blood 78, 2036-2044.

Taylor, R. and Forge, A. (2005). Hair cell regeneration in sensory epithelia from the inner ear of a urodele amphibian. Journal of Comparative Neurology 484, 105-120.

Theos, A., Tenza, D., Matina, J., Hurbain, I., Peden, A., Sviderskaya, E., Stewart, A., Robinson, M., Bennett, D., Cutler, D. et al. (2005). Functions of adaptor protein (AP)-3 and AP-1 in tyrosinase sorting from endosomes to melanosomes. Molecular biology of the cell 16, 5356-5372.

Torres, M., Gomez-Pardo, E. and Gruss, O. (1996). Pax2 contributes to inner ear patterning and optic nerve trajectory. Development 122, 3381-3391.

Tu, T. Y., Chiu, J. H., Shu, C. H. and Lien, C. F. (1999). cAMP mediates transepithelial K+ and Na+ transport in a strial marginal cell line. Hearing Research 127, 149-157.

Tu, T. Y., Chiu, J. H., Yang, W. K., Chang, T. J., Yang, A. H., Shu, C. H. and Lien, C. F. (1998). Establishment and characterization of a strial marginal cell line maintaining vectorial electrolyte transport. Hearing Research 123, 97-110.

Vitelli, F., Viola, A., Morishima, M., Pramparo, T., Baldini, A. and Lindsay, E. (2003). TBX1 is required for inner ear morphogenesis. Human Molecular Genetics 12, 2041-2048.

Waldman, E., Castillo, A. and Collazo, A. (2007). Ablation studies on the developing inner ear reveal a propensity for mirror duplications. Developmental Dynamics 236, 1237-1248.

Wanner, S. and Miller, J. (2007) Regulation of otic vesicle and hair cell stereocilia morphogenesis by Ena/WASP-like (Evl) in Xenopus. Journal of Cell Science 120, 2641-2651.

Wang, Y., Kowalski, P., Thalmann, I., Ornitz, D., Mager, D. and Thalmann, R. (1998). Otoconin-90, the mammalian otoconial matrix protein, contains two domains of homology to secretory phospholipase A2. Proceedings of the National Academy of Sciences of the United States of America 95, 15345-15350.

Wang, W., Grimmer, J., Van De Water, T. and Lufkin, T. (2004). Hmx2 and Hmx3 homeobox genes direct development of the murine inner ear and hypothalamus and can be functionally replaced by Drosophila Hmx. Developmental Cell 7, 439-453.

Wangemann, P., Liu, J. and Marcus, D. (1995). Ion transport mechanisms responsible for K+ secretion and the transepithelial voltage across marginal cells of strial vascularis in vitro. Hearing Research 84, 19-29.

Wangemann, P., Nakaya, K., Wu, T., Maganti, R., Itza, E., Sanneman, J., Harbidge, D., Billings, S. and Marcus, D. (2007). Loss of cochlear HCO3- secretion causes deafness via endolymphatic acidification and inhibition of Ca2+ reabsorption of a Pendred syndrome mouse model. American Journal of Physiology. Renal physiology 292, 1345-1353.

Wells, D., Gutierrez, L., Xu, Z., Krylov, V., Macha, J., Blankenburg, K., Hitchens , M., Bellot, L., Spivey, M., Stemple, D. et al. (2011). A genetic map of Xenopus tropicalis. Developmental Biology. 354(1), 1-8.

Whitfield, T. (2002). Zebrafish as a model for hearing and deafness. Journal of Neurobiology 53, 157-171.

Whitfield, T., Granato, M., van Eeden, F., Schach, U., Brand, M., Furutani-Seiki, M., Haffter, P., Hammerschmidt, M., Heisenberg, C., Jiang, Y. et al. (1996). Mutations affecting development of the zebrafish inner ear and lateral line. Development 123.

Whitfield, T. and Hammond, K. (2007). Axial patterning in the developing vertebrate inner ear. International Journal of Developmental Biology 51, 507-520.

Whitfield, T., Riley, B., Chiang, M. and Philiips, B. (2002). Development of the zebrafish inner ear. Developmental Dynamics 223, 427-458.

Whitfield, T., Sharpe, C. and Wylie, C. (1994). Nonsense-mediated mRNA decay in Xenopus oocytes and embryos. Developmental Biology 165, 731-734.

Woo, K. and Fraser, S. (1998). Specification of the hindbrain fate in the zebrafish. Developmental Biology 197, 283-296.

Wu, D. and Oh, S. (1996). Sensory organ generation in the chick inner ear. Journal of Neuroscience 16, 6454-6462.

Xie, X. and Smart, T. (1991). A physiological role for endogenous zinc in rat hippocampal synaptic neurtransmission. Nature 349, 521-541.

Yamoah, E., Lumpkin, E., Dumont, R., Smith, P., Hudspeth, A. and Gillespie, P. (1998). Plasma membrane Ca2+-ATPase extrudes Ca2+ from hair cell stereocilia. Journal of Neuroscience 18, 610-624.

Yaoi, Y., Suzuki, M., Tomura, H., Sasyama, Y., Kikuyama, S. and Tanaka, S. (2003). Molecular cloning of otoconin-22 complementary deoxyribonucleic acid in the bullfrog endolymphatic sac: effect of calcitonin on otoconin-22 messenger ribonucleic acid levels. Endocrinology 144, 3287-3296.

Yoshino, T., Sato, E., Nakashima, T., Teranishi, M., Nakayama, A., Mori, N., Murakami, H., Funahashu, H. and Imai, T. (2004). The immunohistochemical analysis of pendrin in the mouse inner ear. Hearing Research 195, 9-16.

Young, J., Cherone, J., Doyon, Y., Ankoudinova, I., Faraji, F., Lee, A., Ngo, C., Guschin, D., Paschon, D., Miller, J. et al. (2011). Efficient targeted gene disruption in the soma and germ line of the frog Xenopus tropicalis using engineered zinc-finger nucleases. Proceedings of the National Academy of Sciences of the United States of America 108(17), 7052-7057.

Zhao, X., Yang, H., Yamoah, E. and Lundberg, Y. (2007). Gene targeting reveals the role of Oc90 as the essential organizer of the otoconial organic matrix. Developmental Biology 304, 508-524.

Zhao, Y., Yamoah, E. and Gillespie, P. (1996). Regeneration of broken tip links and restoration of mechanical transduction in hair cells. Proceedings of the National Academy of Sciences of the United States of America 93, 15469-15474.

Zheng, W., Huang, L., Wei, Z., Silvius, D., Tang, B. and Xu, P. (2003). The role of Six1 in mammalian auditory system development. Development 130, 3989-4000.

Zwaenepoel, I., Mustapha, M., Leibovici, M., Verpy, E., Goodyear, R., Liu, X., Nouaille, S., Nance, W., Kanaan, M., Avaraham, K. et al. (2002). Otoancorin, an inner ear protein restricted to the interface between the apical surface of sensory epithelia and their overlying acellular gels, is defective in autosomal recessive deafness DFNB22. Proceedings of the National Academy of Sciences of the United States of America 99, 6240-6245.

# Appendix A

SSLPmarkers

***seasick* (*ssk*)**

| Chromosome | Designation | Scaffold v4 assembly | Location in scaffold (bp) | Forward Primer | Reverse Primer |
|---|---|---|---|---|---|
| 1 | 013H11 | 79 | 847170 | TAACTTTCTCCAGGCACAGC | TGACACAGATCACATCCACAG |
| 2 | 042F05 | 403 | 457604 | CTGCTGCTTTGGAACACTG | TCTTTGCCTGAAAACAATGAG |
| 2 | 016H11 | 13 | 1129479 | AGACAGTGGTTCAATGCAAG | TGTCCTCTTTTACGTCCACC |
| 3 | 017G07 | 397 | 24212 | CAATGATCCCAATGTTAGCC | ATTTCCGATCTGCTATGCTG |
| 5 | 025G05 | 252 | 1282369 | TCCGTTCGATTGAGGATAAG | CTGAGTTGGCAGGTAAATG |
| 5 | 020D03 | 2 | 6966063 | GGCCTTTAATTCCACAGGAC | AGGTTGTGTGCTGGGTTTAC |
| 6 | 025H10 | 46 | 1582986 | GGCATGGCTGAGAAGTTTAC | GATTGGTGATTGGATTCTGG |
| 7 | 010E04 | 376 | 201797 | TAAAAGCATACGCCCAAAAG | TGTGCAAACAGACAATCACC |
| 1 | 096B10 | 17 | 5245000 | TTGTAAGTAAGGGCGTCTGC | ACGGCATTTGTGTGTTTACC |
| 1 | 018E09 | 554 | 582407 | CTCAATAATCAGGGCATGTAATC | GCAGACATAAGCATTGTACCC |
| 1 | 002G02 | 16 | 4953465 | GTCTCAACTGTGCCCTTCTG | ATAGCAAAACAAAGCAAGCG |
| 1 | 018E09 | 554 | 582407 | CTCAATAATCAGGGCATGTAATC | GCAGACATAAGCATTGTACCC |
| 1 | 021H07 | 158 | 2160154 | GTTACACAGCTCAGGGTTCC | TGCATGGTCAACTTTAGTGC |
| 1 | 018G09 | 567 | 270277 | CTTTGTAGCTTTCGTGGTGG | CTTGCTAATGAAGCAGTCAGC |
| 1 | 021G10 | 646 | 176341 | GGCAAACATAATCCGTCAAG | ATACAAGCCACAGCAAAACC |
| 1 | 021H03 | 555 | 22632 | TTACCTTAACCTCCTGTTTGC | AATAGGCACGTCTGTTGACTG |
| 1 | 013H11 | 79 | 847170 | TAACTTTCTCCAGGCACAGC | TGACACAGATCACATCCACAG |
| 1 | 016F05 | 60 | 3337045 | ACAGAACCCATGCTTCAATG | CCACATAAAACAGCCAGGTG |
| 1 | 003F02 | 17 | 2883342 | TAAAGGCGAAGACATTCCAC | GGTACTGAGCTGTCCTGTGC |
| 1 | 030C07 | 311 | 212698 | TTGTATAGCACAAACCCAGTG | TGGCAACATAAATCTCATGC |
| 1 | 071H12 | 656 | 531000 | TTAGATGCAAAGCAAACTTGG | TATGTCTGGGTGACAGGTCC |
| 1 | 087H04 | 112 | | TATATCCAATGCTATGGCCG | GAGGAAGAGCACAGTTGGTG |
| 1 | 028D11 | 112 | 1213293 | TATTTGCCTTCTCCACCAAG | AAGCCCACATAAATGCAGAG |
| 1 | 123G04 | 289 | 485000 | TTGCAGTTACCGTGGTTTG | TTTCATCATCATCCTCCAAC |
| 1 | 327_1 | 327 | 13637 | GGTGCAACCAAAGAAAAACC | GGGCTTGAACCCAAAAAGTT |
| 1 | 327_3 | 327 | 14388 | TGCTAGCATGGACTAAGGTATTCA | ATTATTGCACCCACCACTGC |
| 1 | 327_4 | 327 | 54098 | CAGTGTGGCTTGTCATACAAAT | AGTCAGAGGACTATCAGTCAGATCTAT |

***komimi* (*kom*)**

| Chromosome | Designation | Scaffold v4 assembly | Location in scaffold (bp) | Forward Primer | Reverse Primer |
|---|---|---|---|---|---|
| 2 | 042F05 | 403 | 457000 | CTGCTGCTTTGGAACACTG | TCTTTGCCTGAAAACAATGAG |
| 2 | 016H11 | 13 | 1129000 | AGACAGTGGTTCAATGCAAG | TGTCCTCTTTTACGTCCACC |
| 5 | 009G06 | 74 | 1847904 | TGGATTCTGTGGTTCAAATG | ATCATTGCGTTTTGCGTTAG |
| 6 | 008B05 | 326 | 620484 | ATACACAAACCACCCCAAAG | AGCATTTCCATTGAGTCCTG |
| 7 | 012A04 | 168 | 763326 | TGGTACTTCTGGGCTTCTTG | AGTGCTTATTTGTGTTGGGG |
| 9 | 023G03 | 487 | 11663 | TCAGAAGGTTGTTTTCCTGC | GACCCAAGAGAGAGGGAGAG |
| 10 | 018A06 | 155 | 964747 | CATATCACGGCTTAGGCAAC | CTGATGCAACTGTCAAGCAC |
| 6 | 015G09 | 674 | 468112 | CATTAGGGGTAATTTCATGTGC | AAGCAGAGTGAGAAAGAAAGC |
| 3 | 042A06 | 1202 | 124473 | TGTTTTGTGATGTGTCCCAG | ACTGCCATACAGGGTGCTAC |
| 8 | 049C11 | 671 | 236442 | AATGGCTTTCTCTTTCTCTCTC | GCCCAATACATAAAGGACACC |
| 6 | 016B11 | 104 | 1527715 | AACACACACACACACCATGC | ATGGAGAACCTTAACGGGAC |
| 6 | 121G10 | 96 | 198000 | CAGCTTTAGAATGCCAGCTC | AATTTCCCTACCCCAAACAG |
| 6 | 025E12 | 104 | 1914090 | GCAGCTACACAATCAGGACC | AGAACTTTGCATTCTGCCAC |
| 6 | 008B08 | 326 | 862353 | AAACTATGGGGCTTTATTTGC | TTTTGCTGTTGTTGATGCAC |
| 6 | 047F09 | 260 | 1591033 | AGAAAAGGAACCAGACCACC | AGACTCCCACCACTCTACCC |
| 6 | 048E02 | 96 | 2583939 | AGCAGCACTGACATGAAATG | CTCTTCTGAGCACTTTTGCC |
| 6 | 033H03 | 96 | 1758555 | GGAAACTGCCATTGTACCAG | AATGCACAAACTGCAAATCC |
| 6 | 009H12 | 3 | 212950 | CCCATTCCCACAGTCTATTG | ATACCATTTCCAGGGCTTTC |
| 6 | 010A09 | 3 | 1146249 | AATTGTGAAAAGAAGCGTGG | ACAAGAGTTATCCGCACAGG |
| 6 | 037B05 | 396 | 156052 | CATCTGGGTGCTTTGTATCC | GAACATGGCCCTTATGAGTC |
| 6 | 010B12 | 433 | 830000 | ATCATCCTTTCCTTCCCTTC | AGAGTGCAGCCTAAGTCATTC |
| 6 | 122G03 | 330 | 1234000 | AATTGTGGCAGATAATGAAGC | GGCAGCAGGAGGAACTTTAC |
| 6 | 033G06 | 459 | 60083 | GACATGGGAACAGCAGACTC | CAGATAAACCAAGGGAATGC |
| 6 | 015B02 | 496 | 751305 | TGCTTCTCCTATTGACGACC | TTATTGGTTAAAGACCCGCC |
| 6 | 015A12 | 21 | 2891188 | TCACAATAGTCAAGTTACACTGGG | CAACTGCCTCCTCCATTG |
| 6 | 097H04 | 21 | 3610000 | AGGGGTTAATTTCCGCATAG | GTGTCGGAGTCATTGGAATC |
| 6 | 105H09 | 21 | 3700000 | TCAAGAGAAAGGCAGGAATG | GGAGTTAAGGAAGAGCGGAG |
| 6 | 025H10 | 46 | 1582000 | GGCATGGCTGAGAAGTTTAC | GATTGGTGATTGGATTCTGG |
| 6 | 015B05 | 496 | 280000 | GTGTTTGGGTTAAGTTCCCC | GTACTTCCAGTTGGTGGGTG |

***legolas* (*leg*)**

| Chromosome | Designation | Scaffold v4 assembly | Location in scaffold (bp) | Forward Primer | Reverse Primer |
|---|---|---|---|---|---|
| 1 | 013H11 | 79 | 847170 | TAACTTTCTCCAGGCACAGC | TGACACAGATCACATCCACAG |
| 2 | 016H11 | 13 | 1129000 | AGACAGTGGTTCAATGCAAG | TGTCCTCTTTTACGTCCACC |
| 5 | 026H07 | 206 | 1771000 | GATAAAAGAAAACGACACCCC | TTTCAGGCTATCAGCAAATC |
| 7 | 010E04 | 376 | 201000 | TAAAAGCATACGCCCAAAAG | TGTGCAAACAGACAATCACC |
| 8 | 049C11 | 671 | 236000 | AATGGCTTTCTCTTTCTCTCTC | GCCCAATACATAAAGGACACC |
| 10 | 045F05 | 240 | 908000 | TGCATTTTGTAATGGGGTG | TTTGTCAGGCACAACAAGTC |
| 5 | 026G01 | 172 | 61000 | CCAGATTTTCCCATAGAGCC | TGCCACTAATACACCAGTATGTG |
| 5 | 020G01 | 473 | 504000 | TGACAGATCCAGCTTTCGTC | AGCCACAGAGAGTGACCAAC |
| 5 | 017D07 | 450 | 129000 | ATCTCCCAAGAGGTCTGTCC | GCACCAACATGGGTTTTAAG |
| 5 | 018H10 | 182 | 511000 | GAGAATGGCACAATTTCACTG | TACCTATCTTTCGAGCTGGG |
| 5 | 109C12 | 68 | 1523000 | AACATATACCAAGCCACCTCTG | TCTGTTTTCTTTCTCATTTCTTCC |

***bunny* (*bun*)**

| Chromosome | Designation | Scaffold v4 assembly | Location in scaffold (bp) | Forward Primer | Reverse Primer |
|---|---|---|---|---|---|
| 2 | 113H08 | 802 | 46000 | ATGCTCGGGACTATTTGAAG | TATCAGCAGCACGAACAAAC |
| 2 | 055B07 | 82 | 2902000 | AAATGTCACGTCTCCAGTCC | CAGTTAGACACCAGAACCCG |
| 2 | 019A04 | 171 | 2048000 | TCTAGCAGCACCTTGAGAGG | TGTTGTTATCCATGCCTCAG |
| 2 | 033B04 | 71 | 2309000 | CCTGTGTCTATCAAACAAATGC | AAGGCAATTAAGCAACAACG |

# Appendix B

## Candidate Genes

## Otoconial mineralization

| Candidate Gene | Function | LG | Scaffold Position | Local SSLP | Reference |
|---|---|---|---|---|---|
| *oc22* | otoconial matrix protein | 4 | 390: 368194-520617 | 026F08 | Petko et al., 2007 |
| *oc90* | otoconial matrix protein | 2 | 496: 53614-235898 | 015B05 | Zhao et al., 2007 |
| *tecta* | otoconial membrane protein | 4 | 124: 2,456,088-2,465,047 | 012B08 | Moreno-Pelayo et al., 2008 |
| *opn* | otoconial matrix protein | 7 | 187: 1,812,671-1,829,406 | 005H01 | Takemura et al., 1994 |
| *gp96* | chaperone | 3 | 390: 1277810-1286287 | 109E10 | Sumanas et al., 2003 |
| *atp1a1* | Na-K transporter | 2 | 959: 48266-56376 | 027C04 | Blasiole et al., 2006 |
| *slc26a4* | solute carrier | 8 | 45: 3,280,890-3,303,023 | 070D04 | Brownstein et al., 2008 |
| *calb1* | $Ca^{2+}$ transporter | 2 | 96: 2,621,124-2,652,092 | 048E02 | Buckiova & Syka 2009 |
| *otop1* | extracellular calcium sensor | 1 | 441: 286368-306727 | 050D01 | Hughes et al., 2004 |
| *calr1* | calcium binding protein | 7 | 6: 3,915,120-3,945,494 | 024B06 | Dechesne et al., 1996 |
| *pvalb* | calcium binding protein | 5 | 501: 575,410-590,259 | 035C06 | Heller et al., 2002 |
| *kcnma1* | calcium activated potassium channel | 4 | 265: 797,000-1,089,066 | 037G05 | Beisel et al., 2007 |
| *mcoln3* | ion channel | 7 | 6: 2,046,900 – 2,067,606 | 024B06 | Di Palma et al., 2002 |
| *hps1* | intracellular protein trafficking | 7 | 212: 1,731,324-1,776,402 | 121C07 | Chiang et al., 2003 |
| *hps4* | intracellular protein trafficking | 1 | 17: 2,251,546-2,261,199 | 003D01 | Chiang et al., 2003 |
| *muted* | intracellular protein trafficking | 6 | 33: 1,900,073-1,923,400 | 085G05 | Falcon-Perez et al., 2002 |
| *cappuccino* | intracellular protein trafficking | 6 | 213: 1,720,508-1,726,502 | 017F06 | Ciciotte et al., 2003 |
| *noxo1* | intracellular protein trafficking | 9 | 174:1,992,876-1,997,959 | 082A04 | Kiss et al., 2006 |

## Placode induction and otic vesicle patterning

| Candidate Gene | Function | LG | Scaffold Position | Local SSLP | Reference |
|---|---|---|---|---|---|
| *dlx3* | transcription factor | 10 | 165: 2,180,191 – 2,185,078 | 024G05 | Brown et al., 2005 |
| *dlx4* | transcription factor | 10 | 165: 2,143,034 – 2,160,541 | 024G05 | Brown et al., 2005 |
| *dlx6* | transcription factor | 2 | 400: 432,849-436,979 | 016H01 | Brown et al., 2005 |
| *fgf3* | transcription factor | u.m. | 3249: 5,462-10,121 | - | Maroon et al., 2002 |
| *fgf8* | transcription factor | 4 | 238: 635,262 – 644,317 | 017F12 | Maroon et al., 2002 |
| *fgfr1* | fgf receptor | 7 | 32: 2,250,873-2,297,135 | 032C08 | Maroon et al., 2002 |
| *pax2* | transcription factor | 4 | 204:1487698 - 1542474 | 033F04 | Burton et al., 2004 |
| *pax5* | transcription factor | 1 | 175: 1630926 - 1750137 | 033E03 | Kwak, S. et al., 2006 |
| *pax8* | transcription factor | 7 | 30: 1851403 - 1859593 | 058C06 | Mackereth et al., 2006 |
| *dach1* | transcription factor | 6 | 13:3159589 - 3310616 | 025D03 | Ozacki et al., 2004 |
| *eya1* | transcription factor | 2 | 260: 424,511 – 483,260 | 047F09 | Kozlowski et al., 2005 |
| *eya4* | transcription factor | 9 | 172: 629,719 – 1,681,182 | 026G01 | Wang et al., 2008 |
| *foxi1* | transcription factor | 1 | 280: 516,316 - 521,622 | 036A09 | Pauley et al., 2006 |
| *wnt1* | transcription factor | 2 | 130: 1,689,330 – 1,694,878 | 017E12 | Riccomango et al., 2005 |
| *wnt3* | transcription factor | u.s. | 379: 801,762-853,280 | - | Riccomango et al., 2005 |
| *wnt8* | transcription factor | 8 | 65: 23,443 – 28,463 | 024C03 | Riccomango et al., 2005 |
| *foxg1* | transcription factor | 5 | 37: 1,859,990-1,861,297 | 015B07 | Pauley et al., 2006 |
| *sox10* | transcription factor | 7 | 88: 512,437-514,549 | 074D11 | Breuskin et al., 2010 |
| *hmx2* | transcription factor | 4 | 316: 788,532-790,210 | 055C09 | Wang et al., 2004 |
| *hmx3* | transcription factor | 4 | 316: 762,890-764,716 | 055C09 | Wang et al., 2004 |
| *otx1* | transcription factor | 9 | 473: 715,997-720,114 | 020G01 | Vitelli et al., 2003 |
| *otx2* | transcription factor | 8 | 68: 1,513,190-1,515,996 | 109F10 | Vitelli et al., 2003 |
| *tgfβ2* | secretary signaling molecule | 9 | 182: 1,257,020-1,344,581 | 044F10 | Okano et al., 2005 |

## Semicircular canal development

| Candidate Gene | Function | LG | Scaffold Position | Local SSLP | Reference |
|---|---|---|---|---|---|
| *bmp2* | transcription factor | 9 | 450: 240,133 – 251,862 | 017D07 | Hammond et al., 2009 |
| *bmp4* | transcription factor | 8 | 247: 834,417-860,132 | 029G10 | Chang et al., 2008 |
| *gli3* | signaling molecule | 2 | 57: 312,820 - 442,672 | 012A06 | Bok et al., 2007 |
| *tmie* | transmembrane protein | 2 | 479: 781,729 – 844,245 | 029A05 | Mitchem et al., 2002 |

## Hair cell stereocilia development

| Candidate Gene | Function | LG | Scaffold Position | Local SSLP | Reference |
|---|---|---|---|---|---|
| *atp2b2* | atpase $Ca^{2+}$ transporting plasma membrane 2 | 7 | 88: 2,761,146-2,852,198 | 036C01 | Crouch & Schulte, 1996 |
| *cdh23* | otocadherin | u.s. | 546: 55554-356494 | - | Di Palma et al., 2001 |
| *pcdh15* | kinocilia link | 8 | 65: 3,004,340-3,006,556 | 042D04 | Goodyear et al., 2010 |
| *myoVIIa* | motor protein | 6 | 277: 1,025,547-1,049,491 | 051C06 | Di Leva et al., 2006 |
| *evl* | actin binding protein | 5 | 222: 1049985-1140855 | 007E07 | Wanner & Miller, 2007 |

## Sensory cell differentiation

| Candidate Gene | Function | LG | Scaffold Position | Local SSLP | Reference |
|---|---|---|---|---|---|
| *atoh1* | lateral inhibition | 1 | 276: 130897-131646 | 006A02 | Millimaki et al., 2007 |
| *hes1* | lateral inhibition | 4 | 207: 1,143,438 – 1,145,416 | 016G06 | Haddon et al., 1998 |
| *crb3a* | cell polarity | 7 | 19: 4,641,455-4,668,092 | 048B03 | Omori & Malicki, 2006 |
| *dvl1* | cell polarity | 4 | 390: 692,714-758,849 | 026F08 | Etheridge et al., 2008 |
| *dvl3* | cell polarity | 9 | 132: 303,504-332,181 | 023D01 | Etheridge et al., 2008 |
| *gfi1* | transcription factor | 7 | 70: 2,807,473 – 2,813,181 | 059D10 | Kirjavainen et al., 2008 |
| *prox1* | transcription factor | 4 | 108: 2,095,441-2,138,030 | 114F09 | Kirjavainen et al., 2008 |
| *ngn1* | transcription factor | 8 | 177: 464,024-464,498 | 024C03 | Ma et al., 2000 |
| *nt-3* | neurotrophic factor | 8 | 24: 3,338,298-3,374,682 | 046E03 | Kimitsuki et al., 2003 |

A list of candidate genes, known to display mutant phenotypes resembling the *X. tropicalis* inner ear mutants, has been complied from the literature. The locations of these genes in the *X. tropicalis* genome have been identified in the version 4 genome assembly using the ensembl genome browser (http://www.ensembl.org/Xenopus_tropicalis/Info/Index) and SSLP markers located close to the candidate genes have been identified using the Sater map (Wells et al., 2011).

Key: u. s.: unmapped scaffold

# Appendix C

## OC90 signal peptide prediction

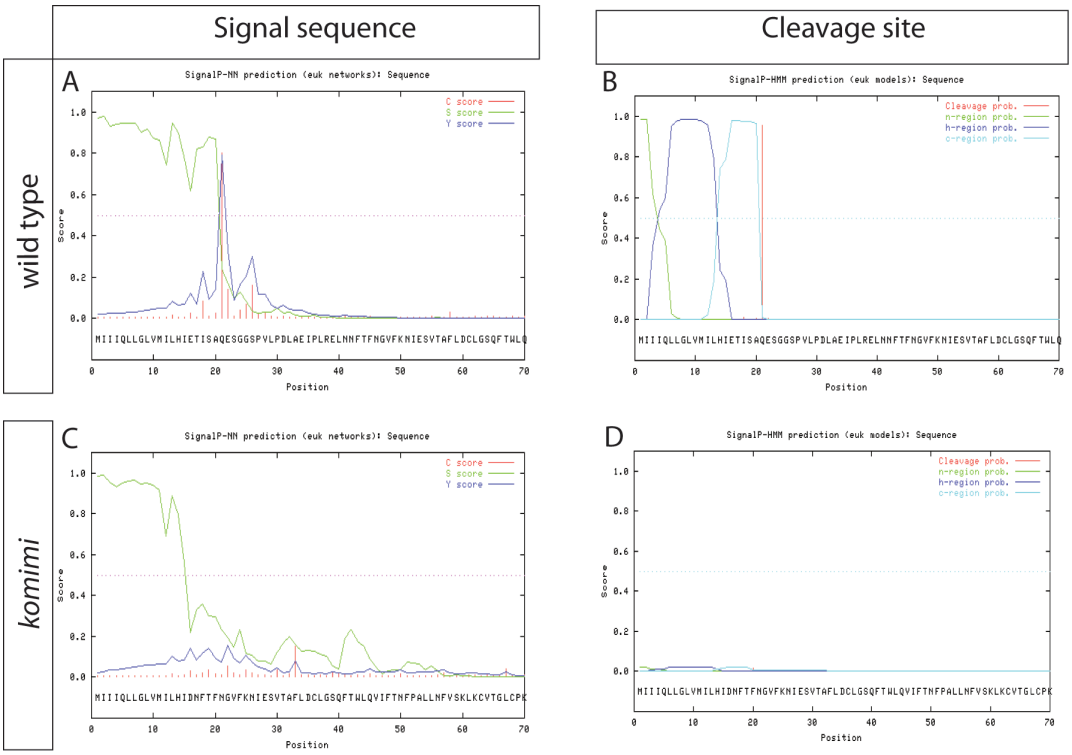


The SignalP software (http://www.cbs.dtu.dk/services/SignalP/) was used to predict the signal peptide for OC90. For the wild type OC90 peptide, the first 21 amino acids have a high probability to be a sectary signal peptide (p=0.983) and the glutamine at position 21 was predicted to be the cleavage site (p=0.954). For the *kom* peptide, the last 6 amino acid of this signal peptide is lost. There is a low probability for the beginning of the kom OC90 to be a signal peptide (p=0.023) and the probability of a peptide cleavage site in this region is low also (p=0.015).